Ontwikkeling en validatie van niet-invasieve diagnostiek voor onderzoek van arteriële stijfheid en golfreflecties met toepassing in sub-Saharisch Afrika

Development and Validation of Non-Invasive Diagnostic Tools for the Assessment of Arterial Stiffness and Wave Reflections with Application in Sub-Saharan Africa

Jan Kips

Promotoren: prof. dr. ir. P. Segers, prof. dr. L. Van Bortel
Proefschrift ingediend tot het behalen van de graad van
Doctor in de Ingenieurswetenschappen: Biomedische Ingenieurstechnieken

Vakgroep Civiele Techniek
Voorzitter: prof. dr. ir. J. De Rouck
Faculteit Ingenieurswetenschappen en Architectuur
Academiejaar 2010 - 2011

UNIVERSITEIT GENT

ISBN 978-90-8578-441-8
NUR 954
Wettelijk depot: D/2011/10.500/45

Supervisors:

Prof.dr.ir. Patrick Segers
Prof.dr. Luc Van Bortel

Research units:

Institute Biomedical Technology
Biofluid, Tissue and Solid Mechanics for Medical Applications
Ghent University
De Pintelaan 185 - Block B
B–9000 Gent
Belgium

Heymans Institute of Pharmacology
Clinical Pharmacology Research Unit
Ghent University
De Pintelaan 185 - Block B
B–9000 Gent
Belgium

Members of the exam committee:

Chairman:	
Prof.dr.ir. Rik Van de Walle	Faculty of Engineering and Architecture, UGent
Secretary:	
Dr.ir. Hans Hallez	Faculty of Engineering and Architecture, UGent
Reading committee:	
Prof.dr. Alun Hughes	Imperial College, London, UK
Dr.ir. Berend Westerhof	BMEYE, Amsterdam, The Netherlands
Dr.ir. Sebastian Vermeersch	Faculty of Engineering and Architecture, UGent
Dr.ir. Hans Hallez	Faculty of Engineering and Architecture, UGent
Other members:	
Prof.dr.ir. Stephen Greenwald	Queen Mary University, London, UK
Dr. Marc Twagirumukiza	Faculty of Medicine, UGent
Prof.dr. Luc Van Bortel	Faculty of Medicine, UGent
Prof.dr.ir. Pascal Verdonck	Faculty of Engineering and Architecture, UGent
Prof.dr.ir. Patrick Segers	Faculty of Engineering and Architecture, UGent

This research was funded by VLIR (Vlaamse Interuniversitaire Raad) research grant VLADOC 2007-0013-396.

Acknowledgements

This book summarizes most of the research I have performed during the past five years. However, there is no way I could have done this alone. Therefore, this is the right moment to express my gratitude to those who supported and helped me in one way or another. I always felt there were great, cool and interesting people around and behind me.

Being a sports freak, I drafted my own *Dream Team*. Allow me to walk you through this league of extraordinary gentlemen/-women:

Goalkeeper:

- Patrick Segers. *Player/coach.*
  Patrick is the first reason I started a PhD. He practically tailored a research project to fit my interests, and managed to be a colleague, a boss and a friend at the same time. Although he manages a research lab of about twenty people, he knows more about my research than I do myself.

Defenders:

- Koen Van Canneyt. *Main organiser.*
  Koen is the second reason I started a PhD, by showing me how much fun research could actually be during our joint Master thesis.

- Dries Mahieu. *Silent force.*
  Dries was my first colleague, the guy who actually introduced me to life as a PhD-student and an amiable *compagnon de route*.

- Grietje Vanacker & Guido Kips. *My first true defenders.*
  My parents. They formed the base of who I am and raised me with loads of love, freedom and patience.

Midfielders:

- Sebastian Vermeersch. *Supports all actions with analogies and arguments.* Seba's amazing eloquence and particular sense of humor make him an extraordinary colleague and friend. His contribution to this PhD can hardly be overestimated.

- Isabelle Fabry. *Eases most actions with happiness.*
  Isabelle brought enthousiasm, naivety and great care to our office.

- Julie Lippens. *Supports all actions with care and love.*
  My wonderful wife, with an endless patience, trust and belief in me, giving me strength and joy in life. She is also the reason why you won't find (m)any typo's in this book.

- Lieselot Kips. *Wonderkid. Relativises all actions.*
  Our daughter. Only 11 weeks old, but every inch drop-dead georgeous. She was born on the very day I finished writing this PhD.

Attackers:

- Kennedy Cruickshank. *Eccentric energetic striker.*
  Apart from the multiple lively and lengthy discussions I enjoyed having with him, Kennedy is also the one who offered me the oppportunity to perform research in Nigeria and Jamaica.

- Marc Twagirumukiza. *Hard-working diplomate. The team's black guy.*
  I had the pleasure to share the office with Marc, and although he often complained that 'life is too hard', it always seemed a bit lighter when he was around.

General manager of this team would be Luc Van Bortel, my co-promotor, who supported me the first year of my PhD and had a distant trust in the completion of this PhD.

Besides this team, there are some other *teams* of people I really want to acknowledge:

My current and former colleagues at the Heymans Institute, in particular Sofie, Majda, Jolyce, Silas, Tine, Ilse and Karen.

My current and former bioMMeda-colleagues, in particular Bram, who helped me run off my frustrations, and Jurgen, who actuallly assembled the Tono-Doppler device described later on in this thesis.

I consider myself lucky to have spent quite some time of my PhD in exotic locations such as South-Africa, Nigeria and Jamaica. On each of these trips, I always felt very welcome. A warm thanks to Hugo, Alta and Edelweiss in South-Africa, Terrence, Alan and Kathryn in Jamaica, Lola, Williams and Yomi in Nigeria.

My friends and family, in particular Lies, Julie, Marie & Ward, thanks for being there and making me forget my PhD when I needed it.

I'm truly grateful to all of you!

Jan
Gent, July 2011

Contents

Samenvatting
Summary

Samenvatting

Dit doctoraatsonderzoek focust op de ontwikkeling en validatie van nieuwe methoden en toestellen ter bepaling van arteriële stijfheid en golfreflecties, twee indicatoren met voorspellende waarde voor de ontwikkeling van hoge bloeddruk (hypertensie) en de hiermee geassocieerde hart- en vaatziekten.

De tekst bestaat uit vijf onderdelen. Het eerste deel bevat algemene achtergrondinformatie, terwijl de voornaamste conclusies worden samengevat in het laatste deel. Het eigenlijke onderzoek is gegroepeerd in de drie middelste delen: delen II en III bundelen een aantal studies over de validatie en ontwikkeling van nieuwe methoden en toestellen ter bepaling van arteriële stijfheid en golfreflecties. In het vierde deel wordt gefocust op de studie van de arteriële eigenschappen van zwarten. Elk deel wordt hierna kort samengevat.

Deel I: Achtergrond

In *hoofdstuk 1* worden de basisprincipes van de cardiovasculaire anatomie, fysiologie en pathofysiologie geïntroduceerd, met bijzondere aandacht voor arteriële wandmechanica en hemodynamica. Hypertensie speelt een cruciale rol als zowel een vorm van hart- en vaatziekte op zichzelf als een risicofactor voor de ontwikkeling van andere types hart- en vaatziekten. Om een beter begrip te krijgen van de verschillende factoren die de ontwikkeling beïnvloeden van hypertensie in het bijzonder en van de eigenschappen van de arteriële circulatie in het algemeen, worden de twee grote klassen van modellen van de arteriële circulatie besproken. In het windketelmodel worden de verschillende eigenschappen van de arteriële boom voorgesteld door een beperkt aantal 'lumped' parameters zoals weerstand, compliantie (of zijn inverse, stijfheid) en inertie. In het tweede soort modellen wordt de arteriële circulatie als een golfsysteem bekeken, waarbij de druk- en snelheidsgolven samengesteld zijn uit voorwaarts lopende golven die zich weg van het hart bewegen en terugwaartse golven die naar het hart toe bewegen na reflectie op uiteenlopende plaatsen in de arteriële boom. Uit deze modellen komen arteriële stijfheid en golfreflecties naar voor als de belangrijkste determinanten van een toename in systolische druk en pulsdruk.

Hoofdstuk 2 gaat dieper in op de verschillende methoden om arteriële stijfheid en golfreflecties te bepalen. Stijfheid kan bepaald worden op een globaal, regionaal of lokaal niveau. Hoewel elke aanpak zijn voor- en nadelen heeft, is de meting van aortastijfheid door middel van de carotis-femoralis golfsnelheid (pulse wave velocity, PWV) momenteel de klinische referentietechniek. Arteriële golfreflecties kunnen gekwantificeerd worden op basis van de vorm van de drukgolf (*golfvormanalyse*) of op basis van een wiskundige opsplitsing van de druk- en snelheidsgolf in voorwaartse en terugwaartse golven, hetzij in het frequentiedomein (*impedantie-analyse*) of in het tijdsdomein (*intensiteitsanalyse)*.

Deel II: Validatie en ontwikkeling van nieuwe methoden

De analyse van golfreflecties en arteriële stijfheid heeft zich de laatste 15 à 20 jaar sterk ontwikkeld en is nu in de overgangsfase tussen klinisch onderzoek en klinische praktijk, zoals geïllustreerd wordt door de inclusie van PWV als een maat voor subklinische orgaanschade in de ESC/ESH[1] richtlijnen sinds 2007.

Met het oog op deze overgang naar de klinische praktijk verschuift de focus in de bepaling van arteriële stijfheid en golfreflecties van een complete, accurate karakterisatie zoals gebruikt (zou moeten worden) in klinisch onderzoek naar een meer pragmatisch compromis tussen nauwkeurigheid en tijds- en kostenefficiëntie van de meettechniek. Gebruik makend van de concepten die in deel I werden aangebracht, valideerden en ontwikkelden we een aantal nieuwe methoden ter bepaling van arteriële stijfheid en golfreflecties.

Hoofdstuk 4 beschrijft de resultaten van een validatiestudie waarin een nieuwe methode van golfseparatie op basis van een gemeten drukgolf en een geschatte (driehoekige) snelheidsgolf wordt vergeleken met de meer traditionele methode van golfseparatie op basis van gemeten druk- en snelheidsgolven. Hoewel deze nieuwe methode benaderend is, heeft ze het voordeel dat de vaak dure en tijdsintensieve meting van de snelheidsgolfvorm vermeden wordt. Deze aanpak werd geïntroduceerd door Westerhof *et al.* voor de bepaling van de reflectiemagnitude (RM), met veelbelovende resultaten in een kleine dataset. Later gebruikten Qasem *et al.* dezelfde methode om transittijden (TT) en golfsnelheid in de aorta te bepalen aan de hand van een centrale drukgolf, de drukgolf ter hoogte van de aorta. De nauwkeurigheid van deze benaderingstechnieken voor de bepaling van RM en TT werd nagegaan door gebruik te maken van beschikbare drukgolven in de carotis en snelheidsgolven in de aorta die op niet-invasieve wijze werden gemeten tijdens de Asklepios studie. Daarnaast werd ook de nauwkeurigheid onderzocht van een meer fysiologische snelheidsgolfvorm als benadering voor de echte, gemeten golfvorm. Hiervoor werd gebruik

[1] ESC: European Society of Cardiology; ESH: European Society of Hypertension

gemaakt van een gemiddelde golfvorm die genormaliseerd en persoonspecifiek in de tijd geschaald werd.

De driehoekige snelheidsgolfvorm, in de tijd geschaald op basis van tijdsinformatie van de gemeten snelheidsgolfvorm, leverde een matige overeenstemming tussen de referentie en de geschatte RM en TT. Zowel voor de RM als voor de TT verslechterde deze overeenstemming nog wanneer de tijdsinformatie van de drukgolf in plaats van die van de snelheidsgolf werd gebruikt. Deze overeenstemming tussen schatting en referentie verbeterde aanzienlijk wanneer de snelheidsgolf benaderd werd door de meer fysiologische golfvorm, al blijven sommige individuele verschillen groot. Het is daarom niet vanzelfsprekend om deze benaderende technieken toe te passen in de klinische praktijk. Besluitend kunnen we stellen dat, in de Asklepios populatie, de benaderende methoden ter bepaling van RM en TT waarden opleveren die grondig verschillen van de referentiewaarden die worden verkregen wanneer zowel gemeten druk- als snelheidsgolfvormen gebruikt worden.

Hoofdstuk 5 is gewijd aan de niet-invasieve bepaling van drukgolven in de halsslagader of carotis. Calibratie van een tonometriecurve op de carotis gebeurt aan de hand van de diastole en gemiddelde bloeddruk gemeten op de bovenarm of brachialis. Deze gemiddelde bloeddruk wordt in het ideale geval bepaald als het rekenkundig gemiddelde van de brachiale drukgolfvorm. Dit impliceert dat voor een correcte niet-invasieve bepaling van de carotisdruk de drukgolf op zowel de brachialis als de carotis moet gemeten worden. Omdat het vaak moeilijk is om goede tonometriecurven te verkrijgen bij zwaarlijvige mensen, kan het gebruik van gecalibreerde distensiecurven een breder toepasbaar alternatief vormen voor tonometrie. Deze aanpak kan in het bijzonder van nut zijn op de brachialis, waar de haalbaarheid van een betrouwbare tonometriemeting in het verleden meermaals in vraag werd gesteld.

Voor deze studie werd gebruik gemaakt van distensie- en tonometriemetingen op de brachialis en carotis van 148 personen. De pulsdruk ter hoogte van de carotis, verkregen op basis van geschaalde distensiemetingen, werd vergeleken met de klassieke (referentie-)calibratiewijze op basis van tonometriecurves, alsook met de recent voorgestelde combinatie van een brachiale tonometriecurve en een lineair of exponentieel geschaalde distensiecurve op de carotis. Het verschil tussen de referentie pulsdruk en de pulsdruk verkregen via geschaalde distensiemetingen was kleiner dan het verschil tussen de referentie pulsdruk en de methodes op basis van één tonometriecurve en één distensiecurve. Omwille hiervan raden we aan om de bloeddruk ter hoogte van de carotis te bepalen aan de hand van twee metingen met dezelfde techniek, hetzij tonometrie, hetzij distensie.

Centrale bloeddruk kan ook geschat worden uit drukgolven gemeten op de voorarmslagaders (radialis) door middel van een zogenaamde transferfunctie. Dit betekent dat de verkregen centrale bloeddrukwaarde zal afhangen van de calibratie van de radiale drukgolf. In *hoofdstuk 6* worden drie calibratiemethoden, toegepast op radiale en carotis tonometriecurven, gemeten in de Asklepios studie: calibratie op basis van brachiale diastole bloeddruk en (i) brachiale systole bloeddruk, (ii) gemiddelde bloeddruk verkregen als één derde van de brachiale pulsdruk (de zogenaamde *één-derde regel*), (iii) gemiddelde bloeddruk verkregen als 40% van de brachiale pulsdruk. Uit deze vergelijking blijkt dat zowel de systole bloeddruk ter hoogte van de carotis als deze ter hoogte van de aorta, verkregen via een transferfunctie, sterk afhankelijk zijn van de calibratie van carotis en radiale drukgolven. Onze data suggereren dat de één-derde regel voor de berekening van de gemiddelde bloeddruk (die wordt beschreven in standaard handboeken) moet vermeden worden, zeker indien de gemiddelde bloeddruk wordt gebruikt voor verdere berekening van aortadruk via een transferfunctie. Het gebruik van 40% van de brachiale pulsdruk als benadering voor de gemiddelde bloeddruk is nauwkeuriger en wordt daarom aanbevolen.

In *hoofdstuk 7* worden de determinanten van een nieuwe stijfheidsindex, de *Ambulatory Arterial Stiffness Index* (AASI), onderzocht aan de hand van een numeriek model van de arteriële circulatie. Op basis van 24-uurs ambulante bloeddrukmetingen kan de AASI berekend worden als één min de helling van de lineaire regressielijn tussen de systole en diastole bloeddruk, en vereist dus geen meting van druk-, snelheids- noch distensiegolfvorm. Hoewel de eenvoud van deze methode aanspreekt, zijn 24-uurs bloeddrukmetingen vereist en is er controverse in hoeverre de AASI een maat is voor arteriële stijfheid en niet beïnvloed wordt door andere hemodynamische parameters. Wij onderzochten de invloed van vijf parameters (arteriële distensibiliteit, perifere weerstand, hartritme, cardiale contractiliteit en veneuze vullingsdruk) op de AASI door elke parameter te variëren van 80% tot 120% van zijn initiële waarde in stappen van 10% om de dagelijkse fluctuaties na te bootsen in een theoretische, normotensieve persoon. Om na te gaan in welke mate de AASI verandert bij grote veranderingen in stijfheid, werden twee bijkomende theoretische personen gesimuleerd met een gemiddelde distensibiliteit van respectievelijk 50% en 25% van de distensibiliteit van de eerste theoretische persoon. Uit deze simulaties is duidelijk dat arteriële distensibiliteit, perifere weerstand en vooral hartritme de belangrijkste determinanten van de AASI zijn. De verstorende invloed van hartritme en perifere weerstand op de AASI betekent een aanzienlijke beperking van de bruikbaarheid van de AASI als maat voor arteriële stijfheid.

Deel III: Validatie en ontwikkeling van nieuwe toestellen

Tesamen met de verhoogde interesse voor de rol van de grote arteriën in de ontwikkeling van hypertensie en in het bijzonder sinds de inclusie van PWV in de ESC/ESH richtlijnen voor de behandeling van hypertensie, is het aantal toestellen om golfreflecties en arteriële stijfheid te meten sterk toegenomen. Dit derde deel beschrijft de validatiestudies die werden ondernomen op twee relatief nieuwe toestellen, alsook de ontwikkeling van een goedkoper toestel voor gebruik in ontwikkelingslanden.

Hoofdstuk 9 bespreekt de resultaten van een numerieke validatie van het werkingsprincipe van de Arteriograph (Tensiomed, Boedapest, Hongarije), een toestel dat beweert de golfsnelheid in de aorta te meten door middel van een eenvoudige manchet ter hoogte van de brachialis. Terwijl de manchet opgeblazen wordt tot boven de systole bloeddruk, wordt een drukcurve opgemeten die twee duidelijke pieken vertoont. De eerste piek is de systole piek, terwijl de tweede piek door de uitvinders wordt toegeschreven aan een reflectie ter hoogte van de splitsing van de aorta in de liesslagaders. De PWV wordt dan berekend als de verhouding van tweemaal de afstand tussen het borstbeen en het schaambeen tot het tijdsverschil tussen de twee pieken in de drukgolfvorm. Om de geldigheid van dit werkingsprincipe te testen maakten we gebruik van een numeriek model van de arteriële circulatie om bloeddrukken en snelheidsgolven te simuleren in de normale configuratie en in een configuratie waarbij de brachialis afgekneld is. Deze laatste configuratie leverde inderdaad een duidelijke tweede piek op in de brachiale drukgolfvorm, maar de timing van deze piek was enkel gerelateerd aan de brachiale en axillaire stijfheid en niet aan de stijfheid van de aorta. Dit wijst er op dat de voorgestelde methode golfreflecties oppikt die zich beperken tot de brachialis en de axillaris, en dat de aldus bekomen PWV-waarden eerder een maat zijn voor de brachiale en axillaire stijfheid dan voor de beoogde aortastijfheid. Onze simulaties stellen als dusdanig het werkingsprincipe van de Arteriograph ernstig in vraag.

In *hoofdstuk 10* worden de resultaten besproken van vergelijkende metingen van de centrale systole bloeddruk (cSBP) tussen de Omron HEM-9000AI (Omron Healthcare, Kyoto, Japan) en de SphygmoCor (Atcor Medical, Sydney, Australië). Centrale bloeddruk wordt beschouwd als een sterkere predictor van cardiovasculaire problemen dan de conventionele brachiale bloeddruk. De Omron HEM-9000AI is de eerste automatische tonometer die de bepaling van cSBP toelaat. Een eerdere studie rapporteerde echter grote verschillen tussen de cSBP-waarde van Omron HEM-9000AI en deze van SphygmoCor, zonder een duidelijke verklaring te geven. Onze studie gaat op zoek naar de oorzaken van het verschil tussen beide centrale bloeddrukschattingen en geeft een indicatie

welke schatting het dichtste bij de werkelijkheid ligt. Hiervoor werd gebruik gemaakt van de aortadruk afgeleid uit de carotisdruk als toestel- en algoritmeonafhankelijke referentie.

143 zwarte Zuid-Afrikanen werden bemeten met zowel een Omron HEM-9000AI (tonometrie op radialis) als een SphgymoCor toestel (tonometrie op radialis, brachialis en carotis). Hoewel de vorm van de met beide toestellen gemeten radiale drukcurves vergelijkbaar was en de cSBP-waarden goed correleerden, was de Omron-schatting gemiddeld 18.8 mmHg hoger dan de SphygmoCor-schatting. De aortadruk lag tussen beide schattingen in. De resultaten van deze studie tonen aan dat het aanzienlijke verschil tussen de centrale bloeddrukschattingen van Omron HEM-9000AI en SphygmoCor te wijten is aan verschillen in algoritme, en suggereert dat de overschatting door Omron HEM-9000AI groter is dan de onderschatting door SphygmoCor.

De beschikbare toestellen ter bepaling van arteriële stijfheid en golfreflecties zijn duur, wat een obstakel kan vormen voor onderzoek in ontwikkelingslanden. Daarom ontwikkelden wij een goedkoper toestel om snelheids- en drukgolven en aldus PWV en lokale bloeddruk te meten. De ontwikkeling en validatie van de hardware en software van dit Tono-Doppler toestel worden beschreven in *hoofdstuk 11*. De hardware is samengesteld uit commercieel beschikbare componenten: snelheidsgolven, gemeten via mobiele Doppler toestellen (Huntleigh Healthcare, Cardiff, UK), en tonometriecurves, gemeten via een micro-tip transducer (Millar Instruments, Texas, USA), worden gedigitaliseerd aan 100 Hz in een data-acquisitie module (NI-9219, National Instruments, Texas, USA). Een ECG-signaal kan mee opgenomen worden door een éénkanaals ECG-module (EG01000, Medlab GmbH, Karlsruhe, Duitsland). Het toestel heeft geen aparte elektrische voeding nodig maar wordt gevoed via de USB-verbinding met een PC of laptop. Specifieke acquisitie- en verwerkingssoftware werden ontwikkeld in Matlab (MathWorks, Natick, Massachusetts, USA) op basis van bestaande code en algoritmes ontwikkeld in het kader van de Asklepios studie. Hard- en software werden afzonderlijk gevalideerd in een validatiestudie op 11 gezonde vrijwilligers. De totale kostprijs van het Tono-Doppler toestel ligt beneden de 4000 €.

Deel IV: Arteriële eigenschappen bij zwarten

Het vierde deel van deze tekst focust op de arteriële eigenschappen bij zwarten, wiens cardiovasculair risicoprofiel duidelijk verschilt van dat van blanken.

Hoofdstuk 13 gaat dieper in op deze verschillen in risicoprofiel en de mogelijke mechanismen die aan de oorzaak ervan liggen. De literatuur rond arteriële eigenschappen bij zwarten wordt besproken, met specifieke aandacht voor de ethnische verschillen in de mechanische eigenschappen van de grote arteriën. De stijfheid van de grote elastische arteriën zoals de aorta en de carotis blijkt hoger in zwarten dan in blanken, terwijl er geen verschil in stijfheid wordt gerapporteerd voor de meer musculaire arteriën zoals de brachialis, noch voor elastische of musculaire arteriën in diabetici en hemodialysepatiënten.

Uit deze literatuurstudie wordt duidelijk dat het overgrote deel van het onderzoek naar ethnische verschillen tussen zwarten en blanken wordt uitgevoerd op zwarten die in Westerse landen leven, zoals de Verenigde Staten en het Verenigd Koninkrijk. Gezien hart- en vaatziekten ook in sub-Saharisch Afrika aan een snelle opmars bezig zijn, is meer onderzoek op zwarten in sub-Saharisch Afrika dringend nodig als een objectieve basis voor beleids- en behandelingsstrategieën.

Tegen deze achtergrond werden twee studies ondernomen in Nigeria, het dichtstbevolkte land in sub-Saharisch Afrika. *Hoofdstuk 14* beschrijft de resultaten van een vergelijkende studie van de arteriële stijfheid en golfreflecties in 184 jonge Nigeriaanse vrouwen en 92 Belgische vrouwen van dezelfde leeftijd. De determinanten van arteriële stijfheid en de gemiddelde waarden van stijfheid en golfreflecties werden vergeleken tussen beide ethnische groepen. We stelden geen verschillen vast in PWV en cSBP, maar de radiale SBP en de centrale augmentatie index waren lager in Nigeriaanse vrouwen. Bovendien was het verschil tussen de carotisdruk en de centrale druk verkregen via een transferfunctie duidelijk groter bij de Nigeriaanse vrouwen dan bij de Belgische vrouwen. Dit vraagt om een specifieke validatie van de transferfunctie in zwarten.

In een tweede studie beschreven in *hoofdstuk 15* werd de aortastijfheid van 264 Nigeriaanse baby's gemeten bij de geboorte, na 3 maanden en opnieuw na 12 maanden, in een poging om de vroegste veranderingen in arteriële distensibiliteit te meten. Omdat het aantal baby's met kwaliteitsvolle metingen sterk varieerde tussen de verschillende follow-up periodes, worden de data voorgesteld als een vergelijking tussen cross-sectionele metingen op drie momenten en als drie subsets van longitudinale data. Uit zowel de cross-sectionele als de longitudinale data blijkt dat de PWV significant toeneemt van de geboorte tot de leeftijd van 3 of 12 maand. Daarentegen werd tussen de opeenvolgende PWV-metingen op dezelfde baby's geen correlatie vastgesteld.

Summary

On the interface between engineering and medicine, this PhD focuses on the development and validation of new methods and devices to assess arterial stiffness and wave reflections, two emerging markers predictive of the development of high blood pressure (hypertension) and concomitant cardiovascular disease (CVD), the leading cause of death worldwide.

The manuscript is subdivided into five parts. The first part provides a general background to the different studies performed during my PhD, while the last part summarizes the most important conclusions. The actual research is grouped in the three middle parts: parts II and III bundle a number of studies on the validation and development of new methods and devices to quantify arterial stiffness and wave reflections. In the fourth part, this knowledge is applied to study the arterial properties in people of African descent. Each part is briefly summarized in the following sections.

Part I: Background

Chapter 1 introduces the basics of cardiovascular anatomy, physiology and pathophysiology, with particular focus on arterial wall mechanics and hemodynamics. Hypertension plays a crucial role, both as a type of CVD as well as a risk factor for the development of other types of CVD. In order to gain a better understanding of the different factors influencing the development of hypertension in particular and the characteristics of the arterial circulation in general, the two main classes of models of the arterial circulation are discussed. In a Windkessel model, the different properties of the arterial tree are represented by a number of discrete, lumped parameters, such as resistance, compliance (stiffness) and inertance. Alternatively, the arterial tree can be viewed as a wave system where the pressure and flow waves are composed of forward waves travelling away from the heart and backward waves travelling towards the heart, reflected at different sites along the arterial tree. From these models, arterial stiffness and wave reflections emerge as the most important determinants of increasing systolic and pulse pressures.

Chapter 2 focuses on arterial stiffness and wave reflections and summarizes the various methods that have emerged to quantify both parameters. Arterial stiffness can be assessed at a global, regional or local level. Though each approach has its pros and cons, the measurement of carotid-femoral pulse wave velocity (PWV) as a means of regional arterial stiffness has gained the status of clinical gold-standard technique. Arterial wave reflections can be quantified on the shape of the pressure wave (*wave shape analysis*) or from mathematical wave separation in forward and backward waves, either in the frequency (*impedance analysis*) or time domain (*wave intensity analysis*).

Part II: Validation and development of new methods

The analysis of wave reflections and arterial stiffness has increasingly gained attention over the last 15-20 years and is now in the transition between clinical research and clinical practice, as illustrated by the inclusion of PWV as a marker of subclinical organ damage in the 2007 ESC/ESH[2] guidelines.

With regard to this (anticipated) introduction in clinical practice, the focus in assessing arterial stiffness and wave reflections has shifted from an accurate, complete characterisation as (should be) used in clinical research to a more pragmatic compromise between accuracy and time- and cost-effectiveness of the measuring technique, applicable in clinical practice. Using the concepts introduced in part I, we validated and developed a number of new methods to quantify arterial stiffness or wave reflections.

Chapter 4 details the results of a validation study in which a new approach of wave separation based on a measured pressure waveform and an estimated (triangular) flow waveform is compared to the more traditional approach of wave separation using a measured pressure and flow waveform. Though approximative, this new approach has the advantage of bypassing the often expensive and time-consuming assessment of an aortic flow waveform. The approach was first introduced by Westerhof *et al.* to estimate reflection magnitude (RM), with promising results in a small dataset. Later, Qasem *et al.* used the same approach to derive pulse transit time (TT) and aortic PWV from a central pressure waveform. We verified these approximation techniques for RM and TT using carotid pressure and aortic flow waveforms measured non-invasively in the Asklepios study and explored the accuracy of approximating the flow waveform by using a person-specific time-scaled normalized average flow waveform.

A triangular flow approximation using timing information from the measured aortic flow waveform yielded moderate agreement between reference and estimated RM and TT. For both RM and TT, agreement between reference and

[2] ESC: European Society of Cardiology; ESH: European Society of Hypertension

approximated values further decreased when the approximated flow waveform was obtained using timing information from the pressure waveform. Approximating the flow by a more physiological waveform significantly improved these results. We conclude that, in our Asklepios population, results from pressure-based approximative methods to derive RM or aortic pulse TT differ substantially from the values obtained when using both measured pressure and flow information.

Chapter 5 relates to the non-invasive assessment of carotid artery pressure waveforms. Calibration of the carotid tonometric curve is based on brachial diastolic blood pressure (DBP) and mean arterial blood pressure (MAP), the latter ideally obtained as the arithmetic average of the brachial pressure waveform. Therefore, proper non-invasive assessment of carotid artery pressure ideally requires waveforms recorded at two anatomical locations: the brachial and the carotid artery. As tonometry recordings are difficult to obtain in obese patients, the use of calibrated diameter distension waveforms could provide a more widely applicable alternative for local arterial pressure assessment than applanation tonometry. This approach might be of particular use at the brachial artery, where the feasibility of a reliable tonometric measurement has been questioned. The aim of this study was to evaluate an approach based on distension waveforms obtained at the brachial and carotid arteries.

Using local brachial and carotid diameter distension and tonometry waveforms recorded in 148 subjects, this approach is compared to traditional pulse pressures obtained through tonometry at both the carotid and brachial arteries (used as a reference) and the more recently proposed approach of combining tonometric readings at the brachial artery with linearly or exponentially calibrated distension curves at the carotid artery. The difference between the reference carotid pulse pressure (PP) and the PP obtained from brachial and carotid distension waveforms was smaller than the difference between the reference carotid PP and the estimates obtained using a tonometric and a distension waveform. We therefore recommend to stick to one technique on both the brachial and the carotid artery, either tonometry or distension, when assessing carotid blood pressure non-invasively.

Central blood pressure can be estimated from radial artery pressure waveforms using a generalized transfer function. However, the obtained central pressure waveform depends on the calibration of the radial waveform. In *chapter 6*, three calibration methods are compared using the radial and carotid tonometric waveforms acquired on 1873 individuals in the Asklepios study: calibration using brachial artery DBP and (i) brachial systolic pressure (SBP), (ii) MAP estimated with the one-third rule and (iii) MAP estimated as 40% of brachial artery pulse pressure. Both carotid artery SBP and central SBP obtained via a

transfer function are highly sensitive to the calibration of the respective carotid artery and radial artery pressure waveforms. Our data suggest that the one-third rule to calculate MAP from brachial cuff BP, which is advocated in standard clinical textbooks, should be avoided, especially when used to calibrate radial artery pressure waveforms for subsequent application of a pressure transfer function. Until more precise estimation methods become available, it is advisable to use 40% of brachial pulse pressure instead of 33% to assess MAP.

In *chapter 7*, the determinants of a newly proposed stiffness index, the Ambulatory Arterial Stiffness Index (AASI) are explored using a numerical model of the arterial circulation. Based on 24-hour ambulatory blood pressure recordings, the AASI is calculated as one minus the slope of the linear regression line between systolic and diastolic blood pressure values and thus does not require the recording of a pressure, flow or diameter distension waveform. Although appealing because of its simplicity, it does require 24-hour blood pressure recordings and there is controversy as to which extent AASI reflects arterial stiffness or is affected by other cardiovascular parameters. We assessed the relative importance of five parameters (arterial distensibility, peripheral resistance, heart rate, cardiac contractility and venous filling pressure) on the AASI by varying each parameter from 80 to 120% of its initial value in steps of 10% to mimick the daily fluctuations in one theoretical, normotensive subject. To assess the ability of AASI to detect large changes in stiffness, two additional subjects were simulated with a distensibility of 50% and 25% of the default distensibility, respectively. From these simulations, it becomes clear that arterial distensibility, vascular resistance and especially heart rate are the main determinants of the AASI. The confounding effects of vascular resistance and heart rate seriously limit the use of the AASI as a marker of stiffness.

Part III: Validation and development of new devices

Along with the increased attention for the role of the large arteries in the development of hypertension and concomitant cardiovascular diseases and especially since the ESC/ESH guidelines include the measurement of PWV for the management of patients with hypertensive disease, the number of devices to measure wave reflections and arterial stiffness has boosted. This third part describes the validation studies that were performed on two relatively new devices, as well as the development of a low-cost device for use in African settings.

Chapter 9 details the results of a numerical validation of the working principle of the Arteriograph (Tensiomed, Budapest, Hungary), a device that claims to assess aortic PWV by means of a simple brachial cuff. Brachial blood pressure is

measured during supra-systolic pressure inflation of the cuff, yielding pressure waveforms with pronounced first and secondary peaks. The secondary peak is ascribed to a reflection from the aortic bifurcation, and PWV is calculated as the ratio of twice the jugulum-symphysis distance (~ aortic root - bifurcation) and the time difference between the two peaks. To test the validity of this working principle we used a numerical model of the arterial tree to simulate pressures and flows in the normal configuration and in a configuration with an occluded brachial artery. A pronounced secondary peak was indeed found in the brachial pressure signal of the occluded model, but its timing was only related to brachial-axillary stiffness and not to aortic stiffness. Our data indicate that the method picks up wave reflection phenomena confined to the brachial and axillary arteries, and derived values of PWV rather reflect the stiffness of the brachial and axillary arteries than the intended aortic stiffness. As such, our simulations question the working principle of the Arteriograph.

Chapter 10 reports on the comparative measurements between the Omron HEM-9000AI (Omron Healthcare, Kyoto, Japan) and SphygmoCor systems in an attempt to validate the central systolic pressure (cSBP) estimate provided by Omron HEM-9000AI. The Omron HEM-9000AI is the first automated tonometer to provide an estimate of cSBP, which is considered to be more predictive of cardiovascular events than the conventional brachial pressure. However, considerable differences between the cSBP-estimate of Omron and that of SphygmoCor have been reported, but not explained. This study assesses the sources of the differences between both cSBP-estimates and provides a handle on which estimate is closest to reality. For this purpose, aortic cSBP derived from calibrated carotid SBP was used as device- and algorithm-independent reference.

A total number of 143 black South Africans were measured with an Omron HEM-9000AI (radial tonometry) and a SphygmoCor device (radial, brachial and carotid tonometry). Each subject was measured with an Omron HEM-9000AI and a SphygmoCor. Though the shape of the recorded radial pressure waves was similar in both devices and the corresponding cSBP-estimates correlated strongly, the Omron-estimate was on average 18.8 mmHg higher than the SphygmoCor-estimate. Aortic SBP was in between both estimates. The results from this study demonstrate that the considerable difference between the central pressure estimates of Omron HEM-9000AI and SphygmoCor is due to algorithm differences, and suggest that the overestimation by Omron HEM-9000AI is larger than the underestimation by SphygmoCor.

The available devices to assess arterial stiffness and wave reflections are expensive, which may pose an obstacle for research in developing countries such as most countries in sub-Saharan Africa. We therefore developed a low-cost

device to acquire flow and pressure waveforms and hence derive PWV and local blood pressure. The development and validation of the hardware and software of this Tono-Doppler device is outlined in *chapter 11*. The hardware is assembled from commercially available components: flow recordings from two handheld Doppler devices (Huntleigh Healthcare, Cardiff, UK) and tonometry recordings from a micro-tip transducer (Millar Instruments, Texas, USA) are digitized at 100Hz in a data-acquisition module (NI-9219, National Instruments, Texas, USA). An ECG can be co-registered by a one-channel ECG module (EG01000, Medlab GmbH, Karlsruhe, Germany). The device does not need to be connected to the mains but is powered from a PC or laptop through USB-connection. Based on existing code and algorithms developed in the framework of the Asklepios study, a dedicated acquisition and processing interface were developed in Matlab (MathWorks, Natick, Massachusetts, USA). Hard- and software were validated separately in a validation study on 11 healthy volunteers. The total price of the Tono-Doppler device is <4000€.

Part IV: Arterial properties in people of African descent

The fourth part of this manuscript focuses on the arterial properties of people of African descent, who display a clearly different cardiovascular risk profile than Caucasians.

Chapter 13 elaborates on this difference in risk profile and the potential mechanisms that may be at the origin of it. The literature on arterial properties of Africans is reviewed, with particular focus on the ethnic differences in mechanical properties of the large arteries. The stiffness of the large elastic arteries such as the aorta and carotid artery was consistently found to be higher in African origin than in people of Caucasian origin. No such difference has been observed for more muscular arteries like the brachial artery, nor for elastic or muscular arteries in subjects with type-2 diabetes or patients on hemodialysis.

From the literature review, it is apparent that most of the research on ethnic differences between Africans and Caucasians is performed on Africans living in Western countries such as the United States and the United Kingdom. Given the increasing rates of cardiovascular disease in sub-Saharan Africa, more research on Africans living in sub-Saharan Africa as a basis for policy and treatment strategies is urgently needed.

Against this background, two studies were undertaken in Nigeria, the most populous country in sub-Saharan Africa. *Chapter 14* details the results of comparative study on the aortic stiffness and arterial wave reflections in 184 young Nigerian women and 92 age-matched Belgian women. Mean levels as well as determinants of PWV, augmentation index (AIx) and local pressure were compared across ethnicity. No ethnic differences in PWV and cSBP in young and

middle aged women were observed, but we did find a lower radial SBP and central AIx in Nigerian as compared to Belgian women. The observed difference between carotid SBP and aortic SBP derived via the radial-to-aortic transfer function in Nigerian women warrants the need for a specific validation of the transfer function in people of African descent.

In a second study described in *chapter 15*, the aortic stiffness of 264 Nigerian babies was asessed at the age of 0, 3 and 12 months in an attempt to track early changes in arterial distensibility. As the number of babies measured at each timepoint varied greatly, data are presented as a comparison of cross-sectional measurements at the three timepoints and as three subsets of longitudinal data. Both the cross-sectional and the longitudinal data report a significant increase in PWV from 0 to 3 months or 12 months. However, no correlation between longitudinal PWV-data was found. Malaria episodes during pregnancy appeared not to influence the PWV during the first year of life.

Introduction

Introduction

Relevance

Cardiovascular diseases (CVDs) are the leading cause of death in Western countries. There are different types of CVDs, such as cerebrovascular disease (stroke), coronary heart disease, elevated blood pressure (hypertension) and heart failure. Of these, hypertension plays a crucial role as it is both a type of CVD and a major risk factor for the development of other types of CVDs.

It is now clear that the elasticity of the large, central arteries plays an important role in the development of hypertension. These vessels form an elastic buffer, in which the blood volume is stored. The stiffer the large arteries, the lesser the pulse pressure is damped. It is well established that a high pulse pressure is directly related to an increased risk of CVD. Therefore, the assessment of arterial function and structure by means of the arterial stiffness and wave reflections is of paramount importance in hypertension research.

In Western countries, there is increasing evidence from large-scale epidemiological studies that the assessment of arterial stiffness has a strong predictive value in predicting cardiovascular events, over and beyond traditional risk factors such as blood pressure, smoking, cholesterol and obesitas. Therefore, the assessment of arterial stiffness and wave reflections is now on the verge of being introduced into clinical practice.

In developing countries, especially in sub-Saharan Africa, the prevalence of CVDs is rapidly increasing and CVDs are expected to surpass infectious diseases such as malaria and AIDS as the leading cause of death in the near future. Furthermore, the cardiovascular risk profile of people of African descent is clearly different from that of people of European descent. Although many different hypotheses have been proposed, the reason for this difference remains largely unknown. Given the role of arterial stiffness in the development of hypertension and concomitant CVD, large artery research on Africans is of particular interest as it may contribute to our understanding of the ethnic difference in cardiovascular risk profile.

Aim

The aim of this thesis is twofold:

- to critically evaluate a number of newly emerged methods and devices for the assessment of arterial stiffness and wave reflections.
- to facilitate large artery research in people of African descent and to perform a number of pilot studies in sub-Saharan Africa.

Structure

This dissertation is divided in five main parts.

The first part provides a general background on arterial physiology and pathophysiology, as well as on the different methods to assess arterial stiffness and wave reflections. The actual research is grouped in the three middle parts: parts II and III bundle a number of studies on the validation and development of new methods and devices to quantify arterial stiffness and wave reflections. In the fourth part, this knowledge is applied to study the arterial properties in people of African descent. Each part starts with a short outline, summarizing and linking the different studies together. In the fifth part, the major conclusions per study are restated and some perspectives for future research are discussed.

One

Background

CHAPTER 1

Arterial physiology and pathophysiology

1.1 The cardiovascular system

The cardiovascular system is a closed circulatory system comprised of the heart and blood vessels. The heart consists of two atria (left and right) and two ventricles (left and right) and can be viewed functionally as two pumps with the pulmonary and systemic circulations situated in between (Figure 1.1). While the pulmonary circulation carries blood to the lungs and back to the heart, the systemic circulation provides all other parts of the human body with blood. Contraction of the right ventricle pumps the blood into the pulmonary circulation where oxygen and carbon dioxide are exchanged within the lung alveoli. Oxygenated blood from the lungs enters into the left atrium, then into the left ventricle, which pumps the blood into the aorta for distribution to the organs via large distributing arteries. Smaller blood vessels within the organs and tissues (primarily capillaries) serve as the primary site of nutrient exchange. Blood leaves the organs and returns to the heart via the venous circulation.

The focus of this PhD dissertation is on the arteries of the systemic circulation. The following references served as a basis for writing this chapter: *Anatomy of the Human Body*[3], *McDonald's blood flow in arteries* [4], *Principles of vascular physiology* [5] and *Snapshots of Hemodynamics* [6].

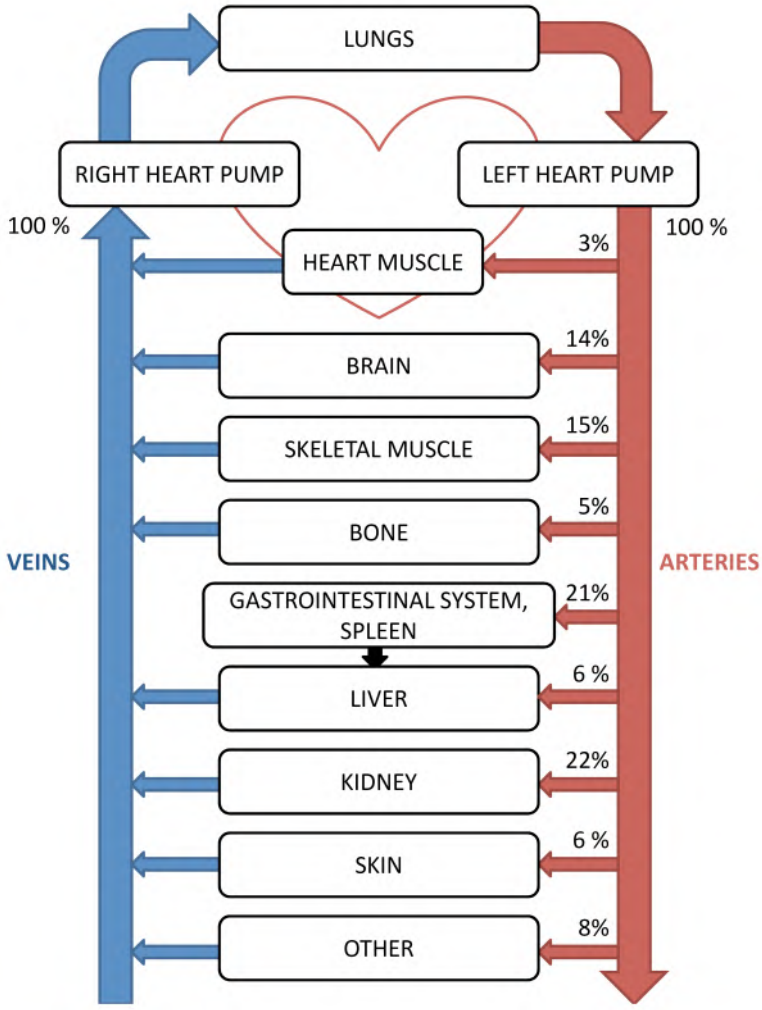

Figure 1.1: Functional view of the cardiovascular system indicating the distribution of the cardiac output in an average resting individual. [1, 2]

1.2 Arterial anatomy

During systole, the contracting left ventricle ejects blood into the aorta, the largest artery of the human body. The aorta forms the trunk of the strongly branched arterial tree. Upon its root, the aorta is about 3 cm in diameter. It ascends for a short distance, arches backwards and to the left side to further descend at the left side of the vertebral column. At around the fourth lumbar vertebra, the aorta, only around 1.75 cm in diameter, ends by dividing into the left and right common iliac arteries [3].

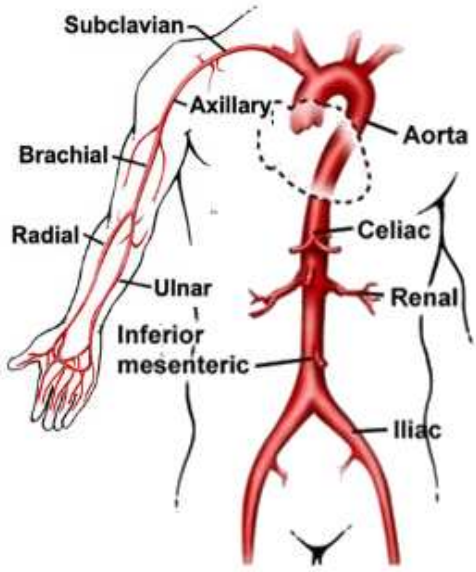

FIGURE 1.2: Large arteries in the thorax, abdomen and upper limb [7].

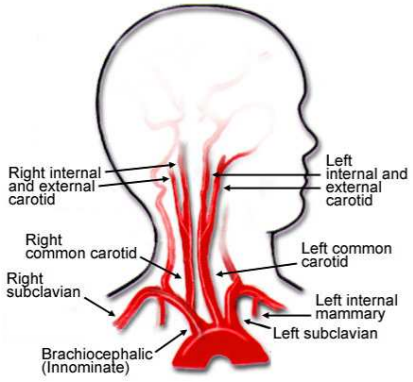

FIGURE 1.3: Large arteries in the neck [8].

Figure 1.2 gives a simplified overview of the numerous large arteries that branch from the aorta. Two coronary arteries branch from the ascending aorta to supply the heart. Three larger arteries branch from the aortic arch: the innominate, the left carotid and left subclavian artery. The largest of these three is the innominate artery, which divides into the right common carotid and right subclavian artery after 4 to 5 cm. Figure 1.3 shows a detailed view of the left and right common carotid arteries, supplying the head and the brain, and the subclavian arteries, supplying the upper extremities. The subclavian artery is

named axillary artery between the outer border of the first rib and the armpit (axilla), and further termed brachial artery between the armpit and the elbow. Here the trunk ends by dividing into two branches: the radial and ulnar artery.

The descending aorta can be divided into a thoracic and abdominal part, corresponding with the two great cavities the aorta traverses. While the branches from the thoracic aorta are rather small, supplying the bronchial tubes, the oesophagus and the spinal column, the abdominal aorta has markedly larger branches, the most important being the celiac artery, supplying the stomach, pancreas and liver, the superior mesenteric artery, supplying the duodenum, and the renal arteries, supplying the kidneys. From the aortic arch towards the peripheral arteries, the vessel diameter decreases gradually, a phenomenon called geometric tapering. Arteries with a diameter below 0.4 mm are called arterioles, whereas capillaries are the smallest type of arteries with a diameter of around 5 μm. Table 1.1 displays a number of structural characteristics for the different types of arteries, such as the internal diameter, the wall thickness and the total cross-sectional area.

Table 1.1: Structural characteristics of the vascular system[1]

	Aorta	Large arteries	Arterioles	Capillaries
Internal diameter	2.5 cm	0.4mm	30μm	5 μm
Wall thickness	2.0 mm	1.0 mm	20 μm	1 μm
Amount	1	160	$5{\cdot}10^7$	10^{10}
Total cross-sectional area	4.6 cm^2	20 cm^2	400 cm^2	4500 cm^2

Though the wall thickness and the relative content can differ among different types of arteries, all arteries have a three-layered structure (figure 1.4):

- The *tunica intima* is the innermost layer and consists of three sublayers: one single layer of endothelial cells, a subendothelial layer of supporting connective tissue (collagen) and an elastic or fenestrated layer consisting of a membrane of longitudinally oriented fibers, the elastic lamina.
- The *tunica media* or middle layer consists of smooth muscle cells (SMCs), nerves and elastic tissue, arranged in lamellae in concentric circles around the vessel wall. This layer accounts for most of the arterial wall thickness.
- The *tunica adventitia* or tunica externa is the outermost layer, mainly composed of collagen and supported by external elastic lamina. The collagen serves to anchor the blood vessel to nearby organs, giving it stability.

A distinction is made between elastic and muscular large arteries. Elastic arteries are the largest arteries close to the heart, such as the aorta and the

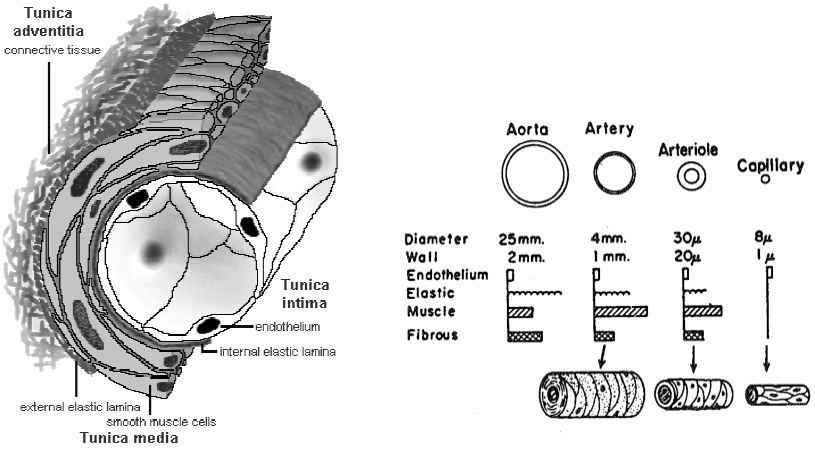

FIGURE 1.4: Left: three-layered wall structure; Right: relative content of endothelium, elastic and fibrous tissues and smooth muscle in different types of arteries, modified from [9].

carotid arteries. They have a thick, highly developed medial layer composed mainly of elastic lamellae, allowing them to distend maximally during systole and thus act as a buffer, temporarily storing blood which is brought into circulation again when the arteries return to their original size. The effect of this recoil is to maintain the pressure during the diastolic phase and to force the blood pumped out of the left ventricle away from the heart, into the systemic vascular system. The large elastic arteries gradually evolve into more muscular arteries which have a media almost entirely composed of SMCs, making them highly contractile. Their degree of contraction or relaxation is controlled by the autonomic nervous system as well as by endothelium-derived vasoactive substances.

1.3 Arterial wall mechanics

1.3.1 Properties of arterial tissue

Due to their three-layered structure and the variety of proteins and cells involved in the arterial wall, arteries behave as incompressible, anisotropic and viscoelastic materials. At low strain levels, elastin dominates the composite behavior, while at high strain levels, collagen becomes increasingly important. This implies that the mechanical wall properties of an artery are pressure-dependent. The stiffness of a material can be expressed by Young's modulus of elasticity (E),

defined as the ratio of stress (σ) and strain (ε): E=σ/ε. For linear elastic materials, this relation is straight and a single Young modulus characterizes the material. The stress-strain curve for arteries, however, as for most other biological tissues, exhibits a curved shape, with its slope, the incremental elastic modulus (E_{inc}), increasing with strain. This indicates a progressive stiffening of the arterial wall with increasing stress and strain, and limits the strain at high stresses, thus protecting against overstretch and damage. A typical value for the incremental elastic modulus of arteries in the normal human is about 500 kPa [6].

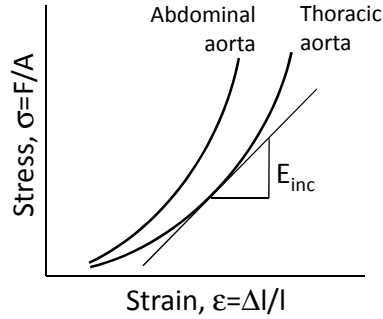

Figure 1.5: Stress-strain relation in the thoracic and abdominal aorta and definition of incremental elastic modulus E_{inc} [10]

Apart from the described non-linear elastic behavior, arterial tissue also exhibits some viscoelastic characteristics when undergoing deformation. One of these characteristics is the hysteresis curve that can be seen when recording stress-strain curves in vivo. Throughout the cardiac cycle, strain lags stress, which leads to dissipation of mechanical energy. Altogether, the effects of viscoelasticity are small and are often neglected in practice.

1.3.2 Forces acting on the arterial wall

There are three types of stress acting on the arterial wall:

- *Tensile, tangential* or *circumferential wall stress (σ)* is the load on the arterial wall caused by the transmural pressure gradient (p). Assuming the ratio of the wall thickness (h) and the lumen radius (r) is small, tensile stress can be calculated using Laplace's law as pr/h. It is apparent that this load increases with decreasing wall thickness and increasing radius, which explains the danger of vascular dilatations such as aneurysms. Increased tensile stress can be compensated by wall thickening.

- *Shear stress* is the frictional stress exerted by the blood flow on the wall. It is determined by the magnitude and the shape of the velocity profile near the wall as well as by the blood viscosity. Shear stress is about 10 000 times smaller than tensile wall stress, but its importance lies in its effect on the endothelium, where it acts as a biomechanical stimulus.

- Arterial pressure causes a *radial wall stress*. The pressure fluctuates between systolic (maximal) and diastolic (minimal) pressure and induces filtration of fluid through the vessel wall.

1.3.3 Vascular remodeling

Upon a change in the mechanical forces acting on the vessel (eg. due to hypertension or a pressure gradient due to stenosis), the vessel wall has the ability to re-establish an equilibrium, a process called vascular remodeling. Blood vessels have hormonal mechanisms that enable them to remodel by modulation of the vascular smooth muscle cells or endothelial cells to produce structural modifications. A distinction can be made between pressure- and flow-induced remodeling.

Adaptation to changes in pressure. An increase in blood pressure causes the tensile stress to rise, which is compensated by hypertrophy or thickening of the arterial wall.

Adaptation to changes in flow. A change in blood flow (Q) has implications for the endothelium, the thin cell layer at the interface of lumen and vessel wall, by means of a change in shear stress. Because shear stress is proportional to Q/r^3, with r the vessel radius, an increase in flow can be compensated by a much smaller increase in vessel radius (vasodilation). Thus, acute changes in blood flow lead to vasodilation or vasoconstriction. Chronic or long term changes in blood flow lead to structural remodeling of the vessel wall, by reorganization of cellular and extracellular wall components [6].

Remodeling is fundamental for normal vessel growth and adaptation, as it allows the vessel to maintain an optimal environment. However, when the vascular environment changes drastically and/or permanently, the remodeling process may contribute to disease progression.

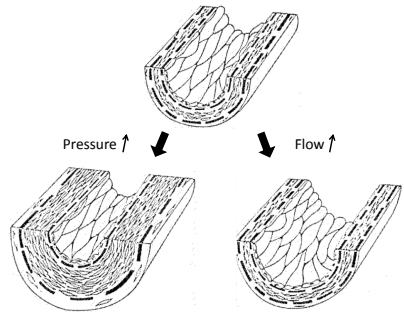

Figure 1.6: Pressure-induced (left) and flow-induced (right) remodeling [6] .

1.4 Arterial hemodynamics

1.4.1 Resistance

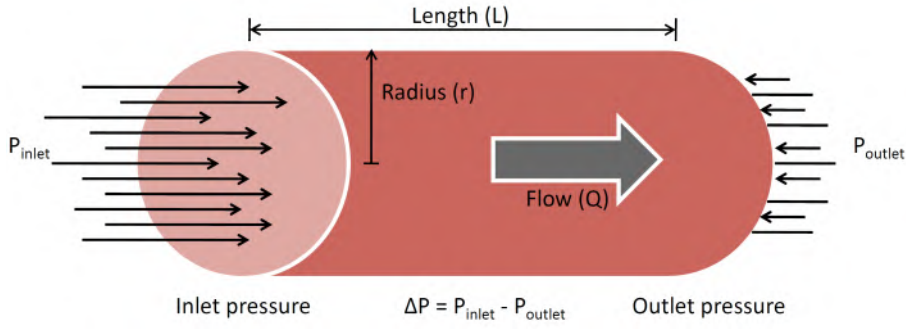

Figure 1.7: Factors influencing blood flow through a tube [2].

When blood flows through an artery, there is a pressure drop along that artery caused by the resistance of the artery to the flow as illustrated in figure 1.7. In the specific case of a circular, stiff tube with a parabolic velocity profile, the law of Hagen-Poiseuille describes the relation between pressure drop (ΔP) and blood flow (Q) under steady flow conditions as:

$$Q = \frac{\Delta P\, r^4}{8\eta l} \tag{1.1}$$

with

r: inner radius of the tube [m]

l: tube length [m]

η: dynamic viscosity [Pa.s]

In analogy to the electrical law of Ohm, where resistance equals voltage drop over current, the resistance (R) of an arterial segment can be expressed as the ratio of the pressure drop along that segment and the flow through the segment under steady flow conditions:

$$R = \frac{\Delta P}{Q} \tag{1.2}$$

Combining equations 1.1 and 1.2, the resistance for the uniform tube can be calculated as

$$R = \frac{8\eta l}{r^4} \tag{1.3}$$

Although this formula is not exactly applicable in the human body as not all underlying conditions are met, it serves to illustrate the strong dependency of resistance on arterial wall radius, and, to a lesser degree, the influence of the vessel length and blood viscosity. Equation 1.2, also called Ohm's law, is more general and can be used in practice. Application of Ohm's law to the arterial tree allows to deduce which type of arteries has the largest resistance, as elegantly explained by Westerhof [6]:
"Again using the electrical analogy, the total resistance (R_{tot}) of two vessels (R_1 and R_2) in parallel is $\frac{1}{1/R1+1/R2}$, while two resistances in series result in a total resistance equal to the sum of the resistances. Using equation (1.3), the resistance of an arteriole can be compared to that of the aorta. Assuming an aortic radius of 15 mm and an arteriole with a radius of 7.5 μm and a length of 1 mm, the resistance of a single arteriole is $3.2 \cdot 10^{10}$ larger than that of a 50 cm long aorta. However, there is only one aorta and there are about $3 \cdot 10^8$ arterioles, which can be considered as parallel to each other. Therefore, the total arteriolar resistance is $\frac{3.2 \cdot 10^{10}}{3 \cdot 10^8} \approx$ 100 times larger than the aortic resistance. Capillaries have diameters of the same order as arterioles, but there are approximately 4 to 5 capillaries per arteriole, reducing their total resistance with a factor 4 to 5."

Figure 1.8 also illustrates that the vascular resistance is almost exclusively determined by the small arteries and arterioles. These are muscular arteries that can regulate the resistance within a wide range by limited changes in diameter. Compared to the resistance of the arterioles, the resistance of the aorta and other large arteries is so low that the mean arterial pressure is practically the same along the large arteries. The large arteries can therefore be interpreted as a supply reservoir with the peripheral resistances (arterioles) adjusting themselves so that the demand of flow to the tissue is met.

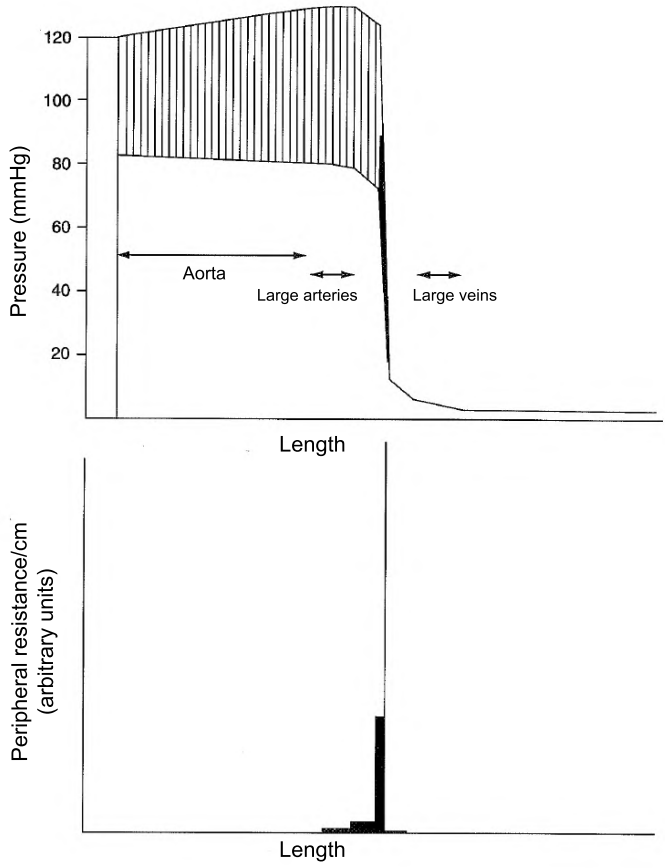

Figure 1.8: The upper panel displays the change in mean pressure and in pulsatile pressure between the ascending aorta and venous circulation. Mean and pulse pressure fall over a short length in the smallest arteries and in the arterioles as a result of the high resistance to blood flow that these vessels present, as illustrated in the lower panel. [11].

When equation 1.2 is applied over the entire systemic circulation, we get:

$$P_a = R_{periph} \cdot CO + P_v \tag{1.4}$$

with

- P_a the mean arterial pressure [Pa]
- R_{periph} the total peripheral resistance [Pa ·s/m^3]
- CO the cardiac output [m^3/s]
- P_v the mean venous pressure [Pa]

Since venous pressure is close to zero, the mean arterial pressure is determined by two main factors: the total peripheral resistance and the cardiac output.

1.4.2 Compliance

When the pressure increases, the artery distends. The change in volume (V) is related to the change in pressure (P) by means of the arterial compliance (C). For arteries, the pressure-volume relation is not straight, as can be seen in figure 1.9. For a small change (Δ) around a chosen working point, compliance can be determined as the local slope of the curve:

$$C = \frac{\Delta V}{\Delta P}. \tag{1.5}$$

The inverse of compliance is the elastance: $E = \Delta P/\Delta V$.

Compliance strongly depends on the chosen working point. Thus, when reporting compliance data one should report the pressure at which the compliance was determined. When comparing arteries of a different size, compliance should be normalised with respect to the arterial volume: $C/V = (\Delta V/V)/\Delta P$, called distensibility.

It is important to note that compliance is a structural property depending on the arterial geometry, as opposed to material properties such as the Young modulus. This is illustrated by the fact that an artery and a vein of about the same size have a similar Young modulus, as venous and arterial walls are composed of the same materials, yet a large difference in compliance is observed. Veins have a far smaller wall thickness making them more compliant than arteries [6].

1.4.3 Inertance

As illustrated in figure 1.10, during the early ejection phase, the left ventricular pressure is higher than the aortic pressure and the blood is accelerated into the aorta. In the late ejection phase, the aortic pressure becomes higher than the ventricular pressure, causing a deceleration of blood.

In this acceleration/deceleration process, the blood mass and the aortic geometry play a role. This is represented by the inertance (L), which can be calculated as

$$L = \frac{\rho l}{A}, \tag{1.6}$$

with

- ρ the blood density [1015 kg/m^3]
- l the vessel length [m]
- A the cross-sectional vessel area [m^2].

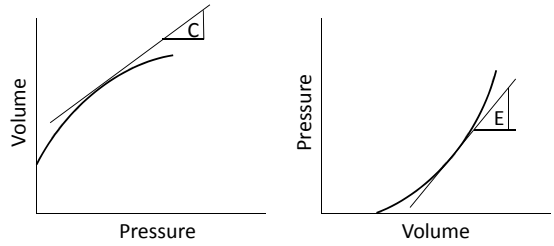

Figure 1.9: Definition of compliance (C) and elastance (E).

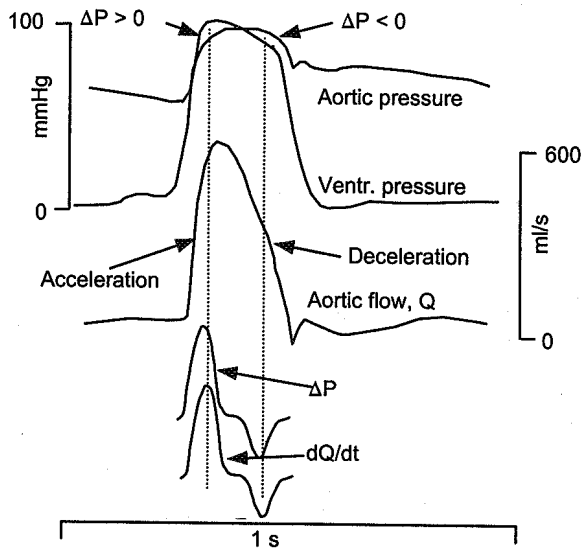

Figure 1.10: Inertance plays a role in accelerating and decelerating the blood: in early systole, when left ventricular pressure is higher than aortic pressure, the blood accelerates and the flow increases; in late systole, aortic pressure is higher than ventricular pressure and the blood velocity decreases. [6].

Inertance links the oscillatory pressure drop with the rate of change of blood flow:

$$\Delta P = L\frac{dQ}{dt} \tag{1.7}$$

The dependence on $1/r^2$ (via $1/A$) implies that inertance plays a larger role than resistance ($\sim 1/r^4$) in the large arteries, while the opposite holds for smaller arteries and arterioles.

1.4.4 Impedance

Vascular impedance (Z) can be considered a more general hemodynamic parameter, integrating resistance, compliance and inertance.
Assuming the arterial system to be linear and in steady state oscillation, the pressure and flow wave can be decomposed into a series of sinusoidal signals (harmonics) using Fourier analysis. The zeroth harmonic represents the steady state pressure (flow), while the frequency of the n-th harmonic is n times the heart rate frequency. Impedance is defined in the frequency domain as the ratio of pulsatile pressure and flow:

$$Z = \frac{P}{Q} \tag{1.8}$$

and is expressed as a modulus and a phase per harmonic.

The three basic hemodynamic elements, resistance, compliance and inertance, can also be represented in the frequency domain as impedances with a modulus and a phase. The relation between the pressure drop over the element and the flow through the element determines its impedance. For resistance, the pressure drop and flow are in phase and their amplitude ratio gives the value of the resistance. For compliance, the flow wave precedes the pressure drop, whereas the opposite holds for the inertance, as illustrated in figure 1.11 [6]. Together, these three basic elements can describe all pressure-flow relations of the arterial system when placed in parallel or series combination (see 1.5.1).

When impedance is measured at the aortic root, it is called 'input' impedance (Z_{in}) and fully characterizes the systemic arterial circulation. Figure 1.12 gives a typical example of a systemic input impedance and the information that can be drawn from it. The total vascular resistance appears as the modulus of the zeroth harmonic. Indeed, total vascular resistance is defined as the ratio of steady state pressure and flow. The contribution of the compliant large arteries is dominant in the first harmonics, causing a decrease in modulus and phase of Z_{in}. For higher harmonics, the modulus oscillates around a constant value, also called the characteristic impedance (Z_c). Z_c can be interpreted as the impedance in the absence of wave reflections and becomes a real number for higher harmonics, which can be obtained as:

$$Z_c = \frac{\rho c}{A} \tag{1.9}$$

with c the wave speed [m/s] and ρ and A the blood density and cross-sectional vessel area as previously defined. In practice, Z_c is estimated as the average modulus of the high frequency harmonics, typically from the 4^{th} to the 10^{th} harmonic.

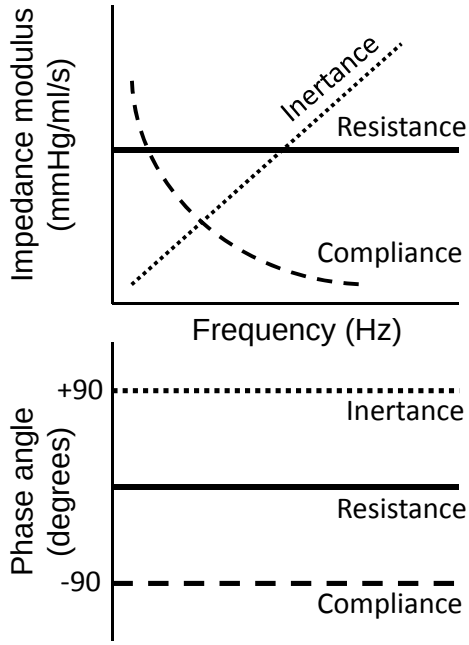

Figure 1.11: Frequency domain representation of vascular resistance, compliance and inertance [6].

1.5 Models of the arterial circulation

A good model approximates and simplifies reality by identifying those factors that are most relevant, and omitting the less relevant factors. Models of the arterial circulation allow us to simulate the effect of a given physiologic change on the arterial system and thus aid in gaining a better understanding of its behavior. There are two main, well established types of models of the arterial system: (i) lumped parameter 'Windkessel' models in which a number of discrete elements model the different properties of the arterial tree and (ii) transmission line/propagative models in which the arterial tree is viewed as a wave system where forward waves travel away from the heart and backward waves reflect at different reflection sites along the arterial tree.

1.5.1 Windkessel models

Derived from the German word for air chamber, Windkessel models originate from the analogy between the buffering function of the large arteries and the working principle of a fire engine, in which a windkessel blunts the intermittent flow of the pump to provide a more steady outflow of water at the fire hose.

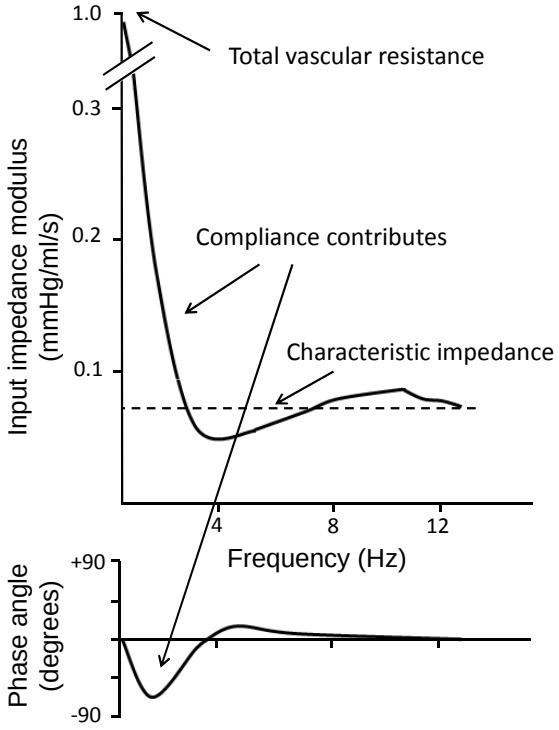

FIGURE 1.12: The input impedance fully characterizes the systemic arterial circulation [6].

Figure 1.13 gives an overview of the different Windkessel models, which can be expressed in hydraulic and electric representations.

In its simplest form, a Windkessel model contains two elements: the total arterial resistance and the total arterial compliance [12]. As described earlier (1.4.1), the total arterial resistance is mainly determined by the smaller arteries and arterioles, while the total arterial compliance is mainly determined by the large elastic arteries. During diastole, the pressure drop follows an exponential decay: $P(t) = P_o e^{-1/RC}$. When comparing the input impedance of the 2-element Windkessel model with the input impedance of the arterial system (figure 1.14), it is clear that the model still differs substantially from the in vivo circulation, especially at higher frequencies. To improve the high-frequency behavior, a 3-element Windkessel model was introduced by Westerhof by adding the characteristic impedance of the aorta in series to the 2-element Windkessel model [13]. Although this model mimics the in vivo input impedance quite well, it overestimates Z_{in} in the lower frequencies. Therefore, Stergiopulos *et al.* [14] proposed the four-element Windkessel model with an inertance (L) in par-

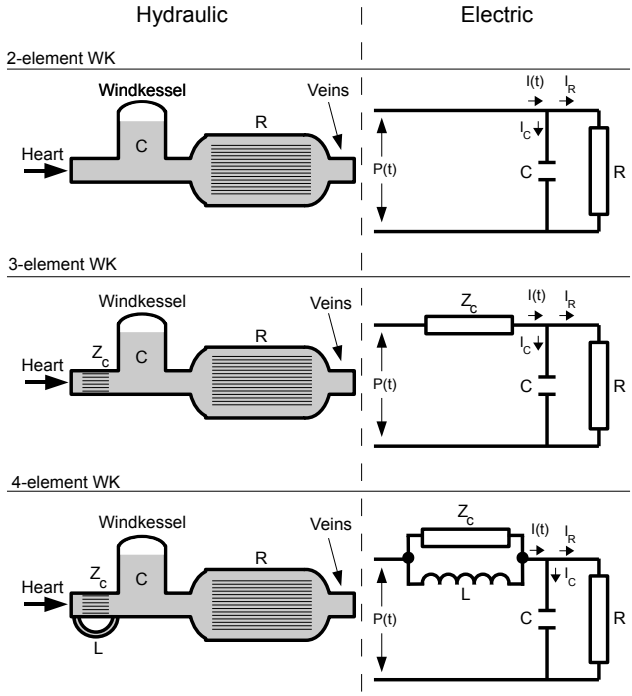

Figure 1.13: Hydraulic and electric representations of the two-element (top), three-element (middle), and four-element (bottom) Windkessel models. R: total peripheral resistance, C: total arterial compliance, Z_c: aortic characteristic impedance, L: arterial inertance $P(t)$: potential difference (pressure) generated by the heart, I: current (flow) [2].

allel with the characteristic impedance. For lower frequencies, Z_c is bypassed through this inertance.

1.5.2 Propagative models

In a propagative or transmission line model of the arterial tree, the observed pressure and flow waveforms are viewed as the resultant of forward and backward travelling waves. Upon contraction of the left ventricle, pressure and flow waves are generated travelling away from the heart into the arterial tree. At every change in impedance, reflections occur, causing backward waves propagating towards the heart. The shape of the resulting pressure and flow waveforms at any location in the arterial tree is determined by the magnitude and the timing of the forward and backward travelling waves. The time at which reflections arrive at a location depends on the distance to the reflection sites and the wave speed. This wave speed, the pulse wave velocity (PWV), is considerably higher (5-15 m/s) than the blood flow velocity ($\approx$ 1 m/s) and is directly related to the

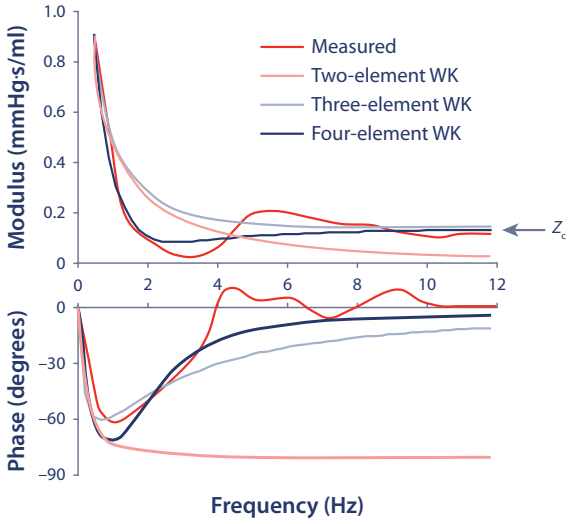

FIGURE 1.14: Aortic input impedance plotted with impedance predicted from a two-, three- and four-element Windkessel model [15].

elasticity of the vessels via the Moens-Korteweg equation:

$$PWV = \sqrt{\frac{hE_{inc}}{\rho D}} \tag{1.10}$$

with

- h the wall thickness
- E_{inc} the incremental elastic modulus
- ρ the blood density
- D the lumen diameter

The Bramwell-Hill equation relates pulse wave velocity to compliance (dV/dP) or the area distensibility ($D_A = dA/A/dP$):

$$PWV = \sqrt{\frac{VdP}{\rho dV}} = \sqrt{\frac{AdP}{\rho dA}} = \sqrt{\frac{1}{\rho D_A}}. \tag{1.11}$$

The location of the wave reflections has been a point of debate for a long time. Several researchers tried to identify one or more distinct reflection points [16–18]. Locations such as the aorta-iliac bifurcation, a major discontinuity,

and the arteriolar bed, with a multitude of bifurcations over a short distance, certainly form major zones of reflections. However, as wave reflections occur at each change of impedance, the continuous change in diameter (geometric tapering) and elastic properties of the arterial tree causes continuous wave reflections, making it practically impossible to identify all the different reflection sites.

To quantify the amount of wave reflection, the complex phenomenon of scattered wave reflection is simplified. Westerhof *et al.* proposed to consider the arterial system as a single viscoelastic tube, in which the pressure and flow wave are seen as the superposition of a single forward and a single backward wave[19]. The forward and backward waves are the integrated representation of all incident and reflected travelling waves. This approach is called *wave separation analysis* and is performed in the frequency domain. As an alternative approach, Parker and Jones introduced the *wave intensity analysis*, in which wave reflections are studied in the time domain. Both approaches are discussed in further detail in section 2.4.

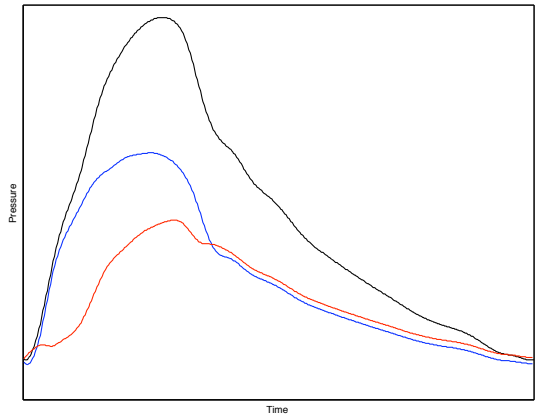

Figure 1.15: Separation of a measured pressure (black) into its forward (blue) and backward (red) components [2].

The propagative model is able to explain some phenomena that can not be explained based on the Windkessel models, such as the shape differences in the pressure waveform at different locations. When comparing the pressure waveform at the ascending aorta with the pressure waveform at the femoral artery as displayed in figure 1.16 for a young subject, it is clear that the femoral waveform is more peaked and has a higher systolic pressure than the pressure waveform at the ascending aorta. This can be explained by noting that the femoral artery is closer to the main reflection sites than the ascending aorta. Whereas the reflected waves arrive at the femoral artery during the systolic phase, thus boost-

ing systolic pressure, the reflections at the ascending aorta arrive later, generally during the diastolic phase. In general, wave reflections cause the pressure waveform to be increasingly peaked when moving away from the heart. This phenomenon is called pulse pressure amplification.

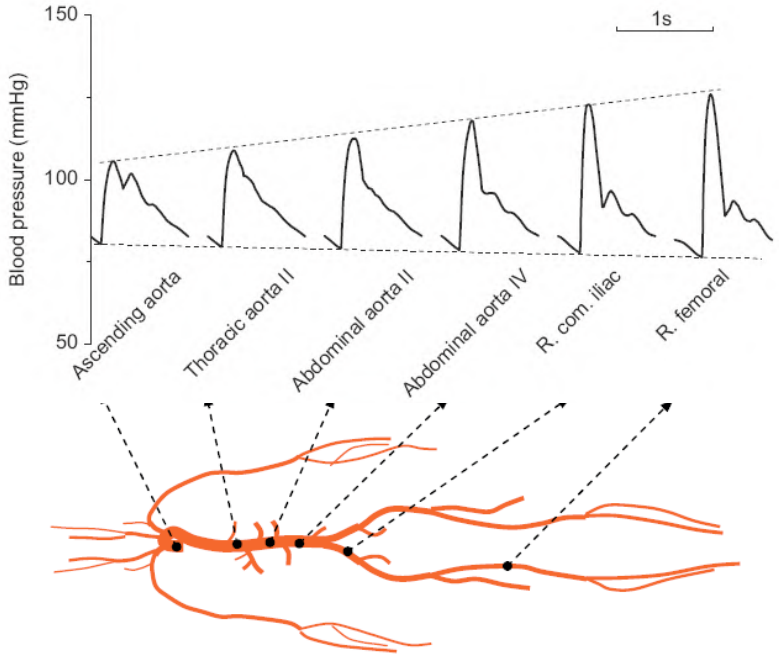

FIGURE 1.16: Snapshots of pressure wave variation along the arterial tree at the age of 25, obtained from a numerical model of the cardiovascular system. [20].

Since blood pressure is usually assessed at the brachial artery, it is important to keep in mind that brachial systolic (SBP) and diastolic blood pressure (DBP) differ from aortic SBP and DBP as a result of the pressure amplification between the aorta and the brachial artery. Ideally, the reflected waves arrive at the heart just as the aortic valve closes. Such timing ensures that the reflected wave does not add to the left ventricular pressure load, but boosts pressure during diastole to enhance coronary perfusion. However, in general, the aortic stiffness increases with age, leading to a higher wave speed (via 1.11) and an earlier return of the reflected wave, causing a boost in systolic aortic pressure and left ventricular afterload and a decrease in pulse pressure amplification.

1.6 Pathophysiology

1.6.1 Cardiovascular disease

Cardiovascular diseases (CVDs) are the main cause of death worldwide, with an estimated 17.1 million worldwide deaths in 2004, representing 29% of all global deaths [21]. A distinction is made between coronary heart disease (myocardial infarction), cerebrovascular disease (stroke), elevated blood pressure (hypertension), peripheral artery disease, rheumatic heart disease, congenital heart disease and heart failure. Of these, coronary heart disease and stroke are the most frequent pathologies, with an estimated 7.2 million and 5.7 million deaths per year, respectively. Apart from the congenital pathologies, the underlying cause of most types of cardiovascular disease is atherosclerosis, a gradually developing process in which cholesterol, fat and fibrous tissue build up in the arterial wall. The pathogenesis of atherosclerosis will be discussed in more detail in section 1.6.3.

1.6.2 Risk factors

Based on the outcome of large-scale population studies, a number of risk factors for the development of CVD have been identified [21, 22]. Approximately 75% of all CVD can be attributed to these risk factors [23], which are classified into modifiable and non-modifiable factors.

The most important *non-modifiable* risk factors are:

- *Age* - A vast majority of people suffering from CVDs is 65 years or older. Therefore, age is recognized as an important risk factor for the development of cardiovascular disease. Throughout life, the blood vessels undergo drastic structural changes. This process is called vascular aging and is described in more detail in 1.6.4. Together with normal vascular aging, a number of gradually evolving long-term processes such as atherosclerosis (see 1.6.3) are at the root of the excess burden of CVDs at older age.

- *Gender* - In general, women are considered to be more protected from CVD until reaching menopause [23]. Although the overall mortality and morbidity of men and women is comparable, specific differences exist in the disease profile per gender. Men have a higher risk of myocardial infarction than women [22, 23], while stroke is markedly more common in women [24].

- *Heredity* - Children of parents with a history of CVD are at higher risk to develop CVD themselves [23]. This also holds for non-congenital CVD. Apart from a family history of CVD, ethnicity also affects the cardiovascular risk profile. African Americans for example have more severe hypertension than Caucasians and a higher risk of heart disease [22].

Among the key *modifiable* risk factors are:

- *Cholesterol* - Mainly produced in the liver, cholesterol is an essential structural component of cell membranes which plays a role in the production of bile acids, steroid hormones, and vitamin D. Cholesterol is transported via the blood by lipoproteins. Two main types of lipoproteins can be discriminated: high-density (HDL) and low-density (LDL) lipoproteins. While HDL is responsible for the transport of excess cholesterol from the cells to the liver and acts anti-atherogenic, LDL is partially ingested by macrophages and foam cells in the vessel wall, potentially leading to atherosclerosis. Therefore, high concentrations of LDL and an imbalance between LDL and HDL are risk factors for the development of CVD. A total cholesterol/HDL-cholesterol ratio more than 5 indicates increased risk [25].

- *Tobacco* - Smoking promotes the development of CVD through a number of mechanisms. It damages the endothelium, increases fatty deposits in the arteries, increases clotting, raises LDL-cholesterol, reduces HDL-cholesterol and promotes coronary artery spasm. Nicotine, the addictive component of tobacco, accelerates the heart rate and raises blood pressure. Smokers have a two- to fourfold risk of developing coronary heart disease compared to non-smokers. Smoking is a powerful independent risk factor for sudden cardiac death in patients with coronary heart disease [8, 22].

- *Hypertension* - Hypertension is the single most important risk factor for stroke [26] and markedly increases the risk of myocardial infarction, kidney failure and congestive heart failure. The number of people suffering from hypertension worldwide is estimated at more than 970 million [27]. The role of hypertension is special in the sense that it is considered both a type of CVD and a risk factor for the development of other CVD types. The pathogenesis and classification of hypertension are discussed in 1.6.5.

- *Physical inactivity* - Physical activity, at any age, protects against a multitude of chronic health problems including all types of CVD. Even moderate levels of daily exercise are beneficial for the blood pressure, blood lipid levels, blood glucose levels, blood clotting factors and the level of vascular stiffness. However, the increasing degree of urbanization and mechanization worldwide has reduced our levels of physical activity. The World Health Organization estimates that more than 60% of the global population is not sufficiently active, exposing those without sufficient daily physical activity to an increased risk of coronary heart disease and stroke of up to 50% [23].

- *Obesity* - People with excess body fat - especially at the waist - are more likely to develop heart disease and stroke even in the absence of other risk factors. Excess weight increases the cardiac load and promotes the development of diabetes. It also raises blood pressure and triglyceride levels, and lowers HDL-cholesterol levels.

- *Diabetes mellitus* - Diabetes mellitus is a metabolic disease characterized by high blood sugar levels which can be classified into two major groups. Type-1 diabetes is characterized by a reduction or total absence of endogenous insulin production, whereas type-2 diabetes is mainly caused by insulin resistance, which causes the cells not to respond to the produced insulin. People with diabetes develop atherosclerosis at a younger age and more severely than people without diabetes. In type-1 diabetics, a two- to three-fold increase in risk of developing CVD is reported. This risk is almost entirely confined to those patients that develop renal disease [28]. In type-2 diabetes, all patients are at increased CVD risk, with women at markedly higher risk than men [25]. About three-quarters of people with diabetes die of CVD [22].

Although different risk factors can be interrelated, the risk of developing CVD increases with a subject's number of risk factors. In an attempt to quantify the overall risk of CVD, several integrated risk scores have been proposed. Categorisation of total CVD risk as low, moderate, high or very high has the merit of simplicity and can therefore be recommended [26]. Based on 12 European cohort studies, the European Society of Cardiology introduced a risk chart called SCORE (Systematic COronary Risk Evaluation) which allows an estimation of the risk of cardiovascular death within a period of 10 years [25]. A distinction is made between countries with high CVD risk (including most Eastern-European countries) and countries with low CVD risk, including Belgium. The 2007 SCORE chart for countries with low CVD risk is shown in figure 1.17. Another commonly used index is the Framingham risk score, which expresses the risk of developing coronary heart disease within the next 10 years. It is derived from the Framingham Heart Study, a long ongoing cardiovascular study in the US with over 5000 subjects which now includes the third generation of participants.

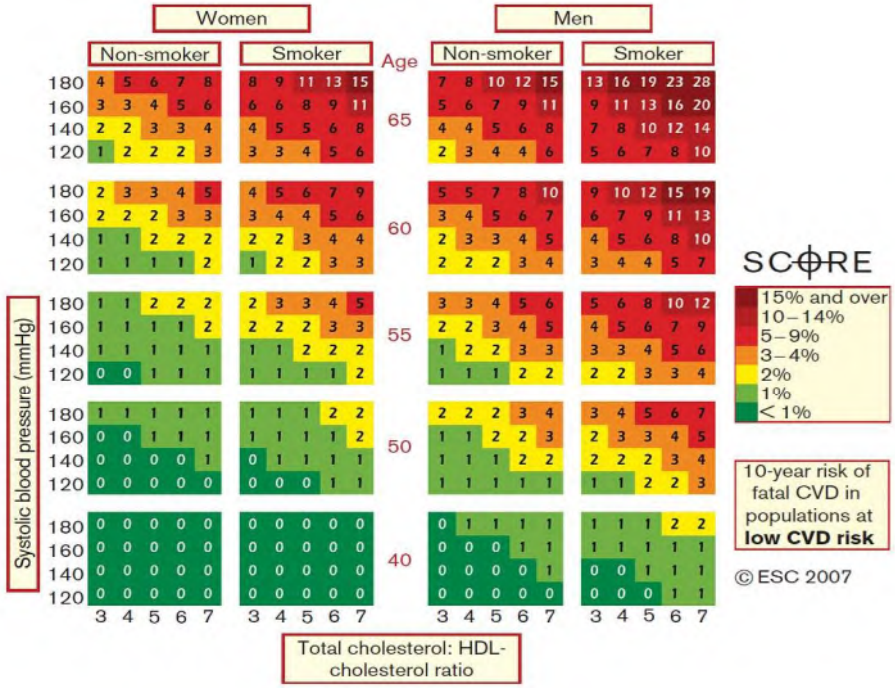

FIGURE 1.17: Score chart: 10-year risk of fatal cardiovascular disease in populations at low CVD risk based on age, gender, smoking, systolic blood pressure and total cholesterol/HDL cholesterol ratio. CVD: cardiovascular disease, HDL: high-density lipoprotein. [25].

1.6.3 Atherosclerosis

Atherosclerosis is a complex and slowly developing process that starts early in life [29, 30] and gradually develops, as illustrated in figure 1.18. Over time, the endothelial function deteriorates, allowing cholesterol rich low-density lipoproteins (LDLs) to enter the arterial intimal layer from the blood stream. This causes a chronic inflammatory reaction in the arterial wall, which in some locations leads to the formation of a plaque: a large core of necrotic and lipid tissue, covered by a fibrous cap.

In a vast majority of cases, the fibrous cap is strong enough to withstand the stress. In these cases, the plaque remains asymptomatic and stable, and hence most often unnoticed. Vulnerable plaques, however, are prone to rupture, which can be a life-threatening event if it is followed by thrombosis [30]. In mechanical terms, plaque rupture occurs when the imposed stress on the plaque exceeds its strength.

For the coronary arteries, a vast majority of the sudden deaths results from plaque rupture followed by thrombosis. In a minority of cases, fatal thrombosis

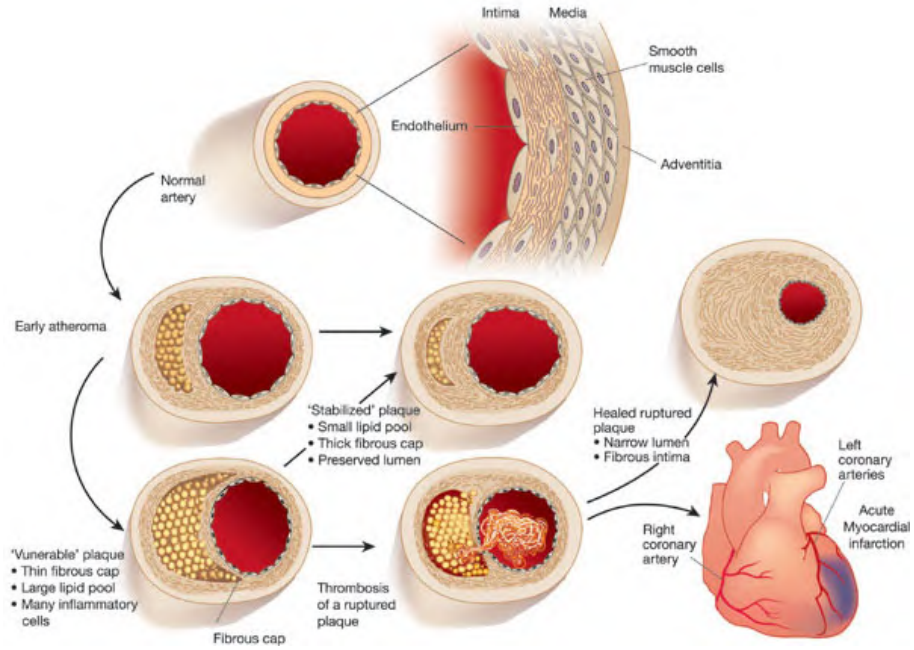

Figure 1.18: Pathogenesis of atherosclerosis.

results from a superficial erosion of the endothelial layer overlying the plaque. Plaque erosion is more common in young victims, in smokers and in women [31–33].

Extensive data confirm that most of the acute infarcts are associated with non-stenotic lesions [33–37]. In this regard, it is important to highlight the role of arterial wall remodeling: the artery responds to plaque growth by increasing its cross-sectional area while retaining sufficiently large lumen dimensions [38, 39]. An immediate consequence is that these plaques do not cause chest pain and can therefore be regarded as silent killers.

1.6.4 Aging

It is debatable whether aging should be considered a pathologic process. Although often associated with atherosclerosis, the increase in stiffness as noted in normal aging is a clearly different process than atherosclerosis. Atherosclerosis is predominantly a disease of the arterial intima and is localized to specific sites in the large arteries. Arterial changes observed in normal aging are diffuse and predominantly affect the arterial media [4]. It is important to note that arterial aging does not simply develop in the elderly but is a gradually developing long-term process starting at young age.

Throughout the course of life, the systemic large arteries undergo pronounced structural changes. Arterial aging phenomena include intimal hyperplasia, calcium deposition, increased collagen content, and, most importantly, progressive thinning and disorganization of the media, with loss of the structural arrangement of elastin fibers and laminae. A logical explanation for this arterial degeneration arises from the application of the principle of material fatigue to the arterial wall. After long-term exposure to cyclic stretch, the elastin cannot be re-synthesized quickly enough, and is gradually replaced with collagen [4]. As a consequence, arteries progressively stiffen with age. The higher pulse pressure caused by this increase in stiffness may in turn cause extra wear of the vessel wall resulting in more breakdown of elastin.

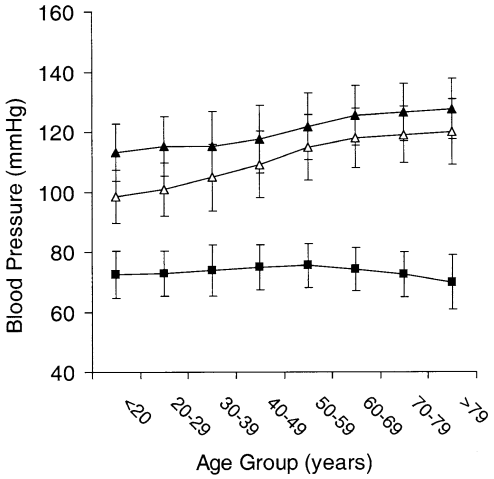

FIGURE 1.19: Evolution of brachial systolic blood pressure (closed triangles), brachial diastolic blood pressure (closed squares) and central systolic blood pressure (open triangles) with age. Mean value ± standard deviation are shown for each decile of age. [40].

Figure 1.19 shows the evolution of brachial SBP and DBP with age in the general population. While SBP rises steadily with age, the DBP reaches a plateau level between the fifth and the sixth decade and decreases progressively at higher age. The increase in pulse pressure (PP) can be explained by an increase in arterial stiffness. During a lifetime, aortic wave speed increases by about a factor two, equalling a decrease in aortic compliance by a factor four (via equation 1.11). Apart from stiffening, the aorta and the central elastic arteries also dilate and become tortuous. Interestingly, these structural changes are virtually confined to the aorta and the central elastic arteries. Unlike the large elastic arteries, no gradual decrease was reported in the distensibility [41, 42] or the PWV [43, 44] of the femoral, radial or brachial arteries with age.

1.6.5 Hypertension

Hypertension mostly occurs as a result of an increase in peripheral resistance and/or an increased level of central arterial stiffness. The inital cause of this increase in either resistance or stiffness is often unclear, as illustrated by the fact that *essential* hypertension, or hypertension of unknown cause, represents 90% of all cases of hypertension [45]. There is, however, a multitude of factors that have been shown to contribute to the pathogenesis of hypertension. Some of these factors are long-term high sodium intake, diabetes mellitus, increased sympathetic nervous system activity and obesity, but also structural and functional factors such as endothelial dysfunction, increased oxidative stress and vascular remodeling.

Whereas an isolated increase in peripheral resistance causes SBP and DBP to rise equally, elevated stiffness is associated with an increase in pulse pressure and SBP. Given the progressive stiffening of arteries at higher pressure, hypertension automatically leads to higher levels of stiffness. The increase in stiffness implies an increase in PWV and aortic impedance, which causes the amplitude of the incident wave to increase and the reflected pressure wave to arrive earlier, thus boosting systolic pressure and aggravating the level of hypertension. Note that an alternative reasoning, based on the windkessel model, leads to a similar conclusion.

When hypertension is sustained, the cardiac load and the stress on the large arteries are increased and cardiovascular degeneration is accelerated. Therefore, the effect of hypertension on the arterial system has many similarities to the aging process and can be regarded as a type of accelerated aging. The effects of hypertension on the more muscular arteries differ from those on the elastic arteries and include intimal hyperplasia, accelerated atherosclerosis [46, 47] and impaired endothelial function [48–50].

Although hypertension itself is recognised as a type of CVD, it also leads to a variety of other cardiovascular events, such as stroke [51] and left ventricular hypertrophy [52]. Therefore, strict follow-up of the blood pressure of those at risk is of paramount importance. The crucial role of hypertension in the estimation of a subject's cardiovascular risk is illustrated in the latest guidelines of the European Society of Hypertension (ESH), where blood pressure figures as a separate marker, while all other risk factors are pooled, as illustrated in figure 1.20). Because clinical evidence shows a continuous relationship between blood pressure and cardiovascular risk, any definition of hypertension is largely arbitrary [53]. In todays clinical practice, hypertension is defined based on brachial blood pressure values. According to the current guidelines [26], a subject is hypertensive if the brachial SBP exceeds 140 mmHg or the brachial DBP exceeds 90 mmHg. Hypertension is further classified in three categories (grades 1, 2 and 3), while the blood pressure of normotensives can be normal or high normal (see figure 1.20).

Blood pressure (mmHg)					
Other risk factors, OD or Disease	Normal SBP 120–129 or DBP 80–84	High normal SBP 130–139 or DBP 85–89	Grade 1 HT SBP 140–159 or DBP 90–99	Grade 2 HT SBP 160–179 or DBP 100–109	Grade 3 HT SBP ≥180 or DBP ≥110
No other risk factors	Average risk	Average risk	Low added risk	Moderate added risk	High added risk
1–2 risk factors	Low added risk	Low added risk	Moderate added risk	Moderate added risk	Very high added risk
3 or more risk factors, MS, OD or Diabetes	Moderate added risk	High added risk	High added risk	High added risk	Very high added risk
Established CV or renal disease	Very high added risk	Very high added risk	Very high added risk	Very high added risk	Very high added risk

Figure 1.20: Stratification of CV risk according to the 2007 ESC/ESH guidelines. SBP: systolic blood pressure, DBP: diastolic blood pressure, CV: cardiovascular, HT: hypertension. OD: subclinical organ damage, MS: metabolic syndrome. Low, moderate, high, and very high risk refer to 10 year risk of a CV fatal or non-fatal event. The term 'added' indicates that in all categories risk is greater than average. The dashed line indicates how the definition of hypertension may be variable, depending on the level of total CV risk [26].

CHAPTER 2

Non-invasive assessment of wave reflection and arterial stiffness: overview of existing methods, devices and associated parameters

2.1 Introduction

Research on hypertension, the most important risk factor for CVD, has been extensive for many decades. Until about 15 years ago, the focus of research and treatment was on peripheral resistance as the main cause of hypertension [10]. More recently, increased emphasis has been given to elevated systolic and pulse pressure, considered to be primarily caused by an increase in arterial stiffness and wave reflections [54]. As a result, arterial stiffness and wave reflections are being increasingly used in the clinical assessment of patients with hypertension and various CV risk factors [55]. The aim of this chapter is to summarize the various methods that have emerged to quantify arterial stiffness and wave reflections. As most of these methods rely on a pressure, flow or diameter distension waveform, the chapter starts with a description of the assessment of these three types of waveforms.

2.2 Waveform acquisition

2.2.1 Pressure waveform

While the use of a cuff-sphygmomanometer allows easy and relatively accurate assessment of the brachial systolic and diastolic pressure, arterial pressure waveforms can be measured non-invasively using either photoplethysmography or applanation tonometry.

Figure 2.1: Nexfin photoplethysmograph (BMEYE, Amsterdam, The Netherlands).

A photoplethysmograph measures the volume change of an organ by illuminating the skin and recording the changes in light absorption. Finger arterial pressure can be assessed by using the volume-clamp or Penaz method. With this method, the finger arteries are clamped at the unloaded diameter, the point at which finger cuff pressure and intra-arterial pressure are equal, thus at which the transmural pressure across the finger arterial walls is zero. A high-speed feedback mechanism allows to keep the artery at this unloaded diameter throughout the cardiac cycle by varying the pressure of the finger cuff. The cuff pressure then equals the intra-arterial finger pressure waveform. Commercial photoplethysmographs include Finometer, PortaPress (FMS, Amsterdam, The Netherlands) and Nexfin (BMEYE, Amsterdam, The Netherlands), as shown in figure 2.1. Although finger pressure waveforms correspond well with radial pressure waveforms in young, healthy subjects, significant differences arise under several (patho)physiologic conditions, due to wave reflections and the pressure gradient in the small finger arteries [56].

Applanation tonometry makes use of a high-fidelity strain micromanometer that records arterial pressure waves when applied on the skin at constant pressure (figure 2.2). It can be applied to various superficial large arteries, provided there is a bone or hard structure under the artery for proper applanation. While it is generally accepted that radial, carotid and femoral artery pressure waveforms can be accurately assessed using applanation tonometry, no consensus exists for brachial artery tonometry. Although the brachial artery lies su-

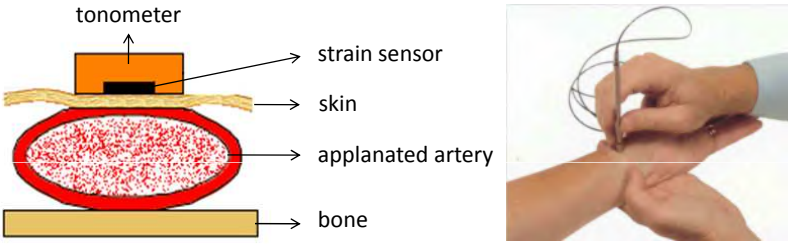

FIGURE 2.2: Applanation tonometry: working principle (left) and application on the radial artery (right).

perficially, it can be difficult to obtain adequate tonometric waveforms in obese individuals or in people with large biceps muscles.

The recorded tonometric waveforms need to be calibrated. At the brachial artery, this can easily be done by using the systolic and diastolic pressures obtained via sphygmomanometry. For the calibration of pressure waveforms at other arterial locations, a more complicated calibration procedure is followed (figure 2.3). Kelly and Fitchett [57] demonstrated that the difference between diastolic and mean arterial pressure remains constant throughout the large arteries. By additionally assuming that also the absolute values of DBP and mean arterial pressure (MAP) remain constant throughout the large arteries [58, 59], the brachial DBP and MAP can be used to calibrate tonometric curves at all other large arteries. Ideally, brachial MAP is obtained as the arithmetic average of a calibrated brachial pressure waveform, and thus requires brachial tonometry. Alternatively, brachial MAP can be approximated by adding 40% of the pulse pressure to the diastolic pressure [60].

Although clinically the most relevant location, the aortic pressure waveform cannot directly be obtained non-invasively. However, based on invasive radial and aortic pressure waves, population-based generalized transfer functions have been constructed to transfer a radial pressure waveform to a synthesized aortic wave. These transfer functions are applied in the time or frequency domain and can be regarded as sophisticated low pass filters since the aortic pressure wave contains fewer higher harmonics than the radial wave. The use of less complicated filters, such as an n-point moving average filter with n one-quarter of the sampling frequency, was recently shown to be capable of accurately predicting central aortic systolic pressure [62].

There are a number of commercially available applanation tonometry systems. The most widespread device is the SphygmoCor (Atcor Medical, Australia), using a pen-type tonometer to manually applanate the artery. The SphygmoCor software has a built-in radial-to-aortic transfer function. For the acqui-

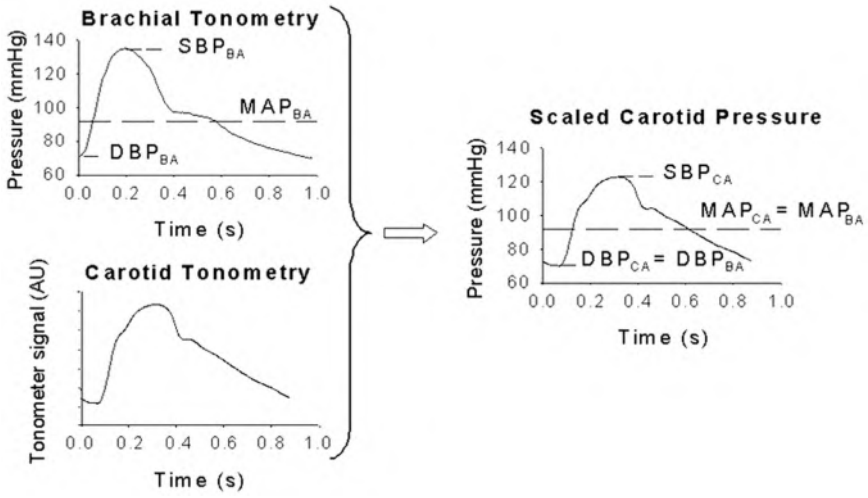

Figure 2.3: Calibration method for carotid artery tonometry waveforms [61]. The same calibration scheme can be used to calibrate waveforms of other superficial large arteries.

sition of radial pressure waves, there are more complex, automated tonometers which, once attached to the wrist by a strap, automatically locate and applanate the artery, such as the BP-508 (Colin Medical Instrumentation, Komaki, Japan) and, more recently, the Omron HEM-9000AI (Omron Healthcare, Kyoto, Japan).

2.2.2 Flow waveform

Flow is obtained as the product of velocity and cross-sectional area. Both velocity and cross-sectional area can be measured non-invasively with ultrasound techniques. An acoustic ultrasound wave, typically at a frequency of between 7 and 12 MHz, propagates in the tissue and reflects on interfaces with a discontinuity in acoustic impedance, such as the wall-lumen interface [63]. When a set of waves is emitted and reflected, a so called B-mode image can be created from the radio frequency (RF) data. By holding the vascular ultrasound probe perpendicular to the axis of the vessel of interest, the cross-sectional area becomes visible and its dimensions can be measured. The velocity waveform is measured with Doppler ultrasound. A distinction can be made between pulsed-wave or continuous-wave Doppler. Continuous-wave Doppler is the simplest mode, whereby flow information is received from all of the moving reflectors in the path of the beam. In pulsed-wave mode, a transducer sends a series of short sound pulses into the body, with pauses between each pulse to allow for the detection of the returning sounds that are echoing back from the red

blood cells. Doppler ultrasound is by default available on vascular ultrasound scanners. Relatively inexpensive handheld Doppler ultrasound systems are also available which employ continuous-wave probes to give Doppler output without the addition of B-mode images. Flow can be measured at the left ventricular outflow tract to provide aortic inflow (figure 2.4), but it can also be measured in any superficial artery, as illustrated in figure 2.5.

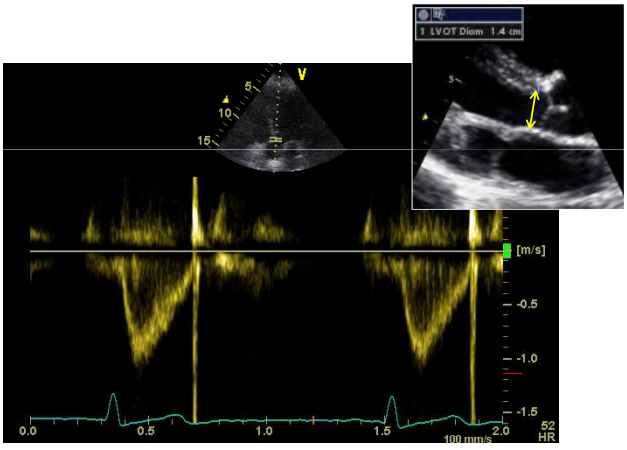

FIGURE 2.4: Aortic flow waveform at the left ventricular outflow tract (LVOT) assessed with Doppler ultrasound. LVOT diameter (top right) is imaged using B-mode ulstrasound.

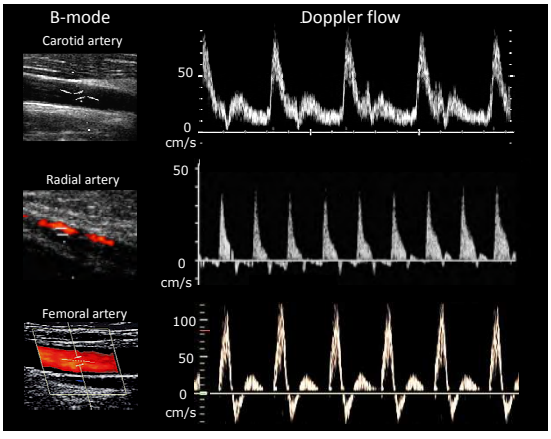

FIGURE 2.5: Examples of carotid, radial and femoral artery flow waveforms assessed with Doppler ultrasound.

2.2.3 Diameter distension waveform

Diameter distension of superficial large arteries can be accurately measured with non-invasive vascular ultrasound. The clear reflections at the lumen-intima and media-adventitia interface allow detection of the posterior and anterior wall, as illustrated in figure 2.6. To optimize accuracy, automated "wall tracking" algorithms have been developed using the RF data to track the displacement of both walls in time. The hence obtained distension waves have an accuracy of less than 5 μm. However, it is worth noting that the arterial distension at the inner wall is about 25% (for relative distension $\Delta D/D$) higher than that at the outer wall [64]. This can be explained by simple geometrical considerations: during systole, the distended vessel wall is thinner than in diastole, because of conservation of wall volume. This leads to a smaller increase in diameter of the outer compared to the inner wall. Because different ultrasound scanners might track another point in the vessel wall, special care should be taken when comparing diameter distensions. In the near future, evolutions in other imaging techniques like CT and MRI may enable the assessment of distension of deeper arteries such as the aorta [63].

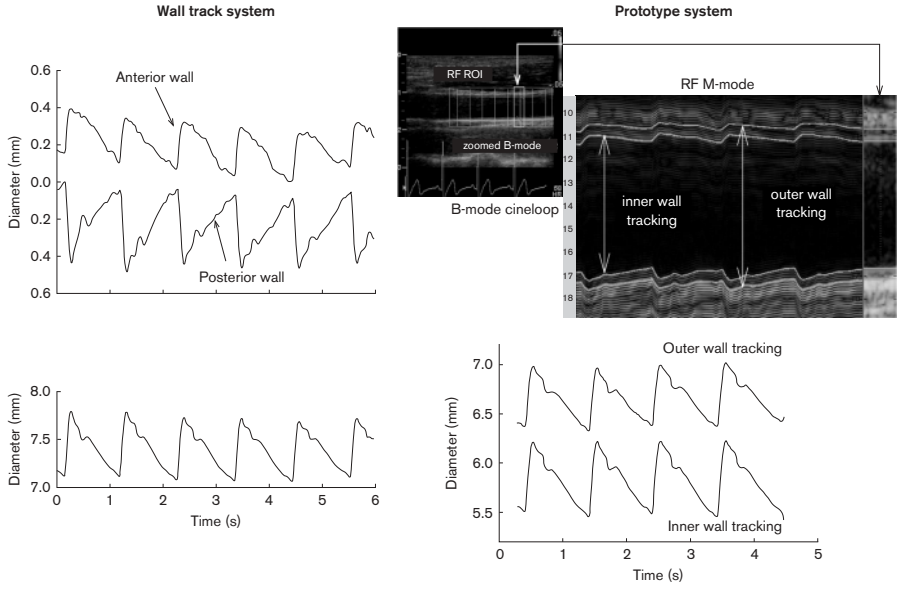

Figure 2.6: A selected region of interest (ROI) in a B-mode image is followed over time and displayed as an M-mode image (upper right). By tracking the displacement of the anterior and posterior wall (upper left), the diameter change over the cardiac cycle can be derived (lower left). Depending on whether the inner or outer wall is tracked, different diameter distension curves are obtained [64].

2.3 Arterial stiffness

Arterial stiffness can be assessed at a local, regional or global level. Each approach has its advantages and disadvantages and is described below in more detail.

2.3.1 Local arterial stiffness

Definition

Arterial compliance, the inverse of stiffness, is the ratio of volume change for a given change in pressure. In practice, the volume of a vessel is difficult to measure and is often replaced by cross-sectional vessel area or diameter. When pressure and diameter are measured continuously over a large pressure interval, S-shaped pressure-area loops can be constructed such as the ones obtained by Langewouters from ex-vivo aortic tissue, shown in figure 2.7.

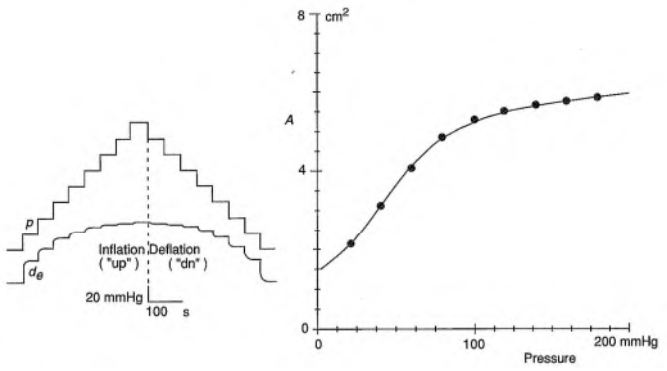

Figure 2.7: Left: aortic pressure (p) and external diameter (d_e) during stepwise in- and deflation. Right: area-pressure relation base measurements during inflation (dots) and fitted data (solid line) [65].

In clinical practice, compliance is calculated over a smaller pressure range, hereby neglecting the nonlinear behavior of the vessel wall within the pressure interval. This approximation yields the compliance coefficient (CC) which represents the buffering capacity of the artery:

$$CC = \frac{\Delta A}{\Delta P} = \pi/4 \frac{2D \cdot \Delta D + \Delta D^2}{\Delta P} \tag{2.1}$$

with

- D the diastolic diameter
- ΔD the difference between maximum and minimum diameter
- ΔP the difference between maximum and minimum pressure

The compliance coefficient, however, is highly dependent on the vessel caliber, and therefore the distensibility coefficient (DC) is a better representation of the elasticity of the artery:

$$DC = \frac{\Delta A/A}{\Delta P} = \frac{2D \cdot \Delta D + \Delta D^2}{D^2 \Delta P} \tag{2.2}$$

In practice, both DC and CC are often calculated over the operating pressure range interval, so ΔP becomes PP and ΔD the wall distension between diastole and systole.

A related parameter is the β-stiffness index, expressing the ratio of logarithm of systolic and diastolic pressures to the relative change in diameter:

$$\frac{\beta = ln(SBP/DBP)}{(D_s - D_d)/D_d} \tag{2.3}$$

with D_s and D_d the systolic and diastolic diameter, respectively.

Measurement

Assessing the distension and compliance coefficients requires pressure and diameter distension waveforms, measured at the same location and time. Since DC and CC strongly depend on the pressure interval over which they are calculated, it is important, when comparing different subjects, to define a common pressure window over which 'isobaric' distension and compliance coefficients can be calculated.

Clinical application

Local stiffness is regularly assessed in clinical studies. Most literature exists for carotid stiffness, since the carotid artery is an easily accessible large elastic artery prone to plaque formation. Carotid stiffness has been shown to be associated with increased CV risk [66] as well as with major CV risk factors such as age [67], hypertension [68], smoking [69] and obesity [70]. When local stiffness is assessed at two locations, conflicting results can be observed: Spek *et al.* found carotid distensibility to decrease with age, while brachial distensibility remained constant for men and even increased for women[67]. This suggests that muscular arteries are able to adapt to the altered conditions [63].

2.3.2 Regional arterial stiffness

Definition

Regional arterial stiffness is typically assessed via the *pulse wave velocity (PWV)*, the wave speed at an arterial segment connecting two locations. Although the stiffness of different arterial regions can be of clinical interest, the most relevant region is the aorta. It represents the largest part of the arterial buffering function and, together with its first branches, is 'seen' first by the left ventricle, and as such is responsible for most of the pathophysiological effects of an increase in arterial stiffness [55]. Aortic PWV is most commonly measured over the carotid-femoral pathway, as these are two superficial arteries which can easily be measured non-invasively (figure 2.8). A less frequently used alternative method measures PWV between the subclavian artery and the abdominal aorta at the position of the umbilicus [71]. Since 2007, PWV is listed in the ESC/ESH guidelines as an established marker of subclinical organ damage. This has given rise to a multitude of devices and methods to assess PWV.

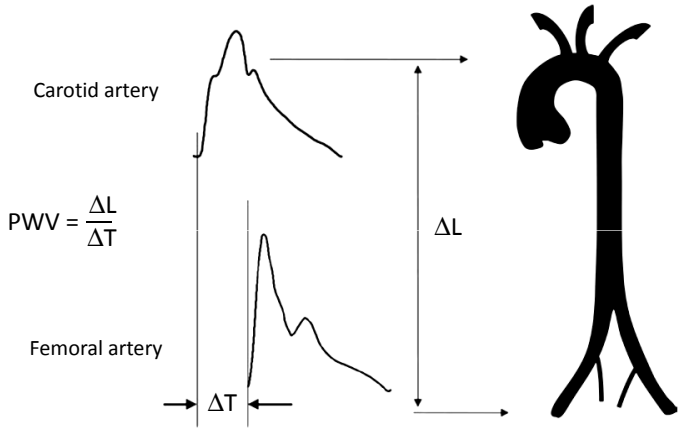

Figure 2.8: Carotid-femoral pulse wave velocity (PWV) [55]

Measurement

Pulse wave velocity is calculated as the ratio of travel distance and travel time. The travel time is the time needed for the wave to travel from the carotid to the femoral artery, and is measured as the time delay (ΔT) between the feet of the carotid and the femoral waveforms, the so-called *foot-to-foot* method. It is assumed that the early part of the wave is little affected by wave reflections and thus reflects the true wave speed. Since pressure, distension and velocity changes at the measuring site are all due to the same perturbation traveling through the arteries, travel time can be assessed from either of these three waves.

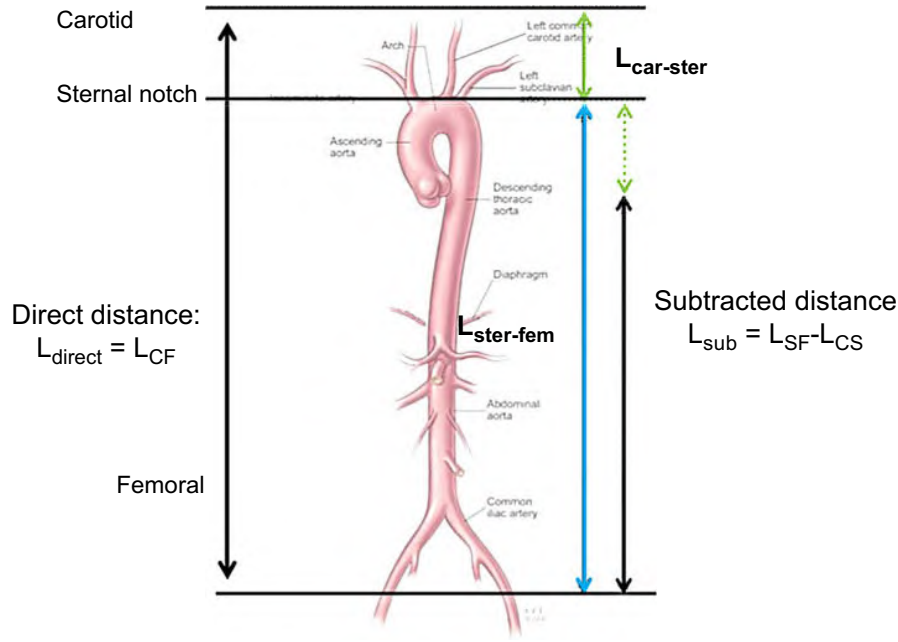

Figure 2.9: Overview of different approaches for defining the path length for PWV calculation [2]

The travel distance is usually measured on the body surface and is therefore only an approximation of the true distance travelled by the waves. As illustrated in figure 2.9, different methods exist: the *direct* distance simply measures the distance over the skin between the two recording sites. Alternatively, the *subtracted* distance is calculated as the distance between the (supra)sternal notch and the femoral measurement site minus the distance between (supra)sternal notch and carotid measurement location. This method takes into account that the direction of the blood flow in the carotid artery is opposite to that in the femoral artery. Since the blood flow in the carotid and femoral arteries originates from the heart, the difference in path length between the heart and the femoral artery minus the path length between the heart and the carotid artery is the true travelled distance. The position of the heart is approximated on the body surface by the suprasternal notch. Both distance methods co-exist, so one must be cautious when comparing different PWVs as the distance method influences the absolute value of PWV. Recently, the use of 0.8 times the direct distance was introduced as a third method [72]. This method proved to yield the smallest error and a high correlation when compared to the true travelled pathlength measured with MRI [73, 74].

Clinical application

The measurement of carotid-femoral PWV is generally accepted as the most robust and reproducible method to determine arterial stiffness [55]. There is a large body of evidence demonstrating its association with incident CV disease (CVD), independent of traditional risk factors and in various populations [71, 75–77]. Recently, Vlachopoulos et al [78] demonstrated that PWV is a strong predictor of future cardiovascular events and all-cause mortality in a meta-analysis including 15,877 follow-up patients. To facilitate the introduction of PWV in routine clinical practice, a set of normal and reference values per blood pressure and age-category was proposed based on data from 13 centres across Europe [72] (see figure 2.10).

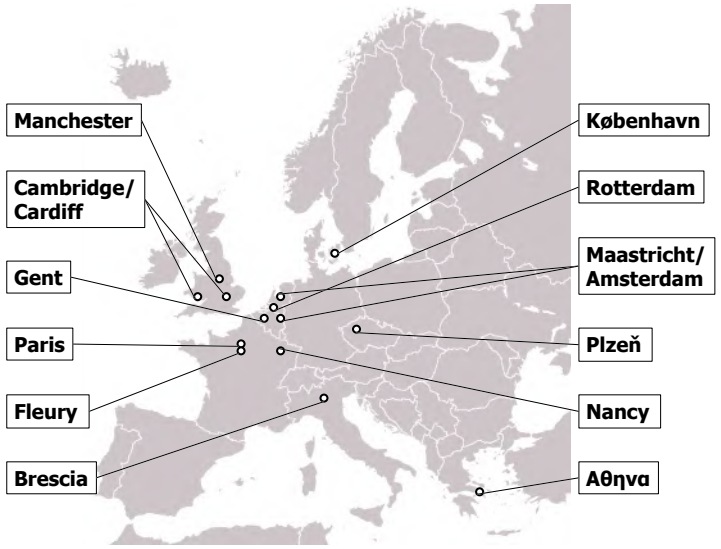

Figure 2.10: Geographic distribution of the centers participating in the reference value project

2.3.3 Global arterial stiffness

Definition

Assessing the global arterial stiffness implies integrating the stiffness of the entire arterial circulation into a single parameter. As a fast approximation, the ratio of stroke volume and pulse pressure (SV/PP) can be used. Although this corresponds with the general understanding of arterial compliance, SV/PP overestimates the true arterial compliance, as it assumes the entire stroke volume to be stored in the large elastic arteries and neglects peripheral outflow [79]. More accurate estimation of the total arterial compliance requires a lumped parameter model of the arterial tree, such as the Windkessel models discussed in section 1.5.1 of Chapter 1.

Measurement

Different methods to calculate the global arterial compliance exist, all of which require the assessment of at least the aortic pressure waveform. A distinction can be made between methods requiring the additional measurement of cardiac output, and others requiring the assessement of the entire flow waveform at the ascending aorta:

1. Decay-time and area method. Assuming a 2-element Windkessel model for the arterial circulation, the pressure *decay* in diastole is exponential, with the time constant τ given by the product of resistance and compliance ($\tau = R.C$) (see 1.5.1). Since R can be calculated as the ratio of mean pressure and mean flow, C can be derived as τ/R. Theoretically, this only holds when there is no flow during diastole, which is only true in the aorta.

Alternatively, the time constant in a 2-element Windkessel model can be derived from the *area* under the pressure curve in diastole as:

$$\tau = \frac{\int_{t_1}^{t_2} P(t)\, dt}{P_{t1} - P_{t2}}, \tag{2.4}$$

with t1 to t2 to be chosen freely between the dicrotic notch and the end of diastole [80]. Again, C is found as τ/R. Both methods are illustrated in figure 2.11.

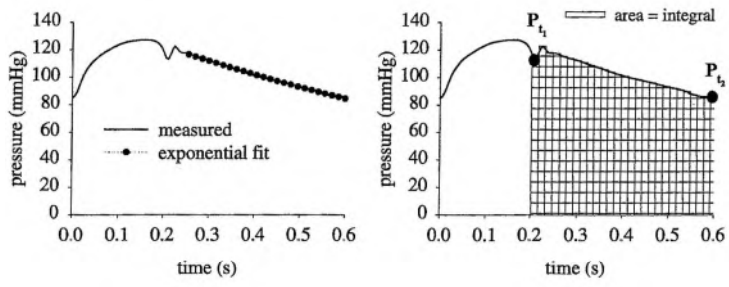

Figure 2.11: The decay-time (left) and the area method (right) [5].

2. Pulse pressure and model fitting method. In the pulse pressure method, R is calculated from the mean pressure and mean flow and an initial value for C is assumed. Using these values as well as the measured flow waveform, the pulse pressure resulting from the model is calculated and compared to the measured pulse pressure. Although it is not possible to accurately reproduce the entire

pressure waveform with a two-element Windkessel model, pulse pressure (low-frequency behavior) can be modeled with more precision. Therefore, an iterative scheme is followed in which the total arterial compliance is changed until the model and the predicted pulse pressure agree within reasonable limits [81]. Similarly, the model fitting method fits the calculated to the measured pressure waveform by changing the input impedance of a 3- or 4-element Windkessel model [6].

Clinical application

The clinical use of the global arterial stiffness is rather limited. In one of the few clinical studies on total compliance, de Simone *et al.* demonstrated that a decreased SV/PP was an independent predictor of cardiovascular outcome in 50 patients followed up over a period of 10 years [82].

2.4 Wave reflections

There are different methods to quantify wave reflection. The gold standard is by separating pressure and flow in their forward and backward components, a method called *wave separation analysis*. This separation can be done in the frequency domain (*impedance analysis*) or in the time domain (*intensity analysis*). Both approaches require the assessment of aortic pressure and flow waveforms. As it is often inconvenient and time-consuming to assess both waveforms, *wave shape analysis* based on the pressure waveform alone might provide an alternative. In this section, the three approaches are described in more detail.

2.4.1 Wave shape analysis

Definition

Although resulting from a multitude of small reflections on different locations, in most cases the apparent arrival of a reflected wave can be identified on the pressure waveform. It is recognized as an inflection (P_i) in the pressure curve and can occur before or after the peak systolic pressure. The augmentation index (AIx) is a surrogate of wave reflections based on the inflection point of the pressure waveform. As illustrated in figure 2.12, the AIx can be calculated in two different ways: either as the ratio of augmented pressure (AP) and pulse pressure (PP), or as the ratio of P2 and P1. Depending on which one occurs first, P1 and P2 are the pulse pressure and the pressure at the inflection point minus diastolic pressure. When the reflected wave arrives before peak systole, a so-called A-type (aged) waveform is obtained where the peak systolic pressure is increased or 'augmented' by the wave reflection. In this case, augmented pressure is positive (as is AP/PP), and P1 equals the pressure at the inflection point while the pulse pressure is P2. In the case of a reflection after peak systole, a so-called C-type (control) waveform is obtained where the systolic pressure is not

augmented, AP/PP is negative and P1 now equals the pulse pressure whereas the pressure at the inflection point is P2. The augmentation index can be calculated on the carotid, radial or synthesized aortic pressure waveforms. An important drawback of this index is its dependence on both the timing and the magnitude of wave reflection.

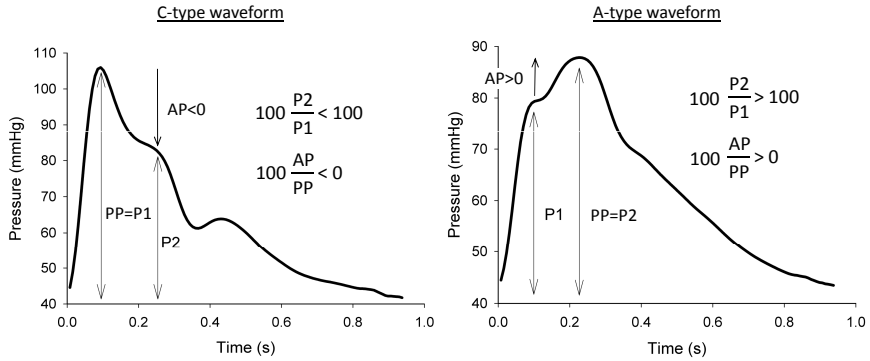

Figure 2.12: Augmentation index defined as 100P2/P1 or 100AP/PP for C-type (left) and A-type waveforms (right). AP=augmented pressure, PP=pulse pressure, P1 and P2 are the pulse pressure and the pressure at the inflection point or vice versa, depending on which one occurs first [40].

Clinical relevance

The augmentation index is the most widely used index of wave reflections. This is mainly due to the availability of relatively inexpensive applanation tonometry systems allowing for reliable non-invasive assessment of the pressure waveform. Following a recent meta-analysis of 11 longitudinal studies, central AIx, calculated on synthetized aortic waveforms, has a significant predictive value of CV events and all-cause mortality, independent of blood pressure and heart rate [83]. Though carotid AIx can be used as a surrogate for central AIx, radial AIx was shown to correlate better with central AIx [84]. Furthermore, the radial inflection point was shown to correspond with the central SBP, rendering radial AIx even more relevant [85].

However, the augmentation index is a composite measure, and although it is related to wave reflection, it is obvious that other factors co-determine its value [86]. One major problem is that the AIx loses sensitivity around the age of 60, where it levels off to a plateau value of 30%, as shown in figure 2.13. This is a bad feature of an index intended for clinical purposes as the majority of subjects suffering from hypertension is older than 60 [87].

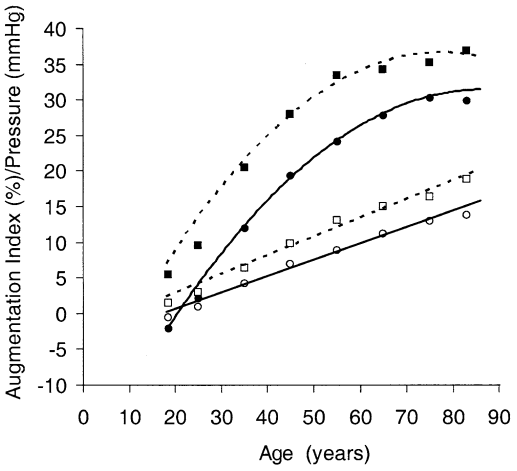

FIGURE 2.13: Evolution of augmentation index (closed circles for males, closed squares for females) and augmented pressure (open circles for males, open squares for females) with age [40]. Data points are the group means for each decile of age.

2.4.2 Wave separation via impedance analysis

Definition

First introduced by Westerhof [19], impedance analysis is performed in the frequency domain, through Fourier-transformation of the pressure and flow waveforms. Therefore, the equations below should be applied for each individual harmonic of pressure and flow. Though Fourier-decomposition of a signal theoretically results in an infinite number of harmonics, in practice, the first 10 to 15 harmonics suffice to reliably describe the pressure and flow waveforms [88].

It is assumed that the pressure and flow harmonics are the sum of a forward and a backward component:

$$P = P_{n,f} + P_{n,b} \tag{2.5}$$

$$Q = Q_{n,f} + Q_{n,b} \tag{2.6}$$

The characteristic impedance (Z_c) relates forward (backward) pressure with forward (backward) flow harmonics:

$$P_{n,f} = Z_c Q_{n,f} \tag{2.7}$$

$$P_{n,b} = -Z_c Q_{n,b} \tag{2.8}$$

The minus sign in the relation for reflected waves results from the fact that flow, compared to pressure, is directional: positive for blood flowing away from the heart and negative for blood flowing towards the heart.

Combining the above equations, each individual harmonic n of the forward and backward waves can be calculated as:

$$P_{n,f} = \frac{P_n + Z_c Q_n}{2} \tag{2.9}$$

$$P_{n,b} = \frac{P_n - Z_c Q_n}{2} \tag{2.10}$$

The complete forward and backward pressure and flow waves can then be reconstructed from these harmonics.

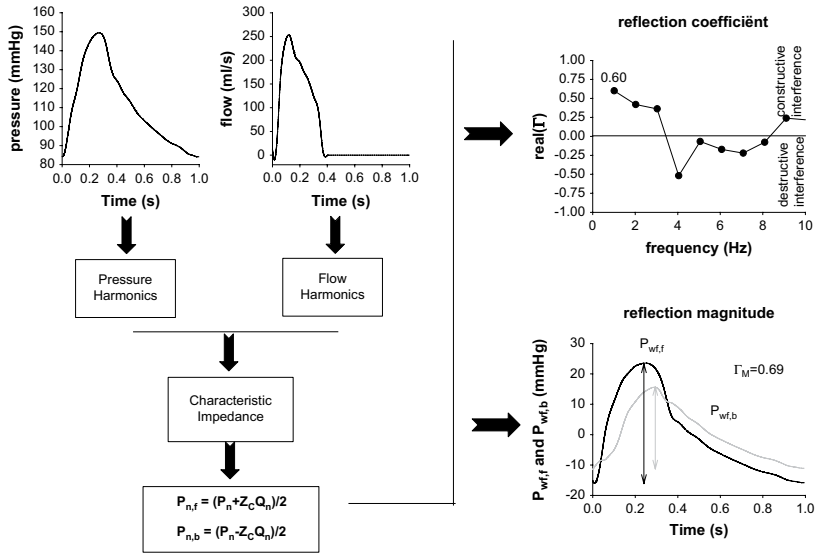

Figure 2.14: Schematic representation of the frequency domain method. Measured pressure and flow are decomposed in a series of harmonics, from which the characteristic impedance (Z_c) is calculated. For each harmonic, the forward and backward component is calculated, which can be used to display the (real part) of the reflection coefficient as a function of frequency. Alternatively, the reflection magnitude can be calculated from the ratio of the amplitudes of the reconstructed forward and backward waves [87].

The amount of wave reflection can be quantified in a number of ways. The *reflection coefficient* (Γ) is obtained as the ratio of the backward and forward waves: $P_{b,n}/P_{f,n}$ for each harmonic n, and thus consists of an amplitude and a phase per harmonic. An elegant way to interpret the reflection at a given location and a given frequency is to express the real part of Γ per harmonic, as illustrated in figure 2.14. A positive real part of Γ indicates constructive interference, while a negative value indicates destructive interference.

Two other reflection indices are based on the global forward and backward wave: the *reflection index (RI)* is defined as the ratio of the amplitudes of the

backward wave and the sum of the forward and backward waves $\frac{|P_b|}{|P_f|+|P_b|}$, while the *reflection magnitude (RM)* expresses the ratio of the amplitude of the backward and the forward wave: $\frac{|P_b|}{|P_f|}$ (see also figure 2.14).

Clinical relevance

Theoretically, pressure and flow should be measured simultaneously at the same location, immediately distal to the aortic valve. In practice, this is only feasible in invasive studies. For most non-invasive studies, carotid pressure is used as a surrogate for aortic pressure. When combining pressure and flow, it is important to align both signals in time in order not to introduce phase errors upon Fourier-decomposition. Furthermore, for the sake of simplicity, the separation of pressure and flow is often performed in the time domain by approximating Z_c by the average of $|P_n|/|Q_n|$ from the 4th to the 10th harmonic [5].

A number of large-scale studies have reported on reflection magnitude and reflection coefficient. Mitchell *et al.* showed that RM as well as AIx were elevated in subjects with systolic hypertension [89]. In an apparently healthy population of middle-aged community-dwellers, Segers *et al.* [86] found a high correlation (R=0.78) between the reflection magnitude and Γ_1, the amplitude of the reflection coefficient at the heart frequency, but a markedly lower correlation between AIx and either of these indices (R<0.6). Between the age of 35 and 55, all three indices of wave reflection increased significantly. However, unlike for AIx, which is systematically higher in women than in men, no gender difference in Γ_1 or RM was observed.

2.4.3 Wave separation via intensity analysis

Definition

Although impedance analysis allows a more accurate study of wave reflections compared to wave shape analysis, the analysis in the frequency domain is less intuitive and quantification of the amount of wave reflection is hampered by the fact that both the amplitudes and the phases have to be taken into account. As an alternative approach, Parker and Jones introduced the wave intensity analysis, which allows to separate pressure and flow in the time domain [90].

Instead of decomposing the pressure and flow waveforms into sinusoidal components, wave intensity analysis considers the arterial pressure and flow velocity waveforms to consist of a summation of infinitesimal 'wavelets' or 'wavefronts'. Wave intensity (dI) is defined as

$$dI = dP \cdot dU \qquad [W/m^2], \tag{2.11}$$

where dP is the change of pressure across a wavefront and dU is the change in velocity across a wavefront.

The wave intensity represents the energy flux carried by the wavefront. dI is positive for forward (+) traveling wavefronts and negative for backward (-) traveling wavefronts. This holds for both compression (dP>0) and expansion (dP<0) waves. When there are simultaneous forward and backward waves in the artery, the wave intensity is the algebraic sum of the wave intensities of the two wavefronts intersecting at the measurement site at the time of measurement. The sign of the net wave intensity therefore immediately reveals whether the forward or the backward waves are dominant, as illustrated in figure 2.15.

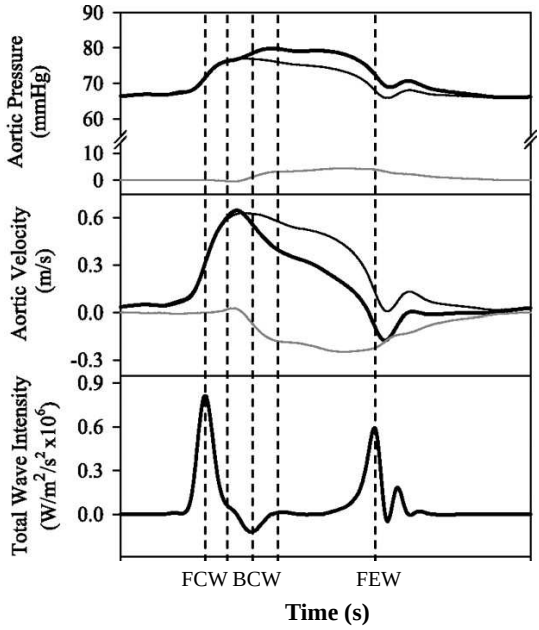

Figure 2.15: Illustration of the wave intensity analysis method. Measured aortic pressure and flow wave (bold line) are separated in their forward (thin line) and backward (grey line) components. Total, forward and backward wave intensity are calculated. FCW: forward compression wave, BCW: backward compression wave, FEW: forward expansion wave [91].

dP and dU are connected via the water hammer equation:

$$dP_{\pm} = \rho c \, dU_{\pm} \tag{2.12}$$

with ρ the blood density and c the local wave speed. Assuming the wavefronts to be additive so that dP = $dP_+ + dP_-$ and dU = $dU_+ + dU_-$, these equations can be rearranged in terms of the forward and backward pressure wavefronts

$$dP_+ = (dP + \rho c \, dU)/2 \tag{2.13}$$

$$dP_- = (dP - \rho c\, dU)/2. \tag{2.14}$$

The corresponding changes in the velocity can be found as

$$dU_+ = (dP + \rho c\, dU)/2\rho c \tag{2.15}$$

$$dU_- = -(dP - \rho c\, dU)/2\rho c. \tag{2.16}$$

The total forward (backward) pressure wave can be obtained by summing all forward (backward) wavefronts

$$P_+ = P_{dia} + \sum_{i=0}^{t} dP_{i+} \tag{2.17}$$

$$P_- = \sum_{i=0}^{t} dP_{i-} \tag{2.18}$$

with P_{dia} the diastolic blood pressure.

Likewise, the forward and backward velocity waves are obtained as

$$U_+ = \sum_{i=0}^{t} dU_{i+} \tag{2.19}$$

$$U_- = \sum_{i=0}^{t} dU_{i-} \tag{2.20}$$

Thus, in order to separate pressure or flow into its forward and backward components, one needs a pressure and a flow wave at one location as well as the local wave speed. This implies that the wave speed measured by the foot-to-foot method (see section 2.3.2) cannot be used in wave intensity analysis, as it is a weighted average of the wave speed between the measurement sites rather than a local wave speed. Local wave speed can be obtained from measured pressure and velocity waveforms using the water hammer equation. In early systole, reflections are assumed to be minimal, so the slope of the P-U loop, the curve obtained when plotting P versus U, equals ρc [92]. In practice, it appears that both impedance and wave intensity analysis give essentially identical results for the determination of the forward and backward waveforms [93].

Clinical relevance

Though wave intensity analysis allows to study local reflections by assessing the change in impedance, it is only the quantification of the overall wave reflections through a global reflection coefficient that has clinical relevance. Therefore, the use of wave intensity analysis in clinical studies lies more in facilitating the interpretation of data or observed phenomena, as it is possible to follow individual waves as they reflect and rereflect within the arterial system [92].

2.5 The Asklepios study

From the above described methods and concepts, it is clear that quantification of arterial wave reflections and arterial stiffness requires the assessment of pressure, flow and/or diameter distension waveforms at different arterial locations. Since these measurements are not (yet) performed in routine daily clinical practice, it is not obvious to obtain such data, surely not at a large scale. Fortunately, the data gathered during the Asklepios study provided a rich source of information that was gratefully used for a number of methodological studies during this PhD.

The Asklepios study is a longitudinal population study focusing on the interplay between aging, cardiovascular hemodynamics and inflammation in (preclinical) cardiovascular disease [94]. The first round was conducted between 2002 and 2004 and included 2524 participants (1301 women), aged 35 to 55 years. Participants were randomly sampled from the twinned Belgian communities of Erpe-Mere and Nieuwerkerken and were free from overt cardiovascular disease at study initiation. All measurements were performed by the same operator. Next to basic clinical data and advanced biochemical analysis, the study has a strong biomechanical component. Both cardiac and vascular structure and function were assessed in detail. Carotid and femoral arteries were scanned for the presence of plaques and the intima-media thickness of both arteries was assessed in high and low shear regions. Flow and diameter distension waveforms were assessed at the carotid and femoral arteries using a Vivid 7 ultrasound scanner (GE Vingmed Ultrasound, Horten, Norway). Pressure waveforms were obtained at the brachial, radial, carotid and femoral arteries using a high-fidelity strain gauge sensor (Millar SPT 301, Millar Instruments, Houston, Texas, USA) and a custom-built acquisition platform.

Two

Validation and development of new methods

CHAPTER 3

Outline

The analysis of wave reflections and arterial stiffness has increasingly gained attention over the last 15-20 years and is now in the transition between clinical research and clinical practice, as illustrated by the inclusion of PWV as a marker of subclinical organ damage in the 2007 ESC/ESH[1] guidelines [26].

With regard to this anticipated introduction in clinical practice, the focus in assessing arterial stiffness and wave reflections has shifted from an accurate, complete characterisation as (should be) used in clinical research to a more pragmatic compromise between accuracy and time- and cost-effectiveness of the measuring technique.

This second part of this PhD-dissertation describes four studies on either the development or the validation of a new method to quantify arterial stiffness or wave reflections:

Chapter 4 details the results of a validation study in which an approach of wave separation based on a measured pressure waveform and an estimated (triangular) flow waveform is compared to the more traditional approach of wave separation using a measured pressure and flow waveform. Though approximative, this new approach has the advantage of bypassing the often expensive and time-consuming assessment of an aortic flow waveform. The approach was recently introduced by Westerhof et al. [95] to estimate reflection magnitude, with promising results in a small dataset. Qasem et al. [96] used the same approach to derive pulse transit time and aortic pulse wave velocity from a central

[1]ESC: European Society of Cardiology; ESH: European Society of Hypertension

pressure waveform. We verified these approximation techniques for reflection magnitude and transit time using carotid pressure and aortic flow waveforms measured non-invasively in the Asklepios study and explored the accuracy of approximating the flow waveform by using a person-specific time-scaled normalized average flow waveform.

Chapter 5 relates to the non-invasive assessment of carotid artery pressure waveforms. Calibration of the carotid tonometric curve is based on brachial DBP and MAP, the latter ideally obtained as the arithmetic average of the brachial pressure waveform. Therefore, proper non-invasive assessment of carotid artery pressure ideally uses waveforms recorded at two anatomical locations: the brachial and the carotid artery. As tonometry recordings are difficult to obtain in obese patients, the use of calibrated diameter distension waveforms could provide a more widely applicable alternative for local arterial pressure assessment than applanation tonometry. This approach might be of particular use at the brachial artery, where the feasibility of a reliable tonometric measurement has been questioned. The aim of this study was to evaluate an approach based on distension waveforms obtained at the brachial and carotid arteries. This approach will be compared to traditional pulse pressures obtained through tonometry at both the carotid and brachial arteries (used as a reference) and the more recently proposed approach of combining tonometric readings at the brachial artery with linearly or exponentially calibrated distension curves at the carotid artery.

Chapter 6 focuses on the impact of radial artery waveform calibration on central blood pressure assessment and calculated pressure amplification. Central blood pressure can be estimated from radial artery pressure waveforms using a generalized transfer-function. However, the obtained central pressure waveform depends on the calibration of the radial waveform. In this study, three calibration methods are compared using the radial and carotid tonometric waveforms acquired in the Asklepios study: calibration using brachial artery DBP and (i) brachial SBP, (ii) MAP estimated with the one-third rule and (iii) MAP estimated as 40% of brachial artery pulse pressure.

In *chapter 7*, the determinants of a newly proposed stiffness index, the Ambulatory Arterial Stiffness Index (AASI) are explored using a previously validated 1D computer model of the arterial circulation [97]. Based on 24-hour ambulatory blood pressure recordings, the AASI is calculated as one minus the slope of the linear regression line between systolic and diastolic blood pressure values [98, 99] and thus does not require the recording of a pressure, flow or diameter distension waveform. Although appealing because of its simplicity, it requires 24-hour blood pressure recordings and there is controversy as to which extent it reflects stiffness or is affected by other cardiovascular parameters. We

assessed the relative importance of five parameters (arterial distensibility, peripheral resistance, heart rate, cardiac contractility and venous filling pressure) on the AASI by varying each parameter from 80 to 120% of its initial value in steps of 10% to mimick the daily fluctuations in one theoretical, normotensive subject. To assess the ability of AASI to detect large changes in stiffness, two additional subjects were simulated with a distensibility of 50% and 25% of the default distensibility, respectively.

CHAPTER 4

Evaluation of non-invasive methods to assess wave reflection and pulse transit time from the pressure waveform alone

The results of this study were published in:
Jan G. Kips, Ernst R. Rietzschel, Marc L. De Buyzere, Berend E. Westerhof, Thierry C. Gillebert, Luc M. Van Bortel, Patrick Segers. *Evaluation of Noninvasive Methods to Assess Wave Reflection and Pulse Transit Time From the Pressure Waveform Alone.* Hypertension 2009, 53:142-149.

4.1 Introduction

The pressure wave can be considered as the composite of a forward pressure wave, travelling from the heart to the periphery, and of a reflected pressure wave, travelling backward towards the heart. Early return of this reflected wave boosts (central) systolic blood pressure, increasing the load on the heart and boosting the amplitude of the pressure wave, factors that have been shown to increase cardiovascular risk [100–103]. Therefore, analysis of pulse wave velocity and pressure wave reflection have been of clinical interest for many years now.

Several methods to quantify wave reflection emerged [55], the most widespread probably being the augmentation index (AIx) [104, 105]. AIx is a parameter

based on analysis of the pressure waveform, and expresses the ratio of augmented pressure (attributed to wave reflection) to pulse pressure. However, because several factors influence its value [40, 95, 106, 107], AIx might not be the most appropriate parameter for an accurate quantification of the magnitude of wave reflection [108].

More accurate methods to assess wave reflection are based on wave separation analysis [4, 19]. These methods are based on measurement of pressure and flow, ideally measured simultaneously and at the same anatomical location, preferentially the central aorta [54]. Although approximated approaches, based on aortic flow and carotid [94] or subclavian [109] pressure measurements are feasible, implementation of these extended measurement protocols in a clinical setting is not evident. In an attempt to merge the benefits of a method based on measurement of pressure waveform alone, and of the wave separation analysis, Westerhof *et al.* recently advocated a new method, where the flow wave is approximated by a triangle. Their analysis yields an approximation of the reflection magnitude (RM), the ratio of the amplitude of the reflected to the forward wave. The method was found to give promising results, but the initial study was, overall, based on a relatively low number of data-sets (29 beats of 19 humans) [95].

In recent work, Qasem and co-workers proposed a new method of deriving pulse transit time and aortic pulse wave velocity from a central pressure waveform. The method is based on assessing the time delay between the forward and backward pressure component, decomposed from a central pressure waveform. The triangular flow wave approximation is used for pressure wave decomposition. Linear regression between calculated and measured carotid-femoral pulse transit time showed promising results in a cohort of 46 subjects [96].

The objective of this study is threefold: (i) to verify the triangular flow wave approximation method and the assessment of the reflection magnitude as proposed by Westerhof *et al.*; (ii) to verify the assessment of aortic pulse wave velocity from a single pulse recording as proposed by Qasem et al.; (iii) to explore the possibility of approximating the flow wave by using a person-specific time-scaled normalised average flow waveform and to assess its impact on the estimates of reflection magnitude and pulse wave velocity.

4.2 Materials and methods

4.2.1 The Asklepios population

A total number of 2325 datasets including non-invasive aortic flow and carotid artery pressure measurements recorded within the framework of the Asklepios Study [94] are used. Carotid pressure waveforms were obtained using applanation tonometry at the left common carotid artery, following an earlier described calibration scheme based on brachial artery tonometry [61, 94]. The aortic flow

waveform was assessed using pulsed Doppler ultrasound (Vivid7, GE Vingmed Ultrasound) in the left ventricular outflow tract (LVOT). Carotid-femoral pulse wave velocity (PWV) was measured by Doppler ultrasound flow measurements in the femoral and carotid artery, respectively. Details on the study protocol and specifications of the measurement techniques and pressure and flow wave processing are found elsewhere [107].

4.2.2 Triangular waveform construction

Following Westerhof *et al.* [95], a triangular flow waveform (Q^{tri}) was constructed. Whereas the authors of that study obtained timing information from the pressure waveform, we approximated the flow using timing information for start, peak and end of flow from the measured flow waveform itself. By doing so, we can evaluate the isolated effect of the triangular shape approximation, independent of errors introduced via the assessment of the timing from the pressure waveform. As such, these results can be considered as the best possible results that can be obtained with a triangular approximation of the flow waveform.

The root mean square error (RMSE) between the approximated flow waveform and the measured one is calculated and expressed as mean (SD).

4.2.3 Linear wave separation analysis and derived parameters

Using flow and pressure, forward (P_f) and backward (P_b) pressure waveforms were calculated using the linear wave separation technique as first described by Westerhof *et al.* [19]. The forward and backward pressure waveforms derived using the measured flow serve as a reference. Agreement between the approximated (derived using approximated flow) and reference forward (and backward) pressure waveform is assessed by calculating the RMSE between the two waveforms. The amplitudes of the approximated forward ($|P_f^{approx}|$) and backward ($|P_b^{approx}|$) pressure waves are compared to the reference forward ($|P_f^{ref}|$) and backward ($|P_b^{ref}|$) pressure wave amplitudes via linear regression analysis (R^2-values) and their mean difference is displayed as mean (SD).

4.2.4 Reflection magnitude assessment

Reference (RM^{ref}) and approximated reflection magnitude (RM^{approx}) are calculated as the ratio of the amplitudes of backward and forward pressure wave: $RM^*=|P_b^*|/|P_f^*|$, with * referring to either the reference or the approximation. Agreement between reference and approximation was studied via linear regression analysis (R^2-values) and Bland-Altman analysis. In addition, we also calculated the augmentation index (AIx) as a measure of wave reflection. We refer to previous work [107] for a description of how AIx was derived.

4.2.5 Pulse wave velocity assessment: time delay between P_f and P_b

To assess the time delay between P_f and P_b, Qasem *et al.* proposed to first modify the pressure waveforms [96] using three criteria:

- $dP_b(t)/dt=0$ $\quad 0 \leq t \leq$ peak flow
- $dP_f(t)/dt<0$ $\quad$ peak flow $\leq t \leq$ end ejection
- $P_f+P_b=P$ $\quad$ at all times

We refer to Qasem *et al.* for details on these assumptions [96]. Basically, it is assumed that the forward pressure wave reaches its peak at the moment of peak flow. The backward pressure wave arrives at the moment of peak flow and only plays a role from that moment on (figure 4.1).

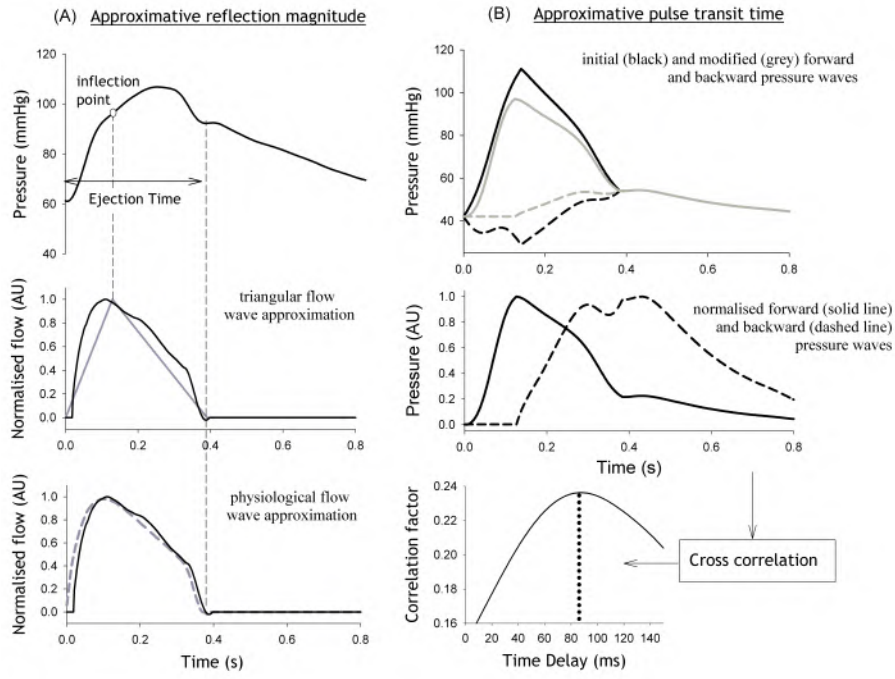

Figure 4.1: (A) Triangular and averaged flow waveform approximation principle. The triangular flow waveform is constructed based on timing of beginning, peak and end of the measured flow waveform. The averaged physiological flow waveform is constructed using measured flows of 74 subjects and stretched in time based on timing of the beginning and end of the measured flow waveform. (B) Pulse transit time (TT) approximation principle, applied with triangular flow waveform. Forward and backward pressure components are modified (see text for modification criteria). Cross-correlation is performed on normalised pressure components. Aortic TT is estimated as half of the time lag at maximum correlation.

After normalization of the modified forward and backward pressure waveforms, the time lag between P_f and P_b was obtained using cross-correlation

techniques, assuming that the correct time-lag is the value for which there is maximum cross-correlation [110] between the two normalized waveforms. Following Qasem *et al.* [96], the pulse transit time (TT) is obtained as half of the time lag.

This method was applied using either the measured flow waveform (Q^{meas}) or the approximated waveform (Q^{tri}). Transit times obtained from these approaches are indicated as TT*, with * referring to either the measured approach or the approximative approach. TT^*s were also compared to the carotid-femoral pulse transit times measured by Doppler ultrasound (TT^{ref}), which serve as a reference here.

4.2.6 Averaged physiological flow waveform

In a third part of this study, approximation via triangular flow waveform profiles was left aside, and the analysis (assessment of RM and TT) was repeated by using a more physiological flow waveform (Q^{avg}) obtained from normalising and averaging measured flow waveforms. Using data from 74 subjects (32 women, 42 men; 3.1 % of the total database), the average flow waveform was calculated after normalising each individual flow curve in time and amplitude. The physiological waveform is mathematically described as a Fourier-series using the first 20 harmonics. The subjects used to construct the physiological flow waveform were subjects where aortic flow was available, but where other data were missing due to various technical reasons. To approximate the actual flow waveform, the averaged and normalised waveform was scaled in time using the timing of beginning and end of each individual measured flow waveform.

4.2.7 Synthesized aortic pressure

The analysis (assessment of RM and TT) was repeated by using synthesized aortic instead of carotid pressure, obtained from radial tonometry via a generalized pressure transfer function [111].

4.3 Results

Basic population and hemodynamic data are given in table 4.1. The mean age of the subjects (1209 women, 1116 men) was 46 years, ranging from 35 to 55 years. A total number of 651 subjects with hypertension was included, of whom 237 were under drug treatment.

4.3.1 Triangular and averaged flow waveform approximation

Table 4.2 gives an overview of the impact of the different flow waveform approximations on the forward and backward pressure waveforms and derived parameters. The RMSE between approximated and measured flow waveform decreases markedly from the triangular (0.12) to the averaged waveform approximation (0.04). Note that these errors are based on a normalised peak flow of 1.0, i.e. the minimal error is 4%.

Table 4.1: Basic clinical data.

Parameter	Data
No. of subjects	2325
Age (years)	45.9 (6.0)
BMI (kg/m^2)	25.6 (4.1)
Systolic BP (mmHg)	127.0 (14.0)
Diastolic BP (mmHg)	80.0 (10.0)
Heart rate (bpm)	63.6 (9.4)

Data are presented as mean (SD) unless otherwise specified. BMI indicates body mass index.

Table 4.2: Approximation errors on flow and forward and backward pressure.

		Flow waveform	
Variable	Measured (Q^{ref})	Triangular (Q^{tri})	Averaged (Q^{avg})
RMSE Q, AU	NA	0.12 (0.02)	0.04 (0.03)
Accuracy of estimating forward component			
RMSE P_f, AU	NA	2.38 (1.50)	1.08 (0.82)
$\lvert P_f \rvert$, mmHg	42.61 (9.45)	48.46 (12.89)	42.60 (9.49)
$\lvert P_f \rvert^{approx}$-$\lvert P_f \rvert^{ref}$, mmHg	NA	5.84 (7.18)	-0.01(3.19)
R^2 approx vs ref	NA	0.70	0.89
Accuracy of estimating backward component			
RMSE P_b, AU	NA	2.38 (1.50)	1.08 (0.82)
$\lvert P_b \rvert$, mmHg	20.22 (5.35)	23.18 (7.65)	20.35 (5.35)
$\lvert P_b \rvert^{approx}$-$\lvert P_b \rvert^{ref}$, mmHg	NA	2.97 (5.59)	0.13 (1.88)
R^2 approx vs ref	NA	0.47	0.88

Q indicates flow; $\lvert P_f \rvert$, amplitude of the forward pressure component P_f; $\lvert P_b \rvert$, amplitude of the backward pressure component P_b; ref, reference; approx, approximate; AU, arbitrary units. Data for RMSE and pressure amplitudes are expressed as mean (SD).

4.3.2 Agreement between approximated and reference reflection magnitude

The RMSE between the approximated and reference forward pressure waves varied between 1.1 mmHg (averaged waveform) and 2.4 mmHg (triangular waveform). Regression analysis between the amplitudes of the approximated forward and backward pressure waves and the reference waves reveals that the highest correlations are found for the averaged waveform. Also, the mean difference $\lvert P_f \rvert$-$\lvert P_f \rvert^{ref}$ (or $\lvert P_b \rvert$-$\lvert P_b \rvert^{ref}$) is smaller when using the averaged waveform, see table 4.2.

Mean reference RM was 0.48 (0.09), while mean RM for triangular and averaged flow waveform were 0.48 (0.10) and 0.48 (0.09), respectively. Figure 4.2 shows the results of the linear regression and Bland-Altman analysis between approximations of RM and RM^{ref}. Bland-Altman analysis shows a constant mean difference around zero for both flow approximations, with a tighter dispersion around the mean when the averaged waveform is used.

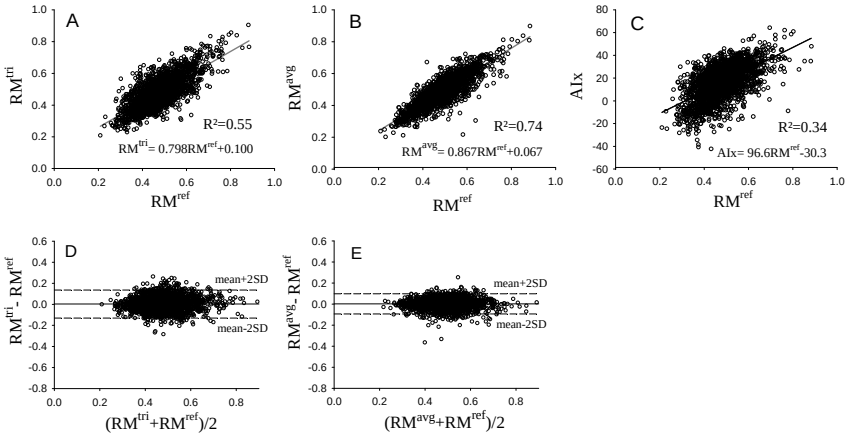

FIGURE 4.2: Panel A-B: Linear regression plots between approximated and reference reflection magnitude (RM). Trend line equations and R^2-values are reported. Panel D-E: Bland-Altman plots between approximations of RM and RM^{ref}. Mean value (solid line) and mean±2SD (dashed lines) are displayed. Panel C shows the relation between augmentation index (AIx) and RM^{ref}. RM^{tri} and RM^{avg} are approximations of RM using triangular flow and averaged flow respectively, whereas RM^{ref} is the reference RM using measured flow.

4.3.3 Agreement between approximated and measured pulse transit time

Pulse transit time (carotid-femoral) measured directly with ultrasound (TT^{ref}) was 67.8 (11.9) ms, while 77.9 (23.3) ms was the mean pulse transit time found based on the principle of wave decomposition using the measured pressure and aortic flow (TT^{meas}). When using a triangular flow approximation, estimated pulse transit time (TT^{tri}) was 72.5 (14.8) ms, whereas the averaged flow approximation yielded a TT^{avg} of 75.9 (20.1) ms. The best agreement between the TT estimated using the measured and either of the approximated flow waveforms was found when using the averaged flow waveform (TT^{avg} ; R^2=0.82). However, when studying the relation between TT^{approx} and TT^{ref}, R^2-values were not higher than 0.28 (figure 4.3). Interestingly, also the agreement between TT^{meas} and TT^{ref} was weak (R^2=0.27, figure 4.3). Bland-Altman plots show a strong trend of overestimation towards higher TT-values for all cases (figure 4.3).

4.3.4 Synthesized aortic pressure

Using synthesized aortic pressure instead of carotid pressure waveforms for the calculation of RM (figure 4.4), agreement ranged from R^2=0.66 (triangular flow) to R^2=0.79 (averaged flow). Transit times were also recalculated using aortic pressure, yielding levels of agreement below R^2=0.13 for both flow waveforms, see figure 4.4.

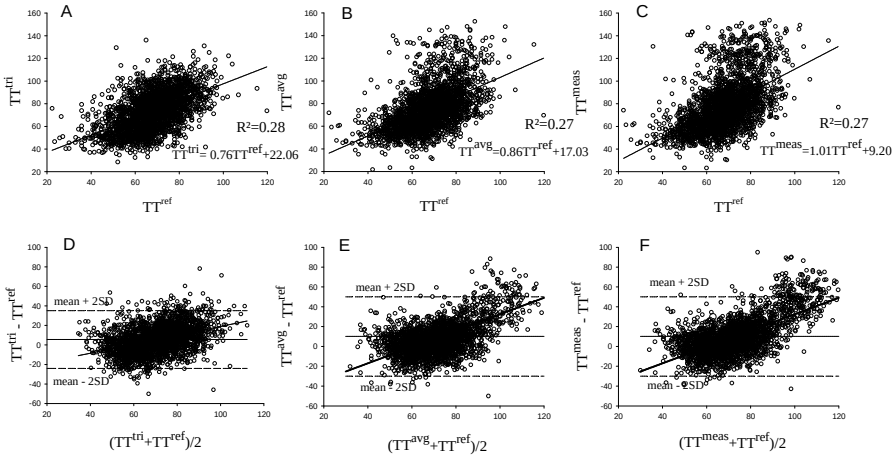

Figure 4.3: Panel A-C: Linear regression plots between approximated and reference pulse transit time (TT). Trend line equations and R^2-values are reported. Panel D-F: Bland-Altman plots between approximations of TT and TT^{ref}. Mean value (solid line) and mean±2SD (dashed lines) are displayed. TT^{tri} and TT^{avg} are approximations of TT using triangular flow and averaged flow respectively, TT^{meas} uses measured flow, whereas TT^{ref} is obtained via the carotid-femoral pathway via Doppler ultrasound.

4.4 Discussion

We applied the triangular flow wave approximation method to estimate reflection magnitude as proposed by Westerhof *et al.* [95], on 2325 non-invasively recorded data sets, consisting of carotid artery pressure and aortic flow waveforms. Despite the fact that we used timing information directly from the measured flow waveforms, the correlation that we found between approximated and actual RM for the triangular flow wave approximations (R^2 = 0.55) is still considerably lower than the values reported by Westerhof *et al.*(R^2 = 0.79 - 0.85). When approximating the flow wave by a subject-specific time-scaled averaged physiological flow waveform, the correlation between approximated and actual RM improved substantially (R^2 = 0.74).

A first issue that needs to be addressed is the question how well the flow waveforms are actually described by a triangle. It is seen from table 4.2 that the triangular approximation yields a RMSE from the measured flow waveform of 0.12, which is three times higher than the value of 0.04 that can be achieved when using a more physiological waveform. Another observation is that, using a triangular flow, the agreement between approximated and actual RM only reached an R^2-value of 0.55, which is still considerably lower than the values

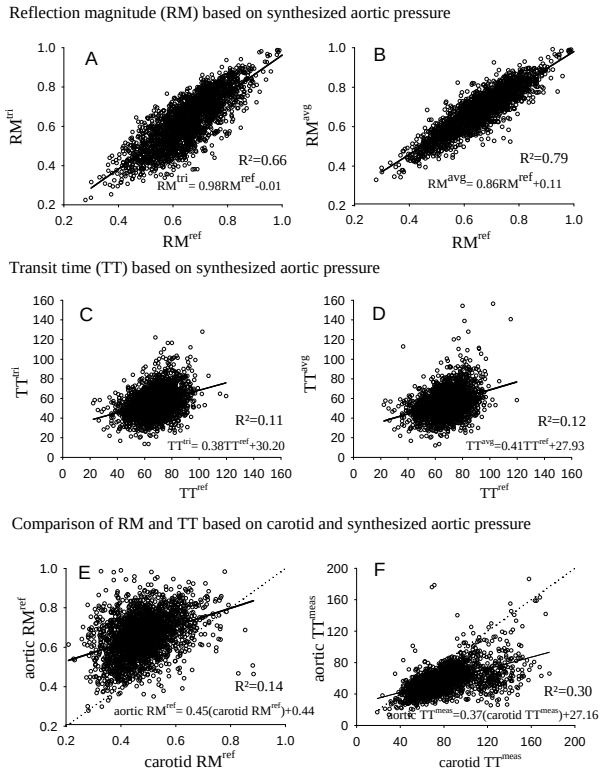

FIGURE 4.4: Panel A-B: Linear regression plots between approximated and reference reflection magnitude (RM), both based on synthesized aortic pressure waveforms. Panel C-D: Linear regression plots between approximated and reference pulse transit time (TT). Panel E-F: Comparison between RM (TT) obtained using carotid pressure and synthesized aortic pressure. The dotted line represents the line of identity. Trend line equations and R^2-values are reported.

reported by Westerhof *et al.* These observations indicate that, at least in our setting, the triangle is a relatively poor approximation of the measured waveforms, which is the main reason for the discrepancy between our findings and those of Westerhof *et al.*

A logical subsequent question is why the triangle is a poorer approximation in this study. A first possible reason can be sought in the different nature of the population. Westerhof *et al.* used a mixed population of 19 subjects, age ranged from 29 to 57 years, with a mean age of 50 years, with data obtained from various sources, including digitised data. All subjects underwent catheterization and were patients. The examples displayed in the manuscript show a more triangular pattern than the waveforms that we measured in our middle-aged, healthy subjects. It is further clear from their figures that mean RM is in the range of 0.6-0.7, which is substantially higher than the value of

0.48 in our study. To assess the impact of RM on the morphology of the measured flow waves, we also calculated averaged, normalised flow waveforms for the database, with subjects grouped into four strata of values of RM (data not shown). The effect of increased RM on the flow wave morphology is a slight shift of the peak to the left, but there is no real better resemblance with a triangular waveform for the higher RM. A second possible reason can be sought in methodological differences between the two studies. The flow waveforms as used by Westerhof *et al.* were aortic flow velocity waveforms, measured with an invasively applied electromagnetic flow velocity sensor, while we used flow velocity waveforms measured using ultrasound in the left ventricular outflow tract. Ultrasound data were measured by an experienced cardiologist following best practice guidelines. On the other hand, literature sources state that both techniques are equivalent [112, 113]; so it is unclear whether the method used to acquire the flow does play a role in our findings.

In an attempt to increase the levels of correlation reported thus far for approximated RM, we tested a new approximation principle, based on an averaged and normalised aortic flow waveform. As clear from table 4.2 and figure 4.2, using an averaged physiological waveform performs significantly better in estimating RM than using a triangular flow waveform. As for the triangular approximations, there is no systematic difference between RM^{avg} and RM^{ref}, as evident from the Bland-Altman plot (figure 4.2).

Another possible reason for the low levels of correlation can be sought in the fact that the pressure waveforms as used by Westerhof *et al.* were not carotid waveforms, but invasively measured aortic waveforms [95]. Although carotid pressure is generally accepted as a surrogate for central aortic pressure, we calculated RMs based on synthesized aortic pressure waveforms to assess whether this methodological difference could possibly explain the different results, but could not find important qualitative differences. Compared to the corresponding values using carotid pressure waveforms, agreement between RM calculated with the measured and approximated flow waveforms was slightly better when using synthesized aortic pressure. On the other hand, agreement between estimated and measured pulse transit times using synthesized pressure waveforms was lower than the corresponding values using carotid pressure.

Interestingly, the agreement between RM obtained using the carotid on the one hand and synthesized aortic waveforms on the other hand, both using the measured flow waveform, showed only poor correlation (R^2=0.14), see figure 4.4. Our data do not allow to address which of the two pressure waveforms, the carotid or reconstructed radial pressure waveform, is closest to the actual central aortic pressure. Nevertheless, it is an important finding that derived parameters, sensitive to wave morphology, can be quite different when using carotid or reconstructed pressure waveforms. This was earlier demonstrated for the augmentation index [84], but this conclusion also seems to pertain to estimates of the RM.

The two reported approximations, RM^{tri} and RM^{avg}, can be considered as the best possible approximations in terms of timing, as they make use of the actual timing of beginning, peak and end of the measured flow to construct an approximated flow waveform. As such, they indicate the theoretical potential of the approximation technique. It is therefore also important to determine the further degradation in accuracy when timing information is obtained from the pressure waveform. An averaged flow waveform was scaled in time, using the start of the systolic upstroke in the pressure waveform as the onset of flow, while the end of the ejection period was assumed to coincide with the dicrotic notch. In a similar way, a triangular flow waveform was constructed. To estimate the timing of the peak of the triangle, we used the timing of systolic blood pressure for waves with late inflection point (C-type waves), while the shoulder point was used for waves with an early inflection point (A-type waves), the shoulder point being identified with an algorithm based on the 4th-order derivative [107, 114]. RM was calculated, using each of these two flow waveforms, and compared to RM^{ref} (data not shown). As expected, the levels of agreement with RM^{ref} were markedly lower, with R^2-values of 0.26 for the triangular waveform, and 0.41 for the averaged waveform.

The main rationale to apply waveform decomposition with an approximated waveform is to find new ways to overcome some of the limitations of the augmentation index, which is an index related to wave reflection but subject to confounding factors such as heart rate and body length. As such, it is relevant to see to what extent these approximated methods provide an improvement over AIx in terms of correlation with RM^{ref}. In fact, we found that the correlation between AIx and RM^{ref} (R^2=0.34, see Figure 4.2) is only slightly worse than the correlation between RM^{ref} and RM^{tri}, and still higher than the decomposition based on the triangular approximation using timing info from the pressure waveform. As such, it is questionable whether these more complex methods offer, at this moment, any added value over AIx.

In a second part of this study, we evaluated a method to estimate pulse transit times from the time delay between the forward and backward pressure waveforms, as previously described by Qasem *et al.* [96]. The correlation we found between estimated and directly measured (carotid-femoral) transit times using approximated flow waveforms was rather limited (R^2<0.29), compared to the values reported by Qasem *et al.*(R^2=0.45-0.64), see figure 4.3. Following Qasem *et al.*, we assessed the time delay between the forward and backward wave using a cross-correlation technique. However, because cross-correlation can be problematic when the waveforms are dissimilar (and may thus be an underlying factor in the poor correlations we found), we tried to limit the cross-correlation to a 'window' around the peak of the modified forward and backward waveforms. Results, however, did not improve (data not shown). Other techniques to assess timing as foot-to-foot delays and the timing of the inflection and shoulder point did not lead to better results (data not shown).

Unlike Qasem *et al.* [96], we also estimated pulse transit times using the measured flow waveform instead of an approximated waveform. Interestingly, agreement with ultrasound-derived carotid-femoral transit times did not increase at all when using the measured flow waveform (figure 4.3). Moreover, Bland-Altman plots show a stronger increasing trend for TT^{meas} than for TT^{tri}. This seems to imply that the modification of the forward and backward pressure components is not appropriate when the measured flow waveform is used to separate pressure. Indeed, when calculating transit times without modifying the forward and backward pressure waveform, mean transit time is 71.2 (26.6) ms, which is closer to TT^{ref} (67.8 ms) than when using modified pressure components, although the agreement remains rather poor ($R^2 = 0.22$). This seems to suggest that methods based on wave decomposition generally perform poorly in estimating transit time. This is in line with recent work from Westerhof *et al.* [115], who demonstrated in a theoretical study that methods based on the time delay between the forward and backward pressure waves should not be used to assess pulse wave velocity. They showed that the moment of return of the reflected wave is not only determined by the wave speed and distance of travel but also by the time shift at the reflection site. As a result, with an assumed location of the reflection site, the PWV cannot be derived. Transit times derived from wave reflection analysis (TT^{meas}, TT^{tri}, TT^{avg}) depend on the pulse wave velocity, the location of reflection and the nature of the reflection [115]. On the other hand, TT^{ref}, measured along the carotid-femoral pathway, depends only on PWV. With increasing age, PWV increases, but it has also been reported that the reflection sites shift in a direction towards the heart [4, 107]. Therefore, in older people, we expect the TT from wave reflection analysis to become progressively lower than TT^{ref}. This is indeed confirmed by figure 4.3, and this phenomenon also explains the trend of overestimation of TT^{ref} for the higher TT-values. This shift of the reflection site towards the heart is not reported by Qasem *et al.* [96], where the effective length of the arterial tree seemed to increase with age, as also earlier reported by Mitchell [116]. We have previously suggested that this finding is related to the fact that identification of the moment of return of the reflected wave based on pressure waveform information (timing of shoulder or inflection point) alone is not accurate enough [107].

Although the mean age of the population in Qasem *et al.* was slightly higher (56±14 years) than ours, they were also healthy volunteers, making it unlikely that differences could be explained by the different nature of the study population. We used transit times measured with Doppler ultrasound as a reference, whereas Qasem *et al.* used tonometry to obtain carotid-femoral transit times. Although both techniques are accepted in literature to measure aortic PWV [55, 71], it is possible that the approximative method based on pressure waves as described by Qasem *et al.* will correlate better with a pressure-derived reference transit time than with a flow-derived transit time between the same anatomical

locations. A second methodological difference is the fact that Qasem *et al.* used synthesized aortic pressure waveforms instead of carotid waveforms. However, when assessing the impact of this methodological difference, we found the agreement between approximation and reference TT to be even lower, with R^2-values below 0.13. Similar as for RM, the agreement between TT obtained using the carotid on the one hand and synthesized aortic waveforms on the other hand, both using the measured flow waveform, yielded weak correlations, see figure 4.4.

4.5 Limitations

The main limitation of this study is that it is entirely based on non-invasively measured data which implies an approximation of the central aortic pressure waveform. Ideally also, pressure and flow are measured simultaneously and at the same anatomical location. For this study, pressure was measured non-invasively using applanation tonometry at the common carotid artery, while flow was measured at the level of the left ventricular outflow tract with Doppler ultrasound. Although carotid pressure is commonly used as a surrogate for central aortic pressure, both curves are not entirely equal, differing from each other in timing and in waveform. The time delay between aortic and carotid pressure waveform is corrected for by visual time-alignment. The difference in waveform persists, and may have an effect on the accuracy of timing approximations for beginning, peak and end of flow used for the flow reconstructions. One could therefore expect better correlations between approximated and actual RM when using invasively measured aortic pressure and flow waveforms, which might also contribute to the better results reported by Westerhof *et al.* In addition, the fact that the results based on the carotid waveforms and synthesized aortic waveforms correlate rather poorly, underlines the need for invasive data. Furthermore, the age range of our study population is rather narrow. This might be a reason why no significant age effects were noticed in the different RM approximation methods. It is also expected that the physiological flow waveform as assessed from this dataset will be less representative for subjects with age or clinical characteristics far beyond those of our Asklepios population.

4.6 Perspectives

Quantification of wave reflection by using a triangular flow wave approximation shows limited accuracy when applied to non-invasively measured pressure and flow data from our Asklepios population database. A newly proposed method making use of a more physiological flow waveform yields a significantly better agreement between approximated and actual reflection magnitude, but considerable deviations still persist. Unlike the findings of Qasem *et al.* [96],

assessment of pulse transit time, and hence of pulse wave velocity from a single pulse recording, shows a rather limited correlation with the pulse transit time measured over the carotid-femoral pathway when tested on our middle-aged population. It cannot be totally excluded that these relatively poor results are to a certain extent due to the non-invasive nature of our study, where the approximation of central aortic pressure by the carotid pressure waveform might introduce some scatter in the data. Another factor that might play a role is the limited age range in our population, testing the methods over a limited range of possible parameter values. However, if the techniques are to be applied clinically, PWV (and wave reflection magnitude) will be determined on an individual basis and based on non-invasive data, and not on a large population with a wide age range. Also, the age range of the Asklepios population, 35-55, might be the range of age to start screening for cardiovascular disease and where sensitive methods are required to identify subjects at increased risk.

CHAPTER 5

The use of diameter distension waveforms as an alternative for tonometric pressure to assess carotid blood pressure

The results of this study were published in:
Jan Kips, Floris Vanmolkot, Dries Mahieu, Sebastian Vermeersch, Isabelle Fabry, Jan de Hoon, Luc Van Bortel and Patrick Segers. *The use of diameter distension waveforms as an alternative for tonometric pressure to assess carotid blood pressure.* Physiological Measurement 2010, 31:543-553.

5.1 Introduction

Central (aortic) blood pressure has gained clinical interest, mainly because some studies have suggested that it has a higher predictive value for cardiovascular events than peripheral (brachial) blood pressure [117–123]. Carotid blood pressure is often used as a surrogate for central aortic blood pressure. An invasive study showed carotid pulse pressure (PP) to differ by only 1.8 mmHg from central aortic PP [59].

Unlike mean arterial pressure (MAP), pulse pressure is not constant throughout the large artery tree, but increases towards the periphery [4, 124], implying that brachial pulse pressure will generally be higher than aortic or carotid pulse pressure. The latter can be obtained non-invasively following a well-known,

linear calibration technique, using applanation tonometry on the brachial and carotid artery combined with brachial oscillometry [61, 84]. However, high-quality tonometric readings require a well-trained operator and may be more difficult to perform in elderly and particularly obese patients [4].

Recently [125], two alternative approaches for estimating carotid artery pressure, using a combination of applanation tonometry performed at the brachial artery and either linearly or exponentially calibrated diameter distension waveforms at the carotid artery, were compared to the more common approach of using applanation tonometry on the brachial and carotid arteries. Using calibrated diameter distension waveforms instead of tonometric waveforms avoids the technical difficulties and necessary operator skills associated with applanation tonometry [59]. The assessment of diameter distension waveforms of superficial arteries can be performed accurately by ultrasound wall tracking algorithms [126–128] which require less training and can more easily be performed in obese patients. For calibration, however, these alternative approaches still rely on tonometry readings performed at the level of the brachial artery, of which the feasibility of performing a reliable tonometric measurement has been questioned recently [129, 130].

It is the aim of this study to evaluate a methodology for non-invasive estimation of carotid pulse pressure based solely on diameter distension waveforms obtained at the brachial and carotid arteries. The results of this approach will be compared to the pulse pressures obtained through tonometry at both the carotid and brachial arteries and to the more recently proposed approach of combining tonometric readings at the brachial artery with linearly or exponentially calibrated diameter distension curves at the carotid artery. As an intermediary step, the morphology of brachial and carotid tonometry and distension waveforms will be compared and the mean arterial pressure (MAP) will be computed using either tonometry or distension curves.

5.2 Methods

5.2.1 Study population

Brachial (BA) and common carotid artery (CCA) distension (D) and tonometer (T) waveforms recorded for two previous studies were used [131, 132]. A total number of 148 subjects was selected, none of whom had a history of cerebrovascular or cardiovascular disease, arterial hypertension (>90/140 mmHg), diabetes mellitus, hyperlipidaemia (total cholesterol >6.5 mmol/l), or were currently pregnant or lactating. Subjects on regular use of vasoactive drugs were excluded. Subjects were allowed 10-15 min of rest in a temperature controlled environment before the examinations.

5.2.2 Measurement of local pressure and distension

Brachial oscillometric blood pressure was measured using either an Omron 705IT (OMRON Healthcare, Hoofddorp, The Netherlands; 100 subjects) or a Dinamap 950 (Critikon Inc, Tampa, Florida; 48 subjects). Applanation tonometry was performed using a Millar pen-type tonometer (SPT 301, Millar Instruments, Houston, Texas) and computer software (SphygmoCor, Atcor Medical, Sydney, Australia). Distension waveforms were obtained with an ultrasound wall tracking system (Esaote AU5 or Scanner 350, Esaote-Pie Medical, the Netherlands). An ultrasound probe holder was used at the brachial artery to ensure that the distension curves were not deformed by the pressure exerted on the probe.

5.2.3 Waveform calibration

At the brachial artery, both tonometry and distension waveforms were linearly calibrated using SBP and DBP obtained from oscillometry. For each waveform type, MAP was calculated as the arithmetic mean of the scaled waveform. Hence, for each subject, two estimates are given: MAP_T obtained from the tonometric waveform, and MAP_D obtained using the distension waveform, respectively. At the carotid artery, diameter waveforms were calibrated using a linear and an exponential calibration scheme. Both calibration schemes are based on the assumption that DBP and MAP remain constant throughout the large arteries. In the linear calibration scheme, the diameter waveform is calibrated by assigning the minimum and mean value of the curve to the brachial DBP and MAP_T or MAP_D, respectively [59]. For the exponential calibration, an iterative procedure was followed as first described by Meinders *et al.* [133]. In brief, the diameter waveforms are scaled assuming an intrinsic exponential relation between pressure and diameter:

$$p(t) = p_d e^{\alpha\left(\frac{d^2(t)}{d_d^2}-1\right)}, \tag{5.1}$$

where p(t) is the pressure waveform, d(t) the diameter waveform, p_d the diastolic blood pressure, d_d the diastolic diameter and α the wall rigidity coefficient. An iterative scheme can be followed to calculate α based on DBP and MAP_T. In summary, by combining brachial and carotid tonometer and distension waveforms, we obtain four different estimates of carotid PP indicated by the following subscripts:

- P_{TT}: using brachial and carotid tonometer waveforms (considered here as the reference value)
- P_{TDlin}: using brachial tonometer and linearly scaled carotid distension waveforms [125]
- P_{TDexp}: using brachial tonometer and exponentially scaled carotid distension waveforms [125]

- P_{DD}: using linearly scaled brachial and carotid distension waveforms

P_{TT} will be considered as the reference method in further analyses since it is accepted to be the most accurate non-invasive method to assess local pressure [59].

5.2.4 Waveform comparisons

To assess whether scaled diameter waveforms can be used as a surrogate for tonometry waveforms and to investigate the impact of the different calibration methods, two morphological parameters are calculated to quantify the overall agreement between the scaled diameter and the tonometric waves. The root-mean-squared error (RMSE) is a measure of the absolute difference between the scaled diameter and tonometry waveforms and, as such, allows to quantify how closely the values of the waveforms match across the entire waveform. RMSE is calculated between the reference carotid waveform (P_{TT}) and each of the five other approaches (generically called 'P_{approx}' hereafter) as :

$$RMSE = \sqrt{\frac{\sum_1^n (P_{approx,i} - P_{TT,i})^2}{n}} \tag{5.2}$$

The form factor (FF) [134] is a measure of how peaked the waveform is, and is defined as the ratio of the difference between the mean and minimum value of the wave and its amplitude (maximal - minimal value): FF=(mean-minimum) / amplitude, see figure 5.1. Unlike RMSE, FF is independent of calibration for the linear calibration scheme, which allows a comparison between carotid distension and tonometry waves, irrespective of which curve was used at the brachial artery. Moreover, the form factors of brachial and carotid curves are important determinants of the carotid pulse pressure, which renders them more relevant for this study than the overall match between two waveforms as expressed by the RMSE-value.

5.2.5 Statistical analysis

Data are presented as mean (SD). Relative errors in mean and peak pressure are reported with respect to pulse pressure measured at the brachial artery with cuff sphygmomanometry. Correlation between variables was assessed using Pearson correlation coefficients. Effects of gender were assessed using ANOVA analysis. P-values lower than 0.05 were considered as statistically significant. To assess the major determinants of the differences in carotid PP estimates, a stepwise forward multiple linear regression analysis was performed including age, gender, length, BMI and brachial PP as potential factors. Only the factors that were significant in univariate analysis were entered into multivariate analysis. A univariate general linear model was constructed to assess whether the form factor differed between the carotid and brachial artery, and between distension and tonometer waveforms. All analyses were performed using SPSS 15 (SPSS Inc., Chicago, IL, USA).

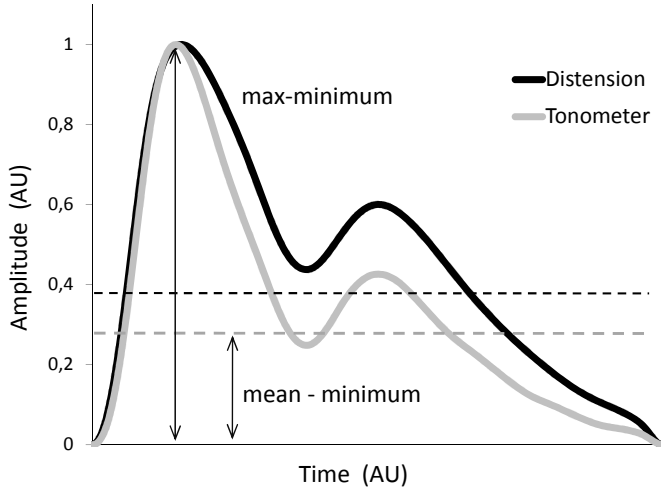

FIGURE 5.1: Distension waves (black) obtained via echo-tracking are less peaked than tonometric waves (grey). The tonometric wave was normalized, whereas the distension wave was calibrated to have same mean and minimal value as the tonometric wave.

5.3 RESULTS

General clinical characteristics of the population can be found in table 5.1.

TABLE 5.1: General description of the study population.

Parameter	Data
Subjects (male/female)	148 (29/119)
Age (years)	29.6 (10.1)
Weight (kg)	66.8 (11.6)
Length (cm)	171.0 (7.8)
BMI (kg/m^2)	22.8 (3.3)
Systolic BP (mmHg)	113.2 (9.8)
Diastolic BP (mmHg)	68.0 (7.1)
PP (mmHg)	45.2 (7.4)
Heart rate (bpm)	64.4 (9.0)

Data are presented as mean (SD) unless otherwise specified. BMI indicates body mass index.

5.3.1 Comparing waveforms by form factor

When comparing tonometry and distension waveforms at the same location by their form factor, we find a higher FF for distension than for tonometry waveforms at both the brachial and the carotid site (table 5.2). When looking at

differences between brachial and carotid artery waveforms, we find brachial FF (both FF_D and FF_T) to be lower than carotid FF. However, the relation between the form factor of the tonometer and distension waveforms is not different for the carotid and brachial artery, as can be seen in figure 5.2. The interaction term between location (brachial or carotid) and technique (tonometer or distension) was not significant (p=0.75) in the general linear model. Additionally, both brachial and carotid FF (both FF_D and FF_T) were significantly higher in women than in men. This difference remained significant after correction for height and heart rate.

Table 5.2: (A): Mean (SD) values of brachial and carotid form factors derived from tonometer (FF_T), linearly scaled distension waves (FF_{Dlin}) and exponentially scaled distension waves (FF_{Dexp}). (B): Mean (SD) values of PP and RMSE for the different carotid pressure waveforms.

(A)		Mean (SD)
brachial	FF_T	40.0 (3.8)
	FF_D	46.2 (3.3)
carotid	FF_T	45.4 (3.3)
	FF_{Dlin}	51.4 (3.0)
	FF_{Dexp}	43.6 (6.3)

(B)	PP (mmHg)	RMSE (mmHg)
P_{TT}	39.9 (8.7)	
P_{DD}	40.8 (7.8)	5.0 (2.1)
P_{TDlin}	35.1 (7.3)	3.5 (1.8)
P_{TDexp}	42.5 (12.7)	3.9 (2.5)

PP, Pulse Pressure; RMSE, root-mean-squared error.

5.3.2 MAP_D versus MAP_T

The use of diameter distension waveforms instead of tonometry waveforms to calculate MAP introduces a difference of 6.2% or 2.8(1.8) mmHg. MAP_D was higher than MAP_T: 88.8(7.8) versus 86.0(8.0) mmHg. There was an excellent correlation between both estimates (R=0.97), but the difference was highly significant (P<0.001), see figure 5.3.

5.3.3 Carotid pulse pressure

Table 5.2 lists the resulting carotid pulse pressure values for the different approaches, as well as the RMSE values associated with each approach. P_{DD}, the pressure waveform obtained via linearly scaled diameter waveforms at the brachial and carotid arteries, yields the carotid PP closest to the reference technique: 40.8 (7.8) mmHg compared to 39.9 (8.7) mmHg for P_{TT}. The difference between both techniques depended on age only (table 5.3). Figure 5.4 shows the correlation between the reference carotid PP (PP_{TT}) and the value obtained

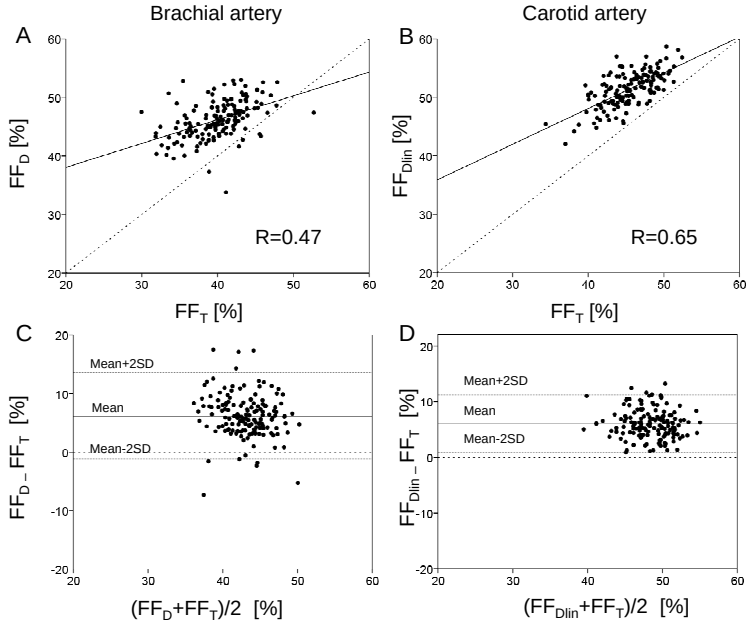

FIGURE 5.2: Relation between distension and tonometric form factors at brachial and carotid artery: regression plots (A,B) and Bland-Altman plots (C,D).

with three other approaches, as well as the corresponding Bland-Altman plots. P_{TDlin}, the approach using brachial tonometry and linearly scaled carotid diameter waveforms yielded the highest correlation (R=0.97) and the smallest RMSE with the reference technique. However, P_{TDlin} underestimates the carotid PP on average by 4.8 mmHg.

TABLE 5.3: Influence of confounding factors on the difference in carotid pulse pressure (PP) estimates.

Variable	Determinant	(cumulative) R^2	β	SE	normalized β
PP_{DDlin} - PP_{TT}	Age	0.10	-0.16	0.04	-0.32
PP_{TDlin} - PP_{TT}	PP_{bra}	0.21	-0.13	0.02	-0.39
	Age + PP_{bra}	0.29	-0.09	0.02	-0.36
	Age + HR + PP_{bra}	0.34	0.06	0.017	0.24
PP_{TDexp} - PP_{TT}	Age	0.42	0.36	0.04	0.53
	Age + HR	0.51	0.21	0.04	0.34
	Age + HR + PP_{bra}	0.54	0.18	0.05	0.20

HR, heart rate (bpm); PP_{bra}, brachial PP from oscillometry (mmHg). We refer to the text for explanation of the abbreviated PP approaches.

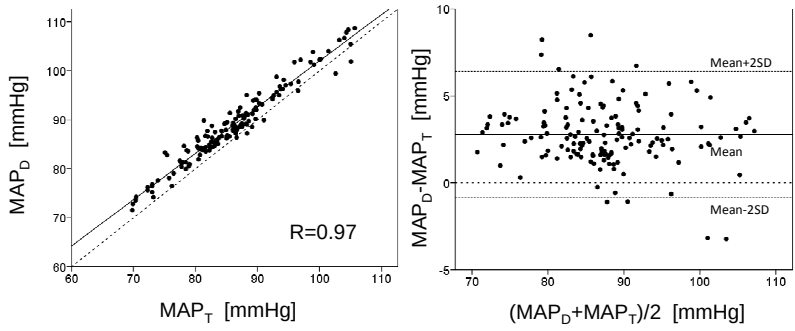

Figure 5.3: Agreement between the (brachial) mean arterial pressure obtained via tonometric waves (MAP_T) and the MAP obtained via distension waves (MAP_D). Regression plot (left) and Bland-Altman plot (right).

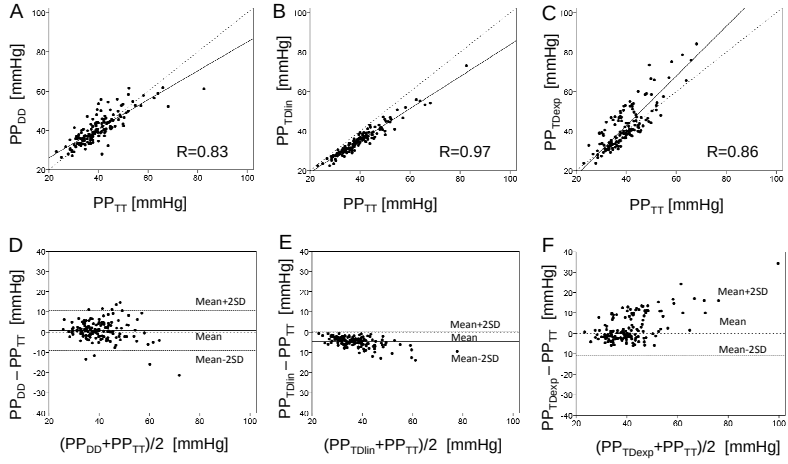

Figure 5.4: Relation between the different estimates of carotid pulse pressure: regression plots (A-C) and Bland-Altman plots (D-F).

5.4 Discussion

The results from the present study suggest that, when diameter distension waves are used as an alternative to tonometry pressure readings at the carotid and/or brachial arteries, it is recommended to measure diameter distension waves at both the brachial and carotid arteries, instead of combining tonometer waves at one artery with distension waves at the other artery. Although previous studies have assessed carotid pressure using only diameter distension waves [59] or using brachial tonometry and carotid distension waves [125], an approach in

which carotid pulse pressure is calculated using brachial and carotid distension curves has not been tested before. Given the reported problems with brachial tonometry, this approach might have clinical relevance. Furthermore, it should be noted that calibrated tonometric curves might not exactly coincide with invasively measured pressure waves, due to limitations inherent to the principle of applanation tonometry. In theory, there should be a constant balance between (internal) blood pressure and applied pressure, i.e. a constant position throughout the cardiac cycle. This creates a problem during peak and late systole where the rebound may temporarily induce an outward motion and, hence, an underestimation of blood pressure. Likewise, a pressure overestimation can be anticipated in early systole. Another issue with applanation tonometry is the questioned reliability in obese subjects. The tonometer has to sense through more (fatty) tissue, and the artery cannot confidently be flattened as there is less direct support of bone behind the artery.

Brachial and carotid distension waveforms were found to be significantly "flatter" (i.e., having a higher form factor) than the corresponding tonometric waves. The fact that distension waveforms were flatter than tonometric waveforms can be explained by the non-linear pressure-diameter relationship, which blunts at higher pressures (i.e., the vessel distends less with increasing pressure due to the increasing recruitment of collagen fibers in the stretched vessel wall). This non-linear relation between pressure and diameter was the rationale for using an exponential calibration scheme [133]. A particular consequence of the difference in "peakedness" between tonometry and diameter-tracings is that the MAP determined from the area under the brachial distension waveform is on average 2.8 mmHg (6.2% of the pulse pressure) higher than MAP obtained via brachial tonometer waveforms. This difference in MAP has an important impact on the differences between the various carotid pressure waves, since each calibration method on the carotid artery is strictly dependent on the (brachial) MAP. Although the two MAP-estimates correlate well, this correlation is highly enhanced by the use of the same (sphygmomanometrically obtained) SBP and DPB to scale the brachial pressure and distension waveforms for each subject. To eliminate this effect, one could compare MAP_T-DBP to MAP_D-DBP. Given, however, the definition of the form factor and the fact that PP at the brachial artery is the same, irrespective of the measurement technique, the 'unscaled' correlation is nothing but the relation between FF_D and FF_T at the brachial artery, which is displayed in figure 5.2. This correlation is notably lower (R=0.47).

When comparing the different carotid pulse pressure values, the difference between PP_{DD} and PP_{TT} is the lowest, being 0.9 (4.9) mmHg or 2.3%. It is even lower than the difference between MAP_D and MAP_T, which seems to imply that a part of the difference introduced by using a distension waveform at the brachial level is compensated by the second use of a distension waveform at the

carotid artery. This can easily be understood when taking into account that

$$PP_{CCA} = \frac{FF_{BA}}{FF_{CCA}} PP_{BA}. \tag{5.3}$$

This illustrates that the pulse pressure at the carotid artery is determined by the ratio of the brachial and carotid form factors. Therefore, systematic differences in FF_{BA} and FF_{CCA} are partially compensated for. MAP, on the other hand, is determined by the brachial form factor only. When using tonometer curves at both sites, the ratio FF_{BA}/FF_{CCA} is 0.88 (see table 5.2) versus 0.90 when using distension data at both sites, explaining why the difference between PP_{DD} and PP_{TT} is smaller than the difference between PP_{TDlin} or PP_{TDexp} and PP_{TT}, respectively (where the ratio FF_{BA}/FF_{CCA} is 0.78 and 0.92, respectively).

Using brachial tonometer and carotid distension waves to calculate carotid pulse pressure (PP_{TDlin}) yielded the estimate with the highest correlation with PP_{TT}, but a considerable underestimation of 4.8(2.5) mmHg when compared to PP_{TT}. This is in line with the results of Vermeersch *et al.*, who found the same approach to underestimate PP_{TT} by 6.4 mmHg in a large population of middle-aged people [125]. They found that the underestimation was highly dependent on brachial PP, with increasing underestimation for higher brachial PP. We could confirm this dependency on brachial PP in our population (table 5.3), which also explains why our PP_{TDlin} performs somewhat better than in the study of Vermeersch *et al.*, where the average brachial pulse pressure was higher (56.2 vs. 45.2 mmHg).

The added value of an exponential calibration scheme for carotid diameter distension waves in combination with brachial artery tonometry is arguable. Although exponential calibration yields a form factor and pulse pressure closer to the reference (FF_T and PP_{TT}, respectively), the overall fit between the exponentially scaled diameter waveform and the tonometric reference waveform was poorer than for a linearly scaled diameter waveform (table 5.2).

Theoretically, two other - non-reported - approaches to obtain a carotid pressure wave are possible: a first one combining brachial distension curves with carotid tonometry, and a second one using linearly scaled brachial distension and exponentially scaled carotid distension curves. Both methods were tested on the study population, but yielded considerable overestimations of carotid PP: 16% and 25%, respectively (data not shown).

One important limitation of this study is the absence of invasive pressure data as a reference to compare the results of the different non-invasive approaches. Furthermore, the limited sample size and age range of our population may hamper the generalizability of our results. A final point of debate is the questioned practical feasibility of brachial applanation tonometry as argued by O'Rourke and colleagues [129, 130]. Figure 5.2 shows that the relation between the form factor of the tonometer and distension waveforms is not different for the carotid

and brachial arteries in our population. Since it can be reasonably assumed that the reliability of distension measurements is the same at the carotid and brachial arteries, this may suggest that applanation tonometry was acquired with a similar degree of reliability at the brachial and carotid arteries and supports the feasibility of applanation tonometry as a reliable technique to obtain non-invasive pressure waveforms at the brachial artery.

5.5 Conclusions

In conclusion we can state that, when aiming to assess carotid artery pressure non-invasively, the use of linearly scaled diameter distension waves at the brachial and carotid arteries introduces only a small error (0.9 mmHg) compared to the reference approach with brachial and carotid tonometry curves. Therefore, it is recommended to stick to one technique, either tonometry or diameter distension waves, rather than using a mix of both techniques.

CHAPTER 6

Non-invasive assessment of central and peripheral arterial pressure waveforms: implications of calibration methods.

The results of this study were published in:
Dries Mahieu, Jan Kips, Ernst R. Rietzschel, Marc L. De Buyzere, Francis Verbeke, Thierry C. Gillebert, Guy G. De Backer, Dirk De Bacquer, Pascal Verdonck, Luc M. Van Bortel, Patrick Segers, on behalf of the Asklepios investigators. *Noninvasive assessment of central and peripheral arterial pressure (waveforms): implications of calibration methods.* Journal of Hypertension 2010, 28:300-305.

6.1 Introduction

The past decade has known an increasing interest in central blood pressure measurement and pressure waveform analysis. Some studies even suggest that central blood pressure has a higher predictive value compared with the traditional sphygmomanometer measurement at the brachial artery level [117, 120].

One non-invasive approach to central blood pressure is to use the carotid (or subclavian) pressure waveform, obtained via applanation tonometry, as a surrogate [61, 84, 135]. It has been shown that carotid tonometry overestimates

central aortic systolic blood pressure by only 1.8 mmHg [59]. Applanation tonometry on the carotid artery, however, implies some difficulties: in addition to the fact that these waveforms require calibration, the absence of underlying bone makes it more difficult to stabilize and flatten the artery, which requires trained personnel. Another technique is to derive central pressure waveforms from non-invasive radial artery pressure waveforms (by applanation tonometry) and applying a generalized transfer function [54, 111, 136–139]. Irrespective of the validity of the principle of using a generalized transfer function [140, 141], the method also requires calibration of the radial pressure waveform.

In a non-invasive procedure, the only information available to calibrate tonometer pressure waveforms is the pressure as measured by cuff sphygmomanometry, generally providing systolic (SBP) and diastolic (DBP) blood pressure. For the calibration of the tonometer curve at the carotid artery, it is most common to calibrate this waveform using diastolic and mean (MAP) blood pressure, assuming that these two pressures (or the difference between them) remain rather constant throughout the arterial tree [58]. MAP is then commonly estimated from SBP and DBP using approximative equations such as the well-known rule of thumb (MAP= DBP + 1/3 PP, with PP=pulse pressure). For the calibration of the radial artery waveform, two approaches can be followed: one can either again use DBP and MAP to calibrate the radial pressure waveform, but it is also common to simply calibrate the radial curve using brachial DBP and SBP. This way, the eventual brachial-to-radial amplification of the pressure pulse is ignored. The debate on the importance of brachial-to-radial amplification is still ongoing [142, 143].

When adhering to the calibration based on DBP and MAP, an issue which is given relatively little attention is the estimate of MAP. Given the fact that it is basically the difference between DBP and MAP (which is in the range of 15 to 20 mmHg in normotensive subjects) that determines the calibration of the radial and carotid pressure waveforms, errors in MAP of a few mmHg may have a large impact on the result obtained after calibration. Some oscillometric devices assess MAP, however these MAPs have never been validated [144–146]. The still most widely used technique is to derive MAP using the well known rule of thumb. Recently, the applicability and accuracy of this simple formula has been questioned, in particular the fraction of PP which should be added to DBP [147, 148]. Bos *et al.* reported that, at the brachial artery site, 40% of PP should be added to DBP instead of 33% as used in the one-third rule [60]. This difference could have an important impact on non-invasive assessment of central blood pressure when applying the methods mentioned above.

The purpose of this study, based on the population data from the Asklepios study [94], is to investigate the influence of different calibration methods of the radial pressure waveform on the estimate of central blood pressure and to analyze the obtained central-to-brachial and brachial-to-radial pulse pressure amplification following the different calibration schemes.

6.2 Materials and methods

The Asklepios study cohort consists of 2524 volunteers (aged between 35 and 55 years) and 1873 subjects were suitable for this specific analysis. For these subjects, applanation tonometry data were available at the radial (RA) and carotid artery (CA). The study was approved by the local ethics committee and written informed consent was obtained from all subjects. All mathematical calculations were done using Matlab (The MathWorks, Natick, Ma), automatically in a blinded way. Subjects were allowed 10-15 min of rest in a temperature controlled environment before the examinations. First, SBP and DBP were measured with a validated oscillometric blood pressure monitor, Omron HEM-907 (Omron Matsusaka Co. Ltd., Japan) [149, 150]. Direct measurement of MAP was not available with this device. This was followed by radial and carotid tonometry (figure 6.1). Tonometry measurements were done using a custom built acquisition system with a pen tonometer (SPT 301, Millar Instruments, Houston, Texas, USA) and a software platform developed in Matlab (The Math Works, Natick, Ma) [61, 84].

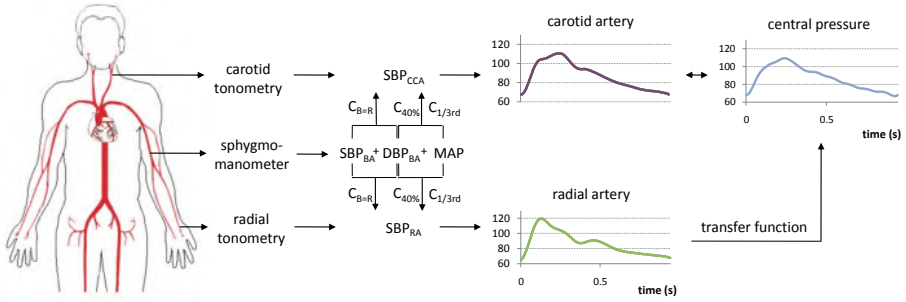

Figure 6.1: Schematic overview of the tonometry measurements and different calibration methods ($C_{B=R}$,$C_{1/3^{rd}}$,$C_{40\%}$). First, the brachial artery pressure waveform is calibrated with absolute blood pressure measured with the sphygmomanometer. Radial and carotid waveforms are calibrated with the three different methods. A transfer function is applied to the calibrated radial pressure waveform in order to assess central blood pressure.

6.2.1 Central blood pressure from radial artery pressure waveforms

Three different calibration methods were used to calibrate the radial pressure waveforms:

- (i) ($C_{B=R}$): In the first method, we assumed the brachial systolic and diastolic blood pressure equal to the radial systolic and diastolic blood pressure .
- (ii) ($C_{1/3^{rd}}$): Secondly, the radial pressure waveforms were calibrated using DBP and MAP, estimated with the one-third rule applied to the PP_{BA}.

- (iii) (C_{40}%): Instead of adding 33% of the pulse pressure to the diastolic blood pressure, we used 40% of the PP_{BA} to assess MAP in a third method (calibration as advocated by Bos *et al.* [60]).

The transfer function (TF), published by Karamanoglu *et al.* [138] was applied to calculate central blood pressure waveforms from the radial pressure waveform. Although not exactly the same, this TF is very similar to the one implemented in the Sphygmocor system or to the TF published by Chen *et al.* [111].

6.2.2 Carotid blood pressure as surrogate for central blood pressure

Carotid tonometry was performed for comparison with estimated central blood pressure. The carotid pressure waveforms were calibrated in the same three different ways as described above.

6.2.3 Central-to-brachial and brachial-to-radial pressure amplification

The absolute central-to-brachial (CTB-amp) and brachial-to-radial systolic pressure amplification (BTR-amp) was determined by the difference between carotid and brachial, brachial and radial pulse pressures respectively, while the relative CTB and BTR-amp was calculated as a percentage of the carotid and brachial PPs respectively. Amplification was calculated for calibration methods (ii) ($C_{1/3^{rd}}$) and (iii) (C_{40}%) while amplification is ignored in method (i).

6.2.4 The form factor

The form factor (FF), defined as the percentage of the amplitude of the waveform to be added to the minimal value to obtain the mean value, was calculated with the following formula:

$$FF = \frac{mean(P_{wf}) - min(P_{wf})}{max(P_{wf}) - min(P_{wf})} \tag{6.1}$$

with P_{wf} the measured pressure waveform and *mean* the calculated arithmetic mean. Min and max are the minimum and maximum of the waveform respectively.

6.2.5 Statistical analysis

Data are presented as mean (standard deviation). A p-value lower than 0.05 was considered statistically significant. Differences were examined by paired-samples t tests or independent-samples t tests where applicable. Statistical analysis was performed using SPSS 15 (SPSS Inc., Chicago, United States).

6.3 Results

The median age of subjects was 46 years (interquartile range [IQR], 41-51 years). A summary of the subject characteristics is presented in table 6.1.

Table 6.1: Subject characteristics for the study cohort of 1873 subjects from the Asklepios population.

	Men	Women
Amount	978	895
Age (years)	46.1 (6.0)	45.5 (6.2)
Height (cm)	175.6 (6.4)	163.2 (6.0)
Body mass index (kg/m^2)	26.0 (3.4)	24.3 (4.1)
Hypertensives (treated)	93	84
Hypertensives (untreated)	222	89
Normotensives	676	735
SBP_{BA} (mmHg)	134.1 (14.0)	128.6 (15.9)
DBP_{BA} (mmHg)	77.9 (10.7)	75.1 (10.7)
MAP_{BA}(mmHg)	101.0 (11.6)	98.4 (12.3)
Heart rate (beats/min)	61.5 (9.8)	65.0 (8.7)

Data are presented as mean (SD). BA, brachial artery.
Hypertension is defined as SBP>140 or DBP>90.

6.3.1 Estimated central blood pressure

Central pressure assessed either via radial artery pressure waveforms and the transfer function or via carotid tonometry, is given in table 6.2 for each calibration method. When estimating central systolic pressure from the radial pressure wave, the value varies from 117.8 (14.2) mmHg ($C_{1/3^{rd}}$) to 126.0 (15.4) mmHg ($C_{40\%}$). Carotid systolic blood pressure varied from 118.4 (14.4) mmHg ($C_{1/3^{rd}}$) to 131.4 (15.2) mmHg ($C_{B=R}$).

Table 6.2: Carotid tonometry and transfer function derived central blood pressure (in mmHg), obtained after application of three different calibration methods to the measured carotid and radial artery pressure waveforms

BTR-amp included?		Calibration method	Carotid artery SBP_{CA}	TF-derived SBP_{TF}	Difference $SBP_{CA} - SBP_{TF}$
No	$C_{B=R}$	SBP_{BA} & DBP_{BA}	131.4 (15.2)	123.5 (15.7)	7.9 (4.9)
Yes	$C_{1/3^{rd}}$	1/3rd rule	118.4 (14.4)	117.8 (14.2)	0.6 (3.1)
Yes	$C_{40\%}$	40% PP	126.8 (15.7)	126.0 (15.4)	0.8 (3.8)

BA, brachial artery; BTR-amp, brachial-to-radial amplification; CA, carotid artery
PP, pulse pressure; TF, transfer function.

6.3.2 Central-to-brachial and brachial-to-radial systolic pressure amplification

When waveforms were calibrated following the one-third rule ($C_{1/3^{rd}}$), the amplification of pulse pressure from carotid to radial artery was 6.7 (5.6) mmHg, with an amplification from carotid to brachial of 13.0 (3.6) mmHg and a damping of -6.3 (4.5) mmHg from the brachial to radial artery. When calibrating the waveforms using $C_{40\%}$ method, the total amplification was 8.1 (6.7) mmHg,

with a carotid-to-brachial amplification of 4.6 (3.8) mmHg, and a brachial-to-radial amplification of 3.4 (5.5) mmHg. The relative central-to-brachial and brachial-to-radial pulse pressure amplification for each calibration method is also presented in figure 6.2. Obviously, when assuming equal carotid, brachial and radial SBP, amplification is ignored.

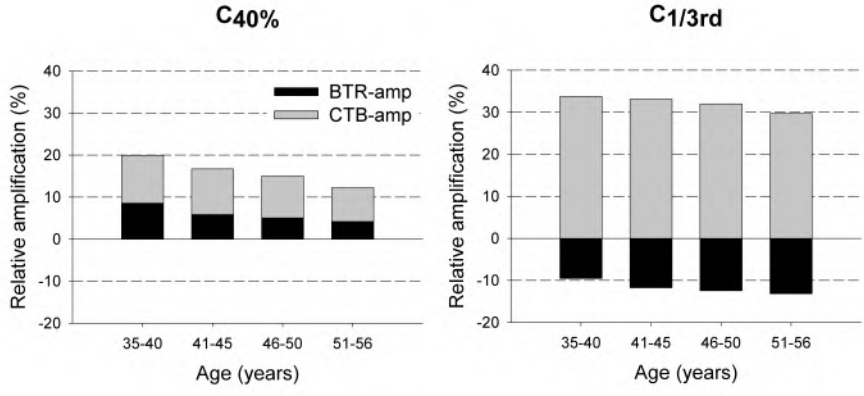

Figure 6.2: Relative pressure amplification, central to brachial (CTB-amp) and brachial to radial (BTR-amp), for calibration method $C_{40\%}$ and $C_{1/3^{rd}}$ for different age ranges.

6.3.3 Form factor

The form factor was higher at the carotid (43.9 (3.3)%) than at the radial artery (38.1 (3.3)%; see also table 6.3.3). FF_{RA} was 2.7 (0.1)% higher in women than in men (p<0.001). FF_{CA} was also significantly higher in women than in men, but only by 0.3% (p<0.05). While FF_{RA} was 0.6 (0.2)% higher in hypertensives compared to normotensives (p<0.001), FF_{CA} was 0.5 (0.2)% lower in hypertensives (p<0.020).

Table 6.3: Radial and carotid FF in the Asklepios population.

	Normotensive (n=1390)	Hypertensive (n=483)	*P*	Men (n=978)	Women (n=895)	*P*	Total (n=1873)
FF_{RA} (%,SD)	37.9±3.3	38.5±3.2	0.001	36.8±3.1	39.5±2.9	0.001	38.1±3.3
FF_{CA} (%,SD)	44.2±3.1	43.7±3.6	0.020	43.8±3.2	44.1±3.4	0.040	43.9±3.3

P-values are given for the difference between normotensives and hypertensives, men and women respectively
FF_{CA}, carotid artery form factor; FF_{RA}, radial artery form factor.

6.4 Discussion

The major finding of this study is that the value of MAP that is used to calibrate applanation tonometry waveforms is of paramount importance for the non-invasive assessment of (central systolic) blood pressure. In particular, the use

of MAP estimated with the widely applied one-third rule leads to results contradicting prevailing insights in arterial physiology and central-to-peripheral pressure amplification. This provides indirect proof that the 1/3rd factor for the calculation of MAP is too low, and is better replaced by a factor close to 40%.

It is clear that the method used to calibrate tonometric waveforms is essential when estimating central blood pressure. As can be seen in table 6.2, for the carotid artery, use of $MAP_{1/3^{rd}}$ or $MAP_{40\%}$ for the calibration introduces a mean difference of around 8 mmHg in estimated carotid systolic blood pressure. Similar differences are found when estimating central systolic blood pressure via the radial artery and a pressure transfer function.

However, it is also observed that when calibration of the radial and carotid waveforms is performed using MAP and DBP (with MAP derived either using $C_{1/3^{rd}}$ or $C_{40\%}$) the difference between TF and carotid derived central pressures is small (below 0.8 mmHg; table 6.2) which is in full agreement with previous findings from our group [84, 151]. This supports the use of TF for estimating central systolic and pulse pressure - provided the radial pressure waveforms are calibrated appropriately [84, 151]. As the TF published by Karamanoglu *et al.* is close to the one used in the SphygmoCor system, we expect our conclusions to be also applicable to this system.

When using the SphygmoCor system, it is common to apply the transfer function to the radial pressure waveform which is calibrated using brachial diastolic and systolic blood pressure, ignoring brachial-to-radial amplification. It can be deduced from table 6.2 that the value found for central systolic pressure (123.5(15.7) mmHg) is relatively close to the value of carotid systolic blood pressure obtained when calibrating the carotid waveform using $C_{40\%}$ (126.8 (15.7) mmHg). Especially given the knowledge that central systolic blood pressure is about 2 mmHg lower than carotid pressure, the two values are remarkably close.

Intriguingly, when we used the one-third rule to assess MAP ($C_{1/3^{rd}}$) for calibration of the radial and carotid waveforms, we found a total carotid-to-radial amplification of 6.7 (5.6) mmHg, but with a very strong amplification up to the brachial artery, followed by damping (a negative value for the brachial-to-radial systolic pressure amplification) over the brachial-to-radial path. This is in contrast with the knowledge of increasing pulse pressure towards the peripheral arteries. We therefore consider this to be non-physiological [4], and important indirect evidence that the one-third rule is not the most accurate method to estimate MAP.

When estimating MAP using the one-third rule, one assumes a form factor of 33%. As can be observed in table 6.3.3, the FFs we found at the carotid and radial level are higher than the conventionally applied 33%, and are in line with the values obtained in the invasive studies by Bos [60] and Chemla [148]. In the former, a form factor of 39.5% was found at the brachial artery. Chemla *et al.* calculated the form factor at aortic root level and found a value of 41.2%. The

somewhat higher values for the FF in our study may be attributable to the non-invasive method used, i.e. applanation tonometry calibrated with an automated blood pressure monitor and a younger population. Also, our population age range was only 20 years (35-55) compared to 34-83 years for the study of Bos *et al.* As early wave reflections in older subjects increase pulse pressure, the lower FF in the study of Bos *et al.* might also (in part) be explained by the difference in age between the groups. Note also that we found the FF to decrease from the carotid (43.9 (3.3)%) to the radial artery (38.1 (3.3)%), which is consistent with a progressive peaking of the pressure waveform and central-to-peripheral pressure amplification.

It is clear from these studies that use of the one-third rule leads to underestimation of MAP. Question is then which value of the form factor should be used to obtain more reliable values of MAP. Bos *et al.* suggest to use 40% at the brachial artery, but a drawback of their study is the lack of normotensive subjects, and their results may only be applicable to hypertensives. On the other hand, our results showed relatively small differences in form factor between normo- and hypertensives. Nevertheless, the FF was higher in women than in men at all locations (table 6.3.3). As such, the optimal formula to estimate MAP from brachial DBP and SBP should account for gender (or hemodynamic and/or body size factors explaining these gender effects).

We previously advocated a method to estimate MAP as the arithmetic mean value of a calibrated brachial tonometric pressure waveform [84, 151]. As our main goal was to demonstrate some of the inconsistencies that are obtained when using $MAP_{1/3^{rd}}$ to calibrate tonometer waveforms, and as there is still some debate regarding the applicability of this method, we chose not to report the data obtained using that method in order not to divert the debate. Anyhow, given the fact that the average FF of the brachial curve is around 42% in our population (data not shown), the results obtained with that method are close to $C_{40\%}$, although that method yields a somewhat lower carotid-to-brachial and higher brachial-to-radial amplification.

6.5 Limitations

It is clear that the most important limitation of the study is the lack of invasive measurements as reference. However, to the knowledge of the authors, this is the first study with non-invasive data supporting the findings of Bos [60] and Chemla [148], which are based on invasive data. Also, carotid tonometry measurements have been used as reference for central blood pressure, while it has been shown that carotid tonometer derived systolic blood pressure in itself is on average 1.8 mmHg higher than the invasive central aortic pressure [59]. In the present study, this difference (between carotid and central systolic pressure derived with a TF) was 0.8 mmHg. Nevertheless, this has no impact on our results in general.

6.6 Conclusion

These findings indicate that the one-third rule should not be used to estimate MAP from brachial artery pressure within the calibration process of non-invasive pressure waveforms. We therefore support the use of the value of 40% above the one-third rule as advocated by Bos *et al.*

CHAPTER 7

Ambulatory Arterial Stiffness Index (AASI): another ambiguous stiffness index

The results of this study are assembled in:
Jan Kips, Sebastian Vermeersch, Philippe Reymond, Pierre Boutouyrie, Nikos Stergiopulos, Stephane Laurent, Luc Van Bortel, Patrick Segers. *Ambulatory Arterial Stiffness Index (AASI) does not accurately assess arterial stiffness*, submitted for publication to Journal of Hypertension.

7.1 Introduction

Arterial stiffness is increasingly recognized as an early marker of and important risk factor for the development of cardiovascular diseases [55, 152]. The gold standard technique to assess arterial stiffness is pulse wave velocity (PWV) [55], which, though straightforward and relatively easy to perform, still requires measurements at two separate arterial locations, remaining cumbersome for routine clinical practice. A relatively new parameter, the Ambulatory Arterial Stiffness Index (AASI) was recently proposed as a surrogate measure for arterial stiffness. This method is based on (24-hour) ambulatory recordings of blood pressure, and is calculated as 1 - (the slope of the linear regression line between systolic and diastolic blood pressure values) [98, 99]. Previous studies have shown that AASI correlates well with PWV [98], and that it has predictive value for cardiovascular mortality [153, 154], in particular for stroke [155].

As such, it appears to provide additional value to the 24-hour blood pressure recording. However, several other studies have questioned whether AASI truly is a measure of arterial stiffness [156–160] and whether it can be used as an alternative for PWV [161]. It has been suggested that the AASI is largely influenced by peripheral resistance and by ventriculo-arterial coupling [158, 159]. Others reported the degree of nocturnal BP fall as an important confounder to AASI and its interpretation as a measure of arterial stiffness [156].

In the present study, this ongoing discussion is addressed using a computer model of the left heart and systemic arterial circulation [97]. The aim of this study is to explore the determinants of the AASI and to assess their relative importance in a well-controlled setting with exact knowledge of all cardiovascular parameters in order to assess to which extent AASI can be used as a measure of arterial stiffness.

7.2 Methods

Ambulatory blood pressure (BP) recordings were simulated using a previously validated and applied 1-D model of the arterial circulation (represented by one hundred and three arterial segments). On the downstream end, terminal beds are mimicked with so-called 3-element Windkessel models. For each segment, properties such as distensibility, diameter, and length can be individually adjusted. Changes in arterial resistance can be simulated by changing the resistance properties in the distal models. The interaction of the heart with the arterial tree is included in the simulations, with the heart modeled as a time-varying elastance model. This implies that blood pressure (or stroke volume) can not directly be altered as an input parameter of the system but is the result of the interaction between the heart and its arterial load, similar to the in vivo situation. We refer to Reymond *et al.* [97] for details on the properties of individual segments and the computational methods used to solve the 1-D flow equations.

7.2.1 AASI in the "default" subject

The AASI of a 'default subject' was calculated by generating multiple BP-values, mimicking regular ambulatory BP-measurements over the course of a day. Each BP-value was the result of a different set of input parameter values. Input parameters that were changed include both cardiac (maximal elastance, heart rate, venous filling pressure) and vascular (resistance, distensibility) parameters. Arterial distensibility, resistance, venous pressure, maximal elastance and heart rate were altered within a ±20% range around their initial value in steps of 10%. Permutations of these five parameters, each with five possible values, lead to 3125 different sets of input parameter values and corresponding BP-values. The initial values of the model parameters were chosen, each within their physiological range, to yield a mean brachial BP of 120/80 mmHg [162, 163]. The applied

variation of ±20% is considered to be representative of the physiological fluctuations occurring over the course of one day. Vascular resistance was changed by multiplication of the default resistance value of each segment with a constant factor (i.e., we did not consider effects of differential changes in the resistance of vascular beds).

To calculate AASI for the default subject, 72 BP-values were randomly picked out of the total number of available BP-values, hereby mimicking the number of BP-recordings obtained during 24-hour ambulatory BP-monitoring with one BP-recording every 20 minutes. This random selection of 72 BP-values was repeated 10 000 times and a histogram of AASI-values was constructed. This approach also serves to illustrate the effect of sampling the continuously varying blood pressure at a number of discrete moments in time, which is unavoidably the case when using ambulatory blood pressure values.

7.2.2 Contribution of cardiac and arterial parameters to AASI in the default subject

Table 7.1 provides an overview of the simulations used to assess the effect of individual parameters. To study the relation between arterial distensibility and AASI, an AASI was calculated for each of the five levels of distensibility. Each value of AASI was therefore based on 625 BP-values corresponding with the variations in resistance, venous pressure, maximal elastance and heart rate at that level of distensibility.

Table 7.1: Overview of the simulations used to assess the effect of individual parameters.

Parameter	C	R	E_{max}	P_v	HR	# simulations
Default subject	↑ 120% ↓ 80%	↑ 120% ↓ 80%	↑ 120% ↓ 80%	↑ 120% ↓ 80%	↑ 120% ↓ 80%	5^5=3125
Effect of C	-	↑ 120% ↓ 80%	↑ 120% ↓ 80%	↑ 120% ↓ 80%	↑ 120% ↓ 80%	$5x5^4$=5x625
Effect of R	-	-	↑ 120% ↓ 80%	↑ 120% ↓ 80%	↑ 120% ↓ 80%	$5x3^5$=5x125
Effect of E_{max}	-	↑ 120% ↓ 80%	-	↑ 120% ↓ 80%	↑ 120% ↓ 80%	$5x5^3$=5x125
Effect of P_v	-	↑ 120% ↓ 80%	↑ 120% ↓ 80%	-	↑ 120% ↓ 80%	$5x5^3$=5x125
Effect of HR	-	↑ 120% ↓ 80%	↑ 120% ↓ 80%	↑ 120% ↓ 80%	-	$5x5^3$=5x125

C, distensibility; R, resistance; E_{max}, maximal cardiac elastance, P_v, venous filling pressure; HR, heart rate.

To study the influence of the other (individual) parameters on the AASI, the same methodology was applied: for each value of the parameter of interest, ranging from 80 to 120% of its initial value in steps of 10%, an AASI was calculated based on the BP-recordings generated by varying the other parameters. As we specifically want to isolate the effect of changes in distensibility from changes in the other parameters, vascular distensibility was held constant

for these analyses, reducing the number of BP-recordings per AASI to 125. For this analysis, AASI was calculated from all available values (i.e., not limiting to subsets of 72 data points).

7.2.3 Ability of AASI to detect large changes in stiffness

To assess the sensitivity of AASI in identifying differences in arterial stiffness among subjects, three theoretical subjects were simulated, each with a clearly different level of arterial stiffness mimicking the increase in arterial stiffness typically occurring with aging. This was done by multiplying the default distensibility of each segment with 100%, 50% and 25% respectively. These levels of arterial distensibility correspond with an average PWV of 5.9, 8.3 and 11.8 m/s, respectively (this theoretical value of PWV was obtained by averaging the PWV for each segment of the aorta, weighted according to the segment lengths; PWV for each segment was calculated from the model parameters as $PWV = 1/\sqrt{\rho D}$; with ρ the blood density (1050 kg/m^3 in the model) and D the distensibility of the segment).

For each theoretical subject, a set of 3125 BP-recordings was generated similarly as before: by varying the distensibility, resistance, maximal cardiac elastance, venous pressure and heart rate from 80 to 120% of their initial value in steps of 10% and calculate the brachial BP for each permutation of these parameters. In order to be useful as a marker of arterial stiffness in clinical practice, the AASI must be clearly different in the three theoretical subjects. This question is addressed by comparing the AASI-histograms.

7.3 Results

7.3.1 AASI in the "default" subject

Figure 7.1A shows all 3125 BP-values generated for the first theoretical subject. The corresponding AASI is 0.43. The different AASI-values obtained by repeated random selection of 72 values out of the total number of 3125 generated BP-values for the first theoretical subject follow a normal distribution with a mean value of 0.43 and a standard deviation of 0.04 (figure 7.1B). This mean value is the same as the value obtained when all available BP-values are taken into account to calculate AASI.

7.3.2 Contribution of cardiac and arterial parameters to AASI in the default subject

For a 120 to 80% decrease in arterial distensibility (increase in stiffness), the AASI increased by 21% from 0.38 to 0.46 as shown in figure 7.2 for three of the five applied levels of distensibility. Figure 7.3 gives an overview of the effect of changes in resistance, heart rate, maximal cardiac elastance and venous pressure on the AASI, when distensibility is kept constant at its default value.

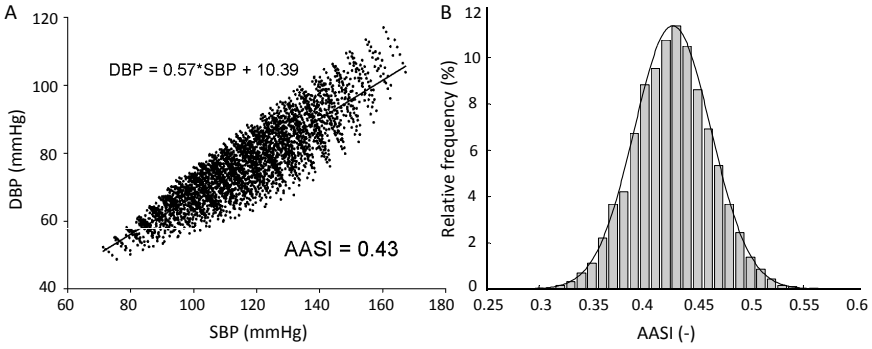

FIGURE 7.1: (A) Scatter plot of all 3125 ambulatory BP-recordings for the default theoretical subject, with corresponding regression line; (B) AASI-histogram for first theoretical subject with overlying normally distributed envelope. The histogram was obtained by calculating an AASI for each of the 10 000 random selections of 72 BP-recordings out of the available 3125 recordings.

While venous pressure and maximal cardiac elastance do not seem to have a pronounced effect on AASI, heart rate, distensibility and resistance considerably alter AASI. An 80 to 120% increase in maximal cardiac elastance changes the AASI by less than 3%, whereas the same relative increase in resistance and heart rate causes the AASI to decrease by 9 and 38%, respectively. Heart rate, distensibility and resistance are all inversely related with AASI. The fact that the AASIs at 100% of the initial value of each individual parameter differ is caused by the fact that they are based on a different set of BP-values, as illustrated for heart rate and venous pressure in the right panel of figure 7.3.

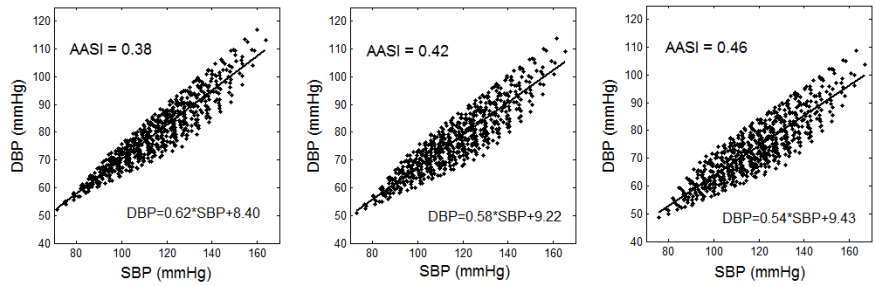

FIGURE 7.2: Relation between AASI and arterial stiffness. Simulated ambulatory BP-recordings and corresponding AASI are shown for 80% (left), 100% (middle) and 120% (right) of the default stiffness value.

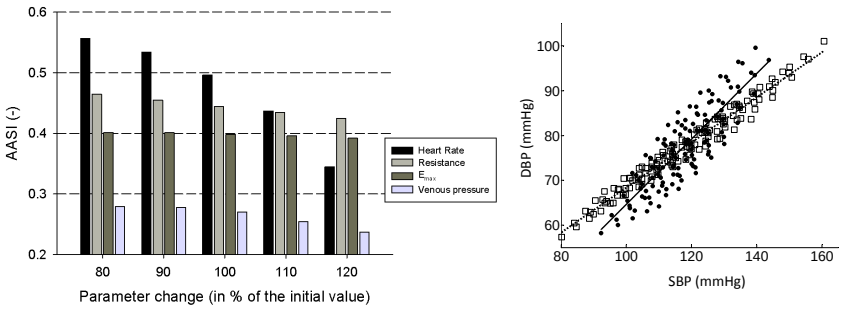

Figure 7.3: Left: influence of maximal cardiac elastance (E_{max}), venous pressure, heart rate and vascular resistance on the AASI. Right: the blood pressure values used to calculate the AASI at 100% of the initial heart rate (open squares) and 100% of the initial venous pressure (closed circles).

7.3.3 Ability of AASI to detect large changes in stiffness

The usefulness of AASI as a marker of stiffness was assessed by considering two additional theoretical subjects with an average distensibility of 50 and 25% of the default theoretical subject, respectively. Figure 7.4 shows the envelopes of the AASI-histograms obtained for the three theoretical subjects. As could be expected from their lower average distensibility, the two additional subjects have a higher mean (SD) AASI: 0.50 (0.04) for the subject with the intermediate distensibility level and 0.67 (0.04) for the subject with the lowest level of arterial distensibility. The overlap between the different envelopes is considerable: 36.8 % between the two more compliant subjects and 3.6 % between the two stiffer subjects.

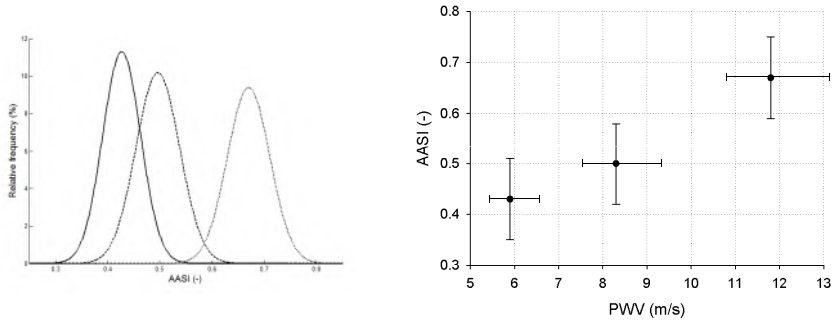

Figure 7.4: Left: envelopes of the AASI-histograms of three theoretical subjects, with a respective average distensibility of 100% (solid line), 50% (dashed line) and 25% (dotted line) of the default theoretical subject. Right: scatterplot of AASI versus PWV for the three theoretical subjects. The error bars denote the mean value plus or minus twice the standard deviation.

7.4 Discussion

The Ambulatory Arterial Stiffness Index (AASI) was recently proposed as a relatively inexpensive and easy-to-measure surrogate marker of arterial stiffness [98, 99], which would provide additional information on arterial stiffness from 24-hour blood pressure recordings. However, there has been quite some debate about this new parameter and the use of AASI as a surrogate for arterial stiffness has repeatedly been questioned. Using a numerical 1D-model of the arterial circulation, this study shows that AASI, although related to arterial stiffness (figure 7.1B), is also largely influenced by vascular resistance and heart rate (figure 7.3). This hampers the usefulness of AASI as a new parameter for risk stratification or as an alternative for PWV as it leads to considerable variability in AASI.

While our simulations clearly demonstrated a strong relation between arterial stiffness and AASI, they also demonstrated that vascular resistance and especially heart rate have an important (inverse) effect on the AASI. In fact, the influence of heart rate on AASI was even stronger than that of distensibility and resistance. This confirms the hypothesis of Westerhof *et al.* [158] that AASI is proportional to T/RC, with T the cardiac period (1/heart rate) and that it reflects ventriculo-arterial coupling rather than arterial stiffness alone (with T/RC representing the coupling parameter, T being the time constant of the heart, and RC the time constant of the arterial circulation). The inverse relation between heart rate and AASI was previously reported by Adiyaman *et al.* [164], but not by Schillaci *et al.* [156] (positive relation) and Li *et al.* [98] (no correlation). This, however, does not necessarily imply that AASI might not be a useful marker of cardiovascular risk, as it has been shown to predict outcome over and beyond classical risk factors [153].

An immediate consequence of the fact that AASI reflects more than stiffness alone, is that, for a given level of stiffness (and variations within the normal physiological range around that value), AASI can vary considerably depending on the concomitant changes in resistance and heart rate. This dependency on the sampling of BP-values is illustrated by the histogram of AASI-values obtained by repeated selections of 72 BP-values out of the total available number of BP-values for one theoretical subject. The standard deviation of 0.04 indicates that, when calculating the AASI based on 72 ambulatory BP-recordings sampled from the available dataset, there is a 32% chance that the true AASI corresponding with that subject is more than 8.5% higher or lower than the calculated value.

To assess to which extent this may hamper its use in clinical practice, three theoretical subjects with a clearly different average level of arterial stiffness were simulated. Whereas there was no overlap in the ranges over which total arterial distensibility (or PWV) varied for the three theoretical subjects, there is a substantial amount of overlap in the AASI histograms. Consider a subject for

whom an AASI of 0.47 is calculated. Based on the histograms in figure 7.4, there is a considerable chance that this value is measurable in both the subject with intermediate stiffness (PWV of 8.3 m/s) as in the subject with the lowest stiffness value (PWV of 5.9 m/s). Assuming that the point at which both histograms cross (AASI = 0.46) is taken as the cut-off point, there is still a 16.0% chance that an AASI-value higher than 0.46 is found for the subject with the lowest stiffness, and a 20.8% chance that an AASI-value lower than 0.46 is found for the subject with intermediate stiffness.

It is not uncommon to assess day- and nighttime values for 24-hour blood pressure recordings and AASI-values could be derived for these subsets. It is, however, not trivial to simulate the physiological effects of sleep in the present model. These involve physiological effects due to the change in posture with associated fluid shifts, hydrostatic pressure differences (affecting distensibility), effects on cardiac preload and changes in sympathetic and parasympathetic tone modulating heart rate, arterial tone, etc. As such, we chose to limit the present analysis to changes of a number of well defined model parameters over a limited range without any attempt to separately model day- and nighttime data.

7.5 Limitations

It is to be acknowledged that this is a theoretical model study with its pros and cons. The model is only an approximation of reality and although it was validated [97] by comparison to non-invasively assessed pressure and flow waveforms of young, healthy volunteers, it cannot be completely excluded that some of the observed effects in this study are exaggerated or masked when compared to reality. However, we took care to limit the changes of the model parameter values to the advocated range [97]. Furthermore, the model does not explicitly include the microcirculation, with vascular resistance modeled as a windkessel model approximation at the distal end of each arterial path. It is possible that the observed range in AASI histograms is slightly exaggerated, as a result of non-physiological combinations of different parameter values. However, we consider a ±20% variation during 24 hours as rather conservative, especially regarding heart rate. Because vascular distensibility is (per definition) pressure-dependent, the reported effects of heart rate and resistance on AASI could be biased by underlying changes in stiffness, as a change in heart rate (resistance) also affects the BP-level and thus distensibility. To assess the importance of this effect, all model simulations were repeated with a pressure-independent distensibility. The results of these simulations did not essentially differ from the original ones.

7.6 Conclusion

Using a computer model of the left heart and the systemic circulation, we identified arterial distensibility, vascular resistance and heart rate as the main determinants of the Ambulatory Arterial Stiffness Index. This seriously limits the use of AASI as a marker of arterial stiffness.

Three

Validation and development of new devices

CHAPTER 8

Outline

Along with the increased attention for the role of the large arteries in the development of hypertension and concomitant cardiovascular diseases and especially since the ESC/ESH guidelines include the measurement of PWV for the management of patients with hypertensive disease, the number of devices to measure wave reflections and arterial stiffness has boosted. This third part of the PhD-dissertation describes the validation studies that were performed on two relatively new devices, as well as the development of a low-cost device for use in African settings (see part IV).

Chapter 9 details the results of a numerical validation of the working principle of the Arteriograph (Tensiomed, Budapest, Hungary), a device that claims to assess aortic pulse wave velocity by means of a simple brachial cuff. Brachial blood pressure is measured during supra-systolic pressure inflation of the cuff, yielding pressure waveforms with pronounced first and secondary peaks. The secondary peak is ascribed to a reflection from the aortic bifurcation, and PWV is calculated as the ratio of twice the jugulum-symphysis distance (~ aortic root - bifurcation) and the time difference between the two peaks. To test the validity of this working principle we used a previously validated [97] numerical model of the arterial tree to simulate pressures and flows in the normal configuration and in a configuration with an occluded brachial artery.

Chapter 10 reports on the comparative measurements between Omron HEM-9000AI (Omron Healthcare, Kyoto, Japan) and SphygmoCor in an attempt to validate the central systolic pressure (cSBP) estimate provided by Omron HEM-9000AI. The Omron HEM-9000AI is the first automated tonometer to provide

an estimate of cSBP, which is considered to be more predictive of cardiovascular events than the conventional brachial pressure. However, considerable differences between the cSBP-estimate of Omron and that of SphygmoCor have been reported [165], but not explained. This study assesses the sources of differences between both cSBP-estimates and provides a handle on which estimate is closest to reality. For this purpose, calibrated carotid SBP was used as device- and algorithm-independent reference.

The available devices to assess arterial stiffness and wave reflections are expensive and not necessarily accurate, as illustrated in chapters 9 and 10. As these relatively high prices may pose an obstacle for research in developing countries such as most countries in sub-Saharan Africa, we developed a low-cost device to acquire flow and pressure waveforms and hence derive PWV, local blood pressure and augmentation index. The development of hardware and software of this Tono-Doppler device is outlined in chapter 11.

CHAPTER 9

Pulse wave velocity from a single brachial cuff recording: the Arteriograph revisited

The results of this study were published in:
B. Trachet, P. Reymond, J. Kips, A. Swillens, M. De Buyzere, B. Suys, N. Stergiopulos, P. Segers. *Numerical validation of a new method to assess aortic pulse wave velocity from a single recording of a brachial artery waveform with an occluding cuff.* Annals of Biomedical Engineering 2010, 38:876-888.

9.1 Introduction

With the increased attention for large artery stiffness and the obvious role of arterial stiffening in the patho-physiology of (isolated) systolic hypertension, the 2007 ESC and ESH guidelines for the management of arterial hypertension [166] now formally recognize large artery stiffness as a factor influencing the prognosis of patients and measurement of arterial stiffness as a useful indicator of vascular damage. Large consensus exists that of all available methods to quantify arterial stiffness or aspects of it, measurement of (carotid-femoral) pulse wave velocity (PWV) is, at present, the only non-invasive comprehensive method which is simple and accurate enough to be considered as a diagnostic procedure feasible on a large scale in a clinical setting, with high values being indicative of stiffened arteries [55, 166]. In essence, measurement of PWV is

simple and straightforward, and it is calculated as the ratio of the distance between two measuring locations and the time it takes for the waves to travel from one location to the other (the pulse transit time). And yet, there is still much ambiguity in measuring PWV, arising on the one hand from difficulties in accurate measurement of the transit time and identification of the foot of the wave front, and on the other hand from measuring the actual travel distance of the waves. The latter is particularly ambiguous for carotid-femoral PWV, where at the moment the wave is picked up at the carotid artery, it is already travelling further down the aorta towards the femoral artery.

With the Arteriograph (Tensiomed, Budapest, Hungary), a new method (and device) to measure pulse wave velocity has recently been introduced onto the market. Unlike most other devices aiming to measure PWV, this device measures the pulse waves at one single location. The device makes use of a brachial cuff that is over-inflated to 35 mmHg over the systolic blood pressure. It is claimed that, as a result of this over-inflation, the reflected wave from the lower body can be detected more easily. The time difference between the first systolic wave and the second reflected wave is then used as the transit time, i.e., the time needed for the wave to travel back and forth to the reflection site. Assuming that the measured external distance from jugulum to symphysis can be used as an approximation of the distance to this reflection site, pulse wave velocity can be computed as the ratio of travelled distance and transit time.

Validation data on the Arteriograph are still rather limited, but they seem to suggest that there is a relation between PWV measured by this new device and PWV measured by more generally accepted methods. However, the underlying principle of this intriguing method is still not fully understood, since no clear explanation has been given for the appearance of a pronounced second peak when the brachial cuff is over-inflated. This second peak is assumed to originate from a reflection of the pressure wave in the lower body, but no reasonable explanation for the fact that this reflection is more pronounced in the case of an over-inflated brachial artery cuff has yet been published. Furthermore, little is known about the underlying assumptions one has to make to calculate PWV with the Arteriograph.

The principal aim of this work is to gain a better understanding and validation of the working principle behind this new method. We used a computer model of the arterial tree to simulate pressure and flow waveforms in a normal arterial system, and in a configuration representing an over-inflated brachial artery (occluded model). The pressure waveforms and wave reflection patterns in the occluded model were studied, and transit time and PWV calculated using the Arteriograph method were compared to the actual transit time and PWV for different stiffness values in the model.

9.2 Materials and methods

9.2.1 Arteriograph: principle of operation

The Arteriograph is basically a simple upper arm cuff connected to a piezoelectric sensor that picks up the pressure signals. Upon operation, the cuff is inflated to a pressure of 35 mmHg over the systolic blood pressure. The pressure in the underlying occluded artery is transmitted through the cuff to the pressure sensor and is reported to show multiple peaks (see figure 9.1). The first is the systolic peak, corresponding to the ejection of blood from the left ventricle into the aorta, while the second peak is assumed to originate from a reflection of the first pressure wave in the lower body. The time difference between the first and second wave in the pressure signal is used as the return time ΔT_{s1-s2}, i.e. the time needed for the pressure wave to travel from the aortic arch to its reflection point and back, with the iliac bifurcation assumed to be the dominant reflection point. The exact algorithm used by the device to determine the transit time is unknown but for our analysis we systematically used the peak-to-peak time difference. The travelled distance corresponding to this return time is twice the distance from aortic arch to iliac bifurcation, which is approximated by measuring the distance between jugulum and symphysis externally (see figure 9.1).

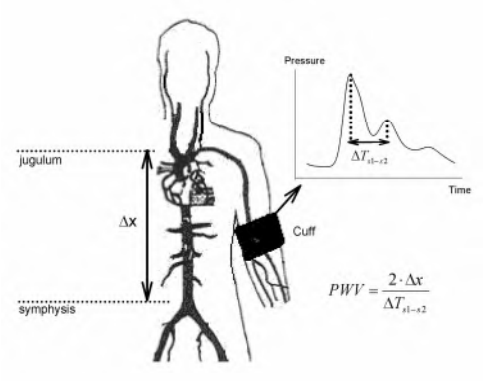

Figure 9.1: Illustration of the working principle of the Arteriograph.

9.2.2 Model simulations

To gain a better insight into the origin of the pressure waveforms occurring during the over-inflation phase of the Arteriograph, we simulated pressure and flow waveforms in the arterial tree using an improved version [97] of the original 1D model of Stergiopulos *et al.* [167]. This model is based on the one-dimensional flow equations and includes nonlinearities arising from geometry and material properties. One hundred and three (103) arterial segments, representing

the various major arteries, are combined and terminated with three-element Windkessel models to form a model of the arterial system. For each segment, properties such as compliance, diameter and length can be adjusted. Resistance can be altered in the distal Windkessel models. We refer to Reymond *et al.* [97] for details on the properties of individual segments and the computational methods used to solve the 1-D Navier-Stokes equations. We used this model to simulate pressure and flow in the normal configuration, and in a configuration with the left brachial artery completely occluded (over-inflation of the Arteriograph cuff). The superfluous segments of the brachial artery were thus removed, resulting in an adjusted model containing only 99 segments (see figure 9.2). The pulse wave velocity in the model was assessed in three different

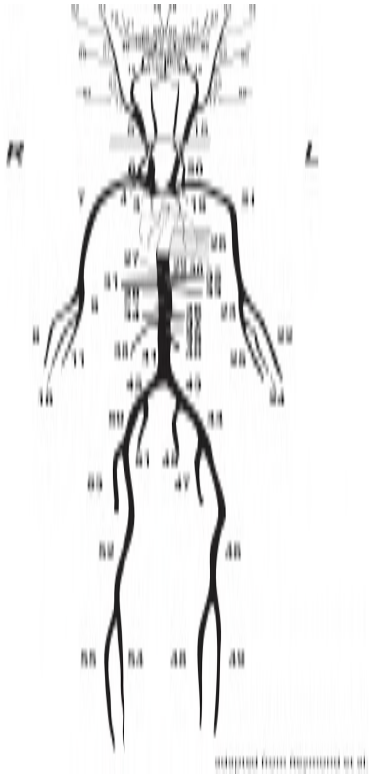

Figure 9.2: Representation of the arterial topology used in the computer model (adapted from [97]). In the occluded model, segments 22-25 were removed in order to simulate the occlusion of the brachial artery by the cuff.

ways.

First, PWV was determined by measuring the foot-to-foot transit time between the pressure signals at the carotid and femoral arteries ($PWV_{car-fem}$).

The foot of the pressure waveform was determined as the maximum of its second derivative [168, 169]. The distance between two nodes could be determined by adding up the lengths of the different segments that connect these nodes. The carotid-femoral distance was then determined as the distance from the aortic root to the femoral artery minus the distance from aortic root to carotid artery, thus correcting for the time the waves are travelling in the opposite direction. The resulting distance was 52.8 cm.

Second, the theoretical PWV value for each segment was calculated from the model parameters as

$$PWV = \frac{1}{\sqrt{\rho D}} \tag{9.1}$$

with ρ the blood density (1050 kg/m^3 in the model) and D the distensibility of the segment. A description of how segment distensibility was determined has been provided by Reymond *et al.* [97]. Averaging of PWV for all segments of the aorta, weighted according to the segment lengths, yielded the theoretical PWV which we considered as the gold standard in this work (PWV_{theor}).

In a third approach, PWV was calculated using the Arteriograph method: the distance from jugulum to symphysis was approximated by adding the segment lengths from the thoracic aorta (starting just after the branch towards the occluded brachial artery) to the aorto-iliac bifurcation, resulting in 37.5 cm. Twice this distance was divided by the transit time between the two peaks in the pressure signal (see also figure 9.1) to find values for pulse wave velocity, PWV_{ATG}.

All simulations were performed for 6 different levels of stiffness of the model, obtained via multiplication of the default compliance value of each segment with a constant compliance factor, changing the compliance from 40% to 140% of its default value in steps of 20%. By changing the compliance in each segment of the arterial tree, we were able to assess the influence of the arterial stiffness on the pulse wave velocity in both configurations of the model. Apart from the compliance of the segments, three more model parameters were varied to test the robustness of the methodology. Extra simulations were run on the occluded model by changing the default arterial resistance of each terminal Windkessel to 80% and 120% of its original value, by changing the duration of a heart cycle to 0.7 and 0.9 seconds instead of the original 0.8 seconds and by changing the maximal elastance (E_{max}) of the heart model to 1.5 and 3.5 mmHg/ml instead of the default value of 2.5 mmHg/ml. This allowed us to compute 7 different PWV-values for each compliance level. We thus found a cloud of PWV's for each of the three methods, and these were analysed using Bland-Altman analysis. To further test the method's sensitivity to isolated changes in stiffness along the brachial trajectory, two extra simulations were performed: in a first simulation only the compliance of the brachial segments was changed (from 40% to 140%

of its default value in steps of 20%) while all other segments maintained their default compliance value. In a second simulation compliance was changed for all segments in the arterial tree except the brachial ones.

For both the occluded and the original model, pressure and flow waveforms were calculated at 5 equidistant locations along the brachial artery using the default model parameters (default compliance and resistance values, heart cycle of 0.8 s, E_{max} of 2.5 mmHg/ml). Furthermore, we also calculated similar data at 5 locations along the ascending, descending and abdominal aorta to investigate whether the propagation of the reflected waves in the abdominal aorta was similar in both models. The obtained pressure and flow waveforms were further processed in Matlab (Mathworks, Natick, MA) [94, 170].

9.2.3 Data and wave reflection analysis

We performed wave intensity analysis on the pressure and flow signals of a simulation on the occluded model with default parameters (default compliance and resistance values, heart cycle of 0.8 s, E_{max} of 2.5 mmHg/ml) to gain more insight into the nature and origin of the different peaks occurring in the signals [87, 90]. The theory of wave intensity analysis was elaborated by Parker and Jones [90] and we refer to their work for details on the method. In brief, disturbances to the flow lead to changes in pressure (dP) and flow velocity (dU), "wavelets", which propagate along the vessels with a wave speed (PWV). Each wavelet is, in its turn, composed of a forward (subscript +) and backward (subscript -) running component, related by

$$dP\pm = PWV \cdot \rho \cdot dU\pm \tag{9.2}$$

with PWV the local PWV_{theor} provided by the computer model. Waves characterized by a dP>0, that is a rise in pressure, are called compression waves, while waves with dP <0 are expansion or suction waves. The nature of a wave was further assessed by analysing the wave intensity, dI, which is defined as the product of dU and dP, and equals the rate of energy flux carried by the wavelet. When dI is positive forward waves are dominant; negative dI indicates dominant backward waves. Wave intensity in itself was then also separated in a net forward and backward wave intensity: $dI_+ = dP_+ \cdot dU_+$ and $dI_- = dP_- \cdot dU_-$, where the "+" denotes a forward travelling wave, while "-" denotes a backward travelling wave. After having computed forward and backward intensity waves in the brachial artery, we computed the distance travelled by these waves to their reflection point. In order to do so, the transit time between a forward wave and its backward reflection is combined with the local theoretical PWV in the brachial artery. Since the wave is travelling back and forth to its reflection site, this allows us to compute the distance to the reflection site as

$$L = \frac{\Delta T\, PWV_{theor}}{2}. \tag{9.3}$$

Beside the wave intensity analysis, we also determined the forward and backward pressure components at different locations in the aortic trunk and in the brachial artery to unravel the patterns of wave reflection in the normal and occluded configuration. Pressure (P) and flow (Q) can be considered to be composed of one forward running component P_f (Q_f) and one backward running component P_b (Q_b), where the single forward and backward running components are the resultant of all forward and backward travelling waves. These forward and backward components were derived as [19]:

$$P_f = \Sigma dP_+ \tag{9.4}$$

$$P_b = \Sigma dP_- \tag{9.5}$$

9.3 Results

9.3.1 Effect of brachial occlusion on the pressure waveform

Figure 9.3 shows pressure waveforms at the distal end of the brachial artery (immediately proximal to the occlusion site) for both the control (top left) and the occluded model (top right). To assess the influence of the stiffness of the arteries on the obtained pulse wave velocity the pressure signals were computed for 6 different levels of arterial compliance, keeping all other model parameters on their default value. The time delay between the first and second systolic peak in the occluded model ΔT_{s1-s2}, that should be related to aortic PWV according to the Arteriograph principle (see figure 9.1), decreased from 0.271 s to 0.123 s for compliance decreasing from 140% to 40% of its original value (not all values are shown in figure 9.3 to improve visibility).

Figure 9.3 also shows the resulting brachial pressure waveforms when compliance of the occluded model is only altered in the brachial segments (bottom left), and in all segments except the brachial ones (bottom right). It is observed that ΔT_{s1-s2} is proportional to the change in compliance when compliance was altered in all segments and when it was altered in the brachial segments only, but there was no change in the time delay between the first and second systolic peaks when the compliance in the brachial segments was not altered.

9.3.2 Impact of model stiffness, resistance and cardiac parameters on PWV

In figure 9.4, the three methods used to determine PWV are compared. For all methods, PWV increased significantly over the simulated range, varying from about 5.2 m/s to 9.2 m/s (theoretically calculated values). This is consistent with a nearly 4-fold decrease in total arterial compliance. There was a good correlation between PWV_{theor} and $PWV_{car-fem}$ (R^2=0.95), but $PWV_{car-fem}$ was systematically lower than PWV_{theor} (difference: 1.08±0.70 m/s). Bland-Altman

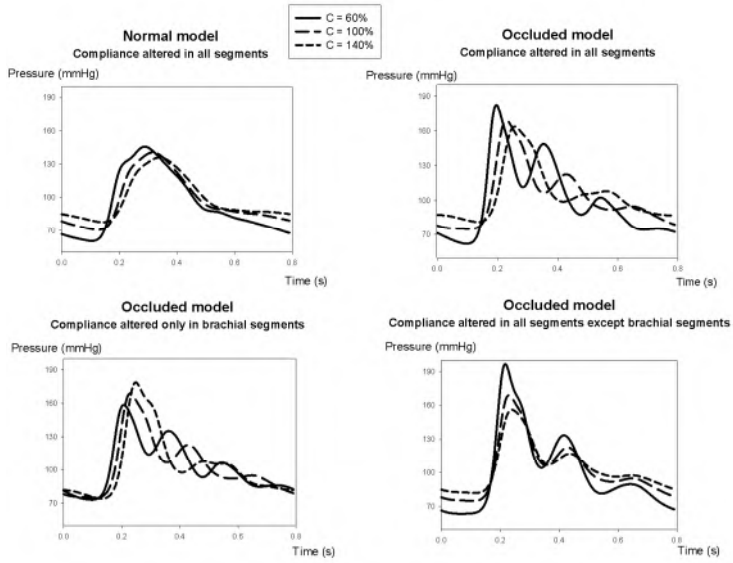

Figure 9.3: Pressure waveforms at the location of the cuff (brachial artery) for three levels of total arterial compliance (in % of the default value). Top left: normal model. Top right: occluded model, compliance altered in all segments. Bottom left: occluded model, compliance altered only in brachial segments. Bottom right: occluded model, compliance altered in all segments except the brachial segments.

analysis showed that the underestimation increased with higher values of PWV (figure 9.4). There was also a good correlation between the theoretical pulse wave velocities and those calculated using the Arteriograph method (R^2=0.94), but again PWV_{ATG} was lower than PWV_{theor} (difference: 2.17±0.42 m/s), the underestimation increasing with higher values of PWV (figure 9.4). Comparing $PWV_{car-fem}$ with PWV_{ATG}, both methods correlate well (R^2=0.90), with $PWV_{car-fem}$ being on average 1.09±0.48 m/s higher than PWV_{ATG}. The difference between both, however, becomes smaller with higher values of PWV. We conclude that, although PWV_{ATG} correlates well with both PWV_{theor} and $PWV_{car-fem}$, the numerical values of the Arteriograph method are clearly lower than those of the other methods.

Reducing the resistance of each terminal Windkessel to 80% of its default value resulted in a decrease of mean blood pressure and, given the non-linear coupling between blood pressure and stiffness, a lowering in PWV with 8±3% of its initial value (average normalized difference ± SD for 18 simulated cases: 3 different methods and 6 compliance levels per method). Increasing the resistance to 120% of its initial value increased PWV with 7±4%. Shortening the heart cycle from 0.8 s to 0.7 s resulted in an increase in (blood pressure and) PWV with 5±3% of its initial value, whereas PWV decreased with 6±3% when the

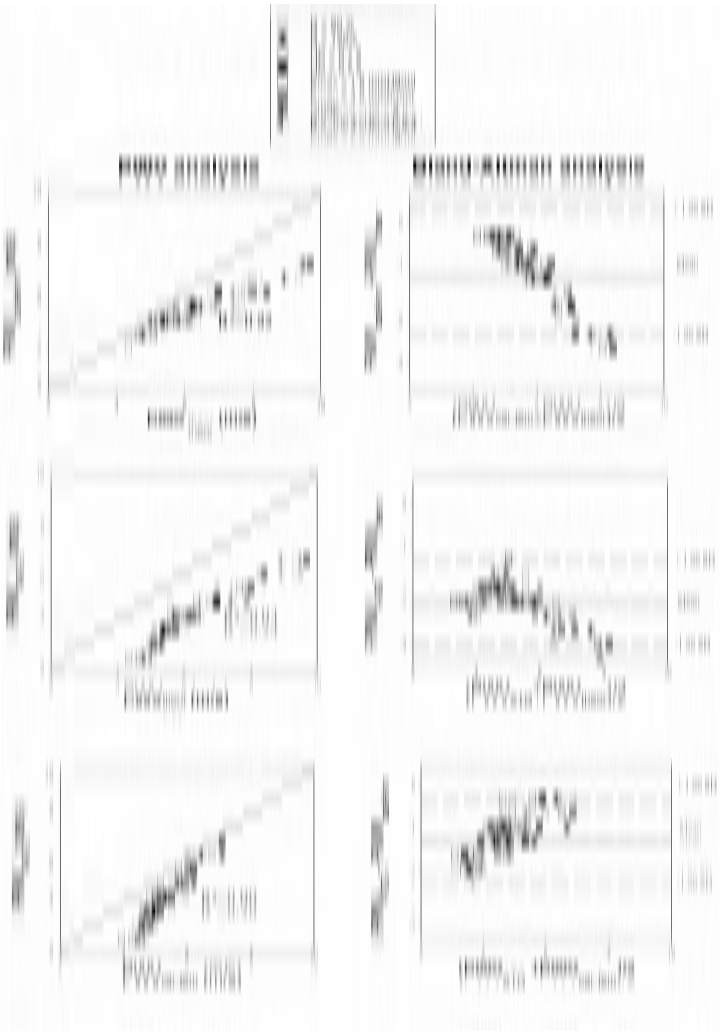

FIGURE 9.4: Correlation between different methods to compute pulse wave velocities with varying model parameters. Resistance (R), heart cycle length (HC) and maximal heart elastance (Emax). Top: carotid-femoral PWV vs theoretical PWV. Middle: arteriograph PWV vs theoretical PWV. Bottom: arteriograph PWV vs carotid-femoral PWV.

heart cycle was elongated to 0.9 s. Finally, PWV values decreased with 14±7% when the maximal heart elastance E_{max} was lowered from 2.5 mmHg/ml to 1.5 mmHg/ml, and PWV values increased with 9±5% when E_{max} was raised to 3.5 mmHg/ml. These changes were again modulated by the changes in operating blood pressure.

9.3.3 What is causing the change in transit time?

In figure 9.5 the influence on PWV_{ATG} of altering compliance in only the brachial segments is compared to the influence of altering compliance in all but the brachial segments. When compliance is decreased in all but the brachial segments, PWV_{theor} and $PWV_{car-fem}$ increase but PWV_{ATG} remains constant. This can also be observed in figure 9.3 (bottom right), since transit times did not change in the occluded model when compliance in the brachial segment was kept at its original value. Similar results are found by altering compliance only in the segments of the aortic trunk, where most of the compliance of the arterial system resides (not plotted). On the other hand, increasing compliance only in the brachial artery results in an increase of PWV_{ATG} whereas PWV_{theor} and $PWV_{car-fem}$ obviously remain constant since stiffness in the aorta is not changing. We also observe that the corresponding transit times (and resulting PWV_{ATG} values) are identical to the simulation where compliance in all segments was altered. This implies that all correlations between PWV_{ATG} and PWV_{theor} or $PWV_{car-fem}$ as they are plotted in figure 9.4 are modulated by the local change in stiffness in the (occluded) brachial artery and not by the change in aortic stiffness of the complete model as such. To further investigate the ori-

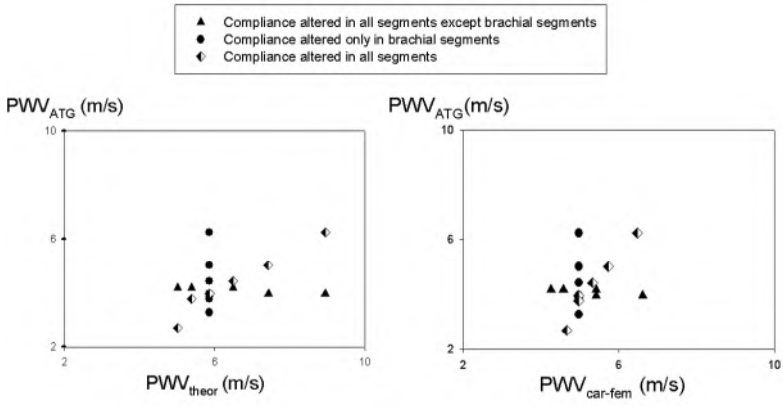

Figure 9.5: Correlation between different methods to compute pulse wave velocities when altering compliance only at the brachial segments, when altering compliance in all segments except the brachial segments, and when altering compliance in all segments (default). Left: Arteriograph PWV vs theoretical PWV. Right: Arteriograph PWV vs. carotid-femoral PWV.

gin of the second peak in the pressure signal of the occluded model, the pressure

waveforms and their forward and backward components are compared on 5 different locations throughout the brachial artery (figure 9.6) and the aortic trunk (figure 9.7). This was done for both the normal and the occluded model using default parameters. In figure 9.6, the timing of the forward waveforms throughout the brachial artery is similar in both models: the more distal in the brachial artery, the greater the time delay since the pressure wave arrives later. The amplitude of the forward waveforms is similar in both models, depending on the compliance. In the backward waveforms, more important differences between both configurations can be noticed. The amplitude of the backward components in the occluded model is much higher. Also in the occluded model, the reflected wave appears first at the occlusion and only later at the proximal part of the brachial artery, while the timing of the backward component is scattered in the non-occluded configuration.

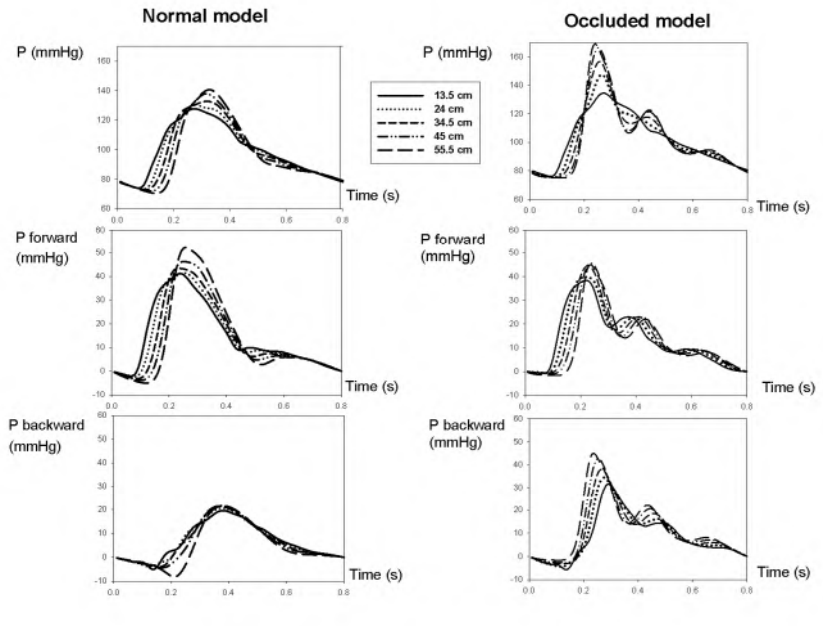

FIGURE 9.6: Pressure waveforms at 6 locations throughout the brachial artery (distances are expressed in cm to the aortic root). Top: total pressure; middle: forward pressure; bottom: backward pressure.

Studying the waveforms (and the forward and backward components) along the aortic trunk (figure 9.7) did not reveal obvious differences between the occluded and non-occluded configuration. This is another indication that the second peak in the pressure signal is probably caused by a local phenomenon in the brachial artery, and is not linked to waves travelling back from the lower body.

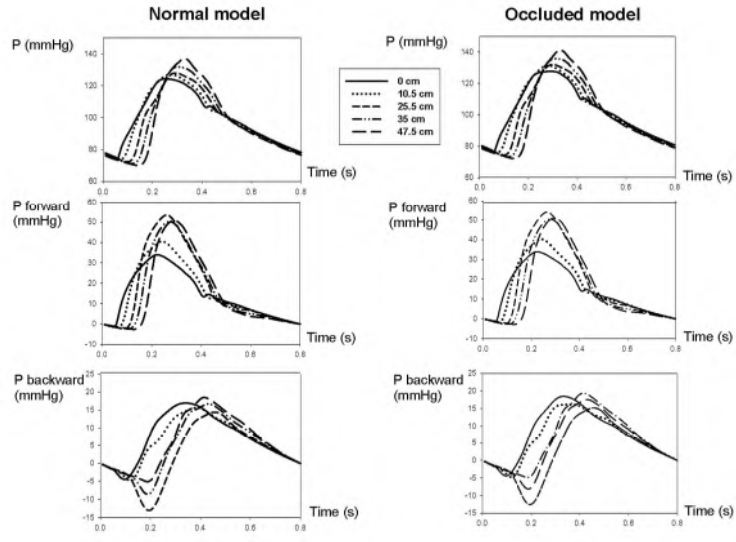

Figure 9.7: Pressure waveforms at 6 locations throughout the descending and abdominal aorta (distances are expressed in cm distal from aortic root). Top: total pressure; middle: forward pressure; bottom: backward pressure.

9.3.4 Wave intensity analysis

The results of the wave intensity analysis performed on the pressure and flow signals just proximal to the occlusion of the brachial artery are shown in figure 9.8. Analysis of the normal model reveals a forward compression wave (P_1), arising from the systolic ejection. This wave is followed by a backward compression wave (P_2), a (positive closed end) reflection of the first forward wave in the brachial artery itself. Then there is a forward expansion wave (P_3) linked with the relaxation of the left ventricle. Performing the same analysis for the model of an occluded brachial artery reveals that now the peak intensity of the first backward compression wave (P_2') is almost three times stronger than in the original model. This strong backward compression wave is caused by the total reflection of the incident wave on the brachial occlusion. Next, we observe a forward expansion wave P_3', that is most probably a reflection of P_2'. To assess the origin of this reflection, the distance travelled by the reflected wave was calculated. Combining the peak-to-peak time difference between P_3' and P_2' and the local theoretical PWV in the brachial segment, the distance from the measurement point to the reflection point was determined to be 29.5 cm. This distance approximates the distance to the point where the subclavian artery, later becoming the brachial artery, branches from the aortic arch (35.05 cm upstream from the location where wave intensity analysis is performed). We therefore

hypothesize that the reflected backward compression wave P_2' is re-reflected at the location where the subclavian branches from the aorta, and is picked up at the location of the cuff as the forward expansion wave P_3'. Next, P_4' is a backward expansion wave caused by the reflection of P_3' on the occlusion and P_5' is again a forward compression wave, caused by the reflection of P_4'. The distance matching the peak-to-peak transit time between P_4' and P_5' is 30.2 cm, thus we can reasonably assume that this wave is reflected at the same point as the previous wave. It is obvious from the timing in figure 9.8 that P_5' is the wave causing the pronounced second peak in the pressure signal picked up by the Arteriograph. Using wave intensity analysis, we have thus shown that P_5' is a forward compression wave, caused by a re-re-re-reflection of the first incident wave. This wave is travelling back and forth between the occlusion of the cuff and the point where the subclavian artery branches from the aortic trunk.

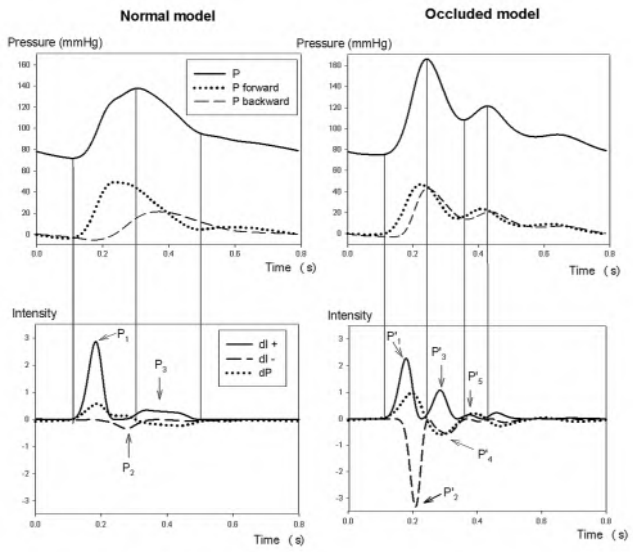

FIGURE 9.8: Wave intensity analysis at the location of the cuff (brachial artery) for C=100%. Bottom: wave intensity analysis in normal model (left) and occluded model (right). Top: effect of wave intensity on pressure signal and forward and backward pressure components in normal model (left) and occluded model (right).

9.4 Discussion

The main conclusions that we can draw from this computer model study are: (i) occlusion of the brachial artery introduces a total reflection at the upper arm which introduces a pronounced second peak in the brachial pressure curve; (ii) when compliance of the model is altered over the complete arterial tree, the pulse wave velocity calculated following the Arteriograph principle is lower than but correlates well with both the theoretical and carotid-femoral PWV; (iii) this correlation, however, is modulated by local stiffness modifications in the brachial artery and is not linked to aortic stiffness in the remaining parts of the arterial system.

Our study questions the working principle of the Arteriograph and, at the same time, also raises some concern with respect to the ability of the device to provide accurate values of PWV, comparable to transit time methods. The main difference between the Arteriograph and most other methods to measure pulse wave velocity from transit times is that the Arteriograph only measures at one location: the upper arm. As such the device has a clear practical advantage over other techniques since it is much easier in use and measurements can be done significantly faster.

As for available in vivo data, in a first validation study, pulse wave velocity measured by the Arteriograph was compared to that of other devices, and a reasonable agreement has been found [171–173]. Baulmann *et al.* [171] determined PWV on 64 patients with three different devices. PWV measured with the Arteriograph was 8.6±1.3 m/s , which was different from that measured by two frequently used transit time based methods (with measurements on the carotid and femoral artery), i.e., the Complior system®(10.1±1.7 m/s) but similar to measurements with Sphygmocor®(8.1±1.1 m/s). The differences in PWV were entirely ascribed to different techniques used to determine the travelled distance, since there was no statistical difference between measured transit times. The correlation between Arteriograph and Complior ($p=0.005$) and Arteriograph and Sphygmocor ($p=0.043$) was significantly worse than the correlation between Complior and Sphygmocor ($p=0.001$). Magometschnig [173] found values of 9.1±1.8 m/s for Arteriograph and 8.4±1.5 m/s for Sphygmocor. However both measurement techniques did not correlate ($r=-0.04$). Illyes [174] also measured PWV as a function of age for 2299 patients and found a linear correlation between measured PWV and age ($r=0.52$). This is in line with the expectations since PWV is known to rise with age.

We tried to match these literature results with the results from the present study. As can be observed from figure 9.3, occlusion of the brachial artery introduces a second peak in the brachial pressure curve which, in normal circumstances, is hardly noticeable. This finding supports the basic working principle of the Arteriograph: inflation of the brachial cuff to a supra-systolic pressure

occludes the artery and leads to an amplification of the second peak making the signal strong enough to be picked up by the sensor embedded in the cuff.

In figure 9.4 the three methods to compute PWV were compared. The excellent correlation between the theoretical PWV and $PWV_{car-fem}$ indicates that this method, which is often used to measure PWV in vivo since these arteries are relatively easy to access with a tonometer or an ultrasound probe [59, 175–177] can be sufficiently accurate to determine pulse wave velocities in vivo. Note, however, that the absolute value of PWV provided by this method is also substantially lower than the theoretical PWV. Moreover, the Bland-Altman plot reveals a trend of underestimation of $PWV_{car-fem}$ for higher values of PWV. We speculate that the discrepancy between the theoretical PWV and $PWV_{car-fem}$ is due to the fact that the theoretical PWV value, derived from the Bramwell-Hill equation [178], applies to the ideal case of an infinitely long tube ignoring effects of viscous friction and wave reflection. Furthermore, an error is introduced via the ambiguity of the travel path of the carotid and femoral pulse [179].

As for PWV_{ATG} - focusing on the simulations where stiffness is altered to the same degree over the complete arterial territory - the correlation with theoretical PWV is similar (R^2=0.94) but the numerical values are systematically lower than $PWV_{car-fem}$. The most obvious explanation for this phenomenon is that, despite the fact that the measured transit times correlate well to the actual PWV values, the distance that was used to calculate PWV from these transit times does not yield correct results. One of the major assumptions made in the Arteriograph is that the second peak in the pressure signal is caused by a reflection of the forward wave at the aorto-iliac bifurcation, which is assumed to be the single reflection point.

In order to further investigate this assumption, we have tried to explain the origin of the secondary peak in the pressure signal of the occluded model by making use of wave intensity analysis (figure 9.8). It is particularly the appearance of a third forward wave (P'5) that is of interest for this analysis. Linking the timing of P'5 to the pressure signal in figure 9.8 shows that this wave is causing the second peak in the pressure signal that is picked up by the Arteriograph and used to determine the PWV_{ATG}. Since both dP and dI are positive, P'5 is a forward compression wave. At first sight this supports the assumption made in the Arteriograph, since a reflection coming from the lower body should be a compression wave travelling in the forward direction in the brachial artery. However, analyzing the wave intensity results and the distances that correspond with the transit times between the different waves, we see that dP'5 is actually a re-reflection of P'3, which in turn is a re-reflection of P'1. Thus, the wave is travelling back and forth between the occlusion and the location where the subclavian artery branches from the aortic arch, and there is no reflection originating from the lower body.

This finding is supported by figure 9.5, showing that the correlation between PWV_{ATG} and aortic PWV is entirely due to local stiffness changes in

the brachial artery, contradicting the supposed working principle of the Arteriograph. If the second peak in the pressure signal would indeed be caused by a wave travelling back from the lower body, its timing should be influenced by a change in aortic stiffness of the aortic segments it is passing through, which is not the case. Also, this wave should be noticeable in the abdominal aorta waveforms, which is not the case either (figure 9.7). In the brachial artery waveforms however, we clearly see a backward travelling wave (figure 9.6). All this leads us to conclude that, even though PWV_{ATG} correlates well to PWV_{theor} and $PWV_{car-fem}$, the underlying principle causing this correlation is probably not a wave reflected from the lower body, but a local reflection occurring in the brachial artery.

The excellent correlation between theoretical PWV and PWV_{ATG} found in figure 9.4 is driven by the fact that the stiffness of the brachial arteries and central vessels was changed to the same extent. Also in humans, stiffness of the upper brachial segment is likely to be related to aortic stiffness [180], which might explain some of the reported in vivo findings. On the other hand, especially for the more peripheral, muscular arteries, there might be discrepancies in the evolution of stiffness with age (and disease) compared to the more central, elastic arteries [125]. The key question therefore remains to what extent the arteries in the brachial segment reflect the properties of the large, central aorta. Anyhow, it follows from our analysis that any value of PWV derived from the Arteriograph is, at best, an indirect and unspecific estimate of the stiffness of the aorta.

9.5 Limitations

This is a computer model simulation study with its inherent strengths and limitations. Its strength lies in the fact that pressure and flow signals can be calculated at every location in the arterial tree with great accuracy without any measurement error. A numerical model, however, remains an approximation of reality: the arterial tree is not modelled into great detail (e.g. the microcirculation has not been taken into account). However the model has been validated and has been shown to produce realistic waveforms [97]. Still, the pressure curves that were simulated in this work represent an ideal case and do not take into account any damping of the pressure signals in the cuff nor the damping that will occur in the transmission of the pressure signal from the brachial artery through the skin towards the pressure sensor. Therefore the curves that are actually measured by the Arteriograph will probably show a less distinct second peak, making it harder to recognize and measure the transit time.

In our simulations the left brachial artery was occluded. Typically, the left subclavian artery (later becoming the brachial artery) arises directly from the aortic arch as the third and final of the great vessels, while the right subclavian artery arises from the bifurcation of the brachiocephalic trunk. Therefore

occlusion of the right brachial artery might result in slightly different wave reflections, although we don't expect large differences.

The exact algorithm used by the device to determine the transit time and the corresponding pulse wave velocity is unknown. We calculated the transit time from the peak-to-peak time difference between the first and second peak. It is generally agreed upon that the foot-to-foot method usually yields the most accurate results, but it is not always easy to determine the foot of the second peak in the signal. It is unclear what method is used by the Arteriograph to determine the transit time, so it is possible that, provided with the same pressure curves, the device would calculate different transit times.

9.6 Conclusions

We have validated the working principle of a newly proposed method to measure aortic pulse wave velocity (the Arteriograph method) using a numerical model of the arterial tree. This method bases its transit time calculation on a second peak in the pressure signal of the over-inflated brachial cuff, which also appeared in our simulations. However, exactly the same change in transit time was observed by altering brachial compliance only, indicating that PWV_{ATG} is only dependent on brachial stiffness and not on stiffness in the remaining part of the arterial tree. Wave intensity analysis also showed that the wave causing the second peak in the pressure signal is travelling back and forth between the occlusion and the location where the subclavian artery branches off from the aorta, and is not originating from a reflection in the lower body. Despite this, numerical values of PWV_{ATG} correlate well to standard methods such as the carotid-femoral transit time or the theoretical Bramwell-Hill equation, but the Arteriograph yields lower absolute values. A possible explanation for this correlation is that the stiffness of the upper brachial segment is likely to be related to aortic stiffness. Finally, one should keep in mind that this is a numerical study aiming to test the theoretical principle behind the Arteriograph, and we cannot make any judgement on the functioning of the device itself. An independent clinical study would be needed to confirm our results and to test the robustness of the device and its algorithms when confronted with non-theoretical measurement data.

CHAPTER 10

Central systolic blood pressure: Omron HEM-9000AI versus SphygmoCor device

The results of this study were published in:
Jan G. Kips, Aletta E Schutte, Sebastian J. Vermeersch, Hugo W. Huisman, Johannes M. Van Rooyen, Matthew C. Glyn, Catharina M. Fourie, Leone Malan, Rudolph Schutte, Luc M. Van Bortel, Patrick Segers. *Comparison of central pressure estimates obtained from SphygmoCor, Omron HEM-9000AI and carotid applanation tonometry.* J Hypertension 2011, accepted for publication.

10.1 Introduction

Central systolic blood pressure (cSBP) has received extensive attention in recent years because there is increasing evidence that it may be a better predictor of future cardiovascular events than brachial pressure [78, 117–119, 121, 123, 181]. The use of central pressures in daily clinical practice is currently hampered by the fact that most measurement devices, although non-invasive, require a trained operator, introducing potential operator dependence. With the recent development of automated and hence operator-independent devices such as the Omron HEM-9000AI (Omron Healthcare, Kyoto, Japan), data collection is facilitated, bringing central pressure a step closer to routine clinical practice. However, Richardson *et al.* [165] recently compared the central pressure estimates from

Omron HEM-9000AI and SphygmoCor (Atcor Medical, Sydney, Australia) in a relatively small (n=33) population sample of healthy Caucasians, aged 20 to 61 years. They found a high correlation (r=0.95), but a mean (SD) difference of 12.2 (4.6) mmHg between both cSBP estimates, the Omron HEM-9000AI yielding the highest estimate. The reason for this difference remains unclear. Although both devices derive cSBP from the radial pressure waveform, SphygmoCor uses a radial-to-aortic generalized transfer function, while Omron HEM-9000AI relies on the relation between cSBP and the second systolic peak (P2) in the radial pressure waveform. Though previous studies [165, 182–184] have used radial P2 as such as an estimate of central pressure, the Omron HEM-9000AI makes use of an additional linear equation to calculate cSBP from the radial P2. The aims of this study are: (1) to perform an extended comparison between the cSBP-estimates of Omron HEM-9000AI and SphygmoCor in a large population sample of rural black South Africans; (2) to assess the sources of differences between both cSBP-estimates, and (3) to assess which of the two methods is most likely to provide the most accurate estimate of central systolic blood pressure. For this last objective, non-invasively measured carotid pressure is used as a reference since it can be measured directly, does not rely on any transfer function and was found to be only 1.8 mmHg higher than central aortic pressure in an invasive study by Van Bortel *et al.* [59, 61].

10.2 Methods

10.2.1 Study population

A total of 143 rural black South Africans (aged 39-91 years), enrolled as part of the Prospective Urban Rural Epidemiology (PURE) study [185], were included in this study. Subjects had fasted and measurements were taken in seated position after at least 10 minutes of supine rest and 5 minutes of seated rest.

10.2.2 Measurements

Radial artery tonometry was performed on the left arm of each subject, first with an Omron HEM-9000AI (acquiring 30 seconds of wave data) and subsequently with a SphygmoCor (acquiring 10 seconds of wave data). Both recordings were calibrated using the cuff blood pressure measured with the Omron HEM-9000AI just prior to central pressure assessment. Additional tonometer measurements were performed on the left brachial artery and the left carotid artery with the SphygmoCor. The quality of the recordings was assured by discarding all Omron recordings with an error message and all SphygmoCor measurements with an operator index below 80. The Omron HEM-9000AI device was operated by two cardiovascular physiologists. All SphygmoCor measurements were performed by a single experienced operator (JK).

10.2.3 Central blood pressure estimation

Central pressure recordings were obtained using the SphygmoCor (cSBP-Sphygmo) and Omron HEM-9000AI (cSBP-Omron) as advocated by their manufacturers and user manuals, i.e. from radial pressure waveforms calibrated using brachial SBP and DBP. Carotid systolic pressure (cSBP-Carotid) was obtained from carotid pressure waveforms recorded by SphygmoCor, calibrated with brachial MAP and DBP obtained from brachial tonometry. This calibration method assumes the MAP and DBP to remain constant throughout the large arteries [59, 61]. Assuming that carotid SBP overestimates the invasive cSBP by 1.8 mmHg [59], an alleged aortic SBP (cSBP-Aortic) was calculated as cSBP-Carotid minus 1.8 mmHg. The calibration method using brachial MAP and DBP has been shown to yield more accurate central pressure estimates, as it takes into account the brachial-to-radial pressure amplification [61]. Therefore, central pressure using radial SphygmoCor recordings was re-calculated using brachial MAP and DBP (cSBP-Sphygmo2).

In order to assess whether potential differences between methods are due to the use of different radial pressure waves as input or due to the different processing algorithms, we additionally calculated central pressures from radial pressure waveforms recorded by Omron HEM-9000AI hardware and processed by SphygmoCor-software (cSBP-OmronSphygmo).

10.2.4 Comparison of measured radial pressure waveforms

To quantify differences in waveform features, the following variables were calculated:

- *form factor (FF)*, defined as the ratio (%) of the difference between the mean arterial pressure (MAP) and the diastolic pressure (DBP) and the pulse pressure (PP): $FF = \frac{MAP-DBP}{PP}$, see figure 10.1. The form factor is a measure of how peaked the waveform is, and is calibration-independent.
- *radial augmentation index (AIx)*, defined as the amplitude of the second systolic peak divided by the amplitude of the first systolic peak (P2/P1) and expressed as percentage (figure 10.1).

Whereas the form factor is a global measure reflecting the overall shape of the waveform, AIx depends on the second systolic peak (P2), a more detailed feature of the wave shape. Moreover, this second systolic peak is used by the Omron HEM-9000AI to calculate cSBP and therefore relevant for this study. For this analysis, both the Omron HEM-9000AI and SphygmoCor recordings were processed with the SphygmoCor-software.

10.2.5 Statistical analysis

Data are presented as mean (SD). The correlation between variables was assessed using Pearson correlation coefficients. Differences between cSBP-estimates were assessed using paired student T-tests. To assess the determinants of the

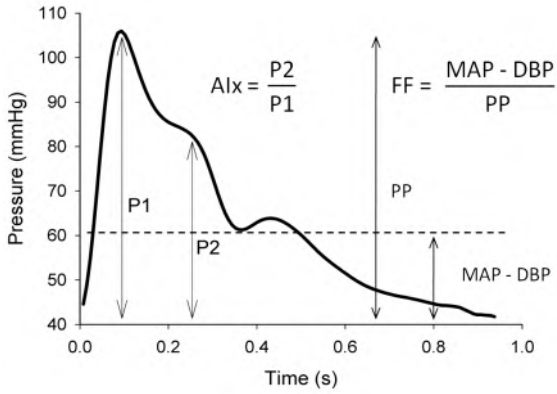

Figure 10.1: Augmentation index (AIx) and form factor (FF).

difference in cSBP between Omron HEM-9000AI and SphygmoCor, a forward multiple regression analysis was performed including age, gender, BMI, brachial SBP and DBP as potential factors. P-values lower than 0.05 were considered as statistically significant. All statistical analyses were performed in PASW Statistics 18 (IBM, Chicago, IL, USA).

10.3 Results

Basic population characteristics are shown in Table 10.1. The ratio male/female was 63/80 and 59 of all subjects were hypertensive according to ESH guidelines (15) (prevalence of 41%).

Table 10.1: Basic population characteristics.

Parameter	Mean (SD)
Age (years)	56.3 (10.6)
Weight (kg)	58.9 (12.8)
Length (cm)	162.1 (8.4)
BMI (kg/m^2)	22.4 (4.8)
Systolic BP (mmHg)	137.7 (25.6)
Diastolic BP (mmHg)	82.1 (12.9)
MAP (mmHg)	104.2 (16.4)
Heart rate (bpm)	70.6 (13.1)

BMI,Body Mass Index; BP, blood pressure;
MAP, mean arterial pressure

Central blood pressure estimation

The mean (SD) values of all central pressure estimates are listed in Table 10.2. When using both devices as advocated by their manufacturers, the corresponding central pressure estimates (cSBP-Omron and cSBP-Sphygmo) correlated strongly ($r=0.99$, $p<0.001$), but the mean difference was substantial: 18.8 (4.3) mmHg, $p<0.001$ (Figure 10.2), with Omron HEM-9000AI yielding the highest estimate and the difference increasing for higher cSBP-values. The only significant determinant of this difference was brachial SBP ($r=0.66$, $p<0.001$).

Table 10.2: Central pressure estimates and second radial systolic peak.

	Mean (SD)
cSBP-Omron	147.9 (27.2)
cSBP-Sphygmo	129.1 (24.1)
cSBP-Carotid	138.0 (26.4)
cSBP-Aortic	136.2 (26.4)
cSBP-OmronSphygmo	129.7 (24.4)
cSBP-Sphygmo2	133.2 (26.2)

Compared to aortic SBP, the Omron cSBP-estimate was on average 11.7 (5.5) mmHg higher, whereas the SphygmoCor cSBP-estimate was on average 7.1 (5.0) mmHg lower. Alternative calibration of the radial SphygmoCor-curves with brachial MAP and DBP instead of brachial pressures yields a central pressure (cSBP-Sphygmo2) that is, on average, 3.0 (4.1) mmHg lower than aortic SBP. In order to focus on differences in waveform features only, the curves from both devices were processed with the same software (SphygmoCor), yielding strongly related central pressure estimates (cSBP-Sphygmo and cSBP-OmronSphygmo; $r=0.99$, $p<0.001$) with a small but significant difference (0.6 (2.1) mmHg, $p<0.001$).

Further comparison of the Omron HEM-9000AI and SphygmoCor waveform features was done by comparing the form factor and augmentation index. Comparison of form factors reveals an average difference of 2.3 (3.0), with FF-Omron the highest ($p<0.001$), see Figure 10.3. The correlation between both FFs was $r=0.65$ ($p<0.001$). The radial AIx of Omron HEM-9000AI and SphygmoCor curves are strongly correlated ($r=0.88$, $p<0.001$) with no significant mean difference (-1.0 (7.4) mmHg; Figure 10.3).

To assess whether the second systolic peak was detected properly in both algorithms, Omron's P2 is compared to the P2 of Omron waves re-analysed through SphygmoCor-software. In this way, potential differences are due to differences in software only. Figure 10.4 shows an average difference of 2.2 (2.7) mmHg, the Omron-software yielding the lowest P2.

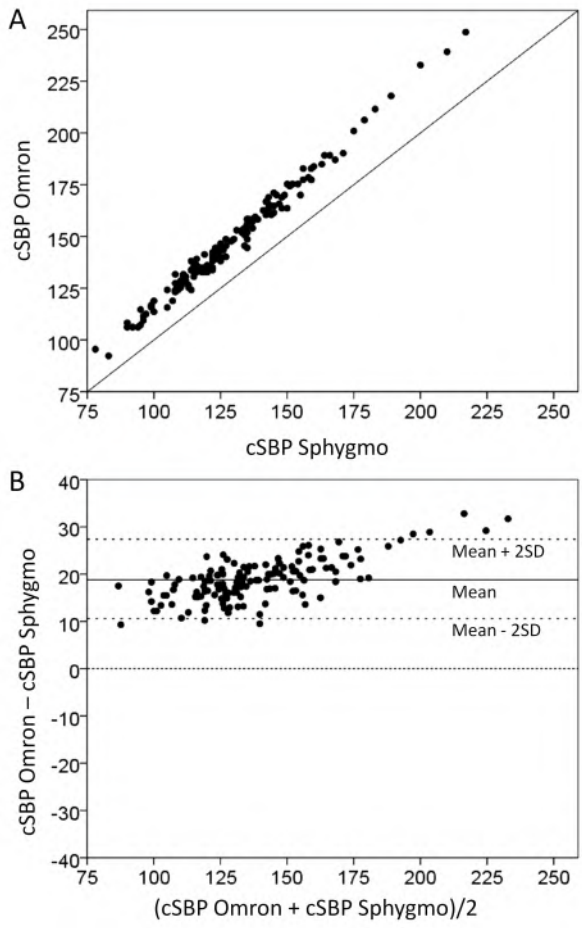

Figure 10.2: Omron HEM-9000AI's versus SphygmoCor's central systolic pressure estimate: regression (A) and Bland-Altman plot (B). cSBP-SphygmoCor was obtained via calibration of the radial waves with brachial pressures.

10.4 Discussion

The results from this study demonstrate a considerable difference between the central pressure estimates from SphygmoCor and Omron HEM-9000AI. Additionally, by comparing both Omron HEM-9000AI and SphygmoCor cSBP-estimates to carotid systolic pressure and derived alleged aortic pressure, this study is the first to provide a handle on which estimate is closest to reality. Furthermore, re-processing of the Omron-waves through SphygmoCor-software allows to clearly separate the impact of any difference in recorded waveforms (due to potential differences in tonometry acquisition) from the impact of the

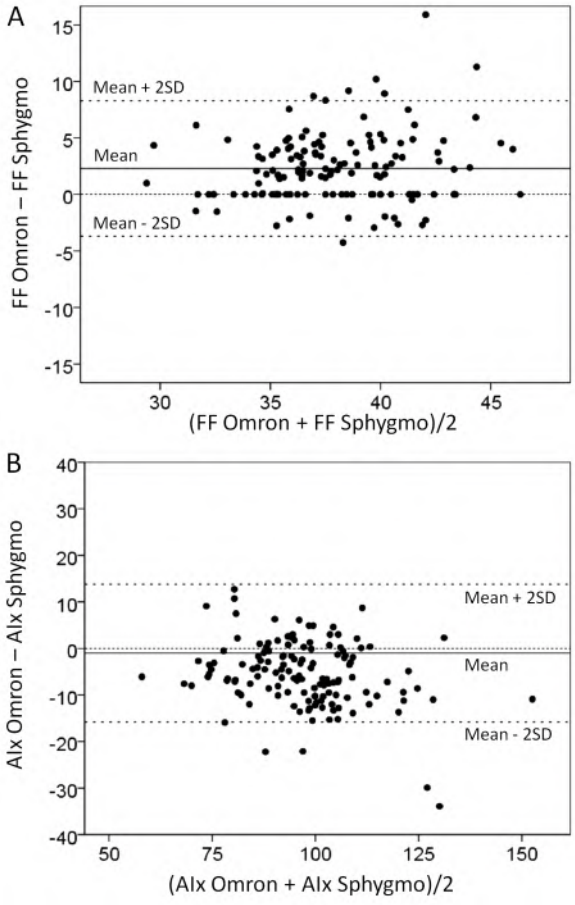

FIGURE 10.3: Comparison of radial pressure waveforms measured by Omron HEM-9000AI and SphygmoCor, both processed with SphygmoCor-software. Bland-Altman plots of the form factor (A) and radial AIx (B).

processing software (due to different tonometry signal processing) on the observed difference in central pressure estimates.

A first important finding is that, when using both devices as advocated by their manufacturers, the mean difference in cSBP was 18.8 (4.3) mmHg. Two factors can contribute to this difference. Firstly, a difference in acquisition-hardware, which would mean that the waveforms recorded with the two devices are not similar, and, secondly, differences in the algorithm to calculate cSBP. To assess the first factor, radial pressure waves recorded by Omron a HEM-9000AI and SphygmoCor were compared by their form factor and augmentation index. The Omron-waveforms had, on average, a higher form factor, indicating that they are less peaked. Although the average AIx was very similar

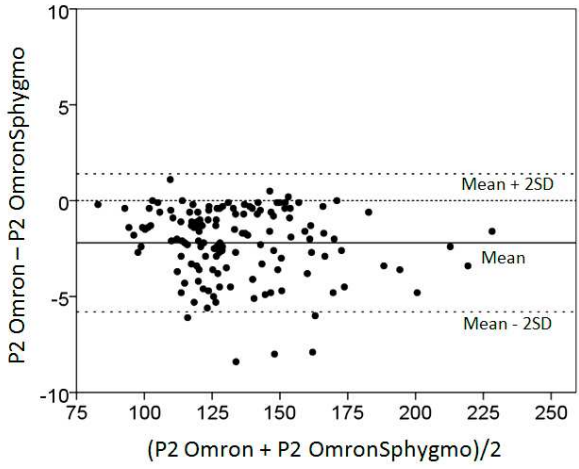

Figure 10.4: Bland-Altman plot of the second systolic peak in radial Omron HEM-9000AI pressure waves, detected with Omron-software (P2-Omron) and with SphygmoCor-software (P2-Omron2).

in Omron- and SphygmoCor-waves, large individual differences in AIx were observed (Figure 10.3). These differences however, seem to have little impact on the estimate of cSBP when using the SphygmoCor software. Indeed, when processing Omron-measured curves with SphygmoCor software, similar cSBP-estimates are obtained: the mean difference between cSBP-OmronSphygmo and cSBP-Sphygmo was 0.6 (2.4) mmHg, or less than 4% of the difference between cSBP-Omron and cSBP-Sphygmo. Unfortunately, the inverse, i.e. to process Sphymocor-measured curves with the Omron software was not possible. Nevertheless, it appears that the main reason for the difference in cSBP is to be sought in differences between the two algorithms, rather than in differences in measured waveforms.

A first potential difference between the two algorithms lies in the detection of the second systolic peak, which is used by the Omron HEM-9000AI to determine cSBP via a linear relationship. An overestimation of P2 by the Omron HEM-9000AI would lead to a higher cSBP via the linear regression equation. Contrary to what could be expected, the Omron-software places the second peak lower than the SphygmoCor-software does (Figure 10.4). Hence, the reason for the difference between cSBP-Sphygmo and cSBP-Omron should not be sought in the detection of the second peak either.

The use of a linear equation to transform P2 to central SBP could be questioned. Previous studies [182, 184, 186] have used untransformed radial P2 as an estimate of central SBP. In our population, radial P2 was on average 3.0 (3.3) mmHg higher than cSBP-Sphygmo.

Another potential difference could be due to the effect of ethnicity. It cannot be excluded that one of the two cSBP-algorithms (or both) perform differently in this black South African population as compared to Caucasian populations. The Omron HEM-9000AI algorithm appears to be based on a regression equation derived from Japanese subjects only [85]. SphygmoCor on the other hand has already been used in Africans [187–189], but was never validated with invasive measurements in a black population, and could therefore also be prone to errors. The applicability of both algorithms to the present population depends on whether the relation between radial and central pressure is different in Africans compared to other ethnicities. Verbeke *et al.* [61] measured carotid and central pressure with SphygmoCor in a middle-aged Caucasian population. They found the carotid pressure to be 9.7 mmHg higher than the central pressure when calibrating radial waveforms with brachial pressures (cfr cSBP-Sphygmo), or 5.7 mmHg when calibrating radial waveforms with brachial MAP and DBP (cfr cSBP-Sphygmo2). This matches very well with the corresponding differences found in the current study: 8.9 mmHg and 4.8 mmHg, respectively. While this only suggests that the relation between carotid and radial pressure does not differ between Caucasians and Africans, it seems reasonable to extrapolate that the relation between radial and central aortic pressure does not differ either[1]. Furthermore, the fact that Richardson *et al.* [165] found a similar difference in cSBP between Omron HEM-9000AI and SphygmoCor in their Caucasian population, renders it unlikely that ethnicity is the main reason for the observed difference in cSBP.

The obvious question remains: which estimate is closest to 'reality'? As invasive data are not available, one approach to answer this question is by comparing the cSBP-estimates to carotid SBP. Carotid SBP is calculated directly from carotid tonometry waveforms calibrated with brachial MAP and DBP, and therefore does not imply any assumption on the relation between radial and central pressure. Carotid SBP is intermediate between cSBP-Omron and cSBP-SphygmoCor, suggesting that the true, invasive cSBP should be sought in- between both estimates. To judge which device yields the closest estimate to the true aortic cSBP, we made use of the reported 1.8 mmHg difference between aortic and carotid SBP from an invasive study [59] and used cSBP-Aortic as the reference cSBP. Compared to cSBP-Aortic, cSBP-Omron provides an average overestimation of 11.7 (5.5) mmHg, while cSBP-Sphygmo provides an average underestimation of 7.1 (5.1) mmHg.

A final factor is the calibration of the radial waveforms. SphygmoCor and Omron HEM-9000AI both calibrate the radial waveforms using brachial pressures, assuming that the brachial-to-radial pressure amplification is negligible

[1]The relation between radial and central aortic pressure in Africans is further assessed in a study in Nigerian women described in chapter 14.

[130]. Verbeke *et al.* [61] however found an average difference of 5.8 mmHg between brachial and radial SBP[2]. They demonstrated that alternative scaling of the radial pressure waveforms using brachial MAP and DBP yields a cSBP-estimate that more closely approximates cSBP-Aortic. In this population, calibrating the radial SphygmoCor-waveforms using radial pressures increased the mean cSBP-estimate by 4.1 mmHg, making it only 3.0 (4.2) mmHg lower than cSBP-Aortic. This alternative calibration procedure was only performed for SphygmoCor-curves since it involves brachial tonometry, which cannot be acquired using the automated Omron HEM-9000AI tonometer.

Although cSBP-Aortic is determined through carotid SBP and therefore clearly not free from limitations, the current data do suggest that the overestimation of cSBP by Omron HEM-9000AI is larger than the underestimation by SphygmoCor ($p<0.001$), especially when the latter is scaled using brachial MAP and DBP. One could argue that, for most actual applications, the absolute value of the central pressure may be of lesser concern than the repeatability, as central pressure is mostly used in addition to brachial pressure. However, when the same parameter (cSBP) measured by two different devices differs more than 15% (18.8 mmHg), any comparison of measurements performed with different devices becomes impossible. While this comparison across devices could be of lesser concern to the individual patient, the large difference also precludes the use of uniform thresholds.

10.5 Limitations

The most important limitation of this study is the lack of invasive central systolic pressure values. Although we consider the cSBP-Aortic used in this study as the best non-invasive guess for central systolic pressure, comparison of the central pressure estimates of Omron HEM-9000AI and SphygmoCor to direct invasive measurements of aortic pressure is still recommended. Furthermore, the Omron HEM-9000AI and SphygmoCor were not applied in a randomised order. For practical reasons, each subject was first measured with Omron HEM-9000AI, and then with SphygmoCor. Although subjects were at rest during both measurements, it cannot be guaranteed that blood pressure remained unchanged. However, since the same brachial BP was used to calibrate the radial waveforms from both devices and given the virtually identical cSBP predicted by the SphygmoCor software using either the SphygmoCor- or the Omron-measured radial waveforms, this effect seems limited.

[2]Chapter 6 describes the impact of different calibration methods on the brachial-to-radial pressure amplification.

10.6 Conclusion

When using SphygmoCor and Omron HEM-9000AI as advocated by their manufacturers in a population of black South Africans, the mean difference in cSBP predicted by both devices was 18.8 (4.3) mmHg. The main reason for this difference in cSBP is to be sought in differences between the two algorithms, rather than in differences in measured waveforms. Analysis of these data using carotid SBP minus 1.8 mmHg as device-independent reference suggests that the 'true' central cSBP is to be sought in-between the Omron HEM-9000AI and SphygmoCor estimates.

CHAPTER 11

Development of a low-cost Tono-Doppler device

11.1 Introduction

As outlined in chapter 2, pulse wave velocity can be obtained from either pressure, diameter or flow waveforms at two anatomical locations. Whereas the acquisition of diameter distension waveforms requires advanced and expensive wall tracking ultrasound scanners, the assessment of flow and pressure waveforms can be done in a much cheaper way. However, the few established commercially available devices for the assessment of PWV (SphygmoCor, Complior) are rather expensive (>20 000 €). Until recently, SphygmoCor was the only commercially available device for applanation tonometry, a monopoly that undoubtedly contributed to its high price. Since the inclusion of PWV as a marker of subclinical organ damage in the ESC/ESH guidelines of 2007, a number of new devices has appeared. These devices are cheaper, often at the expense of accuracy (see for instance chapter 9) or because of new, insufficiently validated algorithms (see chapter 10). As an alternative, we have developed a low-cost device based on existing, validated algorithms to acquire flow and pressure waveforms and hence derive PWV, local blood pressure and augmentation index. The device is specifically built for application in sub-Saharan Africa[1].

[1] Chapter 14 reports the results of a study in Nigerian women measured with the Tono-Doppler device

11.2 Development

11.2.1 Hardware

Figure 11.1 gives a schematic overview of the different components of the Tono-Doppler device. Each component is described in more detail below.

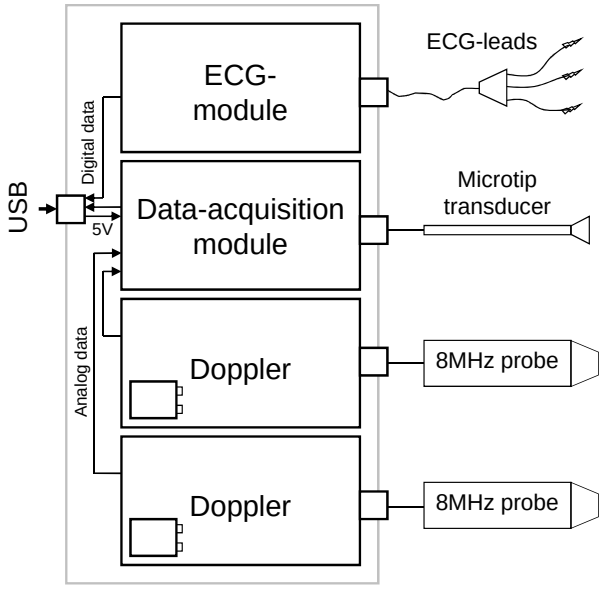

Figure 11.1: Schematic overview of the different components of the Tono-Doppler device.

- *Data-acquisition module* - Pressure and flow waveforms signals are digitized using the NI-9219 (National Instruments, Texas, USA), a data-acquisition hardware module that allows analog-to-digital (ADC) conversion of 4 input channels at a sampling rate of 100Hz and a resolution of 24 bits over a modifiable input voltage range. This range is set at ±125mV for the tonometry signal and at ±1V for the Doppler signal. The digitized signals are transferred to a computer via USB, from which the device also draws power (at 5V). Price is around 1100 €.
- *Micro-tip transducer* - Pressure waveforms are acquired using a SPT-304 micro-tip strain gauge transducer (Millar Instruments, Texas, USA) , the same type of transducer as used by the SphygmoCor device. When pressure is applied on this sensor, a piezoelectric element is compressed causing a voltage difference over a Wheatstone bridge: 25μV/mmHg for a 5V input voltage at the Wheatstone bridge. This voltage signal is digitized at 100Hz in the data-acquisition module. Price is around 1600 €.

- *Doppler devices* - Flow waveforms are acquired using commercially available handheld continuous-wave Doppler devices (Huntleigh Healthcare, Cardiff, UK) with a frequency of 8MHz. These devices have an (amplified) analog output, which is digitized at 100Hz in the data-acquisition module. Price is around 300 €.
- *ECG-module* - A commercially available one-channel module (EG01000, Medlab GmbH, Karlsruhe, Germany) with built-in amplification, filtering and sampling (300Hz) technology provides the electrocardiogram (ECG) needed for synchronization of two consecutively measured pressure or flow waveforms. The module has a serial output, which is converted to USB via a serial-to-USB adapter. Price is around 350 €.
- *Power* - As power supply from the mains is often unreliable or unavailable in sub-Saharan Africa, the Tono-Doppler device is designed to be powered from a laptop. The 5V output of a regular USB-connection is connected to a USB-hub, from where it is distributed to the power supply of the micro-tip transducer, the ECG module and data-acquisition module to serve as a power supply. The Doppler devices are battery powered (9V).

The ensemble is assembled in a ventilated polycarbonate enclosure, as shown in figure 11.2. Total price is below 4000 €.

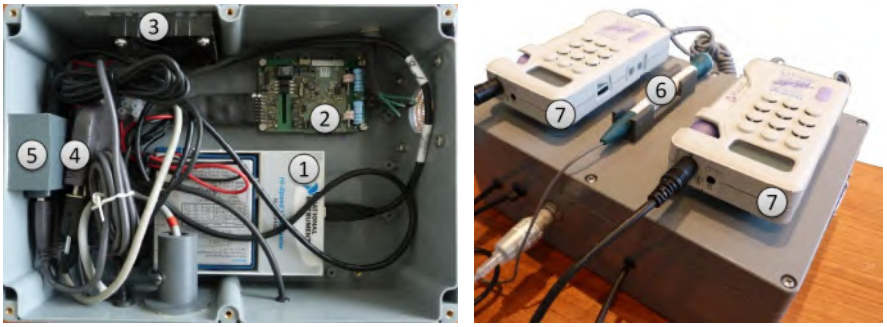

Figure 11.2: Tono-Doppler hardware components: 1: data-acquisition module; 2: ECG-module; 3: ventilator; 4: serial-to-USB adapter; 5: USB-hub; 6: micro-tip transducer; 7: Doppler devices.

11.2.2 Software

Based on existing code and algorithms developed in the framework of the Asklepios study, a dedicated acquisition and processing interface were developed in Matlab (MathWorks, Natick, Massachusetts, USA). During acquisition, the focus of the operator is on getting a quick feedback on the quality of the measurement. This is in contrast with the post-processing, often performed by an

operator with more (technical) background, where the focus is on accuracy. Therefore, the acquisition interface is designed to be straightforward and give multiple visual quality feedback options. The processing interface, on the other hand, allows the user to modify a number of algorithm settings as well as to manually select or deselect individual cycles.

Acquisition interface

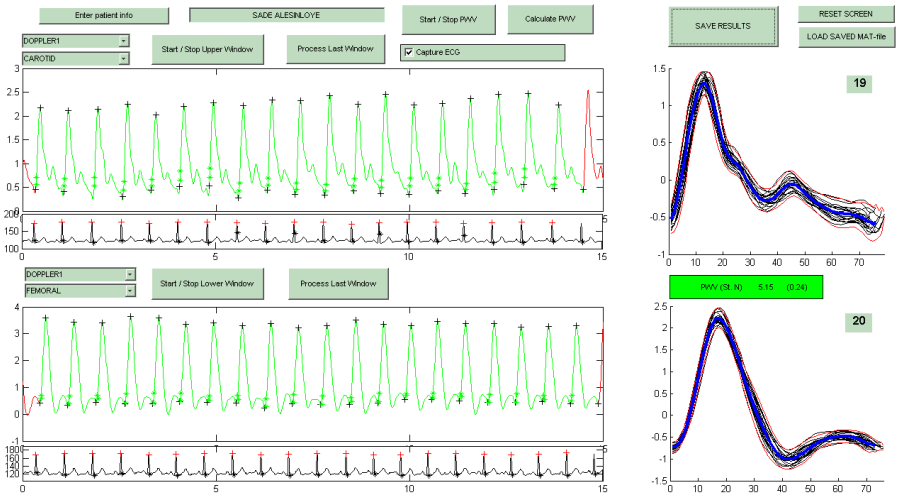

Figure 11.3: Acquisition interface displaying two consecutive Doppler recordings at the carotid (upper panel) and the femoral artery (lower panel), each with co-recorded ECG-signal.

Figure 11.3 displays a screenshot of the acquisition interface. After entering the basic patient information, the user has the choice between the simultaneous assessment of two waveforms (*'start/stop PWV'*) or recording a single waveform (*'start/stop upper (lower) window'*). The technique (Doppler/tonometry) and location (carotid, femoral, radial or brachial artery) can be set in the dropdown boxes at the upper left of the acquisition windows and a checkbox can be selected to measure an ECG along with the Doppler/tonometry curves. When a full window (15 seconds) of data is recorded, the recording can be processed (*'process last window'*) and the average waveform is displayed at the right. Processing includes separating the recorded signal into different cardiac cycles and select the 'usable' cycles based on cycle shape and cycle length criteria, which are detailed in one of the following sections. In contrast to the processing interface, in the acquisition interface, the cycle shape and cycle length criteria are not user-modifiable. The quality of the recording can be assessed by looking at the shape of the average cycle as well as the number of accepted cycles (upper

right of the average cycle window). In the case of a carotid and a femoral recording (either simultaneous or consecutive with ECG-gating as in figure 11.3), the PWV is calculated and colour-coded as an extra feedback on the quality of the recorded waveforms. When the mean PWV-value falls outside the physiologic range (2 m/s-15 m/s), it is coloured red to indicate an unrealistic value. When the mean value is within the physiologic range, it is coloured green when the standard deviation is below 10% of the mean value and orange when the standard deviation is larger than 10%.

In case of simultaneous recordings at the carotid and femoral artery, the travelled time per cycle is obtained by subtraction of the time of the carotid foot from the time of the femoral foot. In this way, an array with beat-to-beat transit times is obtained, from which the mean transit time and standard deviation are easily calculated. In case of two consecutive recordings, the ECG is used to align both recordings in time. For each recording, an array is obtained with the beat-to-beat times between the R-tops of the ECG and the carotid (femoral) feet. The average transit time is obtained from the subtraction of the average value of both arrays, while the standard deviation is obtained as the square root of the sum of the squared standard deviations of each array, following error calculation theory. For both simultaneous and consecutive recordings, the standard deviation of the PWV is obtained as the standard deviation of the transit time multiplied by the ratio of mean PWV and mean transit time.

Processing interface

Figure 11.4 displays a screenshot of the processing window. Upon loading of a recording, the signals are subsampled to 1000Hz (via linear interpolation) to allow a more accurate detection of timing parameters such as the foot of the wave. Individual cycles can be selected or deselected from either the acquisition window (left) or the average waveform window (right). The checkboxes and sliders in the lower panel allow to (de)select and modify the cycle detection and averaging algorithms outlined in the next section.

Algorithms

Both interfaces make use of the following algorithms, which are used in the analysis of both pressure and flow waveforms:

- **Cycle detection**
  To split up a recording into separate cardiac cycles, the points of diastolic pressure need to be identified. This is done by selecting those points of the signal's first derivative that exceed a certain threshold value, as shown by the red line in figure 11.5.

  By default, the threshold is set at 70% of the maximum of the derivative and dynamically lowered until at least 10 sample points are above the threshold. In the processing software, a slider allows manual selection of

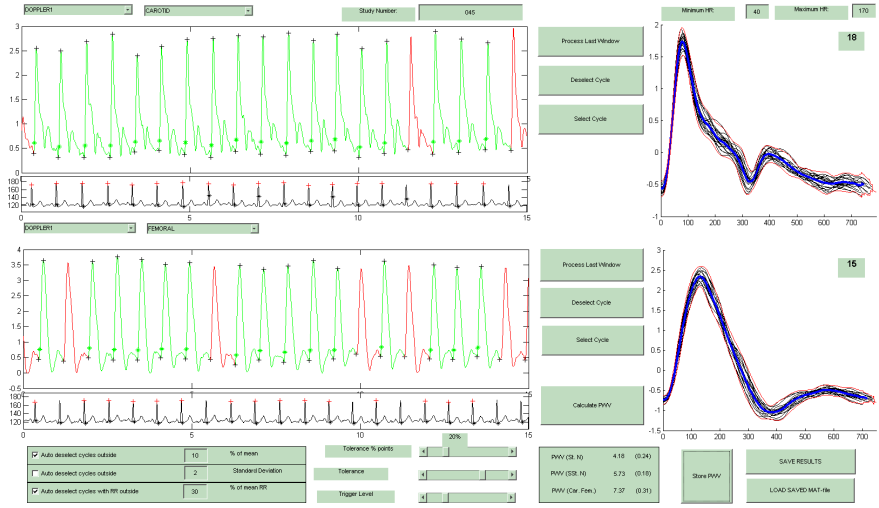

Figure 11.4: Processing interface displaying two consecutive Doppler recordings at the carotid (upper panel) and the femoral artery (lower panel).

the treshold level between 50 and 100% of the derivative amplitude. Per set of consecutive points above the threshold, a local maximum is calculated, as illustrated by the red asterisks in figure 11.5. Diastolic pressure (green asterisk in figure 11.5) is then found by looking for the minimum of the signal between two red asterisks.

- **Average cycle calculation**
  Because recordings often contain irregularities, not all cycles are used to calculate the average cycle. Two criteria are used to select the 'usable' cycles: cycle length and cycle shape. By default, the cycle length criterium deselects the cycles with a length outside interval [mean cycle length - 30%, mean cycle length +30%]. For the cycle shape criterium, a zone is defined around the average waveform, as shown by the red lines in the right panels of figure 11.3 and 11.4. If more than 10% of the points of a cycle fall outside this zone, the cycle is rejected. The upper limit is obtained by adding 10% of the standard deviation of all waveforms to the average waveform, while the lower limit is obtained by subtracting the same 10%. In the processing software, both the cycle length and cycle shape tresholds are user-modifiable.
- **Foot-detection algorithm**
  PWV is obtained as the ratio of travelled distance and transit time (see chapter 2). Travelled distance is measured on the body surface according to multiple definitions and stored along with the 'basic patient info'. The calculation of transit time relies on the identification of wave feet. We

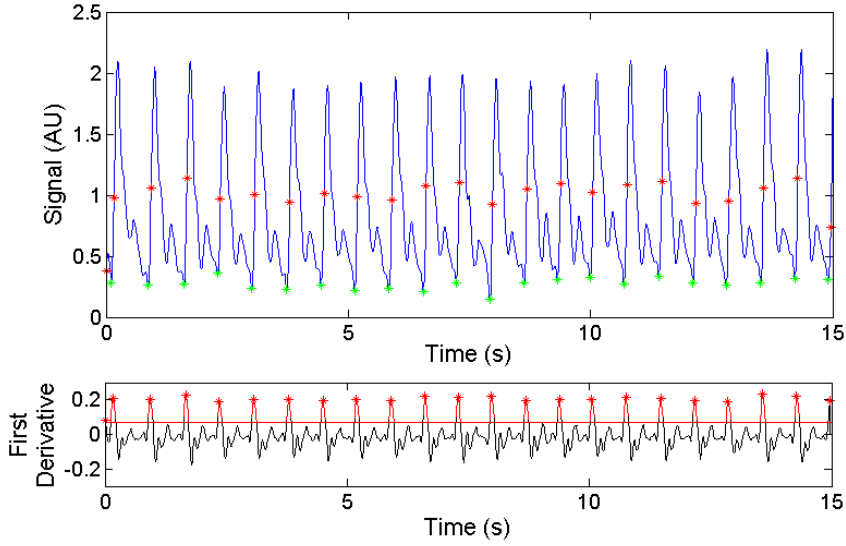

Figure 11.5: Cycle detection algorithm.

defined the foot of the wave as the point at 10% of the cycle pulse height, as illustrated by the green asterisks in figure 11.3 (denoting the last point below and the first point above 10% of the pulse height).

11.3 Validation

Like any other new device, the Tono-Doppler device needs to be validated by comparison to a reference device. We performed a limited validation study on 11 healthy volunteers (5 females), aged 23 to 33 years. Subjects were measured with the Tono-Doppler and the SphygmoCor device, in a random order. Carotid-femoral PWV was assessed from consecutive and simultaneous Doppler recordings with the Tono-Doppler device, and from consecutive tonometry recordings with the SphygmoCor device. Each type of recording was obtained in triplicate. Radial tonometry was performed with both devices. Not all measurements were performed in each subject. Heart rate was monitored as an indicator of the subject's cardiovascular resting condition. Recordings within the same subject were discarded when heart rate differed more than 5 bpm.

When comparing measurements between two devices, potential differences can arise from either the hardware or the software. Therefore, hardware and software are validated separately.

11.3.1 Hardware validation

Since every component of the Tono-Doppler device is commercially available and thus validated by its manufacturer, no separate validation of the ECG-, Doppler- or tonometry-hardware is required. However, as the data-acquisition module has a slightly lower sampling rate than the SphygmoCor device (100Hz vs 128Hz), it cannot be ruled out that the high frequency information of a pressure/flow waveform is not completely captured by the Tono-Doppler device. This could have an impact on the augmentation index (AIx), as this index depends on the higher frequency content of the pressure wave. We compared the AIx between data recorded with the Tono-Doppler and the SphygmoCor device. To isolate any differences in acquisition hardware, the data were processed through the same software (SphygmoCor) and measured with the same tonometer probe (SPT-304, Millar Instruments, Texas, USA). Figure 11.6) shows a Bland-Altman plot of 10 comparative radial tonometry recordings pertaining to 7 volunteers. Mean (SD) difference in AIx is -0.6 (4.8)% between both devices. This difference is comparable to the reproducibility of AIx reported in literature (0.5 (5.4) %, [190], see also figure 11.6), and thus indicates that the high frequency information is sufficiently captured by the Tono-Doppler device.

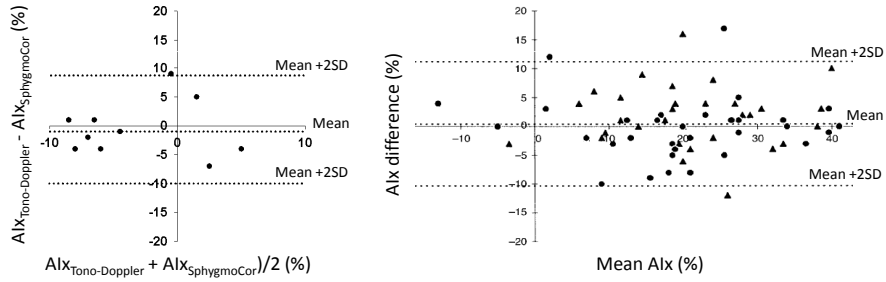

Figure 11.6: Left: Bland-Altman plot of the radial AIx obtained from the Tono-Doppler and the SphygmoCor device. Right: reproducibility of aortic AIx assessed with the SphgymoCor device by two different operators (circles and triangles), as reported by Wilkinson *et al.*[190]

Note that this device comparison is performed in people, whose hemodynamics continuously vary within a small, physiological range, and by manual handling of the tonometer probe, repositioned for each measurement. The term 'hardware validation' should therefore be used with care, as the observed variations in AIx most likely reflect changes in operator and subject's conditions.

11.3.2 Software validation

Acquisition software

A crucial issue in the acquisition process that needs separate validation is the synchronisation between the ECG-signal and the pressure or flow signal. Be-

cause the ECG-signal serves as a reference to align two consecutive pressure/flow recordings in order to calculate the carotid-femoral PWV, it is important that the pressure/flow tracing and the ECG-signal are read simultaneously (or at least with a constant, minor time-delay). As the ECG-signal is digitized within the ECG-module while the pressure/flow signal is digitized in the data-acquisition module, the synchronization between both signals has to be assured by the acquisition sofware. This was verified by comparing the mean carotid-femoral transit time obtained from simultaneous flow recordings with the mean transit obtained from consecutive, ECG-gated flow recordings. Each recording was obtained in triplicate and median values are reported. If the ECG-signal and the flow signal are synchronized correctly, both transit times should be comparable. Comparative measurements on 7 volunteers showed a mean (SD) difference of 3.0 (7.3) ms between both methods. To enable comparison to other reproducibility studies in literature, the transit times are converted to PWV-values by means of the carotid-femoral distance. As can be seen in figure 11.7, our mean (SD) difference of -0.3 (0.7) m/s is within the reproducibility range reported in literature (0.1 (1.2) m/s, Wilkinson *et al.* [190]; 0.3 (2.4) m/s, Frimodt-Moller *et al.* [191]), indicating a correct synchronisation between the ECG-signal and the flow signal.

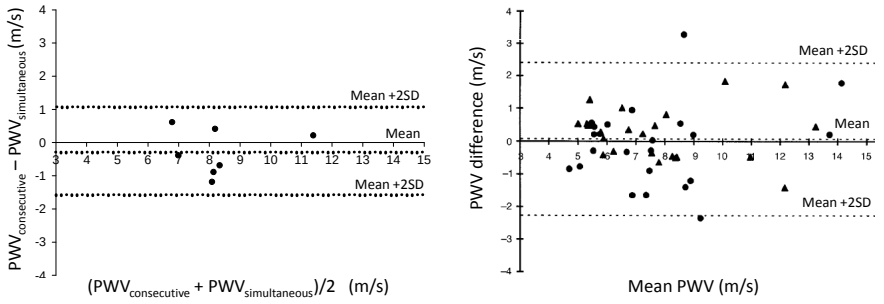

Figure 11.7: Left: Bland-Altman plot of consecutive versus simultaneously measured carotid-femoral PWV from flow recordings with the Tono-Doppler device. Right: reproducibility of carotid-femoral PWV obtained from consecutive tonometer recordings with the SphygmoCor device. The circles and triangles denote measurements by two different operators.[190]

Processing software

Two of the three previously described algorithms, the cycle detection and average cycle calculation algorithms, were previously used in the Asklepios study and as such do not require separate validation. The foot detection algorithm, however, has not been used in a study before and is therefore validated by comparing the transit times calculated by the Tono-Doppler software and the SphygmoCor software. Different foot detection algorithms can be used in SphygmoCor. For this comparison, the algorithm using 10% of the pulse height was selected. To isolate differences in software, the same data (recorded by the SphygmoCor-hardware) were used for processing by both softwares. Figure 11.8 shows the results of a comparison of 15 consecutive carotid and femoral tonometry readings pertaining to 7 subjects. Mean (SD) difference in transit time was 0.4 (2.0) ms, while correlation between both devices was 0.95.

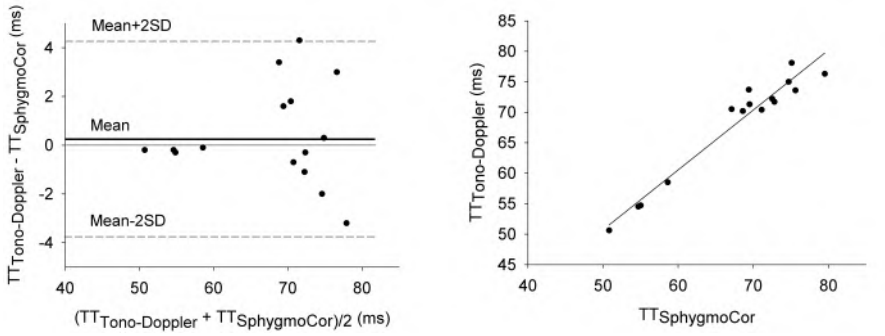

Figure 11.8: Comparison of transit times assessed by Tono-Doppler and SphygmoCor software. Carotid and femoral pressure data are recorded using SphygmoCor hardware.

11.3.3 PWV from Doppler versus PWV from tonometry

With the Tono-Doppler device, one can obtain PWV from either tonometry or Doppler recordings. With SphygmoCor, PWV is obtained from carotid and femoral tonometry recordings. Even though both methods are well accepted in literature and PWV from tonometry and Doppler recordings should be equivalent, comparative measurements on 7 subjects were performed as an extra validation. A Bland-Altman plot of the PWV-values obtained from both methods is given in figure 11.9. Mean (SD) difference is -0.1 (1.2) m/s, indicating no systematic difference between both methods and a range within the previously reported reproducibility range [190, 191].

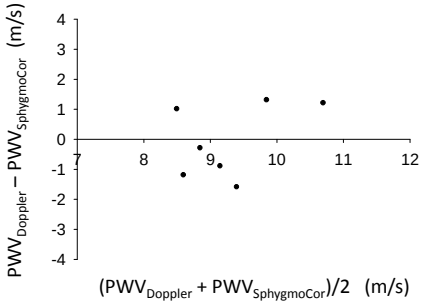

Figure 11.9: Comparison of PWV obtained from flow waveforms via the Tono-Doppler device and from tonometric waveforms via the SphygmoCor device.

11.4 Conclusion

By combining different commercially available hardware components and in-house available signal processing knowhow, we have developed an accurate, low-cost device for the assessment of pulse wave velocity and local pressure. Its mobility and low price (<4000 €) make the Tono-Doppler particularly suited for application in remote settings and developing countries.

Four

Arterial properties in people of African descent

CHAPTER 12

Outline

The fourth part of this manuscript focuses on the arterial properties of people of African descent, who display a clearly different cardiovascular risk profile than Caucasians. Figure 12.1 shows the geographical location of the African studies that were performed during my PhD.

Chapter 13 elaborates on this difference in risk profile and the potential mechanisms that may be at the root of it. The literature on differences in arterial properties between people of African and Caucasian origin is reviewed, with particular focus on the ethnic differences in mechanical properties of the large arteries. From this literature review, it is apparent that most of the research on ethnic differences between Africans and Caucasians is performed on Africans living in Western countries such as the United States and the United Kingdom. Given the increasing rates of cardiovascular disease in sub-Saharan Africa, more research on Africans living in sub-Saharan Africa as a basis for policy and treatment strategies is urgently needed.

Against this background, two studies were undertaken in Nigeria, the most populous country in sub-Saharan Africa. Chapter 14 details the results of comparative study on the aortic stiffness and arterial wave reflections in 184 young Nigerian women and 92 age-matched Belgian women. Mean levels as well as determinants of pulse wave velocity (PWV), augmentation index (AIx) and local pressure were compared across ethnicity.

In a second study described in chapter 15, the aortic stiffness of 264 babies, aged 0-1 year, was asessed in an attempt to track early changes in arterial distensibility. Based on prior findings that the etiology of CVD in adults may have its origin in utero and infancy, aortic pulse wave velocities measured at the age

Figure 12.1: Geographical study locations

of 0, 3 and 12 months were linked to infant and maternal characteristics to gain further insight in the driving factors of early vascular development.

A third study was performed on central blood pressure in rural South-Africa. Given its methodologic nature, the report of this study is given in part II of this manuscript on the validation and development of new methods.

CHAPTER 13

Ethnic differences in arterial properties between Africans and Caucasians in literature

13.1 Cardiovascular risk profile in Africans

People of African descent display a clearly different cardiovascular risk profile than Caucasians. While the prevalence of ischemic or coronary heart disease is generally similar or lower in African-origin people [192, 193], hypertension and diabetes are 1.5 to 3 times more prevalent than in Caucasians [194–198], with the difference most pronounced at young and middle age (20-50 years). The risk of target organ damage associated with these conditions, such as stroke, left ventricular hypertrophy (LVH), insulin resistance and end-stage renal disease is disproportionately greater in those of black African descent even when conventional risk factors are accounted for. In addition, pathophysiologic features of end stage renal failure and LVH appear to be different. Therefore, ethnicity itself has emerged as an important independent risk factor for cardiovascular disease [199, 200].

Over the last 50 years, many different hypotheses for mechanisms underlying this different risk profile have been proposed. One of the theories is that of catch-up growth or Barker's hypothesis [201, 202]. Based on the observation that retarded fetal growth is associated with higher levels of blood pressure in later life, David Barker hypothesized that a pregnant woman can modify the development of her unborn child such that it will be prepared for survival in

an environment in which resources are likely to be scarce, resulting in lower renal glomerular numbers or volumes and hence altered renal handling of salt loads. The increased salt-sensitivity among African-Americans could also be at the base of the observed risk profile. Salt-sensitivity is the impaired ability to excrete ingested salt, leading to an expansion of water volume in the blood vessels, and accompanying elevated blood pressure. The renal vasculature of people of African descent is particularly sensitive to the damaging effects of high blood pressure, as illustrated by the common observation of abundant deposition of extracellular matrix in the renal vessels of hypertensive black patients[203]. Several studies have shown differences in the frequency of gene polymorphisms for several proteins that modulate vascular function [204, 205] between Afro-Caribbean and Caucasian patients. Black subjects also tend to have a higher relative collagen content in the aorta and in the coronary arteries, resulting in stiffer arteries and hence higher blood pressure [206, 207].

Some of these hypotheses are more speculative than others, and the true mechanisms responsible for the difference in risk profile between Africans and Caucasians remain largely unclear. The above listed mechanisms all originated from observed differences in established (non-invasive) markers or predictors of cardiovascular disease. As such, these observations provide the only firm ground to describe ethnic differences in arterial properties. The next section is a brief summary of some of the key differences in cardiovascular risk markers between people of African descent and Caucasians.

13.2 Ethnic differences in arterial properties

13.2.1 Differences in risk markers

There is a number of cardiovascular risk markers that have been consistently reported to differ between Caucasians and subjects of African descent. A first difference is the lower amount of coronary calcium in black subjects, as indicated by a lower coronary calcium score and a lower prevalence of calcified lesions in the coronary arteries [208–211]. This is in line with the reported lower prevalence of coronary heart disease in people of African descent [193, 211]. Secondly, increased levels of carotid intima-media thickness (IMT) were reported in African-Caribbeans and African-Americans at various ages [212–218]. The intima-media thickness increases due to intimal hyperplasia and medial hypertrophy in response to a pulsatile mechanical load, and might therefore indicate a higher carotid pulse pressure [218, 219]. Another consistent finding lies in the hyperemic response in the forearm, also called the flow mediated dilation (FMD). FMD was attenuated in various samples of African-origin subjects [220–225] and is considered indicative of the global impairment of endothelial-dependent and endothelial-independent microvascular vasodilation. Afro-Caribbeans were reported to have lower levels of creatinin-reactive

protein (CRP), an inflammation marker, as well as lower levels of LDL-cholesterol, but higher levels of HDL-cholesterol [226, 227].

13.2.2 Mechanical properties of the large arteries

Given the unique role of the mechanical properties of the large arteries as early markers of atherosclerosis as well as integrated measures of cellular or hormonal changes, the literature on ethnic comparisons of vascular properties involving subjects of black African descent is reviewed in more detail.

Multiple large-scale cross-sectional and follow-up studies have been performed to study the influence and predictive value of markers of arterial stiffness and wave reflections with age, different risk factors and various pathologies [40, 77, 116, 121]. However, nearly all of these studies were performed on subjects of European or Asian descent. The scarce literature on comparative studies on arterial stiffness and arterial wave reflections in people of black African descent versus Caucasians is reviewed using ISI Web of Knowledge. Keywords included 'central blood pressure', 'augmentation index', 'pulse wave velocity', 'wave reflection' or 'arterial stiffness' and 'Africans', 'blacks' or 'ethnic difference'. Bibliographies were manually searched.

When comparing parameters measured in different population samples, it is important to be aware of all the differences between the sampled groups. While differences in continuous, exact parameters like age, blood pressure, weight and height can be statistically corrected for, there are many other differences that cannot be quantified in an exact way, such as differences in lifestyle, environment (do both populations live in a similar environment) or health status (healthy versus diseased). Therefore, these factors should be taken into account for proper comparison across ethnicity. Ethnicity represents a clustering of genetic and environmental factors. While Afro-Caribbeans living in the UK do not differ from Jamaican Afro-Caribbeans in genetical terms, their different environment leads to a clear difference in vascular risk profile [228], suggesting a significant environmental interaction with the development of cardiovascular disease. On the other hand, the impact of the genetic differences between Afro-Caribbeans and Afro-Americans living in the US on their vascular risk profile and arterial mechanical properties was found to be insignificant [229].

A number of studies has assessed arterial stiffness or compliance in more detail, either by measuring carotid-radial PWV in addition to carotid-femoral PWV as a measure of muscular artery stiffness [229–232] or by fitting an advanced Windkessel model including large (C1) and small artery stiffness (C2) to the radial pressure waveform [233, 234]. We have chosen to exclude these parameters from the literature overview, as their interpretation is unclear and their predictive value unproven.

Table 13.1 provides an overview of the comparative studies between people of African descent and Caucasians matching the following criteria:

- arterial stiffness and/or wave reflections are assessed using established markers (see Chapter 2)
- the reported differences are statistically corrected for at least age and blood pressure
- the compared ethnic groups live in the similar environment (in order to minimize environmental differences)

General population

Table 13.1 gives an overview of the literature on differences in the mechanical properties of large arteries between Western and African-origin healthy or general populations.

Table 13.1: Overview of the comparative studies on mechanical properties of large arteries in people of African origin versus Caucasians, in general population samples. .

Parameter	Location	Significant difference?	N Blacks	N Whites	Age	Origin	Author
Aortic stiffness indices							
PWV	car-fem	Yes, higher in blacks	99	103	40-64	UK Caribbean	Chaturvedi [231]
PWV	car-fem	Yes, higher in blacks	25	30	20-25	American	Heffernan [218]
PWV	car-fem	Yes, higher in blacks	88	100	40-68	UK Caribbean	Strain [232]
PWV	car-fem	Yes*	38	82	19-50	Brazilian	Ferreira [207]
PWV	car-fem	No	90	266	70-96	American	Mackey [235]
PWV	car-fem	Yes, higher in blacks	67	85	20-40	American	Wildman [236]
PWV	ao-fem	Yes, higher in blacks	255	659	25-43	American	Chen [237]
DC	aortic	Yes, lower in blacks	414	537	62.1±9.7	American	Malayeri [238]
Carotid stiffness indices							
β-stiffness index	carotid	Yes, higher in blacks	268	2459	475-64	American	Din-Dzietham [239]
β-stiffness index	carotid	Yes, higher in blacks	25	30	20-25	American	Heffernan [218]
Brachial stiffness indices							
β-stiffness index	brachial	No	25	30	20-25	American	Heffernan [218]
PP	brachial	No	166	160	21±0.3	American	Hlaing [240]
Wave reflection indices							
AIx	aortic	Yes, higher in blacks	383	390	49±11	American	Patel [241]
AIx	aortic	Yes, higher in blacks	25	30	20-25	American	Heffernan [218]
PP Amplification	ao-to-bra	Yes, higher in blacks	25	30	20-25	American	Heffernan [218]
PP Amplification	car-to-bra	Yes, higher in blacks	25	30	20-25	American	Heffernan [218]

*lower in black normotensives, higher in black hypertensives. Age is expressed as age range or as mean age ± standard deviation
PWV, pulse wave velocity; DC, distensibility coefficient; PP, pulse pressure; AIx, augmentation index; car-fem, carotid-femoral
N Blacks (Whites), number of blacks (whites); UK Caribbean, Afro-Caribbeans living in the United Kingdom

When aortic stiffness is assessed via what is considered as the gold-standard method (carotid-to-femoral pulse wave velocity) it was found to be consistently higher in people of African origin than in people of Caucasian origin, except for two studies (table 13.1). In the study of Ferreira *et al.* [207] on Brazilian male soldiers, the hypertensive soldiers of African origin had a higher carotid-femoral PWV than their white counterparts, whereas normotensive soldiers of African origin had lower values than their white counterparts. However, the slope of increase of aortic stiffness with systolic blood pressure (SBP) was steeper for Africans than for whites along the entire range of observed BP. In the second discordant study, carotid-femoral PWV did not differ significantly between African-Americans and Caucasians aged 70 to 96 years [235]. It is likely that the high age of this study population is the main reason for not finding a difference in aortic stiffness, as survival bias may have occurred. People reaching the age of 70 and certainly 96 may have beneficial physical characteristics, in particular arterial properties, thus making them less representative of the general population. Furthermore, being marker of subclinical organ damage, PWV is probably less relevant to quantify cardiovascular risk in populations where organ damage is thought to be already beyond the subclinical level.

PWV is inversely related to distensibility via the Bramwell-Hill equation (see equation 1.11 on page 19). As such, the reported lower aortic distensibility coefficient in African-Americans (table 13.1) confirms the reports of a higher aortic stiffness in blacks.

As far as local stiffness is concerned, two studies report a clearly higher *carotid* artery stiffness in African-origin subjects as in whites. At the level of the *brachial* artery, no difference in β-stiffness index nor in pulse pressure (PP), a crude measure of stiffness, was observed.

While the number of studies directly comparing arterial stiffness between people of African descent and Caucasians is low and a majority of the studies focuses on either African-Americans living in the US or African-Caribbeans living in the UK, the available data on ethnic differences in wave reflections are, to the best of my knowledge, limited to two studies, both on African-Americans. In young men [218] and middle-aged men and women [241], arterial wave reflections quantified as augmentation index and pulse pressure amplification, were found to be stronger in African-Americans than in Caucasians.

Populations with specific diseases

The incidence of cardiovascular disease in patients with type-2 diabetes and patients on hemodialysis is much higher than in the general population. These patients therefore provide an interesting subgroup to gain more insight into the etiology and development of cardiovascular disease. Two studies [230, 232] compared PWV in Afro-Caribbean and Caucasian patients with type-2 diabetes

living in the UK. They report no ethnic differences in carotid-femoral PWV. Bellasi *et al.* [242] compared African-American and Caucasian hemodialysis patients and reported no ethnic differences in carotid-femoral PWV nor in aortic AIx.

13.2.3 Critical notes

Some important limitations can be noted about the available data on mechanical arterial properties in people of African descent. A first limitation apparent from table 13.1 is the small number of subjects per study. Apart from the studies of Malayeri [238], Din-Dzietham [239] and Patel [241], the sample sizes are around or below 100 subjects per ethnic group, which makes it dangerous to extrapolate study findings to entire ethnic groups. A second important limitation is the fact that most of the research on people of African descent is performed on *Africans living in Western countries*, such as African-Americans and Afro-Caribbeans living in the UK. Given the potential significant influence of the environment on the development of cardiovascular disease (CVD) [228], this means that the available data cannot readily be extrapolated to sub-Saharan Africa (SSA). The only study I could track on sub-Saharan Africans so far was performed in South-Africa by Shiburi *et al.* [188]. They assessed radial and central AIx as well as carotid-femoral PWV in 347 subjects and proposed preliminary reference values for AIx and PWV in South-Africans, which are clearly higher than similar data in Caucasians [243].

13.3 The need for cardiovascular research in sub-Saharan Africa

The lack of studies on mechanical properties of large arteries in sub-Saharan Africa (SSA) is illustrative for the more general lack of research interest in cardiovascular diseases in this region. However, there are a few good reasons why cardiovascular research in sub-Saharan Africa is relevant and should be intensified. Along with the industrialisation and urbanisation process Africa has been undergoing for decades now, there are associated transitions on the demographic and epidemiological level. On the demographic level, there is a shift from high birth rates, high mortality rates and a short life expectancy towards low birth and mortality rates and a longer life expectancy [244, 245]. Linked to these demographic changes, an epidemiological shift is occurring from communicable or infectious diseases towards non-communicable or degenerative diseases. As a consequence, cardiovascular diseases in SSA are becoming a major health problem with a rapidly increasing prevalence. In 2004, the WHO stated that *"Unless current trends are halted or reversed, over a billion people will die from cardiovascular disease in the first half of the 21st century. The large majority will be in developing countries and much of the life years will be lost in middle*

age. This would be an enormous tragedy, given that research in the last half of the 20th century showed that cardiovascular disease was largely preventable."

While a discussion on treatment strategies for CVD in SSA is certainly beyond the scope of this thesis, it is clear that, ideally, policies should be based on (accurate) data of the prevalence and pathophysiology of CVD in SSA. However, up to date, no such accurate data exist, as illustrated by the above literature review as well as the fact that the most recent estimate of the prevalence of hypertension in SSA showed a 95%-confidence interval ranging from 65 to 93 million [246].

CHAPTER 14

Aortic stiffness and wave reflections: comparison between Nigerian and Belgian middle-aged women

14.1 Introduction

The prevalence of high blood pressure (BP) and resulting cardiovascular disease (CVD) is generally higher among people of African descent than among Europeans or other ethnic groups [27, 198]. Over the last 50 years, many different hypotheses for, and mechanisms underlying this difference have been proposed [247–249]. An almost universal finding has been lower plasma renin in black than in white people at any age which is generally unrelated to blood pressure. Genetic studies thus far failed to identify specific gene variants in a consistent manner. Lower birth weight, possibly leading to lower renal glomerular numbers or volumes and hence renal handling of salt loads, and recently epigenetic mechanisms may be relevant [202, 250]. Another possible mechanism is a difference in mechanical properties of the large arteries, especially arterial stiffness, a structural and functional vascular component, which may be amenable to more specific targeting of treatment.

The current gold-standard technique to assess arterial stiffness is through pulse wave velocity (PWV) measured along the carotid-femoral pathway, which has been shown to have a powerful prognostic value for CVD, independent of BP [55]. Additionally, pulse wave analysis, the assessment of local blood pressure waves through applanation tonometry, can be used to assess local and central augmentation index (AIx) and central systolic blood pressure (cSBP). The

AIx is a measure of wave reflections, while cSBP is the pressure faced by the heart and may be more predictive of CVD than conventional brachial pressure [121]. Pulse wave analysis is usually performed at the radial artery, and aortic parameters are derived via the radial-to-aortic transfer function. However, this transfer function has not been validated for use in people of African ancestry [188]. Tonometer measurements at the common carotid artery can be used as an alternative, as the carotid artery is an elastic, superficial artery very close to the heart and carotid systolic pressure has been reported to be only on average 1.8 mmHg higher than aortic pressure [59].

Several studies have assessed the alleged ethnic difference in mechanical properties of the large arteries non-invasively. However, most of the available data focused on African-Americans [207, 218, 233, 235, 239, 242], African-Caribbeans [71, 231, 251] or African-Europeans [187] rather than Africans living in sub-Saharan Africa. To the author's knowledge, the study by Shiburi *et al.* [188] in South-Africa is the only study so far that measured PWV and pulse wave analysis in sub-Saharan Africa. Whereas the burden of well-known communicable diseases as malaria and HIV in sub-Saharan Africa is decreasing slowly, the estimates and prognoses on the burden of hypertension are alarming. The fact that cardiovascular diseases result in substantial mortality in economically active age groups [27, 252], especially in urbanized regions [246] only adds to this burden. The primary aim of this study was to measure arterial stiffness, aortic pressure and wave reflections in an urban community sample in Nigeria, one of the most densely populated SSA-countries. The results were compared to corresponding values of a European population matched for age and gender. Secondly, the accuracy of the transfer function (TF) to assess central AIx and SBP was evaluated by comparing the TF-derived aortic parameters with AIx and SBP obtained from carotid pulse wave analysis.

14.2 Methods

Study population

A total of 184 healthy, 1-2 year postnatal women (19-45 years) enrolled in the Ibadan Child Growth and Vascular Health study (ICGVH [253]) were recruited at the Adeoyo Maternity Hospital, Ibadan, an urban setting in the southwest of Nigeria.

Measurements

After a minimum of 5 minutes of supine rest, brachial BP was measured with an Omron MIT Elite HEM-7300-WE sphygmomanometer. Carotid-femoral pulse wave velocity (PWV) was obtained in all women with the tono-Doppler device described in chapter 11. Carotid and femoral flow waveforms were acquired sequentially using a handheld continuous wave Doppler device (Huntleigh Healthcare, Cardiff, UK). Transit time was calculated after time-alignment of both

flow waves via co-recorded ECG-signals. The distance between the suprasternal notch and the measurement location at the carotid artery was subtracted from the distance between the suprasternal notch and the femoral measuring location to obtain PWV as the ratio of distance and transit time [2].

Applanation tonometry was performed on the brachial, radial and carotid artery using a Millar pressure sensor in a subset of 36 mothers.

Doppler and tonometry traces were captured at 100Hz using commercially available acquisition hardware (National Instruments, Texas, USA) and displayed and stored using a custom-built hard- and software platform developed in Matlab (Mathworks, Natick, Massachusetts, USA), see also chapter 11. Radial and carotid tonometry waves were calibrated with brachial diastolic (DBP) and mean arterial pressure (MAP), the latter obtained through scaled brachial tonometric waveforms. Radial, carotid and synthesized aortic augmentation index (AIx) and systolic blood pressure (SBP) were calculated using SphygmoCor-software (Atcor Medical, Sydney, Australia) as the ratio of the second and the first peak of the pressure wave expressed in percent. Augmented pressure (AP) was calculated as the difference between the second and the first peak of the pressure wave. In C-type waveforms with an inflection point after the peak systolic pressure, the AP is negative, whereas it becomes positive for A-type waveforms.

Comparison with Belgian population

The results from the Nigerian cohort are compared to a Belgian cohort, composed of women included in two previous studies: the Asklepios study [94] and a study on the vascular effects of migraine [132]. This allowed to cover the age range of the Nigerian population. The Caucasian population was matched to the Nigerian one for age: for every two Nigerian women, one Belgian control subject was included who differed less than two years in age with both Nigerians. For the subset of 36 subjects with tonometry measurements, a separate matching was performed: every Nigerian woman was matched to a Belgian woman of the same age.

Statistics

Data are presented as mean (standard deviation). P-values lower than 0.05 were considered as statistically significant. To assess the determinants of PWV in both populations, a stepwise forward multiple linear regression analysis was performed including age, brachial MAP, body height, BMI and heart rate as potential factors. Only the factors that were significant in univariate analysis were entered into multivariate analysis. All analyses were performed in PASW Statistics 18 (IBM, Chicago, IL, USA).

14.3 Results

Pulse wave velocity

Basic characteristics of the 184 Nigerian and the matched Belgian control women (aged 19-45 years) can be found in table 14.1. The Belgians were on average taller, marginally heavier but still had lower BMI and higher SBP and MAP but not DBP. Average heart rate was lower than in the Nigerian mothers. Pulse wave velocity did not differ significantly between populations; the difference remained insignificant after adjustment for heart rate, BMI, height and SBP. Age, MAP and SBP were all significantly related to PWV in both cohorts after univariate regression analysis. However, multiple regression analysis revealed age and SBP as the main determinants of PWV in the Nigerian cohort (R^2=0.21, p<0.001), whereas SBP was the only factor remaining significant (R^2=0.34, p<0.001) in multiple regression analysis in the Belgian women. Figure 14.1 shows the evolution of PWV with age for both ethnic groups. The increase in PWV with age was slightly but not significantly higher in Nigerian (0.7m/s per decade) than in Belgian women (0.5 m/s per decade).

Table 14.1: Characteristics of Nigerian PWV cohort and its age- and gender-matched Caucasian cohort.

	Nigerians		Belgians		
	Mean	SD	Mean	SD	p-value
N	184		92		
Age (years)	30.6	5.1	30.7	5.9	NS
Height (cm)	159.1	5.2	167.2	6.6	<0.001
Weight (kg)	60.2	11.5	63.1	10.8	NS
BMI (kg/m²)	23.7	4.2	22.5	3.6	0.019
brachial SBP (mmHg)	111.7	12.0	115.1	13.0	0.035
brachial DBP (mmHg)	67.6	9.9	69.2	9.1	NS
brachial MAP (mmHg)	85.3	10.4	88.2	11.1	0.034
HR (bpm)	74.1	8.8	64.4	9.4	<0.001
PWV (m/s)	5.6	1.0	5.8	0.8	NS

BMI, body mass index; SBP, systolic blood pressure; DBP, diastolic blood pressure; MAP, mean arterial pressure; HR, heart rate; PWV, pulse wave velocity

Pulse wave analysis

In the subset of 36 subjects (aged 23-41 years) with tonometry measurements and their matched Belgian controls (Table 2), only body height and heart rate were significantly different between the two groups. When looking at local systolic pressures, only radial SBP was significantly lower in Nigerians than in Belgians. Although synthesized aortic and carotid SBP did not differ significantly

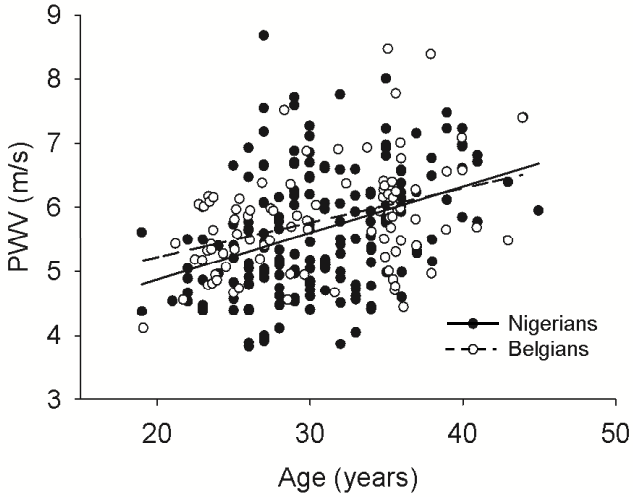

FIGURE 14.1: Evolution of pulse wave velocity (PWV) with age for the Nigerian (black) and Belgian (white) women. Trend lines show a slight but insignificant difference between the Nigerian (solid line) and Belgian cohort (dashed line).

across ethnicity, the difference between both does ($p<0.001$). As for the wave reflection indices, synthesized aortic and carotid AIx and AP differed across ethnicity, unlike radial AIx and AP. After adjustment for heart rate and height, this difference remained significant for carotid AIx ($p=0.03$) and AP ($p=0.02$) and borderline significant for aortic AIx ($p=0.06$) and AP ($p=0.07$). The difference between carotid and aortic AIx did not differ significantly between both ethnic groups.

14.4 Discussion

This study is the first to provide a direct comparison of arterial stiffness and arterial wave reflections between Africans living in sub-Saharan Africa and age-matched Belgians. The results of the present study suggest no ethnic differences in pulse wave velocity and central systolic pressure in young and middle aged women, but we did find a lower radial SBP and central AIx in Nigerian as compared to Belgian women.

Our data can be compared to those of Shiburi *et al.* [188], who studied 108 apparently healthy, normotensive South-African women of comparable age, but with a larger age range (33.5 (13.1) years). They report an average PWV of 5.7 (1.5) m/s and a peripheral and aortic augmentation index of 78.0 (24.1) and 22.5 (15.5), respectively. While the PWV-values match very well, the peripheral AIx

Table 14.2: Characteristics of Nigerian tonometry cohort and its age- and gender-matched Caucasian cohort.

	Nigerians		Belgians		
	Mean	SD	Mean	SD	p-value
N	36		36		
Age (years)	30.3	4.9	30.3	4.9	NS
Height (cm)	159.4	6.5	167.2	7.2	<0.001
Weight (kg)	62.4	17.3	63.5	11.3	NS
BMI (kg/m^2)	24.5	6.3	22.7	3.8	NS
brachial SBP (mmHg)	111.1	10.7	112.9	9.4	NS
brachial DBP (mmHg)	68.0	8.2	68.3	9.2	NS
brachial MAP (mmHg)	85.2	8.9	87.0	8.8	NS
HR (bpm)	77.7	9.1	65.4	11.5	<0.001
Local systolic pressure (mmHg)					
Radial SBP	115.3	11.7	124.2	10.6	0.001
Aortic SBP	103.2	11.4	107.6	9.7	NS
Carotid SBP	110.1	12.1	109.3	10.0	NS
Carotid - aortic SBP	6.8	3.2	1.7	3.5	<0.001
Local augmented pressure (mmHg)					
Radial AP	-16.4	8.4	-20.0	11.6	NS
Aortic AP	2.3	2.6	5.5	6.7	0.009
Carotid AP	-3.2	4.3	1.5	6.7	0.001
Carotid - aortic AP	-5.3	3.3	-4.1	4.9	NS
Local augmentation index (%)					
Radial AIx	66.6	14.3	64.3	19.1	NS
Aortic AIx	107.8	8.2	117.5	19.8	0.009
Carotid AIx	92.6	9.8	104.5	17.9	0.001
Carotid - aortic AIx	-14.4	7.8	-13.0	15.5	NS

BMI, body mass index; SBP, systolic blood pressure; DBP, diastolic blood pressure; MAP, mean arterial pressure; HR, heart rate ; AP, augmented pressure; AIx, augmentation index

in the South-Africans is higher, probably because of a lower heart rate (67.6 (11.8) bpm). Central augmentation index cannot readily be compared, as another definition is used by Shiburi *et al.* (AP/PP instead of P2/P1). Converting our values to this alternative definition, aortic AIx becomes 6.8 (7.0), clearly lower than the values of Shiburi *et al.* who also reported a lower heart rate (67.6 bpm).

In urbanized, westernized settings, most available data on direct ethnic comparisons of arterial characteristics report a higher carotid-to-femoral PWV for people of black African descent, after correction for age and blood pressure.

This was the case for African-American student volunteers (n=25) [218], African-Carribeans living in the UK (n=99, aged 40-64 years) [231], Brazilian black hypertensive male military police soldiers (n=38, aged 19-47) [207] and African-Carribeans living in the UK (n=46, aged 57-60 years) [71]. However, when specific populations were compared, no difference in carotid-to-femoral PWV was found in patients on hemodialysis [242] and patients with type-2 diabetes [230, 251]. All these studies suffer from a relatively small sample size. In a more representative sample from an ARIC sub-cohort [239], carotid artery stiffness was found to be higher in 268 African-Americans compared to 2459 European-origin 45-64 year-olds after adjustment for all vascular risk factors. Whether higher BPs over prolonged periods lead to or are caused by a higher level of aortic stiffness remains uncertain. Our finding that arterial stiffness does not differ between black and white women is therefore in contradiction with current literature. In the absence of other comparative studies directly comparing sub-Saharan Africans to Caucasians, we can only speculate that the previously reported ethnic differences, reported in people of African descent living in developed countries, were more a consequence of lifestyle and environmental factors.

Pulse wave analysis at the carotid artery can be used as an alternative for aortic parameters obtained via the radial-to-aortic transfer function. In this study, both approaches were followed as a way to implicitly assess the accuracy of the transfer function in Africans. In an invasive study by Van Bortel *et al.*, the difference between carotid and invasively measured aortic pressure was 1.8 mmHg, which is in good agreement with the difference between carotid and TF-derived aortic pressure in the Caucasian cohort of this study: 1.7 (3.5) mmHg. However, the difference between the same two non-invasive estimates of central pressure in the Nigerian cohort was much larger: 6.8 (3.2) mmHg. Interestingly, Heffernan *et al.* also reported a higher difference between carotid and TF-derived aortic SBP in African-American than in white students [218]. This might suggest that the transfer function used in the SphygmoCor device is not as accurate when used in people of African descent.

An important point to consider in our study is the effect of ambient temperature which was clearly different between the measurements in the Belgian and Nigerian women. It has been reported that a 10°C increase in indoor temperature reduces brachial SBP by 2 to 5 mmHg [254, 255] as a result of vasodilatation and reduced vascular resistance. As such, this might explain the lower brachial MAP and SBP and the lower radial SBP in the Nigerian women, as well as the lower aortic-to-radial pulse pressure amplification. The fact that PWV nevertheless remains constant can be explained by the fact that the carotid-to-femoral pathway mainly includes elastic arteries, which are less susceptible to vasoregulation with increasing temperature. Assuming that AIx and AP reflect to some

extent the wave reflections in the muscular arteries, the more vasodilated state of the Nigerian women can also account for the lower aortic and carotid AIx and AP observed in Nigerian women.

14.5 Limitations

A first important limitation lies in the danger of extrapolation. The current study comprises only a relatively small number of subjects in a limited age range. Although no ethnic differences in arterial stiffness were found in this population, these results cannot be readily extrapolated. The current findings merely indicate the need for larger-scale epidemiologic research on Africans living in sub-Saharan Africa.

As opposed to studies on ethnic difference in Western countries, any data on Africans living in Africa cannot be compared to people of another ethnicity who live in the same country. Therefore, in this study, a comparison between Nigerian and Belgian women was made. Although this may be statistically correct, this approach has important limitations. Even though both groups were matched for age and gender, there are many other differences between both groups that cannot be quantified and thus not corrected for, such as the differences in lifestyle and environment.

14.6 Conclusion

In contrast to prior studies conducted in Western countries reporting ethnic differences in arterial stiffness and wave reflections between people of African and European descent living in the same (Western) country, the present study suggests no ethnic differences in arterial stiffness, wave reflections or central aortic pressure between young to middle aged Nigerian and Belgian women. The observed difference between carotid SBP and aortic SBP derived via the radial-to-aortic transfer function in Nigerian women warrants the need for a specific validation of the transfer function in people of African descent.

CHAPTER 15

Arterial pulse wave velocity in Nigerian babies

15.1 Introduction

The burden of hypertension-related morbidity and mortality increases inexorably in developing countries, particularly in sub-Saharan Africa [256, 257]. The risk pattern of cardiovascular disease (CVD) is associated with a high prevalence of hypertension and growing rates of obesity and consequent diabetes, especially in women. Maternal characteristics in pregnancy influence neonatal outcome but also early childhood blood pressure (BP) and vascular development [258–260]. Furthermore, the etiology on risk factors for CVD in adults may have its origin in utero and infancy [261, 262] and childhood risk factors are predictive of sub-clinical and overt adult cardiovascular pathology [263, 264]. Higher BP in childhood predicts later hypertension but BP measurement alone is an imprecise way of assessing early development of CVD risk. Aortic pulse wave velocity (aPWV) is a powerful, independent predictor and marker of both subclinical and overt CVD, over and above systolic and pulse pressure [71, 264] probably because aPWV more directly measures vascular distensibility and overall pathology. Studies of arterial distensibility in infancy and childhood are few [265, 266] and there are none to our knowledge in African children.

In this study, we address the early natural history of arterial distensibility by measuring aPWV in a cohort of Nigerian children to examine the relationship between maternal and neonatal characteristics (including malaria) and aPWV at birth, around 3 months and again at 12 months of age. The protocol, method-

ology and equipment were similar to that in our previous study on infants in Britain [267].

15.2 Methods

15.2.1 Participants

Healthy pregnant women aged 18 to 45 were recruited from a semi-urban community, Yemetu-Adeoyo, Ibadan in the relatively affluent South West of Nigeria. HIV positive women were excluded. Their newborn babies were measured at three timepoints: at birth (1-3 days, baseline), at 3 months and at 1 year of age. Preterm deliveries (less than 36 weeks gestation), twins or babies with known syndromes, metabolic defects, sexually transmitted infections, major congenital abnormalities or severe birth trauma were excluded from the study. Ethical approval for the study was obtained from the joint University of Ibadan/University College Hospital ethical committee and from the University of Manchester.

15.2.2 Measurements

Measurements on the mothers

At baseline, weight, height and blood pressure were measured in the mothers. Seated BP was taken in a standard manner, 3 times at every visit during pregnancy after >5 minutes rest, with 1 minute intervals, using a validated Datascope BP monitor with appropriate sized cuffs. The mean value of the last two recordings was used in further analysis. Malaria was determined from thick smear blood samples taken at delivery and up to 3 visits prior to delivery. Mothers were classified as malaria-positive if they had a malaria positive smear in at least one of the visits. Analysis was also done by parasite density count, and four categories were distinguished: no, mild, moderate or severe malaria. The last two are combined in further analysis.

Measurements on the babies

Measurements were carried out at birth and around 3 and 12 months of age. BPs were taken in triplicate using the Datascope BP monitor with appropriate-sized neonatal cuffs. Again the mean value of the last two recordings were analyzed. Babies were weighed naked and length was measured from crown to heel on a stadiometer. Skinfolds (triceps, biceps, subscapular, and suprailiac) were measured using Holtain calipers on the left side of the body. All measurements were obtained in duplicate, or in triplicate if disagreeing by >15%. Mean values of the last two recordings were used in further analysis. All anthropometric measurements were carried out by nurses who had dedicated training based on a WHO manual. Inter-observer and within-observer error were minimized through 3

monthly refresher training sessions where the standard operating procedures and training videos were revisited to ensure standardization of techniques, using the same equipment for women and babies, throughout the study.

Aortic PWV measurement

Babies were in supine position for 2 to 5 minutes before aPWV measurement. Two continuous wave 8MHz Doppler probes (Huntleigh Healthcare, Cardiff, UK) were used, one at the base of the neck to insonate the left subclavian artery and the other peri-umbilically over the abdominal aorta above its bifurcation. The probes were each connected to a Doppler flow velocimeter (MD2, Huntleigh Healthcare), with the output of the velocimeters taken to a custom-made amplifier and analog-to-digital converter, sampling at a rate of 1kHz, and thence to a laptop PC. Flow waveforms were generated, displayed and recorded in real time (figure 15.1). aPWV is obtained as the ratio of travelled distance over transit time. The distance between the subclavian and abdominal sampling sites was measured to the nearest 5 mm by a non-stretch tape measure, whereas the transit time is the time delay between the foot of the subclavian wave and the foot of the abdominal aortic wave [265] and was derived from the waveforms with custom written software using a modification of the algorithm reported by Kontis *et al.* [266]. The software allows to adjust a threshold value for optimal foot detection after which a histogram of the beat-to-beat varying transit times is displayed.

Because of the circumstances in which this study is performed, the often restless babies as well as the lack of quality feedback given by the acquisition software, it can be expected that the quality of the flow recordings is not always high. Therefore, a number of objective criteria was applied to filter out those recordings of sufficient quality for further analysis. Firstly, the histogram of the individual transit times within each recording has to have a Gaussian shape (normal distribution). Secondly, re-analysis of a recording with a different threshold value for foot detection should not change the mean transit time with more than 20%. As variations in transit time become relatively more important in short transit times, there is a cut-off point below which an accurate assessment of the transit time is no longer possible. Therefore, as a third criterium we discarded all recordings with a mean transit time below 20 ms. Since the range of neonatal aPWV-values reported in literature (3 to 6 m/s, Koudsi *et al.* [267]; 2 to 6.5 m/s, Gardiner *et al.* [268]) is well below our cut-off aPWV (which is around 8 m/s for newborns, 9 m/s for babies of 3 months old and 10 m/s for 1 year old babies), the impact of this third criterium on the results is limited.

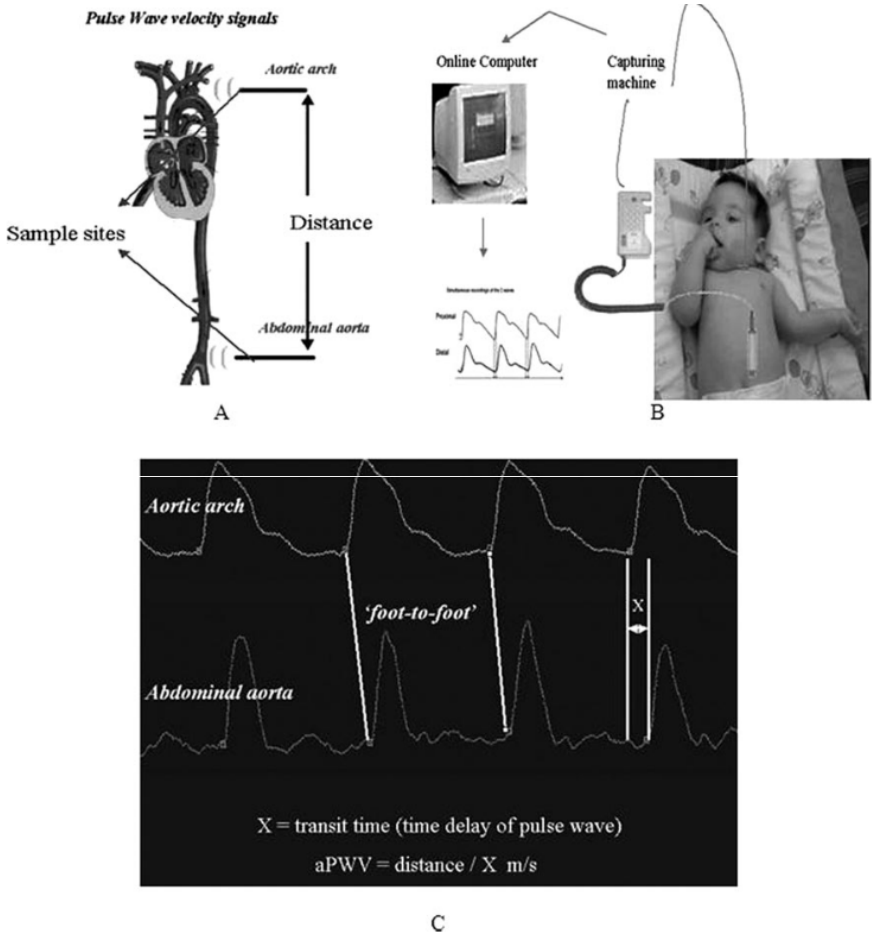

Figure 15.1: Schematic setup for aPWV measurement with Doppler probes at subclavian and abdominal aortic artery. Panel A displays the measured arterial segment; panel B illustrates the use of the probes on a baby; panel C shows the waveforms captured simultaneously from the aortic arch and abdominal aorta and the time delay between the recordings [267].

15.2.3 Statistical analysis

Data are presented as mean (SD). Differences in aPWV between cross-sectional data were assessed using ANOVA, whereas a paired t-test was used in the longitudinal aPWV-data. The influence of maternal malaria on childrens' aPWV was assessed using ANOVA. All analyses were performed using PASW Statistics 18 (SPSS Inc., Chicago, US).

15.3 Results

Out of the 246 babies with PWV-recordings at birth, 124 were retained after application of the quality criteria. Mean age of the mothers was 28.9 (5.1) years, while mean gestational age was 39.3 (1.4) weeks. Mean maternal SBP/DBP was 103.7 (8.7)/60.2 (6.8) mmHg. At the age of three months, 77 of the 249 babies with PWV-recordings were included, 18 of which also had PWV measured at birth. At 12 months of age, 144 of the 267 babies with PWV-recordings were included, 23 of which had PWV measured at 3 months and 40 babies also had measurements at birth, also clear from figure 15.2. Data are presented as a com-

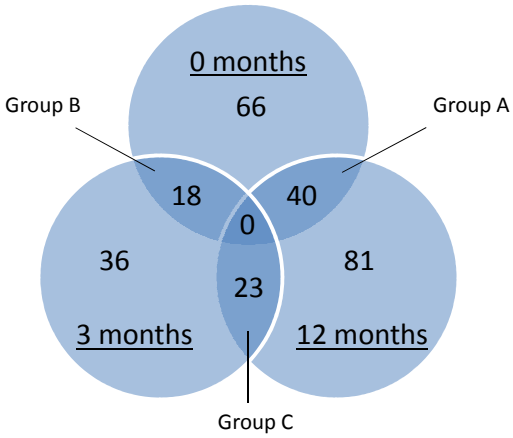

Figure 15.2: Schematic overview of the number of cross-sectional and longitudinal aPWV-data at 0, 3 and 12 months of age.

parison of cross-sectional measurements at the three timepoints and as three subsets of longitudinal data. Table 15.1 shows the characteristics of the cross-sectional data at birth, 3 and 12 months. The cross-sectional data show an increase in aPWV during the first 3 months of life with no significant aPWV-change during the next 9 months (left panel of figure 15.3). The longitudinal data confirm this trend (right panel of figure 15.3) but no significant correlations were found between aPWV at any two timepoints in the longitudinal subsets ($R<0.15$ for all cases).

The influence of malaria on aPWV was studied in more detail. Comparison of aPWV across maternal malaria status, expressed either as 'yes/no' or by degree of parasite density (none, mild, moderate or severe), did not affect neonatal aPWV as illustrated in Table 15.2.

Table 15.1: Basic characteristics of the children measured at 0, 3 and 12 months.

	0 months	3 months	12 months
N	124	77	144
Weight (kg)	3.0 (0.4)	5.8 (0.9)	8.5 (1.3)
Height (cm)	48.7 (2.3)	60.8 (2.9)	73.8 (2.9)
Subscapular skinfold (mm)	4.2 (0.9)	4.3 (0.8)	4.2 (0.8)
Triceps skinfold (mm)	4.2 (0.9)	4.3 (0.8)	4.1 (0.8)
Biceps skinfold (mm)	3.6 (0.7)	3.7 (0.7)	3.7 (0.8)
Suprailiac skinfold (mm)	4.4 (1.0)	4.4 (0.9)	4.4 (0.9)
SBP (mmHg)	71.6 (12.4)	89.1 (8.4)	88.5 (7.5)
DBP (mmHg)	36.1 (8.0)	48.0 (8.7)	64.5 (9.2)
HR (bpm)	126.2 (17.6)	128.0 (16.9)	112.3 (14.2)
PWV	4.5 (1.5)	5.6 (2.1)	5.7 (1.9)

SBP, systolic blood pressure; DBP, diastolic blood pressure; HR, heart rate
PWV, pulse wave velocity

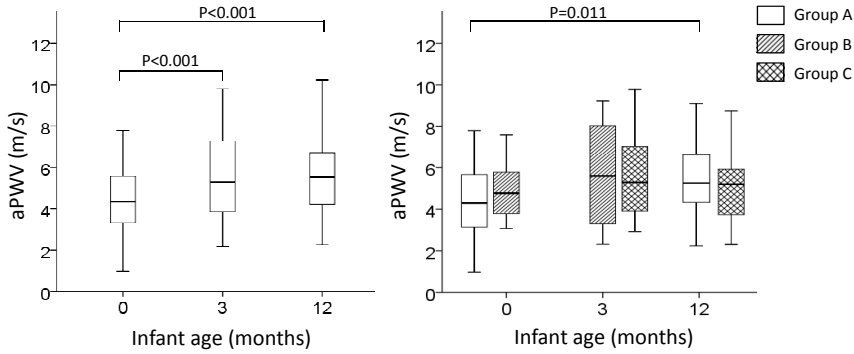

Figure 15.3: Box-plot representation of the aPWV-data at birth, 3 months and 12 months. Left panel: cross-sectional data; right panel: longitudinal data.

15.4 Discussion

By studying the arterial distensibility in young Nigerian children during their first year of life, this study is the first to combine two relatively unexplored research areas: the assessment of early cardiovascular risk development during the first year of life and the study of arterial distensibility in native Africans.

To the best of our knowledge, this study is the first to report on the evolution of aPWV during the first year of life. Previously, Laogun *et al.* [269] described the evolution of aPWV in British schoolchildren, where aPWV fell progressively until the age of 10-12 to increase again afterwards. Although they

Table 15.2: aPWV across maternal malaria status.

	Malarial status		
Age	Positive	Negative	N
0 months	4.5 (1.3)	4.4 (1.6)	61/63
3 months	5.2 (1.9)	5.9 (2.2)	38/39
12 months	5.7 (2.1)	5.6 (1.8)	74/70

N denotes the number of malaria positive and malaria negative babies, respectively

measured aPWV in babies of 3-7 days old, the next timepoint at which aPWV was assessed was between the age of 2 and 3 years. Therefore, the slight increase in aPWV observed in the present study cannot readily be compared to these data. Using the same methodology, Koudsi *et al.* assessed aPWV at birth in 148 British children, reporting a mean aPWV that was fairly similar to ours (4.6 m/s).

Both the cross-sectional and the longitudinal data report a significant increase in aPWV from 0 to 3 months or 12 months. However, no correlation with age in longitudinal aPWV-data was found. It is possible that the number of babies measured at two of the three timepoints was too small for the difference in aPWV to reach statistical significance. Another interpretation could be that, although on average aPWV increases during the first three months of life, individual aPWV can fluctuate considerably throughout the first year of life. The fact that aPWV in this study was not related to BP at any of the three timepoints and therein clearly differs from aPWV measured at later life (where BP is a major determinant of aPWV) might indicate that aPWV is determined by other factors during the first year of life than at later age. A similar phenomenon has been described for the association between weight gain and SBP [270]: while weight gain at 5 years was strongly related to SBP at the age of 22 years, the weight gain at 1 year was not related to the SBP at 22 years.

Maternal malaria during pregnancy has been associated with adverse consequences such as anaemia and low birth weight [271–273]. Therefore, in a region where malaria is pandemic, we anticipated to find a strong positive relation between malarial load in pregnancy and aPWV in early childhood. The fact that no such relation was observed in the present study is surprising. One can only speculate that this is related to the above mentioned hypothesis that, during the first year of life, aPWV is driven by different factors than at later age, so the anticipated positive relation might still be observed during follow-up of these children.

15.5 Limitations

A major drawback of this study is the overall quality of the recordings, with roughly only about 50% of all aPWV-recordings meeting the inclusion criteria. This is probably due to the babies, who cannot stay calm easily for 5 minutes, in particular when being confronted with two Doppler probes touching their skin. In addition, specific to the African setting, the lack of a reliable, continuous electric power supply and the absence of a temperature-controlled room also adds undesired variability to the measurements. Furthermore, the acquisition interface did not provide any direct feedback on the quality of the recording, which lead to many unintentional low-quality recordings.

Therefore, three quality criteria were applied during post-processing to retain only those recordings of sufficient quality. Although these criteria were defined ad-hoc and result from a trade-off between selecting high quality data and retaining a statistically relevant amount of data, the observed mean value as well as the range of aPWV-values is perfectly within the aPWV-values reported in literature on neonates [267, 268].

15.6 Conclusion

Based on the assessment of aortic pulse wave velocity (aPWV) in Nigerian babies, the present study suggests that aortic stiffness increases during the first three months of life by about 1 m/s, with no significant change in the next 9 months. During the first year of life, aPWV can fluctuate considerably and is unrelated to maternal malarial load.

Five

Conclusions

CHAPTER 16

Conclusions

This final chapter first summarizes the main conclusions of each part, after which the current research is put into a broader perspective.

16.1 Validation and development of new methods

The analysis of wave reflections and arterial stiffness has increasingly gained attention over the last 15-20 years and is now in the transition between clinical research and clinical practice, as illustrated by the inclusion of pulse wave velocity (PWV) as a marker of subclinical organ damage in the 2007 ESC/ESH guidelines. The validation and development of new methods to quantify arterial stiffness and wave reflections should be viewed against the background of this anticipated introduction in clinical practice. Whereas research requires the most accurate, complete characterization methods, a more pragmatic compromise between accuracy and time- and cost-effectiveness has to be made in clinical practice. For this reason, a number of new methods and devices has recently emerged, focusing specifically on usability, lower prices and short examination times.

One such method is the quantification of arterial stiffness (transit time) and wave reflections (reflection magnitude) by wave separation using a measured pressure wave and an approximated triangular flow wave, thus bypassing the often expensive and time-consuming assessment of an aortic flow waveform needed in the traditional approach of wave separation. We verified these approximation techniques and demonstrated that a triangular flow approximation yielded only moderate-to-poor agreement between the estimated and the

reference transit time and reflection magnitude. Approximating the flow by a more physiological waveform significantly improved the levels of agreement, but considerable individual deviations still persist. One must therefore be cautious when applying this technique clinically.

This highlights another important difference between research and clinical practice: whereas research is performed on study *populations*, clinical application is on *individuals*. Measuring carotid blood pressure (a surrogate for central aortic blood pressure) requires applanation tonometry recordings at the brachial and the carotid artery. In obese patients, however, tonometry recordings are difficult to obtain, a problem that becomes increasingly important in clinical practice, where each patient needs to be measurable. Therefore, the use of calibrated diameter distension waveforms could provide a more widely applicable alternative for local arterial pressure assessment than applanation tonometry. This approach might be of particular use at the brachial artery, where the feasibility of a reliable tonometric measurement has been questioned. We demonstrated that a technique which makes use of distension waveforms at both the brachial and carotid artery provides estimates of carotid pressure in good agreement with the tonometer-based reference method. As such, further development of cheap ultrasound devices, capable of providing diameter distension waveforms, may provide a clinically useful tool. Note that combining tonometry and diameter distension waveforms performed poorer than use of a single technique.

Another technique to assess central blood pressure which is clinically more useful than the combined brachial-carotid tonometer approach, is the use of radial tonometer waveforms, which are subsequently transformed into central pressure via a transfer function. Not only does this method require a single tonometer reading, the radial artery is also better suited for tonometry and applicable in virtually any subject with normal forearm vasculature. Drawback, however, is the fact that the radial pressure waveform requires calibration, based on information measured at the brachial artery. Different calibration strategies were tested. We demonstrated that, when the radial pressure is calibrated using diastolic blood pressure and an estimate of the mean arterial pressure (MAP), it is advisable to use 40% of the brachial pulse pressure instead of the traditional 33% to assess MAP.

Another newly proposed method to quantify arterial stiffnes, the Ambulatory Arterial Stiffness Index (AASI), was critically evaluated using a previously validated numerical model of the arterial circulation. We identified arterial distensibility, vascular resistance and especially heart rate as the main determinants of the AASI. The confounding effects of vascular resistance and heart

rate seriously limit the use of AASI as a marker of arterial stiffness. While our model-generated data do not allow to exclude that AASI is related to and predictive for cardiovascular disease, they do indicate that this is not due to its ability to adequately capture and quantify arterial stiffness. As such, we discourage the further use of AASI as a marker of arterial stiffness.

16.2 Validation and development of new devices

Along with the increased attention for the role of the large arteries in the development of hypertension and concomitant cardiovascular diseases, the number of devices to measure wave reflections and arterial stiffness has boosted.

The Arteriograph (Tensiomed, Budapest, Hungary) is a newly developed device that claims to assess aortic PWV by means of a simple brachial cuff. To test the validity of the working principle of the Arteriograph, we used a previously validated numerical model of the arterial tree to simulate pressures and flows in the normal configuration and in a configuration with an occluded brachial artery. A pronounced secondary peak was indeed found in the brachial pressure signal of the occluded model (in line with the working hypothesis of the device), but the timing of this secondary peak was only related to the stiffness of the brachio-axillary arterial path and not to aortic stiffness. Our data therefore indicate that the method picks up wave reflection phenomena confined to the brachial and axillary arteries, and derived values of PWV rather reflect the stiffness of the brachial and axillary arteries than the intended aortic stiffness. As such, our simulations invalidate the working principle of the Arteriograph. While these observations do not exclude a potential use of the device in a clinical setting, we do object against the claim of the manufacturer that the device measures aortic pulse wave velocity.

There is increasing evidence that central systolic blood pressure (cSBP) may be a better predictor of future cardiovascular events than brachial pressure. However, the use of central pressures in daily clinical practice is currently hampered by the fact that most measurement devices, although non-invasive, require a trained operator, introducing potential operator dependence. With the recent development of automated and hence operator-independent devices such as the Omron HEM-9000AI (Omron Healthcare, Kyoto, Japan), data collection is facilitated, bringing central pressure a step closer to routine clinical practice. However, when using SphygmoCor and Omron HEM-9000AI as advocated by their manufacturers in a population of black South Africans, the mean difference in cSBP predicted by both devices was as high as 18.8 (4.3) mmHg, which is higher than the difference between central and brachial pressure in most cases. The main reason for this difference in cSBP is to be sought in differences between the two algorithms, rather than in differences in measured

waveforms. Our observations suggest that the 'true' central cSBP is to be sought in between the Omron HEM-9000AI and SphygmoCor estimates, with SphygmoCor probably providing the closest estimate.

As illustrated by the studies on Arteriograph and Omron HEM-9000AI, these newly developed devices are not necessarily accurate. The few established devices on the other hand are all rather expensive, which may pose an obstacle for research in developing countries. Therefore, we developed a low-cost device to acquire flow and pressure waveforms and hence derive PWV and local blood pressure. By combining different commercially available hardware components and in-house available signal processing knowhow, we have developed an accurate, low-cost device for the assessment of PWV and local pressure. Its mobility and low cost make the Tono-Doppler device particularly suited for application in remote settings and developing countries.

16.3 Arterial properties in people of African descent

People of African descent display a clearly different cardiovascular risk profile than Caucasians. To date, the true mechanisms responsible for this ethnic difference remain largely unclear. Most of the research on ethnic differences between Africans and Caucasians is performed on Africans living in Western countries such as the United States and the United Kingdom. Given the increasing rates of cardiovascular disease in sub-Saharan Africa, more research on Africans living in sub-Saharan Africa as a basis for policy and treatment strategies is urgently needed. Against this background, two studies were undertaken in Nigeria, the most populous country in sub-Saharan Africa.

Aortic stiffness and arterial wave reflections were assessed in young Nigerian women and compared to corresponding measurements in age-matched Belgian women. In contrast to prior studies conducted in Western countries, we did not find any ethnic differences in arterial stiffness, wave reflections or central aortic pressure between young to middle age Nigerian and Belgian women. The observed difference between carotid SBP and aortic SBP derived via the radial-to-aortic transfer function in Nigerian women warrants the need for a specific validation of the transfer function in people of African descent.

In a second study, the aortic stiffness of 264 Nigerian babies, aged 0-1 year, was asessed in an attempt to track early changes in arterial distensibility. The results from this study suggest that aortic stiffness increases during the first three months of life, with no significant change in the next 9 months. During the first year of life, PWV can fluctuate considerably and is unrelated to maternal malarial load.

16.4 Perspectives

Since the inclusion of PWV in the 2007 ESC/ESH guidelines, the number of devices and methods for the assessment of arterial stiffness and wave reflection has boosted. To date, no clear framework or regulatory mechanisms exist to validate and ratify these newly developed methods and devices. The results from the methodological research performed during this PhD illustrate that most of these new methods and devices produce results that can differ considerably from the gold-standard. This stresses the need for a better regulation for the development of new devices and methods. In a first step, a 'reference centre' performing a series of standardised comparative measurements with widely accepted gold-standard devices and methods could provide some kind of quality label for new devices and methods. Within this perspective, the initiatives undertaken by the Artery Society can only be welcomed. The society not only coordinates several large multi-center studies to provide reference values for new established parameters and markers (e.g. the reference values on arterial stiffness), it also publishes guidelines for the validation of new devices. Anyhow, up to date, the research field is still quite polarized around 'devices'. Given that the overall purpose is to quantify physical properties of the arterial system, it should ultimately not matter which device was used to measure these properties.

As for the research done in sub-Saharan Africa, the results from the current studies did not identify ethnic differences in arterial properties between Africans and Caucasians, as oppposed to prior studies in Western countries. It should, however, be mentioned that the sample size of the performed studies is far too small to make any extrapolations and draw conclusions for differences between the Africans living in Africa and those living in Western countries. Nevertheless, the performed research does stress the need for more large(r)-scale epidemiological research into the mechanical properties of the large arteries of people in sub-Saharan Africa. In this regard, the developed Tono-Doppler device is a useful tool that can be used in further research. Subject conditions are important when assessing arterial properties, as recognized in the expert consensus document on arterial stiffness listing a set of standardised subject conditions. However, when comparing people from two settings, markedly differing from each other in ambient temperature and humidity, it is unclear whether one should use the same standardised conditions for both groups. Applied to the African setting, the higher average temperature could cause Africans to be more vasodilated, an effect that is no longer present when measured under the standard temperature ($22\pm1^{\circ}C$) mentioned in the expert consensus document. Therefore, a discussion should be held on the standardization of tests and measurements, specifically for the comparison of groups from widely differing settings.

Bibliography

[1] D.E. Mohrman and L.J. Heller. *Cardiovascular physiology*. McGraw-Hill Professional, 2003.

[2] S. Vermeersch. *Applied Arterial Mechanics: from Theory to Clinical Practice*. PhD thesis, Ghent University, 2009.

[3] Henry Gray and Warren H. Lewis. *Anatomy of the human body*. Lea & Febiger, Philadelphia and New York,, 20th edition, 1918.

[4] W.W. Nichols, M.F. O'Rourke, and D.A. McDonald. *McDonald's blood flow in arteries : theoretic, experimental, and clinical principles*. Hodder Arnold ; Distributed in the U.S.A. by Oxford University Press, London New York, 5th edition, 2005.

[5] P. Segers and P. Verdonck. *Principles of vascular physiology*, pages 116–137. Springer-Verlag, Heidelberg, 2002.

[6] N. Westerhof, N. Stergiopulos, and M. Noble. *Snapshots of hemodynamics. An aid for clinical research and graduate education*. Springer Science + Business Media, New York, 2004.

[7] *www.yoursurgery.com*, 2011. (accessed: 20 February 2011).

[8] Texas Heart Institute. *www.texasheartinstitute.org*, 2011. (accessed: 20 February 2011).

[9] R.F. Rushmer. *Structure and Function of the Cardiovascular System*. Saunders, Phildelphia, 1972.

[10] M.F. O'Rourke. *Arterial Stiffness in Hypertension*, chapter Principles and definitions of arterial stiffness, wave reflections and pulse pressure amplification, pages 3–20. Elsevier, 2006.

[11] M.F. O'Rourke. *Arterial function in health and disease*. Churchill Livingstone, 1982.

[12] O. Frank. *Die Grundform des arteriellen Pulses*. Zeitung Biologie, 37:483–526, 1899.

[13] N. Westerhof, F. Bosman, C. J. De Vries, and A. Noordergraaf. *Analog studies of the human systemic arterial tree*. Journal of Biomechanics, 2(2):121–43, 1969.

[14] N. Stergiopulos, B. E. Westerhof, and N. Westerhof. *Total arterial inertance as the fourth element of the windkessel model*. American journal of Physiology, 276(1 Pt 2):H81–8, 1999.

[15] J. W. Lankhaar. *Hemodynamics of pulmonary hypertension*. PhD thesis, Vrije Universiteit Amsterdam, 2008.

[16] M.F. O'Rourke. *Pressure and flow waves in systemic arteries and the anatomical design of the arterial system*. Journal of Applied Physiology, 23(2):139–49, 1967.

[17] R. D. Latham, N. Westerhof, P. Sipkema, B. J. Rubal, P. Reuderink, and J. P. Murgo. *Regional Wave Travel and Reflections Along the Human Aorta - A Study With 6 Simultaneous Micromanometric Pressures*. Circulation, 72(6):1257–1269, 1985.

[18] M. Karamanoglu, D. E. Gallagher, A.P. Avolio, and M.F. O'Rourke. *Functional Origin of Reflected Pressure Waves In A Multibranched Model of the Human Arterial System*. American Journal of Physiology-heart and Circulatory Physiology, 267(5):H1681–H1688, 1994.

[19] N. Westerhof, P. Sipkema, G. C. van den Bos, and G. Elzinga. *Forward and backward waves in the arterial system*. Cardiovascular Research, 6(6):648–56, 1972.

[20] F. Y. Liang, S. Takagi, R. Himeno, and H. Liu. *Biomechanical characterization of ventricular-arterial coupling during aging: A multi-scale model study*. Journal of Biomechanics, 42:692–704, 2009.

[21] World Health Organization. *www.who.int*, 2011. (accessed: 20 February 2011).

[22] American Heart Association. *www.americanheart.org*, 2011. (accessed: 20 February 2011).

[23] J. Mackay, G.A. Mensah, S. Mendis, and K. Greenlund. *Atlas of Heart Disease and Stroke*. World Health Organization, Geneva, 2004.

[24] A. Kattainen, V. Salomaa, T. Harkanen, A. Jula, R. Kaaja, Y. A. Kesaniemi, M. Kahonen, L. Moilanen, M. S. Nieminen, A. Aromaa, and A. Reunanen. *Coronary heart disease: from a disease of middle-aged men in the late 1970s to a disease of elderly women in the 2000s*. European Heart Journal, 27(3):296–301, 2006.

[25] I. Graham, D. Atar, K. Borch-Johnsen, G. Boysen, G. Burell, R. Cifkova, J. Dallongeville, G. De Backer, S. Ebrahim, B. Gjelsvik, C. Herrman-Lingen, A. Hoes, S. Humphries, M. Knapton, J. Perk, S. G. Priori, K. Pyorala, Z. Reiner, L. Ruilope, S. Sans-Menendez, W. S. O. Reimer, P. Weissberg, D. Wood, J. Yarnell, and J. L. Zamorano. *European guidelines on cardiovascular disease prevention in clinical practice: executive summary*. European Heart Journal, 28:2375–2414, 2007.

[26] G. Mancia, G. De Backer, A. Dominiczak, R. Cifkova, R. Fagard, G. Germano, G. Grassi, A. M. Heagerty, S. E. Kjeldsen, S. Laurent, K. Narkiewicz, L. Ruilope, A. Rynkiewicz, R. E. Schmieder, H. A. Struijker Boudier, A. Zanchetti, A. Vahanian, J. Camm, R. De Caterina, V. Dean, K. Dickstein, G. Filippatos, C. Funck-Brentano, I. Hellemans, S. D. Kristensen, K. McGregor, U. Sechtem, S. Silber, M. Tendera, P. Widimsky, J. L. Zamorano, S. Erdine, W. Kiowski, E. Agabiti-Rosei, E. Ambrosioni, L. H. Lindholm, A. Manolis, P. M. Nilsson, J. Redon, H. A. Struijker-Boudier, M. Viigimaa, S. Adamopoulos, V. Bertomeu, D. Clement, C. Farsang, D. Gaita, G. Lip, J. M. Mallion, A. J. Manolis, E. O'Brien, P. Ponikowski, F. Ruschitzka, J. Tamargo, P. van Zwieten, B. Waeber, B. Williams, Hypertension The task force for the management of arterial hypertension of the European Society of, and Cardiology The task force for the management of arterial hypertension of the European Society of. *2007 Guidelines for the management of arterial hypertension: The Task Force for the Management of Arterial Hypertension of the European Society of Hypertension (ESH) and of the European Society of Cardiology (ESC)*. European Heart Journal, 28(12):1462–536, 2007.

[27] P. M. Kearney, M. Whelton, K. Reynolds, P. Muntner, P. K. Whelton, and J. He. *Global burden of hypertension: analysis of worldwide data*. Lancet, 365:217–223, 2005.

[28] N. K. Borch-Johnsen and S. Kreiner. *Proteinuria - Value As Predictor of Cardiovascular Mortality In Insulin-dependent Diabetes-mellitus*. British Medical Journal, 294(6588):1651–1654, 1987.

[29] S. Vaina and C. Stefanadis. *Detection of the vulnerable coronary atheromatous plaque. Where are we now?* International Journal of Cardiovascular Interventions, 7(2):75–87, 2005.

[30] P.K. Shah. *Mechanisms of plaque vulnerability and rupture.* Journal of the American College of Cardiology, 41(4 Suppl S):15S–22S, February 2003.

[31] P. Libby. *Current concepts of the pathogenesis of the acute coronary syndromes.* Circulation, 104(3):365–372, 2001.

[32] A. Farb, A.P. Burke, A.L. Tang, T.Y. Liang, P. Mannan, J. Smialek, and R. Virmani. *Coronary plaque erosion without rupture into a lipid core. A frequent cause of coronary thrombosis in sudden coronary death.* Circulation, 93(7):1354–1363, April 1996.

[33] R. Virmani, F.D. Kolodgie, A.P. Burke, A. Farb, and S.M. Schwartz. *Lessons from sudden coronary death - A comprehensive morphological classification scheme for atherosclerotic lesions.* Arteriosclerosis Thrombosis and Vascular Biology, 20(5):1262–1275, 2000.

[34] A.P. Schroeder and E. Falk. *Vulnerable and dangerous coronary plaques.* Atherosclerosis, 118 Suppl:S141–S149, December 1995.

[35] E. Falk, P.K. Shah, and V. Fuster. *Coronary Plaque Disruption.* Circulation, 92(3):657–671, 1995.

[36] J.A. Ambrose, M.A. Tannenbaum, D. Alexopoulos, C.E. Hjemdahl-Monsen, J. Leavy, M. Weiss, S. Borrico, R. Gorlin, and V. Fuster. *Angiographic progression of coronary artery disease and the development of myocardial infarction.* Journal of the American College of Cardiology, 12(1):56–62, July 1988.

[37] W.C. Little, M. Constantinescu, R.J. Applegate, M.A. Kutcher, M.T. Burrows, F.R. Kahl, and W.P. Santamore. *Can Coronary Angiography Predict the Site of A Subsequent Myocardial-Infarction in Patients with Mild-To-Moderate Coronary-Artery Disease.* Circulation, 78(5):1157–1166, 1988.

[38] S. Glagov, E. Weisenberg, C.K. Zarins, R. Stankunavicius, and G.J. Kolettis. *Compensatory Enlargement of Human Atherosclerotic Coronary-Arteries.* New England Journal of Medicine, 316(22):1371–1375, 1987.

[39] J.R. Crouse, U. Goldbourt, G. Evans, J. Pinsky, A.R. Sharrett, P. Sorlie, W. Riley, and G. Heiss. *Arterial Enlargement in the Atherosclerosis Risk in Communities (Aric) Cohort - In-Vivo Quantification of Carotid Arterial Enlargement.* Stroke, 25(7):1354–1359, 1994.

[40] C. M. McEniery, Yasmin, I. R. Hall, A. Qasem, I. B. Wilkinson, J. R. Cockcroft, and ACCT Investigators. *Normal vascular aging: Differential effects on wave reflection and aortic pulse wave velocity - The Anglo-Cardiff Collaborative Trial (ACCT).* Journal of the American College of Cardiology, 46(9):1753–1760, 2005.

[41] P. Boutouyrie, S. Laurent, A. Benetos, X. J. Girerd, A. P. G. Hoeks, and M. E. Safar. *Opposing Effects of Aging On Distal and Proximal Large Arteries In Hypertensives*. Journal of Hypertension, 10:S87–S91, 1992.

[42] A. Benetos, S. Laurent, A. P. Hoeks, P. H. Boutouyrie, and M. E. Safar. *Arterial Alterations With Aging and High Blood-pressure - A Noninvasive Study of Carotid and Femoral Arteries*. Arteriosclerosis Thrombosis and Vascular Biology, 13(1):90–97, 1993.

[43] A. P. Avolio, S. G. Chen, R. P. Wang, C. L. Zhang, M. F. Li, and M. F. O'Rourke. *Effects of Aging On Changing Arterial Compliance and Left-ventricular Load In A Northern Chinese Urban-community*. Circulation, 68(1):50–58, 1983.

[44] A. P. Avolio, F. Q. Deng, W. Q. Li, Y. F. Luo, Z. D. Huang, L. F. Xing, and M. F. O'Rourke. *Effects of Aging On Arterial Distensibility In Populations With High and Low Prevalence of Hypertension - Comparison Between Urban and Rural Communities In China*. Circulation, 71(2):202–210, 1985.

[45] S. Oparil, A. Zaman, and D. A. Calhoun. *Pathogenesis of hypertension*. Annals of Internal Medicine, 139(9):761–776, 2003.

[46] M.L. Weisfeldt, E. G. Lakatta, and G. Gerstenblith. *Heart disease: A textbook of cardiovascular medicine*, chapter Aging and the heart, pages 1656–1666. WB Saunders Company, 1992.

[47] M. J. Roman, P. S. Saba, R. Pini, M. Spitzer, T. G. Pickering, S. Rosen, M. H. Alderman, and R. B. Devereux. *Parallel Cardiac and Vascular Adaptation In Hypertension*. Circulation, 86(6):1909–1918, 1992.

[48] S. Taddei, A. Virdis, P. Mattei, L. Ghiadoni, C. B. Fasolo, I. Sudano, and A. Salvetti. *Hypertension causes premature aging of endothelial function in humans*. Hypertension, 29(3):736–743, 1997.

[49] C. Giannattasio, A. A. Mangoni, M. Failla, M. L. Stella, S. Carugo, M. Bombelli, R. Sega, and G. Mancia. *Combined effects of hypertension and hypercholesterolemia on radial artery function*. Hypertension, 29(2):583–586, 1997.

[50] M. E. Safar. *Mechanical factors predicting cardiovascular risk and drug treatment of hypertension*. Journal of Hypertension, 20(3):349–352, 2002.

[51] G. Pickering. *High blood pressure*. Churchil, J. &A., 1968.

[52] D. Levy, M. G. Larson, R. S. Vasan, W. B. Kannel, and K. K. L. Ho. *The progression from hypertension to congestive heart failure*. Journal of the American Medical Association, 275(20):1557–1562, 1996.

[53] G. Pickering. *Hypertension. Definitions, natural histories and consequences*. American Journal of Medicine, 52:570–583, 1972.

[54] S. Laurent and P. Boutouyrie. *Recent Advances in Arterial Stiffness and Wave Reflection in Human Hypertension*. Hypertension, 49:1202–1206, 2007.

[55] S. Laurent, J. Cockcroft, L. Van Bortel, P. Boutouyrie, C. Giannattasio, D. Hayoz, B. Pannier, C. Vlachopoulos, I. Wilkinson, and H. Struijker-Boudier. *Expert consensus document on arterial stiffness: methodological issues and clinical applications*. European Heart Journal, 27(21):2588–605, 2006.

[56] W. J. W. Bos, A. H. Vanden Meiracker, K. H. Wesseling, and M. A. D. H. Schalekamp. *Effect of Regional and Systemic Changes In Vasomotor Tone On Finger Pressure Amplification*. Hypertension, 26(2):315–320, 1995.

[57] R. Kelly and D. Fitchett. *Noninvasive determination of aortic input impedance and external left ventricular power output: a validation and repeatability study of a new technique*. Journal of the American College of Cardiology, 20(4):952–963, October 1992.

[58] A.L. Pauca, S.L. Wallenhaupt, N.D. Kon, and W.Y. Tucker. *Does radial artery pressure accurately reflect aortic pressure?* Chest, 102(4):1193–1198, October 1992.

[59] L.M. Van Bortel, E.J. Balkestein, J.J. van der Heijden-Spek, F.H. Vanmolkot, J.A. Staessen, J.A. Kragten, J.W. Vredeveld, M.E. Safar, H.A. Struijker Boudier, and A.P. Hoeks. *Non-invasive assessment of local arterial pulse pressure: comparison of applanation tonometry and echo-tracking*. Journal of Hypertension, 19(6):1037–1044, June 2001.

[60] W.J.W. Bos, E. Verrij, H.H. Vincent, B.E. Westerhof, G. Parati, and G.A. van Montfrans. *How to assess mean blood pressure properly at the brachial artery level*. Journal of Hypertension, 25(4):751–755, 2007.

[61] F. Verbeke, P. Segers, S. Heireman, R. Vanholder, P. Verdonck, and L.M. Van Bortel. *Noninvasive assessment of local pulse pressure: importance of brachial-to-radial pressure amplification*. Hypertension, 46(1):244–248, July 2005.

[62] B. Williams, P.S. Lacy, P. Yan, C. Hwee, C. Liang, and C. Ting. *Development and Validation of a Novel Method to Derive Central Aortic Systolic Pressure From the Radial Pressure Waveform Using an N-Point Moving Average Method*. Journal of the American College of Cardiology, 57(8):951–961, 2011.

[63] L.M. Van Bortel and P. Segers. *Arterial Stiffness in Hypertension*, chapter Direct measurement of local arterial stiffness and pulse pressure, pages 35–51. Elsevier, 2006.

[64] P. Segers, S. I. Rabben, J. De Backer, J. De Sutter, T. C. Gillebert, L. Van Bortel, and P. Verdonck. *Functional analysis of the common carotid artery: relative distension differences over the vessel wall measured in vivo*. Journal of Hypertension, 22(5):973–81, 2004.

[65] G. J. Langewouters, K. H. Wesseling, and W. J. Goedhard. *The static elastic properties of 45 human thoracic and 20 abdominal aortas in vitro and the parameters of a new model*. Journal of Biomechanics, 17(6):425–35, 1984.

[66] J. Blacher, B. Pannier, A. P. Guerin, S. J. Marchais, M. E. Safar, and G. M. London. *Carotid arterial stiffness as a predictor of cardiovascular and all-cause mortality in end-stage renal disease*. Hypertension, 32(3):570–574, 1998.

[67] J. J. van der Heijden-Spek, J. A. Staessen, R. H. Fagard, A. P. Hoeks, H. A. S. Boudier, and L. M. Van Bortel. *Effect of age on brachial artery wall properties differs from the aorta and is gender dependent - A population study*. Hypertension, 35(2):637–642, 2000.

[68] C. Bussy, P. Boutouyrie, P. Lacolley, P. Challande, and S. Laurent. *Intrinsic stiffness of the carotid arterial wall material in essential hypertensives*. Hypertension, 35(5):1049–1054, 2000.

[69] M. J. F. Kool, A. P. G. Hoeks, H. A. J. Boudier, R. S. Reneman, and L. M. A. B. Van Bortel. *Short-term and Long-term Effects of Smoking On Arterial-wall Properties In Habitual Smokers*. Journal of the American College of Cardiology, 22(7):1881–1886, 1993.

[70] E. J. Giltay, J. Lambert, J. M. H. Elbers, L. J. G. Gooren, H. Asscheman, and C. D. A. Stehouwer. *Arterial compliance and distensibility are modulated by body composition in both men and women but by insulin sensitivity only in women*. Diabetologia, 42(2):214–221, 1999.

[71] K. Cruickshank, L. Riste, S. G. Anderson, J. S. Wright, G. Dunn, and R. G. Gosling. *Aortic pulse-wave velocity and its relationship to mortality in diabetes and glucose intolerance: an integrated index of vascular function?* Circulation, 106(16):2085–90, 2002.

[72] F. U. S. Mattace-Raso, A. Hofman, G. C. Verwoert, J. C. M. Witteman, I. Wilkinson, J. Cockcroft, C. McEniery, Yasmin, S. Laurent, P. Boutouyrie, E. Bozec, T. W. Hansen, C. Torp-Pedersen, H. Ibsen,

J. Jeppesen, S. J. Vermeersch, E. Rietzschel, M. De Buyzere, T. C. Gillebert, L. Van Bortel, P. Segers, C. Vlachopoulos, C. Aznaouridis, C. Stefanadis, A. Benetos, C. Labat, P. Lacolley, C. D. A. Stehouwer, G. Nijpels, J. M. Dekker, I. Ferreira, J. W. R. Twisk, S. Czernichow, P. Galan, S. Hercberg, B. Pannier, A. Guerin, G. London, J. K. Cruickshank, S. G. Anderson, A. Paini, E. A. Rosei, M. L. Muiesan, M. Salvetti, J. Filipovsky, J. Seidlerova, M. Dolejsova, and Reference Values Arterial Stiffnes. *Determinants of pulse wave velocity in healthy people and in the presence of cardiovascular risk factors: 'establishing normal and reference values'*. European Heart Journal, 31(19):2338–2350, 2010.

[73] J. Sugawara, K. Hayashi, T. Yokoi, and H. Tanaka. *Age-Associated Elongation of the Ascending Aorta in Adults*. JACC-Cardiovascular Imaging, 1(6):739–748, 2008.

[74] S.A.M. Huybrechts, D. Devos, S. Vermeersch, D. Mahieu, R. Achten, Segers P, and Van Bortel L. *Aortic path length via MRI*. submitted to Journal of Hypertension.

[75] T. Willum-Hansen, J. A. Staessen, C. Torp-Pedersen, S. Rasmussen, L. Thijs, H. Ibsen, and J. Jeppesen. *Prognostic value of aortic pulse wave velocity as index of arterial stiffness in the general population*. Circulation, 113(5):664–70, 2006.

[76] K. Sutton-Tyrrell, S. S. Najjar, R. M. Boudreau, L. Venkitachalam, V. Kupelian, E. M. Simonsick, R. Havlik, E. G. Lakatta, H. Spurgeon, S. Kritchevsky, M. Pahor, D. Bauer, and A. Newman. *Elevated aortic pulse wave velocity, a marker of arterial stiffness, predicts cardiovascular events in well-functioning older adults*. Circulation, 111(25):3384–90, 2005.

[77] F. U. Mattace-Raso, T. J. van der Cammen, A. Hofman, N. M. van Popele, M. L. Bos, M. A. Schalekamp, R. Asmar, R. S. Reneman, A. P. Hoeks, M. M. Breteler, and J. C. Witteman. *Arterial stiffness and risk of coronary heart disease and stroke: the Rotterdam Study*. Circulation, 113(5):657–63, 2006.

[78] C. Vlachopoulos, K. Aznaouridis, M.F. O'Rourke, M.E. Safar, K. Baou, and C. Stefanadis. *Prediction of cardiovascular events and all-cause mortality with central haemodynamics: a systematic review and meta-analysis*. European Heart Journal, 31(15):1865–1871, 2010.

[79] P. Segers, S. Brimioulle, N. Stergiopulos, N. Westerhof, R. Naeije, M. Maggiorini, and P. Verdonck. *Pulmonary arterial compliance in dogs and pigs: the three-element windkessel model revisited*. American Journal of Physiology, 277(2 Pt 2):H725–31, 1999.

[80] Z. Liu, K. P. Brin, and F. C. Yin. *Estimation of total arterial compliance: an improved method and evaluation of current methods*. American Journal of Physiology, 251(3 Pt 2):H588–600, 1986.

[81] N. Stergiopulos, J. J. Meister, and N. Westerhof. *Simple and accurate way for estimating total and segmental arterial compliance: the pulse pressure method*. Annals of Biomedical Engineering, 22(4):392–397, 1994.

[82] G. de Simone, M. J. Roman, M. J. Koren, G. A. Mensah, A. Ganau, and R. B. Devereux. *Stroke volume/pulse pressure ratio and cardiovascular risk in arterial hypertension*. Hypertension, 33(3):800–5, 1999.

[83] C. Vlachopoulos, K. Aznaouridis, and C. Stefanadis. *Prediction of Cardiovascular Events and All-Cause Mortality With Arterial Stiffness A Systematic Review and Meta-Analysis*. Journal of the American College of Cardiology, 55(13):1318–1327, 2010.

[84] P. Segers, E. Rietzschel, S. Heireman, M. De Buyzere, T. Gillebert, P. Verdonck, and L. Van Bortel. *Carotid tonometry versus synthesized aorta pressure waves for the estimation of central systolic blood pressure and augmentation index*. American Journal of Hypertension, 18(9):1168–1173, 2005.

[85] K. Takazawa, H. Kobayashi, N. Shindo, N. Tanaka, and A. Yamashina. *Relationship between radial and central arterial pulse wave and evaluation of central aortic pressure using the radial arterial pulse wave*. Hypertension Research, 30(3):219–228, 2007.

[86] P. Segers, E. R. Rietzschel, M. L. De Buyzere, S. J. Vermeersch, D. De Bacquer, L. M. Van Bortel, G. De Backer, T. C. Gillebert, and P. R. Verdonck. *Noninvasive (input) impedance, pulse wave velocity, and wave reflection in healthy middle-aged men and women*. Hypertension, 49(6):1248–55, 2007.

[87] A. Swillens and P. Segers. *Assessment of arterial pressure wave reflection: Methodological considerations*. Artery Research, 2:122–131, 2008.

[88] W.R. Milnor. *Hemodynamics*. Williams & Wilkins, Baltimore, 2nd edition, 1989.

[89] G. F. Mitchell, Y. Lacourciere, J. P. Ouellet, J. L. Izzo, J. Neutel, L. J. Kerwin, A. J. Block, and M. A. Pfeffer. *Determinants of elevated pulse pressure in middle-aged and older subjects with uncomplicated systolic hypertension - The role of proximal aortic diameter and the aortic pressure-flow relationship*. Circulation, 108(13):1592–1598, 2003.

[90] K. H. Parker and C. J. Jones. *Forward and backward running waves in the arteries: analysis using the method of characteristics*. Journal of Biomechanical Engineering, 112(3):322–6, 1990.

[91] D. J. Penny, J. P. Mynard, and J. J. Smolich. *Aortic wave intensity analysis of ventricular-vascular interaction during incremental dobutamine infusion in adult sheep*. American Journal of Physiology-heart and Circulatory Physiology, 294(1):H481–H489, 2008.

[92] K.H. Parker. *An introduction to Wave Intensity Analysis*, 2010. (accessed on 26 February 2011).

[93] A. D. Hughes and K. H. Parker. *Forward and backward waves in the arterial system: impedance or wave intensity analysis?* Medical and Biological Engineering and Computing, 47(2):207–210, 2009.

[94] E.R. Rietzschel, M.L. De Buyzere, S. Bekaert, P. Segers, D. De Bacquer, L. Cooman, P. Van Damme, P. Cassiman, M. Langlois, P. van Oostveldt, P. Verdonck, G. De Backer, T.C. Gillebert, and Investigators Asklepios. *Rationale, design, methods and baseline characteristics of the Asklepios Study*. European Journal of Cardiovascular Prevention & Rehabilitation, 14(2):179–191, 2007.

[95] B.E. Westerhof, I. Guelen, N. Westerhof, J.M. Karemaker, and A. Avolio. *Quantification of wave reflection in the human aorta from pressure alone - A proof of principle*. Hypertension, 48(4):595–601, 2006.

[96] A. Qasem and A. Avolio. *Determination of Aortic Pulse Wave Velocity From Waveform Decomposition of the Central Aortic Pressure Pulse*. Hypertension, 51(2):188–195, 2008.

[97] P. Reymond, F. Merenda, F. Perren, D. Rufenacht, and N. Stergiopulos. *Validation of a one-dimensional model of the systemic arterial tree*. American Journal of Physiology-Heart and Circulatory Physiology, 297(1):H208–H222, 2009.

[98] Y. Li, J.G. Wang, E. Dolan, E. O'Brien, L. Thijs, T. Nawrot, and J.A. Staessen. *Response to correlating ambulatory blood pressure measurements with arterial stiffness: A conceptual inconsistency*. Hypertension, 48(6):E109–E109, 2006.

[99] E. Dolan, Y. Li, L. Thijs, P. McCormack, J.A. Staessen, E. O'Brien, and A. Stanton. *Ambulatory arterial stiffness index: rationale and methodology*. Blood Pressure Monitoring, 11(2):103–105, 2006.

[100] A.W. Haider, M.G. Larson, S.S. Franklin, and D. Levy. *Systolic blood pressure, diastolic blood pressure, and pulse pressure as predictors of risk for congestive heart failure in the Framingham Heart Study*. Annals of Internal Medicine, 138(1):10–16, 2003.

[101] Y. Nakayama, K. Tsumura, N. Yamashita, K. Yoshimaru, and T. Hayashi. *Pulsatility of ascending aortic pressure waveform is a powerful predictor of restenosis after percutaneous transluminal coronary angioplasty*. Circulation, 101(5):470–472, 2000.

[102] J.A. Chirinos, J.P. Zambrano, S. Chakko, A. Veerani, A. Schob, G. Perez, and A.J. Mendez. *Relation between ascending aortic pressures and outcomes in patients with angiographically demonstrated coronary artery disease*. American Journal of Cardiology, 96(5):645–648, 2005.

[103] G.F. Mitchell, L.A. Moye, E. Braunwald, J.L. Rouleau, V. Bernstein, E.M. Geltman, G.C. Flaker, and M.A. Pfeffer. *Sphygmomanometrically determined pulse pressure is a powerful independent predictor of recurrent events after myocardial infarction in patients with impaired left ventricular function*. Circulation, 96(12):4254–4260, 1997.

[104] M.F. O'Rourke, A. Avolio, and A. Qasem. *Clinical assessment of wave reflection*. Hypertension, 42(5):–e15, 2003.

[105] R. Kelly, C. Hayward, A. Avolio, and M. Orourke. *Noninvasive Determination of Age-Related-Changes in the Human Arterial Pulse*. Circulation, 80(6):1652–1659, 1989.

[106] D. Lemogoum, G. Flores, W. Van den Abeele, A. Ciarka, M. Leeman, J.P. Degaute, P. van de Borne, and L. Van Bortel. *Validity of pulse pressure and augmentation index as surrogate measures of arterial stiffness during beta-adrenergic stimulation*. Journal of Hypertension, 22(3):511–517, 2004.

[107] P. Segers, E.R. Rietzschel, M.L. De Buyzere, Bacquer D. De, L.M. Van Bortel, Backer G. De, T.C. Gillebert, and P.R. Verdonck. *Assessment of pressure wave reflection: getting the timing right!* Physiological Measurement, 28(9):1045–1056, September 2007.

[108] P. Segers, J. De Backer, D. Devos, S.I. Rabben, T.C. Gillebert, L.M. Van Bortel, J. De Sutter, A. De Paepe, and P.R. Verdonck. *Aortic reflection coefficients and their association with global indexes of wave reflection in healthy controls and patients with Marfan's syndrome*. American Journal of Physiology-Heart and Circulatory Physiology, 290(6):H2385–H2392, 2006.

[109] S. Aakhus, C. Soerlie, A. Faanes, S.O. Hauger, K. Bjoernstad, L. Hatle, and B.A. Angelsen. *Noninvasive computerized assessment of left ventricular performance and systemic hemodynamics by study of aortic root pressure and flow estimates in healthy men, and men with acute and healed myocardial infarction*. American Journal of Cardiology, 72(3):260–267, 1993.

[110] R Bracewell. *The Fourier Transform and Its Applications.*, chapter Pentagram Notation for Cross Correlation., pages 46–243. McGraw-Hill, New York, 1999.

[111] C.H. Chen, E. Nevo, B. Fetics, P.H. Pak, F.C. Yin, W.L. Maughan, and D.A. Kass. *Estimation of central aortic pressure waveform by mathematical transformation of radial tonometry pressure. Validation of generalized transfer function*. Circulation, 95(7):1827–1836, April 1997.

[112] A.J.S. Coats, C. Murphy, J. Conway, and P. Sleight. *Validation of the Beat to Beat Measurement of Blood Velocity in the Human Ascending Aorta by A New High Temporal Resolution Doppler Ultrasound Spectral Analyzer*. British Heart Journal, 68(2):223–229, 1992.

[113] J.A. Innes, C.J. Mills, M.I.M. Noble, K. Murphy, S. Pugh, A.C. Shore, and A. Guz. *Validation of Beat by Beat Pulsed Doppler Measurements of Ascending Aortic Blood Velocity in Man*. Cardiovascular Research, 21(1):72–80, 1987.

[114] K. Takazawa, N. Tanaka, M. Fujita, O. Matsuoka, T. Saiki, M. Aikawa, S. Tamura, and C. Ibukiyama. *Assessment of vasoactive agents and vascular aging by the second derivative of photoplethysmogram waveform*. Hypertension, 32(2):365–370, 1998.

[115] B.E. Westerhof, J.P. van den Wijngaard, J.P. Murgo, and N. Westerhof. *Location of a reflection site is elusive - Consequences for the calculation of aortic pulse wave velocity*. Hypertension, 52(3):478–483, 2008.

[116] G.F. Mitchell, H. Parise, E.J. Benjamin, M.G. Larson, M.J. Keyes, J.A. Vita, R.S. Vasan, and D. Levy. *Changes in arterial stiffness and wave reflection with advancing age in healthy men and women - The Framingham Heart Study*. Hypertension, 43(6):1239–1245, 2004.

[117] E. Agabiti Rosei, G. Mancia, M.F. O'Rourke, M.J. Roman, M.E. Safar, H. Smulyan, J.G. Wang, I.B. Wilkinson, B. Williams, and C. Vlachopoulos. *Central blood pressure measurements and antihypertensive therapy: a consensus document*. Hypertension, 50(1):154–160, July 2007.

[118] J.A. Chirinos, J.P. Zambrano, S. Chakko, A. Veerani, A. Schob, H.J. Willens, G. Perez, and A.J. Mendez. *Aortic pressure augmentation predicts adverse cardiovascular events in patients with established coronary artery disease*. Hypertension, 45(5):980–985, 2005.

[119] A.M. Dart, C.D. Gatzka, B.A. Kingwell, K. Willson, J.D. Cameron, Y.L. Liang, K.L. Berry, L.M.H. Wing, C.M. Reid, P. Ryan, L.J. Beilin, G.L.R. Jennings, C.I. Johnston, J.J. Mcneil, G.J. MacDonald, T.O. Morgan, and M.J. West. *Brachial blood pressure but not carotid arterial waveforms predict cardiovascular events in elderly female hypertensives*. Hypertension, 47(4):785–790, 2006.

[120] C.M. McEniery, B. McDonnell, M. Munnery, S.M. Wallace, C.V. Rowe, J.R. Cockcroft, I.B. Wilkinson, and Collaborative Tr Anglo-Cardiff. *Central pressure: Variability and impact of cardiovascular risk factors - The Anglo-Cardiff Collaborative Trial II*. Hypertension, 51(6):1476–1482, 2008.

[121] M.J. Roman, R.B. Devereux, J.R. Kizer, E.T. Lee, J.M. Galloway, T. Ali, J.G. Umans, and B.V. Howard. *Central pressure more strongly relates to vascular disease and outcome than does brachial pressure - The strong heart study*. Hypertension, 50(1):197–203, 2007.

[122] M.E. Safar, J. Blacher, B. Pannier, A.P. Guerin, S.J. Marchais, P.M. Guyonvarc'h, and G.M. London. *Central pulse pressure and mortality in end-stage renal disease*. Hypertension, 39(3):735–738, 2002.

[123] B. Williams, P.S. Lacy, S.M. Thom, K. Cruickshank, A. Stanton, D. Collier, A.D. Hughes, H. Thurston, and A.S.C.O. CAFE Investigators. *Differential impact of blood pressure-lowering drugs on central aortic pressure and clinical outcomes - Principal results of the Conduit Artery Function Evaluation (CAFE) study*. Circulation, 113(9):1213–1225, 2006.

[124] M.E. Safar and G.M. London. *Textbook of Hypertension*, chapter The arterial system in human hypertension, pages 85–102. Blackwell Scientific, London, 1994.

[125] S.J. Vermeersch, E.R. Rietzschel, M.L. De Buyzere, D. De Bacquer, G. De Backer, L.M. Van Bortel, T.C. Gillebert, P.R. Verdonck, and P. Segers. *Determining carotid artery pressure from scaled diameter waveforms: comparison and validation of calibration techniques in 2026 subjects*. Physiological Measurement, 29(11):1267–1280, 2008.

[126] A.P.G. Hoeks, P.J. Brands, F.A.M. Smeets, and R.S. Reneman. *Assessment of the Distensibility of Superficial Arteries*. Ultrasound in Medicine and Biology, 16(2):121–128, 1990.

[127] A.P.G. Hoeks, C. Willekes, P. Boutouyrie, P.J. Brands, J.M. Willigers, and R.S. Reneman. *Automated detection of local artery wall thickness based on M-line signal processing*. Ultrasound in Medicine and Biology, 23(7):1017–1023, 1997.

[128] S.I. Rabben, S. Bjaerum, V. Sorhus, and H. Torp. *Ultrasound-based vessel wall tracking: An auto-correlation technique with RF center frequency estimation*. Ultrasound in Medicine and Biology, 28(4):507–517, 2002.

[129] M.F. O'Rourke and W. W. Nichols. *Aortic diameter, aortic stiffness, and wave reflection increase with age and isolated systolic hypertension*. Hypertension, 45(4):652–8, 2005.

[130] M.F. O'Rourke and K. Takazawa. *Flawed Measurement of Brachial Tonometry for Calculating Aortic Pressure?* Hypertension, 54(5):E131–E131, 2009.

[131] J.N. de Hoon, J.M. Willigers, J. Troost, H.A. Struijker-Boudier, and L.M. Van Bortel. *Cranial and peripheral interictal vascular changes in migraine patients*. Cephalalgia, 23(2):96–104, 2003.

[132] F.H. Vanmolkot, L.M. Van Bortel, and J.N. Hoon. *Altered arterial function in migraine of recent onset*. Neurology, 68(19):1563–1570, 2007.

[133] J.M. Meinders and A.P.G. Hoeks. *Simultaneous assessment of diameter and pressure waveforms in the carotid artery*. Ultrasound in Medicine and Biology, 30(2):147–154, 2004.

[134] D. Chemla, J.L. Hebert, E. Aptecar, J.X. Mazoit, K. Zamani, R. Frank, G. Fontaine, A. Nitenberg, and Y. Lecarpentier. *Empirical estimates of mean aortic pressure: advantages, drawbacks and implications for pressure redundancy*. Clinical Science, 103(1):7–13, 2002.

[135] C.H. Chen, C.T. Ting, A. Nussbacher, E. Nevo, D.A. Kass, P. Pak, S.P. Wang, M.S. Chang, and F.C. Yin. *Validation of carotid artery tonometry as a means of estimating augmentation index of ascending aortic pressure*. Hypertension, 27(2):168–175, February 1996.

[136] B. Fetics, E. Nevo, C.H. Chen, and D.A. Kass. *Parametric model derivation of transfer function for noninvasive estimation of aortic pressure by radial tonometry*. IEEE Trans.Biomed.Eng, 46(6):698–706, June 1999.

[137] D. Gallagher, A. Adji, and M.F. O'Rourke. *Validation of the transfer function technique for generating central from peripheral upper limb pressure waveform*. American Journal of Hypertension, 17(11 Pt 1):1059–1067, November 2004.

[138] M. Karamanoglu, M. F. O'Rourke, A. P. Avolio, and R. P. Kelly. *An analysis of the relationship between central aortic and peripheral upper limb pressure waves in man*. European Heart Journal, 14(2):160–7, 1993.

[139] K. Takazawa, M.F. O'Rourke, M. Fujita, N. Tanaka, K. Takeda, F. Kurosu, and C. Ibukiyama. *Estimation of ascending aortic pressure from radial arterial pressure using a generalised transfer function*. Zeitung Kardiologie, 85 Suppl 3:137–139, 1996.

[140] S.A. Hope, I.T. Meredith, D. Tay, and J.D. Cameron. *'Generalizability' of a radial-aortic transfer function for the derivation of central aortic waveform parameters*. Journal of Hypertension, 25(9):1812–1820, September 2007.

[141] E.D. Lehmann. *Regarding the accuracy of generalized transfer functions for estimating central aortic blood pressure when calibrated non-invasively*. Journal of Hypertension, 18(3):347–349, March 2000.

[142] S.A. Hope, I.T. Meredith, and J.D. Cameron. *Effect of non-invasive calibration of radial waveforms on error in transfer-function-derived central aortic waveform characteristics*. Clinical Science, 107(2):205–211, August 2004.

[143] T.G. Papaioannou, J.P. Lekakis, E.N. Karatzis, C.M. Papamichael, K.S. Stamatelopoulos, A.D. Protogerou, M. Mavrikakis, and C. Stefanadis. *Transmission of calibration errors (input) by generalized transfer functions to the aortic pressures (output) at different hemodynamic states*. International Journal of Cardiology, 110(1):46–52, June 2006.

[144] G. Drzewiecki, R. Hood, and H. Apple. *Theory of the Oscillometric Maximum and the Systolic and Diastolic Detection Ratios*. Annals of Biomedical Engineering, 22(1):88–96, 1994.

[145] G. W. Mauck, C. R. Smith, L. A. Geddes, and J. D. Bourland. *Meaning of the Point of Maximum Oscillations In Cuff Pressure In the Indirect Measurement of Blood-pressure .2.* Journal of Biomechanical Engineering-transactions of the Asme, 102(1):28–33, 1980.

[146] M. Ursino and C. Cristalli. *A mathematical study of some biomechanical factors affecting the oscillometric blood pressure measurement*. IEEE Transactions On Biomedical Engineering, 43(8):761–778, 1996.

[147] W.J. Bos, E. Verrij, H.H. Vincent, B.E. Westerhof, G. Parati, and G.A. van Montfrans. *reply on: Thumb-rule for the proper assessment of mean blood pressure at the brachial artery level: what should be changed?* Journal of Hypertension, 25(8):1741–1742, August 2007.

[148] D. Chemla, M. Brahimi, and A. Nitenberg. *Thumb-rule for the proper assessment of mean blood pressure at the brachial artery level: what should be changed?* Journal of Hypertension, 25(8):1740–1741, August 2007.

[149] S. Omboni, I. Riva, A. Giglio, G. Caldara, A. Groppelli, and G. Parati. *Validation of the Omron M5-1, 145-1 and HEM-907 automated blood pressure monitors in elderly individuals according to the International Protocol of the European Society of Hypertension*. Blood Pressure Monitoring, 12(4):233–242, 2007.

[150] M. A. El Assaad, J. A. Topouchian, B. M. Darne, and R. G. Asmar. *Validation of the Omron HEM-907 device for blood pressure measurement*. Blood Pressure Monitoring, 7(4):237–241, 2002.

[151] P. Segers, S. Carlier, A. Pasquet, S. I. Rabben, L. R. Hellevik, E. Remme, T. De Backer, J. De Sutter, J. D. Thomas, and P. Verdonck. *Individualizing the aorto-radial pressure transfer function: feasibility of a model-based approach*. American Journal of Physiology-Heart and Circulatory Physiology, 279(2):H542–9, 2000.

[152] S. Laurent, P. Boutouyrie, R. Asmar, I. Gautier, B. Laloux, L. Guize, P. Ducimetiere, and A. Benetos. *Aortic stiffness is an independent predictor of all-cause and cardiovascular mortality in hypertensive patients*. Hypertension, 37(5):1236–41, 2001.

[153] M. Kikuya, J.A. Staessen, T. Ohkubo, L. Thijs, H. Metoki, K. Asayama, T. Obara, R. Inoue, Y. Li, E. Dolan, H. Hoshi, J. Hashimoto, K. Totsune, H. Satoh, J.G. Wang, E. O'Brien, and Y. Imai. *Ambulatory arterial stiffness index and 24-hour ambulatory pulse pressure as predictors of mortality in Ohasama, Japan*. Stroke, 38(4):1161–1166, 2007.

[154] E. Dolan, L. Thijs, Y. Li, N. Atkins, P. McCormack, S. McClory, E. O'Brien, J.A. Staessen, and A.V. Stanton. *Ambulatory arterial stiffness index as a predictor of cardiovascular mortality in the Dublin outcome study*. Hypertension, 47(3):365–370, 2006.

[155] T.W. Hansen, J.A. Staessen, C. Torp-Pedersen, S. Rasmussen, Y. Li, E. Dolan, L. Thijs, J.G. Wang, E. O'Brien, H. Ibsen, and J. Jeppesen. *Ambulatory arterial stiffness index predicts stroke in a general population*. Journal of Hypertension, 24(11):2247–2253, 2006.

[156] G. Schillaci, G. Parati, M. Pirro, G. Pucci, M.R. Mannarino, L. Sperandini, and E. Mannarino. *Ambulatory arterial stiffness index is not a specific marker of reduced arterial compliance*. Hypertension, 49(5):986–991, 2007.

[157] S. Laurent. *Surrogate measures of arterial stiffness - Do they have additive predictive value or are they only surrogates of a surrogate?* Hypertension, 47(3):325–326, 2006.

[158] N. Westerhof, J.W. Lankhaar, and B.E. Westerhof. *Ambulatory arterial stiffness index is not a stiffness parameter but a ventriculo-arterial coupling factor*. Hypertension, 49:E7–E7, 2007.

[159] A. Benetos and P. Lacolley. *From 24-hour blood pressure measurements to arterial stiffness - A valid short cut?* Hypertension, 47(3):327–328, 2006.

[160] B. Gavish. *Correlating ambulatory blood pressure measurements with arterial stiffness: A conceptual inconsistency?* Hypertension, 48(6):E108–E108, 2006.

[161] P. Jerrard-Dunne, A. Mahmud, and J. Feely. *Ambulatory arterial stiffness index, pulse wave velocity and augmentation index - interchangeable or mutually exclusive measures?* Journal of Hypertension, 26(3):529–534, 2008.

[162] P. Verdecchia, C. Porcellati, G. Schillaci, C. Borgioni, A. Ciucci, M. Battistelli, M. Guerrieri, C. Gatteschi, I. Zampi, A. Santucci, C. Santucci, and G. Reboldi. *Ambulatory Blood-Pressure - An Independent Predictor of Prognosis in Essential-Hypertension*. Hypertension, 24(6):793–801, 1994.

[163] T.W. Hansen, J. Jeppesen, S. Rasmussen, H. Ibsen, and C. Torp-Pedersen. *Ambulatory blood pressure and mortality - A population-based study*. Hypertension, 45(4):499–504, 2005.

[164] A. Adiyaman, D.G. Dechering, J. Boggia, Y. Li, T.W. Hansen, M. Kikuya, K. Bjorklund-Bodegard, T. Richart, L. Thijs, C. Torp-Pedersen, T. Ohkubo, E. Dolan, Y. Imai, E. Sandoya, H. Ibsen, J.G. Wang, L. Lind, E. O'Brien, T. Thien, J.A. Staessen, and Int Database Ambulatory Blood Pres. *Determinants of the Ambulatory Arterial Stiffness Index in 7604 Subjects From 6 Populations*. Hypertension, 52(6):1038–1U30, 2008.

[165] C.J. Richardson, Kaisa M. Maki-Petaja, Barry J. McDonnell, Stacey S. Hickson, Ian B. Wilkinson, and Carmel M. McEniery. *Comparison of estimates of central systolic blood pressure and peripheral augmentation index obtained from the Omron HEM-9000AI and SphygmoCor systems*. Artery Research, 3(1):24–31, February 2009.

[166] A. Bonny, F. Lacombe, M. Yitemben, B. Discazeaux, J. Donetti, P. Fahri, R. Megbemado, and B. Estampes. *The 2007 ESH/ESC Guidelines for the management of arterial hypertension*. Journal of Hypertension, 26(4):825–825, 2008.

[167] N. Stergiopulos, D.F. Young, and T.R. Rogge. *Computer-Simulation of Arterial Flow with Applications to Arterial and Aortic Stenoses*. Journal of Biomechanics, 25(12):1477–1488, 1992.

[168] Y. C. Chiu, P. W. Arand, S. G. Shroff, T. Feldman, and J. D. Carroll. *Determination of Pulse-wave Velocities With Computerized Algorithms*. American Heart Journal, 121(5):1460–1470, 1991.

[169] S. C. Millasseau, A. D. Stewart, S. J. Patel, S. R. Redwood, and P. J. Chowienczyk. *Evaluation of carotid-femoral pulse wave velocity: influence of timing algorithm and heart rate*. Hypertension, 45(2):222–6, 2005.

[170] P. Segers, E. Rietzschel, S. Vermeersch, M. De Buyzere, D. De Bacquer, G. De Backer, P. Verdonck, T. Gillebert, L. Bortel, and Asklepios Investigators. *Carotid artery structure and large artery stiffness in 2524 middle-aged men and women (Asklepios study): Integrating morphology and mechanics*. Journal of Hypertension, 26:S63–S63, 2008.

[171] J. Baulmann, U. Schillings, S. Rickert, S. Uen, R. Dusing, M. Illyes, A. Cziraki, G. Nickering, and T. Mengden. *A new oscillometric method for assessment of arterial stiffness: comparison with tonometric and piezoelectronic methods*. Journal of Hypertension, 26(3):523–528, 2008.

[172] I. Horvath, L. Papp, and M. Illyes. *Invasive Validations of a User Independent Oscillometric Device (Arteriograph) for Measuring Augmentation Index and Aortic Pulse Wave Velocity*. Artery Research, 1:75–76, 2007.

[173] D. Magometschnigg. *Blood pressure and arterial stiffness. A comparison of two devices for measuring augmentation index and pulse wave velocity.* Wiener Medizinische Wochenschrift, 155:404–410, 2005.

[174] M. Illyes. *A new and fast screening method for measuring complex hemodynamical parameters and arterial stiffness non-invasively with a simple arm cuff*. American Journal of Hypertension, 18(5):15A–15A, 2005.

[175] B.. Jiang, B. Liu, K. L. McNeill, and P. J. Chowienczyk. *Measurement of pulse wave velocity using pulse wave Doppler ultrasound: comparison with arterial tonometry*. Ultrasound in Medicine and Biology, 34:509–512, 2008.

[176] E. D. Lehmann. *Noninvasive measurements of aortic stiffness: methodological considerations*. Pathologie Biologie, 47(7):716–730, 1999.

[177] J. J. Oliver and D. J. Webb. *Noninvasive assessment of arterial stiffness and risk of atherosclerotic events*. Arteriosclerosis Thrombosis and Vascular Biology, 23(4):554–566, 2003.

[178] J.C. Bramwell and A.V. Hill. *The velocity of the pulse wave in man.* Proceedings of the Society for Experimental Biology and Medicine, 93:298Ű306, 1922.

[179] P. Segers, D. Mahieu, J. Kips, E. Rietzschel, M. De Buyzere, D. De Bacquer, S. Bekaert, G. De Backer, T. Gillebert, P. Verdonck, and L. Van Bortel. *Amplification of the Pressure Pulse in the Upper Limb in Healthy, Middle-Aged Men and Women*. Hypertension, 54(2):414–420, 2009.

[180] N. Bjarnegard and T. Lanne. *Arterial properties along the upper arm in humans: age-related effects and the consequence of anatomical location*. Journal of Applied Physiology, 108(1):34–38, 2010.

[181] G. Schillaci and G. Grassi. *Central blood pressure: getting to the heart of the matter*. Journal of Hypertension, 28(2):237–239, 2010.

[182] A.L. Pauca, N.D. Kon, and M.F. O'Rourke. *The second peak of the radial artery pressure wave represents aortic systolic pressure in hypertensive and elderly patients*. British Journal of Anaesthesia, 92(5):651–657, 2004.

[183] A. Adji, K. Hirata, S. Hoegler, and M.F. O'Rourke. *Noninvasive pulse waveform analysis in clinical trials: Similarity of two methods for calculating aortic systolic pressure*. American Journal of Hypertension, 20:917–922, 2007.

[184] S. Munir, A. Guilcher, T. Kamalesh, B. Clapp, S. Redwood, M. Marber, and P. Chowienczyk. *Peripheral augmentation index defines the relationship between central and peripheral pulse pressure*. Hypertension, 51(1):112–118, 2008.

[185] K. Teo, C.K. Chow, M. Vaz, S. Rangarajan, S. Yusuf, and Pure Investigators-Writing Grp. *The Prospective Urban Rural Epidemiology (PURE) study: Examining the impact of societal influences on chronic noncommunicable diseases in low-, middle-, and high-income countries*. American Heart Journal, 158(1):1–7, 2009.

[186] S.S. Hickson, M. Butlin, F.A. Mir, J. Graggaber, J. Cheriyan, F. Khan, A. A. Grace, Yasmin, J.R. Cockcroft, I.B. Wilkinson, C.M. McEniery, and on behalf of the Anglo-Cardiff Collaboration Trial Investigators. *The accuracy of central SBP determined from the second systolic peak of the peripheral pressure waveform*. Journal of Hypertension, 27(9):–, 2009.

[187] D. Lemogoum, L. Van Bortel, M. Leeman, J.P. Degaute, and P.V. de Borne. *Ethnic differences in arterial stiffness and wave reflections after cigarette smoking*. Journal of Hypertension, 24(4):683–689, 2006.

[188] C.P. Shiburi, J.A. Staessen, M. Maseko, W. Wojciechowska, L. Thijs, L.M. Van Bortel, A.J. Woodiwiss, and G.R. Norton. *Reference values for SphygmoCor measurements in South Africans of African ancestry*. American Journal of Hypertension, 19(1):40–46, 2006.

[189] A.J. Woodiwiss, N. Molebatsi, M.J. Maseko, E. Libhaber, C. Libhaber, O.H.I. Majane, J. Paiker, P. Dessein, R. Brooksbank, P. Sareli, and G.R. Norton. *Nurse-recorded auscultatory blood pressure at a single visit predicts target organ changes as well as ambulatory blood pressure*. Journal of Hypertension, 27(2):287–297, 2009.

[190] I. B. Wilkinson, S. A. Fuchs, I. M. Jansen, J. C. Spratt, G. D. Murray, J. R. Cockcroft, and D. J. Webb. *Reproducibility of pulse wave velocity and augmentation index measured by pulse wave analysis*. Journal of Hypertension, 16(12):2079–2084, 1998.

[191] M. Frimodt-Moller, A. H. Nielsen, A. L. Kamper, and S. Strandgaard. *Reproducibility of pulse-wave analysis and pulse-wave velocity determination in chronic kidney disease*. Nephrology Dialysis Transplantation, 23(2):594–600, 2008.

[192] J. E. Keil, S. E. Sutherland, R. G. Knapp, D. T. Lackland, P. C. Gazes, and H. A. Tyroler. *Mortality-rates and Risk-factors For Coronary-disease In Black As Compared With White Men and Women*. New England Journal of Medicine, 329(2):73–78, 1993.

[193] C. Agyemang, R. Bhopal, and W. K. Redekop. *Does the pulse pressure in people of European, African and South Asian descent differ? A systematic review and meta-analysis of UK data*. Journal of Human Hypertension, 21:598–609, 2007.

[194] J. A. Stewart, R. Dundas, R. S. Howard, A. G. Rudd, and C. D. A. Wolfe. *Ethnic differences in incidence of stroke: prospective study with stroke register*. British Medical Journal, 318(7189):967–971, 1999.

[195] S. Y. Li, D. D. McAlpine, J. N. Liu, S. L. Li, and A. J. Collins. *Differences between blacks and whites in the incidence of end-stage renal disease and associated risk factors*. Advances In Renal Replacement Therapy, 11(1):5–13, 2004.

[196] J. Cornoni-Huntley, A. Z. Lacroix, and R. J. Havlik. *Race and Sex Differentials In the Impact of Hypertension In the United-states - the National-health and Nutrition Examination Survey-i Epidemiologic Follow-up-study*. Archives of Internal Medicine, 149(4):780–788, 1989.

[197] B. Kissela, A. Schneider, D. Kleindorfer, J. Khoury, R. Miller, K. Alwell, D. Woo, J. Szaflarski, J. Gebel, C. Moomaw, A. Pancioli, E. Jauch, R. Shukla, and J. Broderick. *Stroke in a Biracial Population - The excess burden of stroke among blacks*. Stroke, 35(2):426–431, 2004.

[198] V. L. Burt, J.A. Cutler, M. Higgins, M. J. Horan, D. Labarthe, P. Whelton, C. Brown, and E. J. Roccella. *Trends In the Prevalence, Awareness, Treatment, and Control of Hypertension In the Adult Us Population - Data From the Health Examination Surveys, 1960 To 1991*. Hypertension, 26(1):60–69, 1995.

[199] S. J. Kittner, L. R. White, K. G. Losonczy, P. A. Wolf, and J. R. Hebel. *Black-white Differences In Stroke Incidence In A National Sample - the Contribution of Hypertension and Diabetes-mellitus*. Journal of the American Medical Association, 264(10):1267–1270, 1990.

[200] H. F. McGruder, A. M. Malarcher, T. L. Antoine, K. J. Greenlund, and J. B. Croft. *Racial and ethnic disparities in cardiovascular risk factors among stroke survivors - United States 1999 to 2001*. Stroke, 35(7):1557–1561, 2004.

[201] J. K. Cruickshank, F. Mzayek, L. Liu, L. Kieltyka, R. Sherwin, L. S. Webber, S. R. Srinavasan, and G. S. Berenson. *Origins of the "black/white" difference in blood pressure - Roles of birth weight, postnatal growth, early blood pressure, and adolescent body size - The Bogalusa Heart study*. Circulation, 111(15):1932–1937, 2005.

[202] D.J. Barker. *Mothers, Babies and Health in Later Life*. Churchill Livingstone, 1998.

[203] M. E. Safar and G. M. London. *Arterial and Venous Compliance In Sustained Essential-hypertension*. Hypertension, 10(2):133–139, 1987.

[204] H. G. Xie, R. B. Kim, C. M. Stein, J. V. Gainer, N. J. Brown, and A. J. J. Wood. *alpha(1A)-Adrenergic receptor polymorphism: association with ethnicity but not essential hypertension*. Pharmacogenetics, 9(5):651–656, 1999.

[205] J. Barley, A. Blackwood, N. D. Carter, D. E. Crews, J. K. Cruickshank, S. Jeffery, A. O. Ogunlesi, and G. A. Sagnella. *Angiotensin-converting Enzyme Insertion/deletion Polymorphism - Association With Ethnic-origin*. Journal of Hypertension, 12(8):955–957, 1994.

[206] B. J. Meyer, A. C. Meyer, J. J. Theron, and W. J. Pepler. *Atherosclerosis In Europeans + Bantu*. Circulation, 29(3):415–&, 1964.

[207] A. V. L. Ferreira, M. C. Viana, J. G. Mill, R. G. Asmar, and R. S. Cunha. *Racial differences in aortic stiffness in normotensive and hypertensive adults*. Journal of Hypertension, 17(5):631–637, 1999.

[208] T. M. Doherty, W. Y. Tang, and R. C. Detrano. *Racial differences in the significance of coronary calcium in asymptomatic black and white subjects with coronary risk factors*. Journal of the American College of Cardiology, 34(3):787–794, 1999.

[209] T. C. Lee, P. G. O'Malley, I. Feuerstein, and A. J. Taylor. *The prevalence and severity of coronary artery calcification on coronary artery computed tomography in black and white subjects*. Journal of the American College of Cardiology, 41(1):39–44, 2003.

[210] A. B. Newman, B. L. Naydeck, K. Sutton-Tyrrell, A. Feldman, D. Edmundowicz, and L. H. Kuller. *Coronary artery calcification in older adults to age 99 - Prevalence and risk factors*. Circulation, 104(22):2679–2684, 2001.

[211] M. J. Budoff, T. P. Yang, R. M. Shavelle, D. H. Lamont, and B. H. Brundage. *Ethnic differences in coronary atherosclerosis*. Journal of the American College of Cardiology, 39(3):408–412, 2002.

[212] A. R. Bhuiyan, S. R. Srinivasan, W. Chen, T. K. Paul, and G. S. Berenson. *Correlates of vascular structure and function measures in asymptomatic young adults: The Bogalusa Heart Study*. Atherosclerosis, 189(1):1–7, 2006.

[213] M. A. Collins, M. L. Millard-Stafford, E. M. Evans, T. K. Snow, K. J. Cureton, and L. B. Rosskopf. *Effect of race and musculoskeletal development on the accuracy of air plethysmography*. Medicine and Science In Sports and Exercise, 36(6):1070–1077, 2004.

[214] T. A. Manolio, A. M. Arnold, W. Post, A. G. Bertoni, P. J. Schreiner, R. L. Sacco, M. E. Saadi, R. L. Detrano, and M. Szklo. *Ethnic differences in the relationship of carotid atherosclerosis to coronary calcification: The Multi-Ethnic Study of Atherosclerosis*. Atherosclerosis, 197(1):132–138, 2008.

[215] H. Markus, Z. Kapozsta, R. Ditrich, C. Wolfe, N. Ali, J. Powell, M. Mendell, and M. Cullinane. *Increased common carotid intima-media thickness in UK African Caribbeans and its relation to chronic inflammation and vascular candidate gene polymorphisms*. Stroke, 32(11):2465–2471, 2001.

[216] B. I. Freedman, F. C. Hsu, C. D. Langefeld, S. S. Rich, D. M. Herrington, J. J. Carr, J. Xu, D. W. Bowden, and L. E. Wagenknecht. *The impact of ethnicity and sex on subclinical cardiovascular disease: the Diabetes Heart Study*. Diabetologia, 48(12):2511–2518, 2005.

[217] R. B. D'Agostino, G. Burke, D. OLeary, M. Rewers, J. Selby, P. J. Savage, M. F. Saad, R. N. Bergman, G. Howard, L. Wagenknecht, and S. M. Haffner. *Ethnic differences in carotid wall thickness - The Insulin Resistance Atherosclerosis Study*. Stroke, 27(10):1744–1749, 1996.

[218] K. S. Heffernan, S. Y. Jae, K. R. Wilund, J. A. Woods, and B. Fernhall. *Racial differences in central blood pressure and vascular function in young men*. American Journal of Physiology-heart and Circulatory Physiology, 295(6):H2380–H2387, 2008.

[219] H. Tanaka, F. A. Dinenno, K. D. Monahan, C. A. DeSouza, and D. R. Seals. *Carotid artery wall hypertrophy with age is related to local systolic blood pressure in healthy men*. Arteriosclerosis Thrombosis and Vascular Biology, 21(1):82–87, 2001.

[220] D. Lemogoum, L. Van Bortel, W. Van den Abeele, A. Ciarka, J. P. Degaute, P. van de Borne, and M. Leeman. *Effect of beta-adrenergic stimulation on pulse wave velocity in black and white subjects*. Journal of Hypertension, 22(12):2349–2353, 2004.

[221] C. M. Stein, C. C. Lang, R. Nelson, M. Brown, and A. J. J. Wood. *Vasodilation in black Americans: Attenuated nitric oxide-mediated responses*. Clinical Pharmacology and Therapeutics, 62(4):436–443, 1997.

[222] C. M. Stein, C. C. Lang, I. Singh, H. B. He, and A. J. J. Wood. *Increased vascular adrenergic vasoconstriction and decreased vasodilation in blacks - Additive mechanisms leading to enhanced vascular reactivity*. Hypertension, 36(6):945–951, 2000.

[223] D. A. Rosenbaum, M. Pretorius, J. V. Gainer, D. Byrne, L. J. Murphey, C. A. Painter, D. E. Vaughan, and N. J. Brown. *Ethnicity affects vasodilation, but not endothelial tissue plasminogen activator release, in response to bradykinin*. Arteriosclerosis Thrombosis and Vascular Biology, 22(6):1023–1028, 2002.

[224] D. F. Kahn, S. J. Duffy, D. Tomasian, M. Holbrook, L. Rescorl, J. Russell, N. Gokce, J. Loscalzo, and J. A. Vita. *Effects of black race on forearm resistance vessel function*. Hypertension, 40(2):195–201, 2002.

[225] C. C. Lang, C. M. Stein, R. M. Brown, R. Deegan, R. Nelson, H. B. He, M. Wood, and A. J. J. Wood. *Attenuation of Isoproterenol-mediated Vasodilatation In Blacks*. New England Journal of Medicine, 333(3):155–160, 1995.

[226] G. Y. H. Lip and C. J. Boos. *Ethnic differences in arterial responses, inflammation, and metabolic profiles - Possible insights into ethnic differences in cardiovascular disease and stroke*. Arteriosclerosis Thrombosis and Vascular Biology, 25(11):2240–2242, 2005.

[227] A. H. Heald, S. G. Anderson, F. Ivison, I. Laing, J. M. Gibson, and K. Cruickshank. *C-reactive protein and the insulin-like growth factor (IGF)-system in relation to risk of cardiovascular disease in different ethnic groups*. Atherosclerosis, 170(1):79–86, 2003.

[228] L. Kalra, C. Rambaran, E. Iveson, P. J. Chowienczyk, I. Hambleton, J. M. Ritter, A. Shah, R. Wilks, and T. Forrester. *The role of inheritance and environment in predisposition to vascular disease in people of African descent*. Journal of the American College of Cardiology, 47(6):1126–1133, 2006.

[229] L. Salciccioli, H. Kamran, G. Qureshi, C. Philip, G. Jean-Louis, F. Zizi, E. H. Ko, and J. M. Lazar. *Indices of Arterial Stiffness in African American and African Caribbean Subjects*. Journal of the National Medical Association, 101(10):992–998, 2009.

[230] C. Rajkumar, R. Mensah, K. Meeran, S. Armstrong, and C.J. Bulpitt. *Peripheral arterial compliance is lower in Afro-Caribbeans compared to white Caucasians with type 2 diabetes after adjustment for blood pressure*. Journal of Human Hypertension, 13(12):841–843, 1999.

[231] N. Chaturvedi, C. J. Bulpitt, S. Leggetter, R. Schiff, P. Nihoyannopoulos, W. D. Strain, A. C. Shore, and C. Rajkumar. *Ethnic differences in vascular stiffness and relations to hypertensive target organ damage*. Journal of Hypertension, 22(9):1731–1737, 2004.

[232] W. D. Strain, N. Chaturvedi, F. Dockery, R. Shiff, A. C. Shore, C. J. Bulpitt, and C. Rajkumar. *Increased arterial stiffness in Europeans and African Caribbeans with type 2 diabetes cannot be accounted for by conventional cardiovascular risk factors*. American Journal of Hypertension, 19(9):889–896, 2006.

[233] E. M. Urbina, T. J. Brinton, A. Elkasabany, and G. S. Berenson. *Brachial artery distensibility and relation to cardiovascular risk factors in healthy young adults (The Bogalusa Heart Study)*. American Journal of Cardiology, 89(8):946–951, 2002.

[234] M. H. Weinberger, N. S. Fineberg, and S. E. Fineberg. *Effects of age, race, gender, blood pressure, and estrogen on arterial compliance*. American Journal of Hypertension, 15(4):358–363, 2002.

[235] R.H. Mackey, K. Sutton-Tyrrell, P.V. Vaitkevicius, P.A. Sakkinen, M.F. Lyles, H.A. Spurgeon, E.G. Lakatta, and L.H. Kuller. *Correlates of aortic stiffness in elderly individuals: A subgroup of the Cardiovascular Health Study*. American Journal of Hypertension, 15(1):16–23, 2002.

[236] R. P. Wildman, G. N. Farhat, A. S. Patel, R. H. Mackey, S. Brockwell, T. Thompson, and K. Sutton-Tyrrell. *Weight change is associated with change in arterial stiffness among healthy young adults*. Hypertension, 45(2):187–192, 2005.

[237] W. Chen, S. R. Srinivasan, and G. S. Berenson. *Differential impact of heart rate on arterial wall stiffness and thickness in young adults: The Bogalusa Heart Study*. Journal of the American Society of Hypertension, 2(3):152–157, 2008.

[238] A. A. Malayeri, S. Natorl, H. Bahrami, A. G. Bertoni, R. Kronmal, J. A. C. Lima, and D. A. Bluemke. *Relation of aortic wall thickness and distensibility to cardiovascular risk factors (from the Multi-Ethnic Study of Atherosclerosis [MESA])*. American Journal of Cardiology, 102(4):491–496, 2008.

[239] R. Din-Dzietham, D. Couper, G. Evans, D. K. Arnett, and D. W. Jones. *Arterial stiffness is greater in African Americans than in whites - Evidence from the Forsyth County, North Carolina, ARIC Cohort*. American Journal of Hypertension, 17(4):304–313, 2004.

[240] W. M. Hlaing, S. Koutoubi, and F. G. Huffman. *Differences in arterial stiffness and its correlates in tri-ethnic young men and women*. Ethnicity and Disease, 16(4):837–843, 2006.

[241] R. S. Patel, A. Morris, Y. Ahmed, N. Stoyanova, I. Al Mheid, N. Kavtaradze, D. Coverson, L. P. Zhao, A. Bidulescu, Z. M. Chen, K. L. Brigham, R. Din-Dzietham, V. Vaccarino, R. W. Alexander, G. Gibbons, and A. A. Quyyumi. *African Americans Have Worse Arterial Compliance Than Whites, Independent of Risk Factor Burden and Framingham Risk Estimates*. Circulation, 120(18):S478–S478, 2009.

[242] A. Bellasi, E. Veledar, E. Ferramosca, C. Ratti, G. Block, and P. Raggi. *Markers of vascular disease do not differ in black and white hemodialysis patients despite a different risk profile*. Atherosclerosis, 197(1):242–249, 2008.

[243] W. Wojciechowska, J. A. Staessen, K. Stolarz, T. Nawrot, J. Filipovsky, M. Ticha, G. Bianchi, E. Brand, M. Cwynar, T. Grodzicki, T. Kuznetsova, H. A. Struijker-Boudier, V. Svobodova, L. Thijs, L. M. Van Bortel, K. Kawecka-Jaszcz, and European Project Genes Hypertensio. *Association of peripheral and central arterial wave reflections with the CYP11B2-344C allele and sodium excretion*. Journal of Hypertension, 22(12):2311–2319, 2004.

[244] S. Yusuf, S. Reddy, S. Ounpuu, and S. Anand. *Global burden of cardiovascular diseases - Part II: Variations in cardiovascular disease by specific ethnic groups and geographic regions and prevention strategies*. Circulation, 104(23):2855–2864, 2001.

[245] J. A. Salomon and C. J. L. Murray. *The epidemiologic transition revisited: Compositional models for causes of death by age and sex*. Population and Development Review, 28(2):205–+, 2002.

[246] T Twagirumukiza, De Bacquer D, Kips, and L.M. De Backer G.and Van Bortel. *Current and Projected Prevalence of Arterial Hypertension in Sub-Saharan Africa by Gender, Age and Habitat: an Estimate from Population Studies.* Journal of Hypertension, page accepted for publication, 2010.

[247] A. Sherwood, C.W. May, W.C. Siegel, and J.A. Blumenthal. *Ethnic-Differences in Hemodynamic-Responses to Stress in Hypertensive Men and Women*. American Journal of Hypertension, 8(6):552–557, 1995.

[248] D.W. Moskowitz. *Hypertension, thermotolerance, and the "African gene": An hypothesis*. Clinical and Experimental Hypertension, 18(1):1–19, 1996.

[249] H.P. Dustan. *Does Keloid Pathogenesis Hold the Key to Understanding Black-White Differences in Hypertension Severity*. Hypertension, 26(6):858–862, 1995.

[250] J. T. Wright, M. Rahman, A. Scarpa, M. Fatholahi, V. Griffin, R. Jean-Baptiste, M. Islam, M. Eissa, S. White, and J. G. Douglas. *Determinants of salt sensitivity in black and white normotensive and hypertensive women*. Hypertension, 42(6):1087–1092, 2003.

[251] E.S. Pinto, R. Mensah, K. Meeran, J.D. Cameron, N. Murugaesu, C. Bulpitt, and C. Rajkumar. *Peripheral arterial compliance differs between races*. Diabetes Care, 28(2):496–496, 2005.

[252] J. Addo, L. Smeeth, and D.A. Leon. *Hypertension in sub-Saharan Africa - A systematic review*. Hypertension, 50:1012–1018, 2007.

[253] O.O. Ayoola, J.G. Kips, S. Greenwald, P. Segers, L. Van Bortel, P.E. Clayton, and J.K. Cruickshank. *Impact of maternal malaria and blood pressure on aortic pulse wave velocity at birth in Nigerian infants: 'The Ibadan childhood growth and vascular health study'*. Hormone Research, 72:424–424, 2009.

[254] S.K. Kunutsor and J.W. Powles. *The effect of ambient temperature on blood pressure in a rural West African adult population: a cross-sectional study*. Cardiovascular Journal of Africa, 21(1):17–20, 2010.

[255] A.G. Barnett, S. Sans, V. Salomaa, K. Kuulasmaa, A.J. Dobson, and Monica Project Who. *The effect of temperature on systolic blood pressure*. Blood Pressure Monitoring, 12(3):195–203, 2007.

[256] K.S. Reddy. *Cardiovascular disease in non-Western countries*. New England Journal of Medicine, 350(24):2438–2440, 2004.

[257] R. Beaglehole. *International trends in coronary heart disease mortality and incidence rates*. Journal of Cardiovascular Risk, 6(2):63–68, 1999.

[258] A. Himmelmann, A. Svensson, and L. Hansson. *Relation of Maternal Blood-pressure During Pregnancy To Birth-weight and Blood-pressure In Children - the Hypertension In Pregnancy Offspring Study*. Journal of Internal Medicine, 235(4):347–352, 1994.

[259] C. M. Law, M. eswiet, C. Osmond, P. M. Fayers, D. J. P. Barker, A. M. Cruddas, and C. H. D. Fall. *Initiation of Hypertension Inutero and Its Amplification Throughout Life*. British Medical Journal, 306(6869):24–27, 1993.

[260] S. H. Zinner, Y. H. Lee, B. Rosner, W. Oh, and E. H. Kass. *Factors Affecting Blood Pressures In Newborn-infants*. Hypertension, 2(4):I99–I101, 1980.

[261] D.J.P. Barker and S.P. Bagby. *Developmental antecedents of cardiovascular disease: A historical perspective*. Journal of the American Society of Nephrology, 16(9):2537–2544, 2005.

[262] P. Bateson, D. Barker, T. Clutton-Brock, D. Deb, B. D'Udine, R.A. Foley, P. Gluckman, K. Godfrey, T. Kirkwood, M.M. Lahr, J. McNamara, N.B. Metcalfe, P. Monaghan, H.G. Spencer, and S.E. Sultan. *Developmental plasticity and human health*. Nature, 430(6998):419–421, 2004.

[263] O.T. Raitakari, M. Juonala, M. Kahonen, L. Taittonen, T. Laitinen, N. Maki-Torkko, M.J. Jarvisalo, M. Uhari, E. Jokinen, T. Ronnemaa, H.K. Akerblom, and J.S.A. Viikari. *Cardiovascular risk factors in childhood and carotid artery intima-media thickness in adulthood - The Cardiovascular Risk in Young Finns Study*. Journal of the American Medical Association, 290(17):2277–2283, 2003.

[264] G.S. Berenson, S.R. Srinivasan, W.H. Bao, W.P. Newman, R.E. Tracy, W.A. Wattigney, and Heart Study Bogaulas. *Association between multiple cardiovascular risk factors and atherosclerosis in children and young adults*. New England Journal of Medicine, 338(23):1650–1656, 1998.

[265] J.S. Wright, J.K. Cruickshank, S. Kontis, C. Dore, and R.G. Gosling. *Aortic Compliance Measured by Noninvasive Doppler Ultrasound - Description of A Method and Its Reproducibility*. Clinical Science, 78(5):463–468, 1990.

[266] S. Kontis and R.G. Gosling. *Online Doppler Ultrasound Measurement of Aortic Compliance and Its Repeatability in Normal Subjects*. Clinical Physics and Physiological Measurement, 10(2):127–135, 1989.

[267] A. Koudsi, J. Oldroyd, P. McElduff, M. Banerjee, A. Vyas, and J.K. Cruickshank. *Maternal and neonatal influences on, and reproducibility of, neonatal aortic pulse wave velocity*. Hypertension, 49(1):225–231, 2007.

[268] H.M. Gardiner, M.J.O. Taylor, A. Karatza, T. Vanderheyden, A. Huber, S.E. Greenwald, N.M. Fisk, and K. Hecher. *Twin-twin transfusion syndrome - The influence of intrauterine laser photocoagulation on arterial distensibility in childhood*. Circulation, 107(14):1906–1911, 2003.

[269] A.A. Laogun and R.G. Gosling. *In vivo arterial compliance in man*. Clinical Physics and Physiological Measurement, 3(3):201–212, 1982.

[270] C.M. Law, A.W. Shiell, C.A. Newsome, H.E. Syddall, E.A. Shinebourne, P.M. Fayers, C.N. Martyn, and M. de Swiet. *Fetal, infant, and childhood growth and adult blood pressure - A longitudinal study from birth to 22 years of age*. Circulation, 105(9):1088–1092, 2002.

[271] R.W. Steketee, J.J. Wirima, and C.C. Campbell. *Developing effective strategies for malaria prevention programs for pregnant African women*. American Journal of Tropical Medicine and Hygiene, 55(1):95–100, 1996.

[272] B.J. Brabin. *An Analysis of Malaria in Pregnancy in Africa*. Bulletin of the World Health Organization, 61(6):1005–1016, 1983.

[273] M. Cot, J.Y. Le Hesran, T. Staalsoe, N. Fievet, L. Hviid, and P. Deloron. *Maternally transmitted antibodies to pregnancy-associated variant antigens on the surface of erythrocytes infected with Plasmodium falciparum: Relation to child susceptibility to malaria*. American Journal of Epidemiology, 157(3):203–209, 2003.

Appendices

Publications

First author

- Kips JG, Segers P, Van Bortel LM. *Identifying the vulnerable plaque: A review of invasive and non-invasive imaging modalities.* Artery Research 2008, 2:21-34.

- Kips JG, Rietzschel ER, De Buyzere ML, Westerhof BE, Gillebert TC, Van Bortel LM, Segers P. *Evaluation of Noninvasive Methods to Assess Wave Reflection and Pulse Transit Time From the Pressure Waveform Alone.* Hypertension 2009, 53:142-149.

- Kips JG, Vanmolkot F, Mahieu D, Vermeersch SJ, Fabry I, de Hoon J, Van Bortel LM, Segers P. *The use of diameter distension waveforms as an alternative for tonometric pressure to assess carotid blood pressure.* Physiological Measurement 2010, 31:543-553.

- Kips JG, Schutte AE, Vermeersch SJ, Huisman HW, Van Rooyen JM, Glyn MC, Fourie CM, Malan L, Schutte R, Van Bortel LM, Segers P. *Comparison of central pressure estimates obtained from SphygmoCor, Omron HEM-9000AI and carotid applanation tonometry.* Journal of Hypertension 2011, 29:1115-1120.

Submitted for publication

- Kips JG, Vermeersch SJ, Reymond P, Boutouyrie P, Stergiopulos N, Laurent S, Van Bortel LM, Segers P. *Ambulatory Arterial Stiffness Index (AASI) does not accurately assess arterial stiffness.*, submitted to Journal of Hypertension.

Co-author

- Segers P, Mahieu D, Kips JG, Van Bortel LM. *The use of a generalized transfer function: different processing, different results!* Journal of Hypertension 2007, 25:1783-1787.

- Van Canneyt K, Kips JG, Mareels G, Baert E, Van Roost D, Verdonck PR. *Experimental and numerical modelling of the ventriculosinus shunt (El-Shafei shunt).* Proceedings of the Institution of Mechanical Engineers Par H - Journal of Engineering in Medicine 2008, 222:455-464.

- Swillens A, Lovstakken L, Kips JG, Torp H, Segers P. *Ultrasound Simulation of Complex Flow Velocity Fields Based on Computational Fluid Dynamics.* IEEE Transactions on Ultrasonics, Ferroelectrics and Frequency Control 2009, 56:546 -556.

- Segers P, Mahieu D, Kips JG, Rietzschel ER, De Buyzere ML, De Bacquer D, Bekaert S, De Backer G, Gillebert TC, Verdonck PR, Van Bortel LM, on behalf of the Asklepios investigators. *Amplification of the Pressure Pulse in the Upper Limb in Healthy, Middle-Aged Men and Women.* Hypertension 2009, 54:414-420.

- Segers P, Mahieu D, Kips JG, Rietzschel ER, De Buyzere ML, Van Bortel LM. *Flawed Measurement of Brachial Tonometry for Calculating Aortic Pressure? Response.* Hypertension 2009, 54: E132-E132.

- Segers P, Kips J, Trachet B, Swillens A, Vermeersch SJ, Mahieu D, Rietzschel ER, De Buyzere ML, Van Bortel LM. *Limitations and pitfalls of non-invasive measurement of arterial pressure wave reflections and pulse wave velocity.* Artery Research 2009, 3:79-88.

- Mahieu D, Kips JG, Rietzschel ER, De Buyzere ML, Verbeke F, Gillebert TC, De Backer G, De Bacquer D, Verdonck PR, Van Bortel LM, Segers P, on behalf of the Asklepios investigators. *Noninvasive assessment of central and peripheral arterial pressure (waveforms): implications of calibration methods.* Journal of Hypertension 2010, 28:300-305.

- Twagirumukiza M, Kayumba PC, Kips JG, Vrijens B, Vander Stichele RV, Vervaet C, Remon JP, Van Bortel LM. *Evaluation of medication adherence methods in the treatment of malaria in Rwandan infants.* Malaria Journal 2010, 9:206.

- Twagirumukiza M, Annemans L, Kips JG, Bienvenu E, Van Bortel LM. *Prices of antihypertensive medicines in sub-Saharan Africa and alignment to WHO's model list of essential medicines.* Tropical Medicine & International Health 2010, 15:350-361.

- Trachet B, Reymond P, Kips JG, Swillens A, De Buyzere ML, Suys B, Stergiopulos N, Segers P. *Numerical validation of a new method to assess aortic pulse wave velocity from a single recording of a brachial artery waveform with an occluding cuff.* Annals of Biomedical Engineering 2010, 38:876-888.

- Fabry I, De Paepe P, Kips JG, Vermeersch SJ, Van Bortel LM. *Different effects of tocolytic medication on blood pressure and blood pressure amplification.* European Journal of Clinical Pharmacology 2011, 67:11-17.

- Trachet B, Reymond P, Kips JG, Vermeersch SJ, Swillens A, Stergiopulos N, Segers P.*Validation of the Arteriograph working principle: questions still remain.* Journal of Hypertension 2011, 29:619-619.

- Twagirumukiza M, De Bacquer D, Kips JG, De Backer G, Vander Stichele R, Van Bortel LM. *Current and projected prevalence of arterial hypertension in sub-Saharan Africa by gender, age and habitat: an estimate from population studies.* Journal of Hypertension 2011, 29:1243-1252.

- Chirinos JA, Kips JG, Roman MJ, Medina-Lezema J, Li Y, Woodiwiss AJ, Norton GR, Yasmin, Van Bortel LM, Wang JG, Cockcroft JR, Devereux RB, Wilkinson IB, Segers P, McEniery CM. *Ethnic Differences in Arterial Wave Reflections and Normative Equations for Augmentation Index.* Hypertension 2011, 57:1108-1116.

Submitted for publication

- Chirinos JA, Kips JG, Brumback L, Kronmal R, Bluemke DA, Jacobs D, Duprez DA, Vermeersch SJ, Townsend RR, Segers P. *Central pressure profiles as predictors of incident cardiovascular events: The Multiethnic Study of Atherosclerosis (AE 042).* submitted to The New England Journal of Medicine

Abbreviations and Symbols

Abbreviations

AASI	Ambulatory arterial stiffness index
AIx	Augmentation index
AP	Augmented pressure
aPWV	Aortic pulse wave velocity
BA	Brachial artery
BMI	Body mass index
BP	Blood pressure
CCA	Common carotid artery
CO	Cardiac output
cSBP	central systolic blood pressure
CV	Cardiovascular
CVD	Cardiovascular disease
SMC	Smooth muscle cell
DBP	Diastolic blood pressure
ECG	Electrocardiogram
FMD	Flow-mediated dilation
HR	Heart rate
IMT	Intima media thickness
LDL	Low-density lipoprotein
LVH	Left ventricular hypertrophy
LVOT	Left ventricular outflow tract
MAP	Mean arterial pressure
PhD	Doctor of philosophy
PP	Pulse pressure
PWV	Pulse wave velocity
RM	Reflection magnitude
RMSE	Root-mean-squared error
SBP	Systolic blood pressure
SD	Standard deviation

SSA	sub-Saharan Africa
TF	Transfer function
TT	Transit time
WHO	World health organisation

Symbols

A	Cross-sectional area	[m^2]
C	Compliance	ml/mmHg
c	Wave speed	[m/s]
D	Diameter	[m]
η	Dynamic viscosity	[Pa.s]
E	Elastance	[mmHg/ml]
E	Young modulus of elasticity	[Pa]
h	Thickness	[m]
L	Inertance	[$Pa.s^2/m^3$]
l	Length	[m]
P	Pressure	[mmHg]
Q	Flow rate	[m^3/s]
ρ	Mass density	[kg/m^3]
R	Resistance (electric)	[Ω]
R	Resistance (hydraulic)	[$mmHg.s/m^3$]
r	Radius	[m]
σ	Stress	[Pa]
τ	Strain	[]
T	Cardiac period	[s]
V	Volume	[m^3]
Z	Impedance	[kg/m^4]

Operators

Δ	Difference
d	Derivative
Σ	Sum

Subscripts

A	area
a	arterial
approx	approximated
b	backward
c	characteristic

D	diameter distension
exp	exponential
f	forward
in	input
inc	incremental
lin	linear
max	maximal
periph	peripheral
T	tonometer
v	venous
wf	waveform

Superscripts

avg	averaged
meas	measured
tri	triangular

Units

bpm	beats per minute
cm	centimeter
Hz	hertz
kg	kilogram
m	meter
min	minute
mmHg	millimeter of mercury
Ω	ohm
Pa	pascal
s	second
V	volt

List of Figures

List of Tables